# PRINCIPAL COMPONENT ANALYSIS FOR SIGNAL-BASED SYSTEM IDENTIFICATION

by

**Murat Hasan Tan**

A thesis submitted for the degree of

**Doctor of Philosophy**

Supervisor

**Prof. J. K. Hammond**

University of Southampton

Faculty of Engineering, Science and Mathematics

Institute of Sound and Vibration Research

April 2005

# ACKNOWLEDGEMENTS

First and foremost, I must thank Professor Joe Hammond for his ***broadband*** support throughout my ISVR experience since 1996.

I would also like to thank:

Professor Paul White for his crucial technical advice on various signal processing problems;

Mrs. Maureen Strickland for everything she has done since my first day in the department;

Ms. Alison Gunn for the unlimited extensions on library loans;

Mrs. Norma Martin for her time spent on my junk e-mails;

and My Family for their patience ...

# CONTENTS

## Glossary of Symbols

| | |
|---|---|
| $t$ | time |
| $f$ | linear frequency |
| $\omega$ | angular frequency |
| $\Delta$ | time delay |
| $\tau$ | time lag |
| $a$ | gain |
| $a(t)$ | time-varying gain |
| $e$ | error in time domain |
| $E$ | error in frequency domain |
| $J$ | cost function |
| $E[\,]$ | expectation operator |
| $x(t)$ | original time history of signal $x$ |
| $x_m(t)$ | measured time history of signal $x$ |
| $n_x(t)$ | time history of noise on signal $x$ |
| $h(t)$ | impulse response function |
| $H(f)$ | frequency response function |
| $X(f)$ | Fourier transform of signal $x$ |
| $X_m(f)$ | Fourier transform of measured signal $x$ |
| $\hat{S}_{xx}(f)$ | power-spectral density estimate of signal $x$ |
| $\hat{S}_{xy}(f)$ | cross-spectral density estimate between signals $x$ and $y$ |
| $\gamma^2_{xy}(f)$ | ordinary coherence function between signals $x$ and $y$ |
| $T$ | truncated time record length |
| $i$ | sample index |
| $N$ | number of samples |
| $k$ | segment index |
| $K$ | number of segments |
| $\mathbf{x}$ | bivariate time domain measurement vector |
| $\mathbf{z}$ | principal components vector |

| | |
|---|---|
| $\mathbf{R}_{xx}$ | bivariate covariance matrix |
| $\mathbf{R}_{mm}$ | multivariate covariance matrix |
| $\mathbf{R}(f)$ | spectral correlation matrix |
| $\mathbf{m}$ | multivariate time domain measurement vector |
| $\sigma$ | standard deviation |
| $\sigma^2$ | variance |
| $\mu$ | mean |
| $\lambda$ | eigenvalue |
| $\mathbf{\Lambda}$ | diagonal eigenvalue matrix |
| $\mathbf{t}$ | eigenvector |
| $\mathbf{T}$ | transformation matrix |
| $\mathbf{Q}$ | orthonormal transformation matrix |
| $\boldsymbol{\theta}(f)$ | frequency domain measurement vector |
| $\kappa(f)$ | ratio of input-output measurement noise spectra |
| $s$ | Laplace variable |
| $\Pr\{\ \}$ | probability density function |
| $L$ | log likelihood function |
| $\tilde{\mathbf{R}}$ | adjoint of spectral correlation matrix |
| $Var\{\ \}$ | variance |
| $F(t)$ | excitation force |
| $\xi$ | viscous damping coefficient |
| $\omega_0$ | undamped natural frequency |
| $\omega_0(t)$ | time-varying undamped natural frequency |
| $R_{xx}(0)$ | auto-correlation function of signal $x$ |
| $R_{xy}(\tau)$ | cross-correlation function between signals $x$ and $y$ for lag $\tau$ |
| $\mathbf{R}(\tau)$ | covariance matrix for lag $\tau$ |
| $h(t,\tau)$ | time-varying impulse response function |
| $H(t,\omega)$ | time-varying frequency response function |
| $H(t,s)$ | time-varying transfer function |

# Chapter One

# INTRODUCTION

## 1.1 Aim of the Research

*"Identification is the determination, on the basis of input and output, of a system within a classified class of systems, to which the system under test is equivalent."*

-L. Zadeh, (1962)

The study of system identification in signal processing is huge with a vast literature and methodology ranging from the totally standard (e.g. frequency response function estimation for linear time-invariant and parametric estimation) to innovative and developing techniques.

In this thesis the term system identification addresses the generalised process of obtaining useful information to describe the system characteristics from the relationships between the measurable input-output data sets within the system's boundary. The primary mathematical tool we use in order to accomplish this task is the classical Principal Component Analysis (PCA) technique.

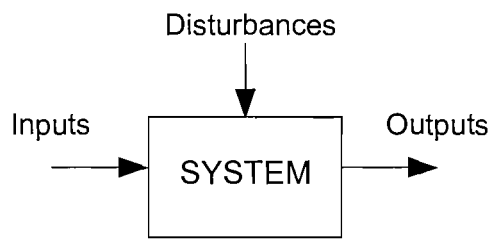


**Figure 1.1** Illustration of a generic system to be identified.

PCA, created over 60 years ago, is one of the most powerful statistical multivariate data analysis techniques. It has been widely used for a variety of applications in different fields ranging from natural and social sciences to several branches of engineering. The aim of this method is to introduce *parsimony* to the investigation by reducing the dimensionality, without any explicit assumptions on the probability density characteristics of the data set. With the use of PCA, an original set of independent variables are transformed into a possibly smaller set of *uncorrelated* virtual variables that are easier to understand and treat for further analysis. Eigen-Value Decomposition (EVD) of the measurement covariance matrix forms the basis of this technique.

Our work focuses on developing PCA-based data processing/analysis strategies in order to be able to extract the features of various forms of physical systems under investigation. It has been shown that, when the data to be analysed through the use of PCA consists of the measured input(s) and the output(s), the eigenvalues and the eigenvectors of the associated covariance (or spectral correlation) matrix give a direct indication of the degree of linearity with respect to the system's transfer characteristics. This crucial observation forms the primary novel contribution of our research. Originating from this fundamental aspect, we demonstrate how eigen-analysis can be used as an effective practical procedure for the identification and/or interpretation of the properties of different types of systems including linear/non-linear time-invariant, pure delay and non-stationary.

## 1.2 Scope and Contents of the Thesis

The necessary theoretical background and mathematical preliminaries for fundamental signal processing concepts and statistical methods covered in this thesis are summarised in Chapter 2. These include an overview of signals and systems theory in the context of transfer function estimation as well as the basic principles of the Least Squares Method and PCA.

In Chapter 3, a detailed analytical review and statistical assessment of the existing Single-Input-Single-Output (SISO) system transfer function estimation methods are presented. The performances of the three *standard* least squares estimators are compared both theoretically and computationally on the basis of a generic measurement system exhibiting various cases of uncorrelated additive noise contamination on the input and/or output signals. Furthermore, a generalised Total Least Squares (TLS) estimation scheme is proposed from a geometric viewpoint allowing one to readily interpret the relationships between these estimators.

Chapters 4 and 5 introduce the concept of PCA-based input-output investigation with reference to Linear Time-Invariant (LTI) systems considered in both time and frequency domains. Work presented in this part of the thesis forms the foundations of our overall signal analysis/processing strategy which is later extended to other types of systems with appropriate modifications. Initially, the methodology is described in terms of gain estimation in SISO and Multi-Input-Single-Output (MISO) systems based on real variables (Chapter 4) for simplicity and hence providing a clear picture of the associated procedures. The problem of Frequency Response Function (FRF) estimation in the corresponding dynamical systems is covered in detail in Chapter 5 where it is also shown that the SISO PCA and TLS FRF estimators are equivalent for the special case of equal input-output measurement noise. In addition to the above, a statistical inference based approach is considered for SISO FRF estimation through the use of the principle of the Maximum Likelihood (ML) leading to a novel development of a generalised PCA/TLS regime. The theoretical material covering the work contained in these chapters is validated by computational simulations whose results are also used in order to give a direct comparison between the existing and the proposed techniques.

Chapter 6 deals with the application of PCA to non-linear processes with particular reference to linear equivalent transfer function estimation and non-linearity detection. By using the eigenvalues and the eigenvectors of the input-output covariance (or spectral correlation) matrix, a form of linearization of the non-linear system is considered. It is shown analytically that the EVD of the data set leads to the derivation of a parameter, equivalent to the virtual coherence function. Computational simulations are undertaken for the performance assessment of the proposed approximation procedure in a typical Duffing oscillator model. An experimental investigation for fault detection of a typical multi-output rotating machine is studied where measured system output pairs for several operating conditions are analysed using the PCA-based coherence, the so called Non-Linearity Detection Ratio (NDR), and the Ordinary Coherence Function (OCF).

In Chapter 7, non-dispersive time-delay detection in several forms of single- and multi-path systems using EVD-based input-output analysis is introduced. The merit of carrying out the data processing in the time domain as opposed to frequency domain is verified analytically. In essence, the procedure implemented differs from those in the rest of the thesis with respect to the formation of statistical information matrices: An array of negative and positive lag input-output covariance matrices are formed whose eigenvalues are subsequently computed and observed for further interpretation. The results of computational simulations demonstrate the robustness of the proposed delay detection scheme under extreme Signal-to-Noise Ratios (SNRs).

Chapter 8 introduces the proposed Short-Term Spectral PCA (STSPCA) for time-varying transfer function estimation. Data processing strategy is based on moving-segment EVD of a series of spectral correlation matrices formed by simultaneous truncation of the input-output signals of a non-stationary system. The results of computational simulations on a Single Degree of Freedom (SDOF) system with time-varying natural frequency proves the procedure to be a practical and effective alternate to the classical Short-Time Fourier Transform (STFT) spectrogram technique.

General conclusion of the thesis and considerations for future research are given in Chapter 9.

# Chapter Two

# STATISTICAL METHODS FOR SIGNAL-BASED SYSTEM IDENTIFICATION

## 2.1 Introduction

This chapter presents the necessary theoretical background for various fundamental signal processing concepts, the problem of transfer function estimation and the two commonly used statistical multivariate data analysis techniques that are referred to in this thesis.

The next section covers the conventional methodology of transfer/frequency response function introducing the concepts such as system/data classification, power/cross spectral densities and the ordinary coherence function.

Section 2.3 introduces the widely used statistical technique, the so called the Least Squares Method, whose more detailed coverage is presented in Chapter 3 in the context of existing gain and Frequency Response Function (FRF) estimators.

In the last section the primary statistical technique on which our work has been based on, the so called Principal Component Analysis (PCA), is covered giving its basic principles, mathematical description and geometrical interpretations which is helpful in order to follow the rest of the thesis both conceptually and mathematically.

## 2.2 Transfer Function Estimation

In the simplest form, a system may have only one input and one output. Such systems are called *single-input single-output* (SISO) systems as depicted in the block diagram in Figure 2.1.

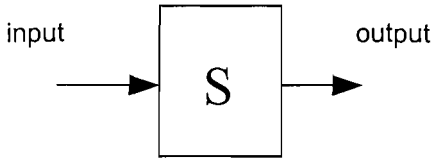


**Figure 2.1** Block Diagram of a single-input single-output (SISO) system.

In the more general case, systems have several inputs and outputs. Such systems are said to be multivariable and called *multi-input multi-output* (MIMO) systems. These can be represented by a block diagram of the type shown in Figure 2.2.

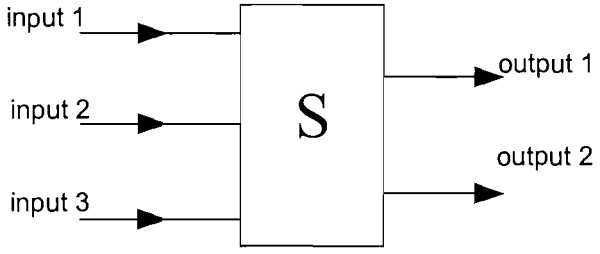


**Figure 2.2** Block Diagram of a multi-input multi-output (MIMO) system.

A system is said to be *static* if its response at any time depends only on the present value of its excitation. Such a system may also be regarded as *memoryless* or constant as in the case of the relationship between the input $x$ and the output $y$ of a SISO system that is given by

$$y(t) = x^3(t) \tag{2.1}$$

where $t$ is the time index.

A system is said to be *dynamic* if its response depends on the past as well as the present values of its excitation. Such systems may also be regarded as having a *memory*. An example for this class of systems can be defined by the input-output relationship

$$\frac{dy}{dt} = x \quad \Rightarrow \quad y(t) = \int x(t)dt + \text{constant} \tag{2.2}$$

In this case, the system operates as an Integrator and does not forget the past values of the input ever.

A system is said to be *linear* if it obeys the principle of *superposition*. Superposition requires the property of *additivity* and the property of *homogeneity*. A system is said to be *non-linear* if it does not meet the requirements of superposition. In practice, no real system component is completely linear, however, frequently the range of operation is such that linearity can be assumed.

A system is *time varying* if its the behaviour and characteristics are fluctuating over time and is *time invariant* if its behaviour and characteristics are fixed over time.

System signals e.g. inputs and outputs are functions of time and records of them are referred to as *time histories*. Although signals can be classified in many different ways, they may be divided into two main categories, namely, *deterministic* or *random*. Deterministic signals are able to be predicted or deduced whereas random signals are not exactly predictable. Deterministic signals may also be divided into two main groups: *periodic* or *non-periodic*. Non-periodic signals can be either *transient* or *almost periodic*. Non-deterministic (random) signals can be either *stationary* or *non-stationary*.

The problem of Transfer Function Estimation relies on the analysis of the relationship between input and output signals. If both input and output are measurable then this can be carried out by applying some specific controlled input signal to the system under investigation (unless there is already a naturally occurring measurable input), measuring the resulting response, and subsequently determining the transfer function using the appropriate mathematical manipulation.

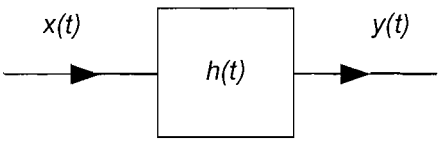


**Figure 2.3** SISO Linear Time-Invariant System

The dynamic characteristics of a Linear Time-Invariant System, that is also assumed to be stable and causal such as depicted in Figure 2.3, can be described by its impulse response (or weighting) function *h(t)* which is defined as the output of the system at any time to a *unit impulse* (delta function) input applied a time *t* before. The theoretical relationship between its input and output is given by

$$y(t) = h(t) * x(t) \tag{2.3}$$

i.e. the convolution (*) of the system impulse response *h(t)* and the system input *x(t)* is the system output *y (t )*. Commonly the solution to the problem of estimating the transfer function of a linear time-invariant system is considered in the *frequency domain*. The convolution form of the time domain is very much simplified when the Fourier Transform is applied and the frequency domain equivalent of the above relationship is given by

$$Y(f) = H(f) . X(f) \tag{2.4}$$

The transformation from the time domain into the frequency domain for any time history *a(t)* is defined as

$$A(f) = \int_{-\infty}^{\infty} a(t) e^{-j2\pi ft} dt \tag{2.4a}$$

i.e. *Y(f)* is the Fourier Transform of the output, *X(f)* is the Fourier Transform of the input and *H(f)* is the Fourier Transform of the system impulse response called the Frequency Response Function at each frequency *f*.

However, when traditional experimental response testing procedures are involved difficulties arise: in particular the measurements can often be violated by various factors such as non-linear system behaviour, change of system characteristics with time, instability and most commonly the contamination by additive measurement noise on the data to be analysed. This can affect either the input or output, or both.

If a time-invariant, stable linear system is driven by a stationary random process the output is also stationary random. Figure 2.4 illustrates the generic measurement SISO system in the presence of additive measurement noise when the input is a stationary random process and forms the basis for the general signal-based estimation problem for the FRF where all signals are also represented by their Fourier Transforms (FT) i.e. in the frequency domain.

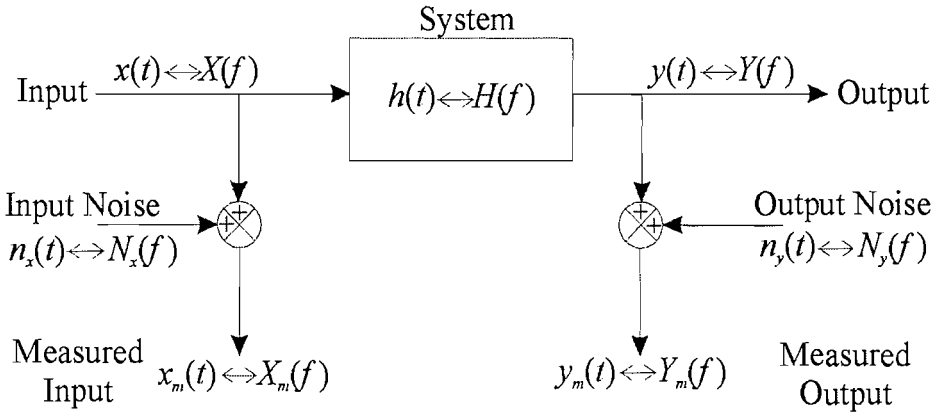


**Figure 2.4** Generic Measurement Diagram of a Linear Time-Invariant SISO System with uncorrelated additive measurement noise

In practice, taking a finite length of data results in truncation of input and output i.e. a sample time history of length $T$, and a relationship between the input and output in the frequency domain is given by

$$Y_T(f) \approx H(f) \cdot X_T(f) \tag{2.5}$$

where $Y_T(f)$ is the Fourier Transform (FT) of the finite length realization of the output and $X_T(f)$ is the Fourier Transform of the finite length realization of the input. Also from Figure 2.4 it is clear that

$$\begin{aligned} X_m(f) &= X(f) + N_x(f) \\ Y_m(f) &= Y(f) + N_y(f) \end{aligned} \tag{2.6a,b}$$

It is central to the problem of statistical estimation that the relationships between the time domain descriptors (mean, covariance etc.) and the frequency domain descriptors (spectral density functions) are clearly emphasised since they form the basis of the whole process. Spectral density functions can be defined in various ways [1, 2] e.g. through the correlation functions or the finite Fourier Transforms or the filtering-squaring-averaging operations. In its most commonly used form (through the finite F.T.), the two-sided power spectral density function of a finite length realization $x_T(t)$ is given by

$$S_{xx}(f) = \lim_{T\to\infty} \frac{1}{T} E\left[\left|X_k(f,T)\right|^2\right] \tag{2.7}$$

where $T$ is the record length of the $k^{\text{th}}$ data segment, $f$ is the frequency, $X_k(f,T)$ is the F.T. of the segmented data and E[ ] denotes the expectation operator (see (2.13)).

This is the frequency composition of a random function described in terms of the spectral density of its *mean square value (average power in the time domain).* In practice the length of the data segment and the number in the ensembles over which the averaging operation is taken will always be finite. This formula is normally implemented by the Fast Fourier Transform (FFT) available in most of the software packages and analysers that are commonly in use today. Similarly, the two-sided cross-spectral density function of the finite length realizations $x_T(t)$ and $y_T(t)$ is given by

$$S_{xy}(f) = \lim_{T\to\infty} \frac{1}{T} E\left[X_k^*(f,T)Y_k(f,T)\right] \tag{2.8}$$

where ' * ' denotes the complex conjugate operator.

An extremely important property of the cross-spectral density function is that it is bounded by the cross-spectrum inequality (see also the corresponding cross-correlation inequality, [1, 2, 3]) and this is given by

$$\left|S_{xy}(f)\right|^2 \le S_{xx}(f)S_{yy}(f) \tag{2.9}$$

This result relates to the property of the *ordinary coherence function* (sometimes called the *coherency squared* function) which is defined as

$$\gamma_{xy}^2(f) = \frac{\left|S_{xy}(f)\right|^2}{S_{xx}(f)S_{yy}(f)} \tag{2.10}$$

which by (2.9) satisfies the condition

$$0 \le \gamma_{xy}^2(f) \le 1 \tag{2.11}$$

for all frequencies. This function can be described as the measure of the degree of linear association between two signals. If the system under investigation is linear the coherence function can be considered as the fractional proportion of the mean square value at the output which is contributed by the input at the given frequency. Hence for the ideal case such as given in Figure 2.3, the coherence function will be unity for all frequencies. However, if the coherence function has the value between zero and unity, it should be expected to have one or more of: extraneous measurement *noise*, *non-linear* system behaviour or output $y(t)$ due to the input $x(t)$ as well as *other inputs.*

## 2.3 The Method of Least Squares

It is very often of great importance in the statistical analysis of data to know whether a relationship exists between two or more variables. In the case of two variables, data is then termed *bivariate* i.e. there are two observations or measurements associated with each item. Suppose, an experiment has been carried out and pairs of data $(x_i,y_i)$ have been observed for values, $i=1,...,N$. These data may be regarded as controlled variable *input* $x$ and dependent (response) variable *output* $y$. It should be noted that this input-output notion is not necessary. In more usual situations some relation between two variables is sought i.e. it is suspected that there is some relationship between $x$ and $y$. The likely relationship between these two variables can be easier to see on a scatter diagram where the controlled (independent) variable $x$ is normally plotted on the horizontal axis. Having established some relationship by eye on the plotted scatter diagram between $x$ and $y$, a more quantified relationship needs to be specified in order to be able to answer some questions about the problem. For example one might seek a linear relationship between the variables. The main concept in such a *linear regression* problem is that using the sample data in the problem, the resulting *sample regression line* is estimated in order to give the best approximation to the assumed theoretical or *population regression line.*

There are a number of possible ways in order to be able to obtain a line adjustment to best-fit the scatter of points. In the above example, if it is assumed that a linear relationship between $x$ and $y$ is expected to be in the form of $y=ax$, then three different types of error can be defined in the measured data as the consequence of additive measurement noise. These are listed as below and also shown in the Figure 2.5.

***Case I*** → $e_y$ : errors are defined in output data $y_i$, assuming input data $x_i$ are error-free;

***Case II*** → $e_x$ : errors are defined in input data $x_i$, assuming output data $y_i$ are error-free;

***Case III*** → $e_t$ : error line is normal to the best-fit line assuming errors to be present in both input and output data.

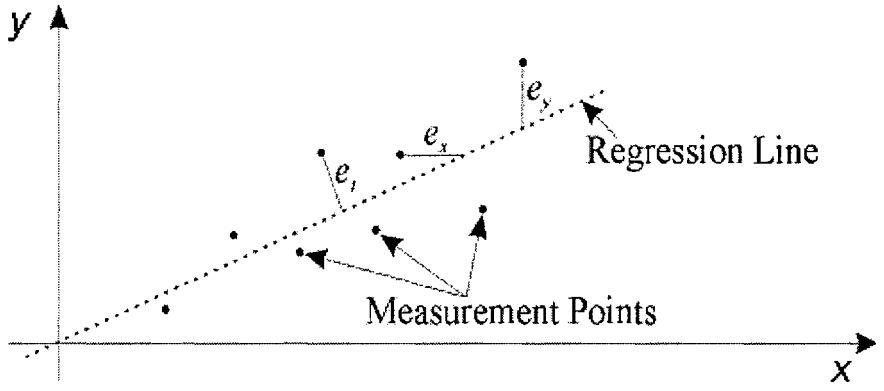


**Figure 2.5** Possible types of error defined in the measured bivariate data.

The principle that is widely used in linear curve-fitting, is the method of least squares and is also an approach to the transfer function (gain or FRF) estimation problem with no assumptions on the probability distributions of the data sets. The basic principle of the method is that, for a given set of data an estimator that minimizes the total squared error (distance) from a central location i.e. the sum of square errors for each item (point), is chosen. For the above example given by the linear relationship $y=ax$, this criterion is obtained by the minimization of a *measurement error cost function* with respect to the unknown variable $a$. If one minimises the sum of the squared vertical errors ($e_y$) between the fitted line and the data points then the estimator $a_1$ or $H_1(f)$ is obtained, whereas if the sum of the squared horizontal errors ($e_x$) is the quantity to be minimised then the estimator $a_2$ or $H_2(f)$ results. Whereas if it is the sum of the perpendicular errors ($e_t$) that is minimised then the Total Least Squares (TLS) estimator $a_{TLS}$ or $H_v(f)$ is realised (see Chapter 3 for more details).

## 2.4 Principal Component Analysis

Principal Components Analysis (PCA) is one of the most effective Multivariate Data Analysis Techniques which focuses on inter-object correlations and depends upon the fact that at least some of the variables in the original data set are mutually *correlated.* No assumptions on the probability distributions of the data sets are required. It is closely related to the Karhunen-Loéve and the Hotelling transforms.

Each variable forming the original data set can be considered as an axis of variability. PCA transforms the original axes in order to represent the same amount of the variability i.e. the total variance contained in the original variables in such a way that the first principal component (axis) accounts for the maximum proportion of the total variance, the second principal component (axis) accounts for the maximum proportion of the remaining variance and so on. New linear combinations are ordered according to their variation and the first few of the new axes represent the most of the variation contained in the original variables.

With this technique, a large number of correlated variables can be reduced into a smaller set of *uncorrelated* variables that is easier to understand and treat for further analysis. For a single random vector the *uncorrelatedness condition* between its components is defined as its covariance matrix being an $n$ x $n$ *diagonal matrix* where $n$ is the number of components i.e. for a random vector $\mathbf{x}$

$$\mathbf{R}_{xx} = E\left[(\mathbf{x}-\boldsymbol{\mu}_x)\cdot(\mathbf{x}-\boldsymbol{\mu}_x)^T\right] = \mathbf{D} \tag{2.12}$$

where $\boldsymbol{\mu}_x$ is the mean vector and $E[\ ]$ denotes the expectation operator. For any real single-valued continuous function g($\mathbf{x}$) of a random vector $\mathbf{x}$ the expected value is defined by [4]

$$E\{g(\mathbf{x})\} = \int_{-\infty}^{+\infty} g(\mathbf{x}) p_x(\mathbf{x}) d\mathbf{x} \tag{2.13}$$

where $p_x(\mathbf{x})$ is the probability density function of $\mathbf{x}$ and the integral is computed over all the components which are random variables. There is usually no knowledge of the probability density of a random vector although a set of $N$ samples are available and the expectation can be estimated using the formula [4].

$$E\{g(\mathbf{x})\} \approx \frac{1}{N}\sum_{i=1}^{N} g(\mathbf{x}_i) \tag{2.14}$$

The principal component method searches for the uncorrelated linear combinations of the variables in the original data set which contains most of the information. An original $p$-dimensional set of variables can be characterised as a $p$-dimensional random vector, $\mathbf{x} = (x_1, x_2, \ldots, x_p)$ that can be linearly transformed by $y = a_1x_1 + a_2x_2 + \ldots + a_px_p$ into a one dimensional variable $y$.

In algebraic terms the first principal component is a linear combination of this $p$-dimensional random vector $\mathbf{x}$ i.e.

$$y_1 = \sum_{i}^{p} a_{1i} x_i$$

where $i = 1,2,\ldots,p$ and its variability is maximised with the constraint that the sum of the squared weights is one i.e.

$$\sum_{i}^{p} a_{1i}^{\ 2} = 1$$

The variance of the second principal component

$$y_2 = \sum_{i}^{p} a_{2i} x_i$$

is maximised with the constraint that it is orthogonal to the first principal component i.e. uncorrelated, and it involves determining a secondary weighting factor. This process can be continued in order to obtain as many principal components as possible according to the number of the variables in the original data set. Normally the first few principal components represent the main proportion of the total variance of the original variables and are of great importance. Each weighting factor obtained is associated with one principal component and its variance.

The set of original variables for each *object* is the *data array* to be analysed where the variables are taken as the *columns* and the objects are taken as the *rows* or vice versa. The dependencies of variables and the objects are defined relative to some central point because the possible major weight differences between certain variables raises the requirement of scaling them. This can be done by *centring, normalisation* or *standardisation.* Although in many cases the measured original variables are in the same units the variance of each measured variable may differ from another one by a considerable amount.

Geometrical interpretation of the principal components is very appropriate and particularly for the two variable case, is quite simple to visualise and draw. Suppose an experiment has been carried out with $n$ observations in the two dimensional variable space forming a scatter of points recorded as in the linear regression problem given by Figure 2.5. For the reason that there is some positive correlation between these two variables the dots lie in an ellipsoidal band extending from lower left to upper right instead of being scattered randomly over the whole graph.

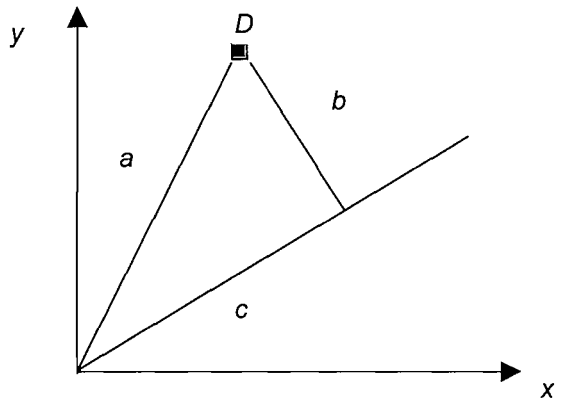


**Figure 2.6** Projection onto the principal axis.

The projections of the points on the first axis are to be as stretched as possible and this means that the variance of the projections are maximised such as that shown in Figure 2.6 where $D$ is the data point, $a$ is the distance of data point from the origin, $b$ is the distance of data point from the principal axis and $c$ is the projection of the position vector of $D$ onto the principal axis. By Pythagoras' Theorem

$$a^2 = b^2 + c^2$$

for the single data point the distance $a$ is constant, therefore in order to obtain the best choice of the principal axis, $b$ is minimised while $c$ is maximised. For the sampled population of the data points the sum of the squared errors is obtained by the summation of the same operation over all points. The first new axis is drawn through the points and in this case the first principal component is the line of the closest fit to the scatter of points minimising the sum of the squared deviation of the $n$ number of

observed data from the sample mean i.e. the estimator (principal component) for $y=ax$. Similarly, the second principal component is the line of closest fit to the residuals from the first principal component and is *orthogonal* i.e. being at right angles to the first. The two principal components together constitute a best fitting plane defining the locations of the scatter of points.

Derivation of principal components is based on a straightforward geometric technique. Since the problem is to define the relationship between the original axes and the principal axes i.e. to describe the *transformation of one co-ordinate system to another*, the solution to the problem is illustrated below in Figure 2.7 [5] where $X_1$ and $X_2$ are the original axes, $Y_1$ and $Y_2$ are the principal axes, and $D$ is a single data point. $\theta$ denotes the angle between the original axes and the principal axes.

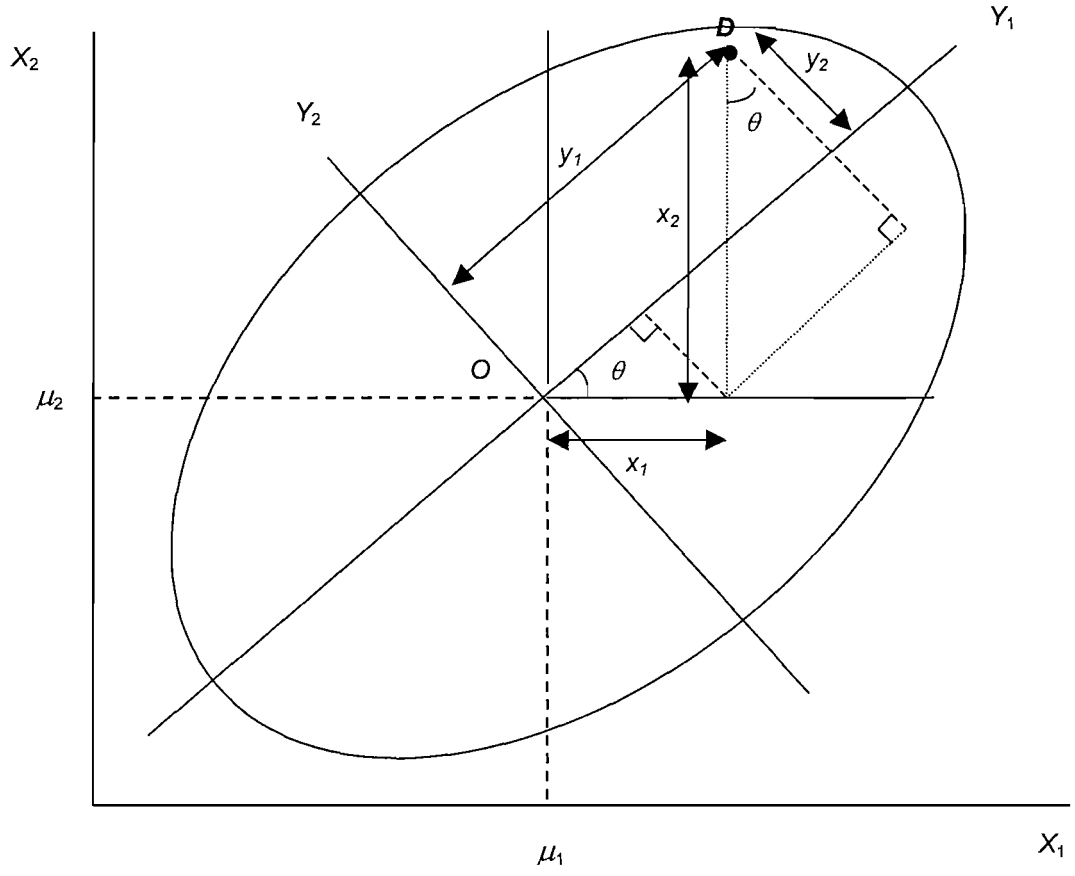


**Figure 2.7** Transformation of one co-ordinate system to another.

The origin, $O$, is defined at the intersection point of the mean values of the two original variables i.e. at the point $(\mu_1,\mu_2)$. This means that the variables have been centred to have zero means. The co-ordinates of the data point $D$ can be defined as $(X_1-\mu_1,X_2-\mu_2)$ or as the deviations from the mean i.e. $(x_1 , x_2)$. It can also be clearly seen that the co-ordinates of the data point $D$ can be given in terms of the principal components $(y_1, y_2)$. Using trigonometric relationships one can show that [5] the principal components are given by

$$y_1 = x_1 \cos\theta + x_2 \sin\theta \tag{2.15a}$$

and

$$y_2 = -x_1 \sin\theta + x_2 \cos\theta \tag{2.15b}$$

These relationships can also be written in matrix form

$$\begin{bmatrix} y_1 \\ y_2 \end{bmatrix} = \begin{bmatrix} \cos\theta & \sin\theta \\ -\sin\theta & \cos\theta \end{bmatrix} \begin{bmatrix} x_1 \\ x_2 \end{bmatrix} \tag{2.16}$$

or

$$\mathbf{y} = \mathbf{A}\mathbf{x} \tag{2.17}$$

and hence

$$\mathbf{x} = \mathbf{A}^{-1}\mathbf{y} \tag{2.18}$$

where $\mathbf{A}$ is an orthogonal matrix i.e. $\mathbf{A}^T=\mathbf{A}^{-1}$. Therefore the transformation of the original co-ordinate system to principal axes is an orthogonal transformation that with each vector $\mathbf{x}$ in the real vector space $\boldsymbol{R}^n$ such a transformation assigns a vector $\mathbf{y}$ in the vector space $\boldsymbol{R}^n$. This is simply the plane rotation through the angle $\theta$ and it can be shown that any orthogonal transformation in the plane or in the three-dimensional space is a rotation [6]. Now, assume that the variables $X_1$ and $X_2$ given above are mutually correlated. If a set of $N$ objects are measured on these variables then one can form a $2xN$ (or $N$x2) matrix defining the data array to be analysed such that

$$\mathbf{x}_i = \begin{bmatrix} X_{1i} \\ X_{2i} \end{bmatrix}, \text{ for } i=1,2,\ldots,N \tag{2.19}$$

The 2x2 *covariance matrix* of the variables $X_1$ and $X_2$ can be defined as

$$\mathbf{R}_{xx} = \overline{\mathbf{x}_i \mathbf{x}_i^{\mathrm{T}}} \tag{2.20}$$

where $\mathbf{x}_i = \begin{bmatrix} (X_{1i} - \mu_1) \\ (X_{2i} - \mu_2) \end{bmatrix} = \begin{bmatrix} x_{1i} \\ x_{2i} \end{bmatrix}$, for $i$=1,2,…,$N$; the operator "—" denotes the average over the sample population of $N$ objects. The 2x2 matrix $\mathbf{R}_{xx}$ is symmetric i.e. $\mathbf{R}_{xx}^{\mathrm{T}}=\mathbf{R}_{xx}$ and it has an orthonormal basis of 2 eigenvectors. The transformation of the uncorrelated *virtual* variables $y_1$ and $y_2$ to the original correlated variables $x_1$ and $x_2$ can be defined by

$$\mathbf{x} = \mathbf{T}\mathbf{y} \tag{2.21}$$

where $\mathbf{y} = \begin{bmatrix} y_1 \\ y_2 \end{bmatrix}$ with $y_1$ and $y_2$ are mutually uncorrelated i.e. the orthogonal principal axes and $\mathbf{T}$ is the transformation matrix. So (2.20) can be written as

$$\mathbf{R}_{xx} = \overline{\mathbf{x}\mathbf{x}^{\mathrm{T}}} = \mathbf{T}\overline{\mathbf{y}\mathbf{y}^{\mathrm{T}}}\mathbf{T}^{\mathrm{T}} \tag{2.22}$$

where $\mathbf{y}\mathbf{y}^{\mathrm{T}}=\mathbf{R}_{yy}$ i.e. the covariance matrix of the new variables. Therefore the above expression takes the form of

$$\mathbf{R}_{xx} = \mathbf{T}\mathbf{R}_{yy}\mathbf{T}^{\mathrm{T}} \tag{2.23}$$

From Similarity Transformation and Diagonalisation Theorem of Matrices [6], it can be shown that the matrix $\mathbf{R}_{yy}= \mathbf{\Lambda}$ is diagonal with the eigenvalues $(\lambda_1, \lambda_2)$ of the covariance matrix ($\mathbf{R}_{xx}$) of the original variable as the entries on its main diagonal and $\mathbf{T}$ is the orthonormal transformation matrix, i.e. $\mathbf{T}^{-1}=\mathbf{T}^{\mathrm{T}}$, containing the corresponding eigenvectors as its columns. Multiplying both sides of (2.23) by $\mathbf{T}$ from the right gives

$$\mathbf{R}_{xx}\mathbf{T} = \mathbf{T}\mathbf{R}_{yy} \tag{2.24}$$

or

$$\begin{bmatrix} x_{11} & x_{12} \\ x_{21} & x_{22} \end{bmatrix} \cdot \begin{bmatrix} t_{11} & t_{12} \\ t_{21} & t_{22} \end{bmatrix} = \begin{bmatrix} t_{11} & t_{12} \\ t_{21} & t_{22} \end{bmatrix} \cdot \begin{bmatrix} \lambda_1 & 0 \\ 0 & \lambda_2 \end{bmatrix} \tag{2.25}$$

From this result one can verify that the orthogonal transformation preserves the value of the inner product of vectors and hence the sum of the eigenvalues is equal to the total variance of the original variables. i.e. for the two variable case above

$$\sum_{i=1}^{2} \lambda_i = \sum_{i=1}^{2} \sigma_i^2 \tag{2.26}$$

where $\sigma_i^2$ denotes the variance of the $i^{th}$ variable. This result is of great importance and will be looked at in detail in the following chapters since it forms the basis for the application of the method in system identification.

## 2.5 Summary

This chapter has presented the necessary theoretical background for the statistical principles and multivariate data analysis techniques used in the following chapters in the context of signal-based system identification through input-output relationships.

In the next chapter the conventional transfer function estimators based on the least squares approach are analysed and in Chapter 4 the application of the method of principal component on time series for the gain estimation in memoryless systems is investigated in detail both analytically and computationally leading to Chapter 5 which covers the extension of the same approach in the frequency domain for the Frequency Response Function (FRF) estimation in dynamical systems.

Application of PCA to the problem of system identification is further investigated and several novel approaches are introduced in the Chapters 6, 7 and 8 for linear equivalent transfer function estimation, non-linearity detection, delay detection and non-stationary data analysis respectively.

# Chapter Three

# LEAST SQUARES TRANSFER FUNCTION ESTIMATORS

## 3.1 Introduction

This chapter presents the analysis of the existing transfer function estimators based on the least squares error minimisation techniques for Single-Input Single-Output (SISO) systems in the contexts of gain estimation and frequency response function estimation respectively. The primary reason to include this review is that, in Chapters 4 and 5 the problem of transfer function estimation will be presented through an approach using Principal Component Analysis (PCA) forming a part of this thesis in terms of original contributions. The background information from this chapter will be used in order to give a direct comparison between the existing and the proposed techniques.

In the first part (Section 3.2) a simple gain system is considered and the derivations of various least squares estimators are given with corresponding cost functions describing the optimisation landscape for each procedure. Noisy conditions under which these estimators exhibit biasing effects are also shown.

In the second part (Section 3.3) the generalisation of the Total Least Squares (TLS) gain estimation is introduced from a geometric point of view. A single error distance between the measured data and the true input-output transfer relationship is defined which is dependant on an angle that allows one to interpret the relationships between the standard least squares based estimators by selecting its value appropriately.

Section 3.4 covers the least squares transfer function estimation scheme in the frequency domain where the commonly used Frequency Response Function (FRF) estimators have been covered, revealing their most significant properties, advantages and disadvantages under different conditions followed by computational simulations for assessing the statistical behaviours of these estimators. A summary and outline of the concluding remarks are given in Section 3.5.

## 3.2 Least Squares Gain Estimators

It is crucial to the problem of FRF estimation that the most appropriate statistical estimation procedure is followed in order to obtain an accurate estimate for the identification of the system under investigation (see Figure 2.4). There are two classical transfer function estimators commonly in use; these estimators are based on least squares optimisation methods and are commonly referred to as $H_1(f)$ and $H_2(f)$. Both of these methods are commonly regarded within the framework of least squares estimation, which assumes that any noise is present on only one of the measured signals. An alternative technique, in which noise is assumed on both signals, is based on the concept of TLS and is commonly referred to as $H_s(f)$. All three methods have been widely applied and are integral to many analysis tasks. The above standard transfer function estimators can be derived by regression analysis based on the observation that in the absence of noise the input-output relationship of a linear time-invariant system is given by (2.4) [7]. The problem is to estimate the function $H(f)$ based on $N$ observations corresponding to the Fourier Transforms (FTs) of each segment, i.e. $X_{m_n}(f)$ and $Y_{m_n}(f)$ for $n=1,\ldots,N$. In the next three subsections, in order to visualise these estimators we shall temporarily consider that $X_{m_n}(f)$ and $Y_{m_n}(f)$ are real valued and describe the procedure in terms of the transfer function estimation of a simple gain system. Figure 2.5 shows a set of measured points and various error measures that can be adopted and the minimisation procedures could be based on. The measured system input and the measured system output are defined as

$$x_m = x + n_x \tag{3.1a}$$

and

$$y_m = y + n_y \tag{3.1b}$$

where $x$ is system input, $y$ is system output, $x_m$ is measured input, $y_m$ is measured output, $n_x$ is additive input measurement noise and $n_y$ is additive output measurement noise. If the system under investigation is considered as a pure gain of the true value $a$ then the resulting system output can be written as

$$y_m = a.x + n_y \tag{3.2}$$

From hereon in this chapter it is assumed that the signals within the system's boundary are stationary random time histories i.e. each consists of a mean value and a zero mean random variable such that

$$x = \mu_x + r_x \tag{3.3}$$

$$n_x = \mu_{nx} + r_{nx} \tag{3.4}$$

$$n_y = \mu_{ny} + r_{ny} \tag{3.5}$$

$$y = a(\mu_x + r_x) \tag{3.6}$$

where $\mu$ denotes the mean value and $r$ denotes the zero mean random variable. For each $i^{th}$ sample data of the time histories, the zero mean random variable $r_i$ is assumed to have some probability distribution from which the sample value of $r$ is drawn.

### 3.2.1 Optimal Estimator for Output Noise

With reference to Figure 2.5, if it is assumed that the errors are defined as occurring in the $y$-direction i.e. for the case of additive measurement noise on the system output, then for each data point the error distance can be given by the relationship

$$e_y^i = y_i - a_1 x_i \tag{3.7}$$

where $a_1$ is the estimator for the slope of the best-fit linear regression line in the presence of the errors defined in the output data and $i$ is the sample index. Using the least squares approach one can form a cost function for the sum of the squared errors i.e. for the deviations from the central location $y=a_1x$ such that

$$J_1 = \frac{1}{N}\sum_{i=1}^{N}(e_y^i)^2 = \frac{1}{N}\sum_{i=1}^{N}(y_i - a_1 x_i)^2 \tag{3.8}$$

where $N$ is the number of the data points observed. The above expression is a quadratic function of $a_1$, with respect to which minimising the cost function $J_1$ can be obtained from the solution of

$$\frac{dJ_1}{da_1} = \frac{2}{N}\sum_{i=1}^{N}(y_i - a_1 x_i)(-x_i) = 0 \tag{3.9}$$

from which $a_1$ is given by

$$a_1 = \frac{\sum_i x_i y_i}{\sum_i x_i^2} \tag{3.10}$$

where the numerator represents the cross-correlation between the two variables and the denominator represents the variance of the variable $x$ i.e. this estimator uses the ratio of the cross-correlation between input $x$ and output $y$ and the power of input $x$. (N.B. the division $N$ may be used in numerator and denominator as appropriate).

Considering the system given by Figure 2.4 as a pure gain with the input-output relationship $y=ax$, if it is assumed that $n_x=0$ and $n_y\neq 0$, one can rewrite the cost function given by (3.8) using the expectation operator in order to minimise the sum of the squared errors over the samples such that

$$J_1 = E\left[(e_y^i)^2\right] = E\left[\left(y_m^i - a_1 x^i\right)^2\right] \tag{3.11}$$

where $i$ denotes the sample index.

Using the relationships given from (3.1) to (3.6) and substituting the symbol $\sigma^2$ as appropriate to denote the signal variance, (3.11) is rearranged to give

$$J_1 = (a-a_1)^2 \cdot (\mu_x^2 + \sigma_x^2) + \mu_{ny}^2 + \sigma_{ny}^2 \tag{3.12}$$

which can be plotted as a function of the estimator $a_1$ at the fixed value of the true gain $a=3$ such as that shown in the Figure 3.1 showing that the true value of the gain factor at the local minimum of the error surface is at $a_1=3$ when only the output data is noise contaminated.

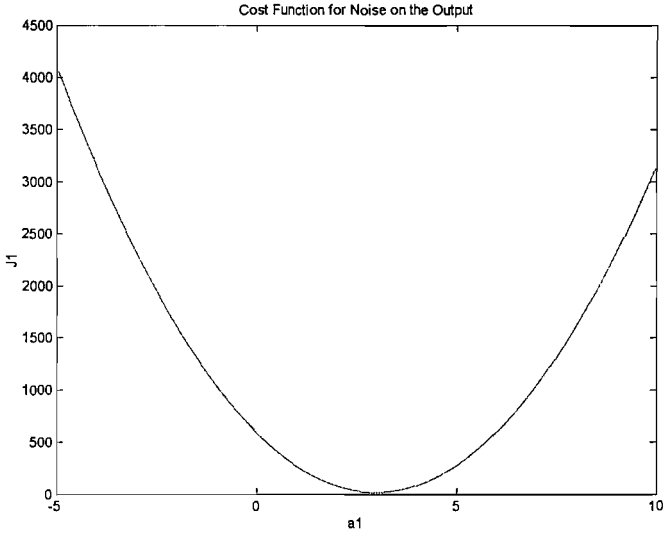


**Figure 3.1** Theoretical Cost Function for the Noise on the Measured Output for zero mean signals with input variance 64 and noise variance 16 (Output SNR: 15dB).

In the presence of additive measurement noise on the system input the computational expression (3.10) defining estimator $a_1$ (assuming a theoretical average) takes the form

$$a_1 = \frac{a^2\mu_{nx}\mu_y + a\mu_y^2 + a\sigma_y^2}{a^2\mu_{nx}^2 + a^2\sigma_{nx}^2 + \mu_y^2 + \sigma_y^2 + 2a\mu_{nx}\mu_y} \tag{3.13}$$

which can be simplified for zero-mean signals and written as

$$a_1 = \frac{a\sigma_y^2}{a^2\sigma_{nx}^2 + \sigma_y^2} \tag{3.14}$$

This means that estimator $a_1$ is always biased when used for the cases where the measured system input is noise contaminated regardless of the mean value of the signals. Figure 3.2 shows the results from computational simulations which illustrates this biasing effect for zero-mean signals by giving a comparison with the true gain of value $a$=3.

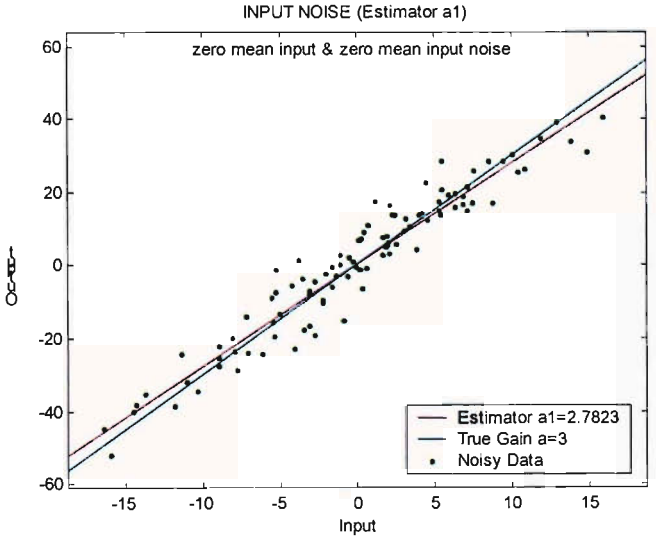


**Figure 3.2** Comparison between the true gain $a$=3 and its estimate $a_1$ for zero mean signals in the presence of additional measurement noise on the system input derived from the Computational Cost Function of a single set of 100 normally distributed random data for the Noise on the Measured Input with input variance 64 and noise variance 4 (Input SNR: 12dB).

### 3.2.2 Optimal Estimator for Input Noise

In the case of additive measurement noise on the input (Figure 2.5, Case II), errors are defined in the measured data in the $x$-direction and the error distance for each data point is given by the relationship

$$e_x^i = x_i - \frac{y_i}{a_2} \tag{3.15}$$

where $a_2$ is the estimator for the slope of the best-fit linear regression line in the presence of the errors defined in the input data and $i$ is the sample index. One can form the quadratic cost function for the sum of the squared errors i.e. for the deviations from the central location $y=ax$ such that

$$J_2 = \frac{1}{N}\sum_{i=1}^{N}(e_x^i)^2 = \frac{1}{N}\sum_{i=1}^{N}\left(x_i - \frac{y_i}{a_2}\right)^2 \tag{3.16}$$

The value of $a_2$ minimising the cost function $J_2$ can be obtained from the solution of

$$\frac{dJ_2}{da_2} = \frac{2}{N}\sum_{i=1}^{N}\left(x_i - \frac{y_i}{a_2}\right)\left(\frac{y_i}{a_2^2}\right) = 0 \tag{3.17}$$

from which $a_2$ is given by

$$a_2 = \frac{\sum_i y_i^2}{\sum_i x_i y_i} \tag{3.18}$$

where the numerator represents the variance of the variable $y$ and the denominator represents the cross-correlation between the two variables. In contrast to Estimator $a_1$ this uses the ratio of the power of the output and the cross-correlation between the input and output.

For the gain system given in the previous section if it is assumed that $n_x \neq 0$ and $n_y=0$, one can rewrite the theoretical cost function given by (3.16) in a similar way for the case of additive measurement noise on the system input as

$$J_2 = E\left[(e_x^i)^2\right] = E\left[\left(x_m^i - \frac{y_m^i}{a_2}\right)^2\right] \tag{3.19}$$

which can be rearranged using the relationships (3.6) to (3.11) to give

$$J_2 = \left[ \mu_x^2 + \mu_{nx}^2 + \sigma_x^2 + \sigma_{nx}^2 + 2\mu_x\mu_{nx} + \frac{a^2}{a_2^2} \cdot \left(\mu_x^2 + \sigma_x^2\right) - \frac{2a}{a_2}\left(\mu_x^2 + \sigma_x^2 + \mu_x\mu_{nx}\right) \right] \tag{3.20}$$

As in the previous example the above expression can be plotted as a function of the estimator $a_2$ at the fixed value of the true gain $a$=3 such as that shown in Figure 3.3. Also for this case it can be seen from the curve whose shape differs from the parabola shown in the previous case that minimizing the cost function will lead to the true gain factor i.e. the local minimum occurs at $a_2$=3.

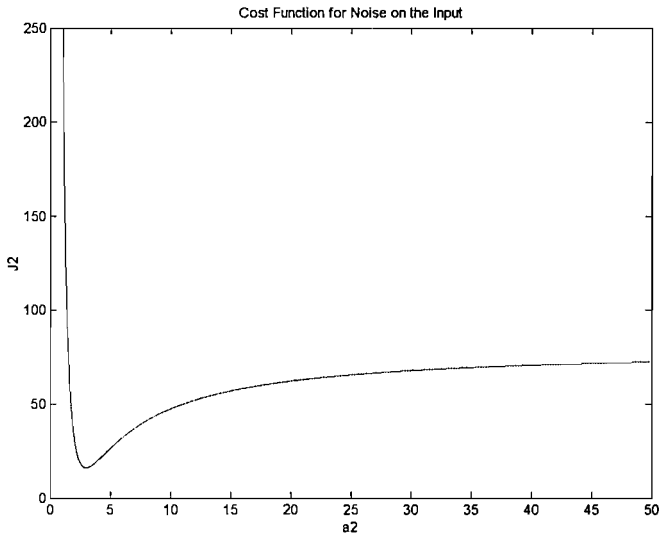


**Figure 3.3** Theoretical Cost Function for the Noise on the Measured Input for zero mean signals with input variance 64 and noise variance 16 (Input SNR: 6dB).

In the case of output noise the computational expression (3.18) defining Estimator $a_2$ can be expanded as

$$a_2 = \frac{(a\mu_x + \mu_{ny})^2 + a^2\sigma_x^2 + \sigma_{ny}^2}{a\mu_x^2 + a\sigma_x^2 + \mu_x\mu_{ny}} \tag{3.21}$$

which for zero-mean signals take the form

$$a_2 = a + \frac{\sigma_{ny}^2}{a\sigma_x^2} \tag{3.22}$$

The above expressions show that this estimator always gives biased results for output noise. Results from the computational simulations are illustrated in Figure 3.4 for the case of zero-mean signals verifying the biasing effect on this estimator when output data is noise contaminated.

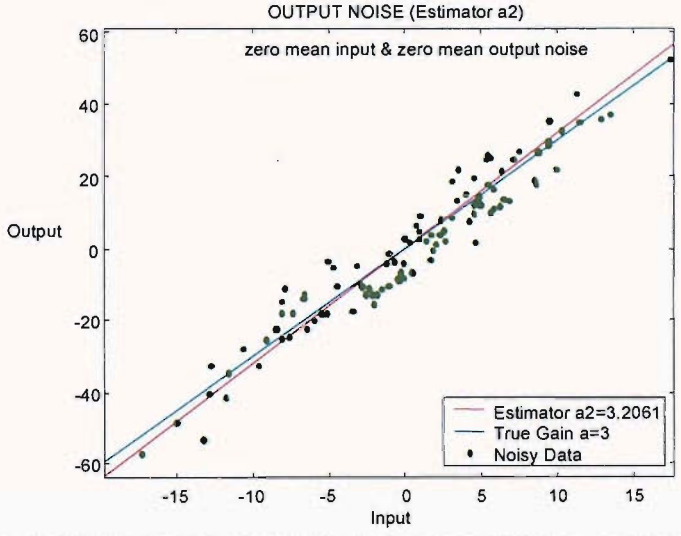


**Figure 3.4** Comparison between the true gain $a=3$ and its estimate $a_2$ for zero mean signals in the presence of additional measurement noise on the system output derived from the Computational Cost Function of a single set of 100 normally distributed random data for the Noise on the Measured Input with input variance 64 and noise variance 4 (Output SNR: 21dB).

### 3.2.3 Optimal Estimator for Input & Output Noise

In the case of the additive measurement noise on both the input and output, the error is defined as normal to the best-fit line assuming errors to be present in both input and output data such as that shown in Figure 2.5. For each data point, the error distance normal to the regression line can be given by

$$e_T^i = \frac{y_i - a_{\mathrm{TLS}} x_i}{\sqrt{1 + a_{\mathrm{TLS}}{}^2}} \tag{3.23}$$

where $a_{\mathrm{TLS}}$ is the estimator for the slope of the best-fit linear regression line in the presence of the errors defined in both input and output data. Similarly, using the least squares approach one can form a cost function for the sum of the squared errors i.e. for the deviations from the central location $y=a_{\mathrm{TLS}}x$ such that

$$J_T = \frac{1}{N}\sum_{i=1}^{N}(e_T^i)^2 = \frac{1}{N}\sum_{i=1}^{N}\frac{(y_i - a_{TLS}x_i)^2}{\left(1 + a_{TLS}{}^2\right)} \tag{3.24}$$

The expression (3.24) is a non-quadratic function of $a_{\mathrm{TLS}}$ and therefore one can expect to obtain more than one extreme value by differentiating the cost function $J_T$ with respect to $a_{\mathrm{TLS}}$ and equating to zero from the solution of

$$\frac{dJ_T}{da_{TLS}} = \frac{1}{N}\sum_{i=1}^{N}\frac{2(y_i - a_{TLS}x_i)(-x_i)}{\left(1 + a_{TLS}{}^2\right)} - \frac{1}{N}\sum_{i=1}^{N}\frac{(y_i - a_{TLS}x_i)^2 2a_{TLS}}{\left(1 + a_{TLS}{}^2\right)^2} = 0 \tag{3.25}$$

It can be shown that the Estimator $a_{\mathrm{TLS}}$ is given by the positive signed root of (3.25) and thus

$$a_{TLS} = \frac{\sum_i (y_i^2 - x_i^2) + \sqrt{\left[\sum_i (y_i^2 - x_i^2)^2 + 4\sum_i (x_i y_i)^2\right]}}{2\sum_i x_i y_i} \tag{3.26}$$

For the gain system such as that given in Sections 3.2.1 and 3.2.2 if it is assumed that $n_x \neq 0$ and $n_y \neq 0$, one can rewrite the theoretical cost function given by (3.24) for the case of additive measurement noise on both the system input and the system output as

$$J_T = E\left[(e_T^i)^2\right] = E\left[\frac{\left(y_m^i - a_{TLS}\, x_m^i\right)^2}{1 + a^2{}_{TLS}}\right] \tag{3.27}$$

Using the same relationships given from (3.6) to (3.11) and after some algebra the above expression can be rearranged to give

$$J_T = \left(\frac{1}{1+a^2{}_{TLS}}\right)\cdot\left(a^2\mu_x^2 + a^2\sigma_x^2 + \mu_{ny}^2 + \sigma_{ny}^2 + a_{TLS}^2\mu_x^2 + a_{TLS}^2\sigma_x^2 + a_{TLS}^2\mu_{nx}^2 + a_{TLS}^2\sigma_{nx}^2 - 2a_{TLS}a\mu_x^2 - 2a_{TLS}a\sigma_x^2\right) \tag{3.28}$$

and plotted as a function of the estimator $a_{\mathrm{TLS}}$ at the fixed value of the true gain $a$=3 such as that shown in Figure 3.5. This cost function has two extreme values and the optimisation is based on the minimum value at $a_{\mathrm{TLS}}$=3 that is equal to the true gain factor only for the case where the variances of input and output noise are equal although at reasonable Signal-to-Noise Ratios (SNRs) the difference between noise variances cause slight biasing effects tending towards overestimation of the true value for higher output noise and towards underestimation for higher input noise.

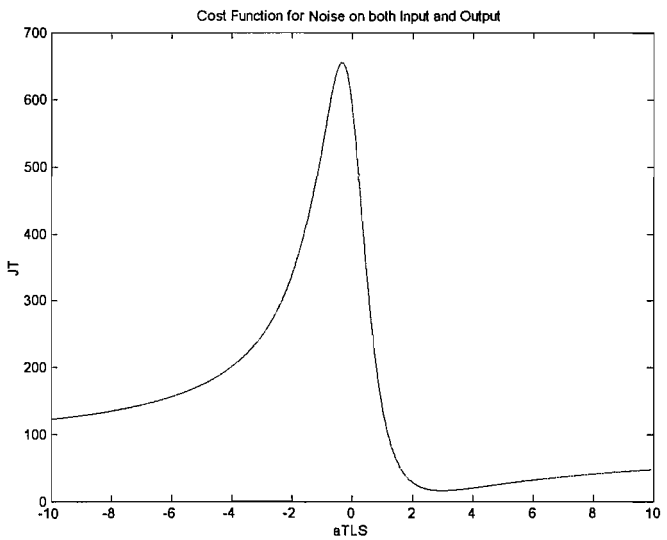


**Figure 3.5** Theoretical Cost Function for the Noise on both the Measured Input and the Measured Output for zero mean signals with input variance 64 and noise variances 16 (Input SNR: 6dB ; Output SNR: 15dB).

### 3.2.4 Comparison of Least Squares Gain Estimators

In an attempt to compare the biasing effects of the least squares gain estimators, computational procedures have been carried out and the *estimator means* and *variances* have been calculated. The method used is based on ensemble averaging over 1000 sample populations (ensembles) each consisting of also 100000 randomly generated set of data points representing the stationary random processes within the boundary of the model system under investigation. The true gain factor has been set to 3 in order to give a direct comparison between various estimator performances. All the signals used for computations have Gaussian probability distributions. Eight different cases for various additive measurement noise and signal mean conditions have been covered and these are

Case 1 – Output Noise / Zero Mean Signals

Case 2 – Input Noise / Zero Mean Signals

Case 3 – Equal Input & Output Noise / Zero Mean Signals

Case 4 – Input Noise > Output Noise / Zero Mean Signals

Case 5 – Input Noise < Output Noise / Zero Mean Signals

Case 6 – Output Noise / Non-Zero Mean Signals

Case 7 – Input Noise / Non-Zero Mean Signals

Case 8 – Input & Output Noise / Non-Zero Mean Signals

Input variance and the noise variance for the corresponding cases are set to 64, 16 and 9 respectively whereas for the cases of equal input-output noise both noise variance have been set to 16. The results are presented in Tables 3.1 and 3.2. It can be clearly seen that the mean of the estimator $a_{TLS}$ takes values in the range [ $a_1$ , $a_2$ ] and is optimal when both input and output noise are present in the measured signals whereas for output noise the estimator $a_1$ and for input noise the estimator $a_2$ gives the best results for the true gain factor respectively. It should be noted that the most accurate estimates obtained using the TLS estimator is for Case 3 where the input-output measurement noises have equal variance.

In the next section, the derivation of the above estimators is given through a different approach that allows one to be able to generalise the least squares based estimation procedure and validates the computational results of this subsection analytically.

| | | | |
|---|---|---|---|
| **Case 1** – Output Noise / Zero Mean Signals | | | |
| $\sigma_x^2 = 64$ / $\sigma_{nx}^2 = 0$ / $\sigma_{ny}^2 = 16$ / $\mu_x = 0$ / $\mu_{noise} = 0$ | | | |
| $a_{TRUE} = 3$ | $a_1 = 3.00$ | $a_2 = 3.07$ | $a_{TLS} = 3.06$ |
| **Case 2** – Input Noise / Zero Mean Signals | | | |
| $\sigma_x^2 = 64$ / $\sigma_{nx}^2 = 16$ / $\sigma_{ny}^2 = 0$ / $\mu_x = 0$ / $\mu_{noise} = 0$ | | | |
| $a_{TRUE} = 3$ | $a_1 = 2.39$ | $a_2 = 3.00$ | $a_{TLS} = 2.93$ |
| **Case 3** – Equal Input & Output Noise / Zero Mean Signals | | | |
| $\sigma_x^2 = 64$ / $\sigma_{nx}^2 = 16$ / $\sigma_{ny}^2 = 16$ / $\mu_x = 0$ / $\mu_{noise} = 0$ | | | |
| $a_{TRUE} = 3$ | $a_1 = 2.41$ | $a_2 = 3.10$ | $a_{TLS} = 3.00$ |
| **Case 4** – Input Noise > Output Noise / Zero Mean Signals | | | |
| $\sigma_x^2 = 64$ / $\sigma_{nx}^2 = 16$ / $\sigma_{ny}^2 = 9$ / $\mu_x = 0$ / $\mu_{noise} = 0$ | | | |
| $a_{TRUE} = 3$ | $a_1 = 2.40$ | $a_2 = 3.04$ | $a_{TLS} = 2.96$ |
| **Case 5** – Input Noise < Output Noise / Zero Mean Signals | | | |
| $\sigma_x^2 = 64$ / $\sigma_{nx}^2 = 9$ / $\sigma_{ny}^2 = 16$ / $\mu_x = 0$ / $\mu_{noise} = 0$ | | | |
| $a_{TRUE} = 3$ | $a_1 = 2.62$ | $a_2 = 3.08$ | $a_{TLS} = 3.03$ |
| **Case 6** – Output Noise / Non-Zero Mean Signals | | | |
| $\sigma_x^2 = 64$ / $\sigma_{nx}^2 = 0$ / $\sigma_{ny}^2 = 16$ / $\mu_x = 8$ / $\mu_{noise} = 4$ | | | |
| $a_{TRUE} = 3$ | $a_1 = 2.53$ | $a_2 = 2.60$ | $a_{TLS} = 2.60$ |
| **Case 7** – Input Noise / Non-Zero Mean Signals | | | |
| $\sigma_x^2 = 64$ / $\sigma_{nx}^2 = 16$ / $\sigma_{ny}^2 = 0$ / $\mu_x = 8$ / $\mu_{noise} = 4$ | | | |
| $a_{TRUE} = 3$ | $a_1 = 2.35$ | $a_2 = 2.57$ | $a_{TLS} = 2.54$ |
| **Case 8** – Input & Output Noise / Non-Zero Mean Signals | | | |
| $\sigma_x^2 = 64$ / $\sigma_{nx}^2 = 16$ / $\sigma_{ny}^2 = 16$ / $\mu_x = 8$ / $\mu_{noise} = 4$ | | | |
| $a_{TRUE} = 3$ | $a_1 = 2.35$ | $a_2 = 2.60$ | $a_{TLS} = 2.57$ |

**Table 3.1** Estimator means for various cases.

| | | |
|---|---|---|
| **Case 1** – Output Noise / Zero Mean Signals | | |
| $\sigma_x^2 = 64$ / $\sigma_{nx}^2 = 0$ / $\sigma_{ny}^2 = 16$ / $\mu_x = 0$ / $\mu_{noise} = 0$ | | |
| $Var(a_1) = 2.49e\text{-}6$ | $Var(a_2) = 2.56e\text{-}6$ | $Var(a_{TLS}) = 2.62e\text{-}6$ |
| **Case 2** – Input Noise / Zero Mean Signals | | |
| $\sigma_x^2 = 64$ / $\sigma_{nx}^2 = 16$ / $\sigma_{ny}^2 = 0$ / $\mu_x = 0$ / $\mu_{noise} = 0$ | | |
| $Var(a_1) = 1.48e\text{-}5$ | $Var(a_2) = 2.22e\text{-}5$ | $Var(a_{TLS}) = 2.32e\text{-}5$ |
| **Case 3** – Equal Input & Output Noise / Zero Mean Signals | | |
| $\sigma_x^2 = 64$ / $\sigma_{nx}^2 = 16$ / $\sigma_{ny}^2 = 16$ / $\mu_x = 0$ / $\mu_{noise} = 0$ | | |
| $Var(a_1) = 1.56e\text{-}5$ | $Var(a_2) = 2.72e\text{-}5$ | $Var(a_{TLS}) = 2.43e\text{-}5$ |
| **Case 4** – Input Noise > Output Noise / Zero Mean Signals | | |
| $\sigma_x^2 = 64$ / $\sigma_{nx}^2 = 16$ / $\sigma_{ny}^2 = 9$ / $\mu_x = 0$ / $\mu_{noise} = 0$ | | |
| $Var(a_1) = 1.64e\text{-}5$ | $Var(a_2) = 2.53e\text{-}5$ | $Var(a_{TLS}) = 2.56e\text{-}5$ |
| **Case 5** – Input Noise < Output Noise / Zero Mean Signals | | |
| $\sigma_x^2 = 64$ / $\sigma_{nx}^2 = 9$ / $\sigma_{ny}^2 = 16$ / $\mu_x = 0$ / $\mu_{noise} = 0$ | | |
| $Var(a_1) = 1.13e\text{-}5$ | $Var(a_2) = 1.60e\text{-}5$ | $Var(a_{TLS}) = 1.48e\text{-}5$ |
| **Case 6** – Output Noise / Non-Zero Mean Signals | | |
| $\sigma_x^2 = 64$ / $\sigma_{nx}^2 = 0$ / $\sigma_{ny}^2 = 16$ / $\mu_x = 8$ / $\mu_{noise} = 4$ | | |
| $Var(a_1) = 1.34e\text{-}6$ | $Var(a_2) = 1.19e\text{-}6$ | $Var(a_{TLS}) = 1.20e\text{-}6$ |
| **Case 7** – Input Noise / Non-Zero Mean Signals | | |
| $\sigma_x^2 = 64$ / $\sigma_{nx}^2 = 16$ / $\sigma_{ny}^2 = 0$ / $\mu_x = 8$ / $\mu_{noise} = 4$ | | |
| $Var(a_1) = 5.16e\text{-}6$ | $Var(a_2) = 5.51e\text{-}6$ | $Var(a_{TLS}) = 5.86e\text{-}6$ |
| **Case 8** – Input & Output Noise / Non-Zero Mean Signals | | |
| $\sigma_x^2 = 64$ / $\sigma_{nx}^2 = 16$ / $\sigma_{ny}^2 = 16$ / $\mu_x = 8$ / $\mu_{noise} = 4$ | | |
| $Var(a_1) = 6.05e\text{-}6$ | $Var(a_2) = 6.82e\text{-}6$ | $Var(a_{TLS}) = 6.73e\text{-}6$ |

**Table 3.2** Estimator variances for various cases.

## 3.3 Generalisation of TLS Gain Estimation

In view of the theoretical and computational review of the gain estimators presented in the previous section, here we seek to develop a generalised approach for the least squares estimation scheme from a geometric viewpoint. As has already been explained in detail, for the basic memoryless input-output linear relationship $y=ax$, the least squares optimisation is obtained by the minimisation of a *cost function,* that is the sum of the squared measurement errors, with respect to the unknown gain $a$. To summarise, with reference to Figure 2.5, if one minimises the sum of the squared vertical errors between the fitted line and the data points then the estimator $a_1$ is obtained, whereas if the sum of the squared horizontal errors is the quantity to be minimised then the estimator $a_2$ results. When the sum of the perpendicular errors is minimised then the TLS estimator $a_{TLS}$ is realised. From the statistical performance assessment of these estimators we have also seen that the TLS gain estimator always gives results between the 1st and the 2nd least squares estimators.

Our motivation here is that by using geometric relationships we can obtain a *general term* for the least squares error distance to be minimised from which it would be possible to derive each of the individual estimators presented above by appropriate manipulation. For our analysis, let us first define a new measurement error distance between the true input-output line and the data points such that its position vector with respect to the corresponding data point is at an angle $\theta$ to the vertical distance $(e_y)$ that is associated with the estimator $a_1$. This is illustrated in Figure 3.6 where $(x_i,y_i)$ gives the co-ordinates of the data point, $e_\theta$ is the new error distance and $e_t$ is the perpendicular TLS distance. Using trigonometric relationships (angles in radians for convenience) we get

$$\frac{e_t}{y_i - ax_i} = \sin\left(\frac{\pi}{2} - \psi\right) = \cos\psi \tag{3.29}$$

Since $\tan\psi = a$, then

$$\frac{e_t}{y_i - ax_i} = \frac{1}{\sqrt{1+a^2}} \tag{3.30}$$

and hence the TLS error distance is

$$e_t = \frac{y_i - ax_i}{\sqrt{1+a^2}} \tag{3.31}$$

The relationship between the perpendicular (standard TLS) error distance and the new (generalised TLS) error distance is given by

$$e_\theta = \frac{e_t}{\sin\phi} \tag{3.32}$$

From Figure 3.6 it can be clearly seen that

$$\phi = \pi/2 + (\theta - \psi) \tag{3.33}$$

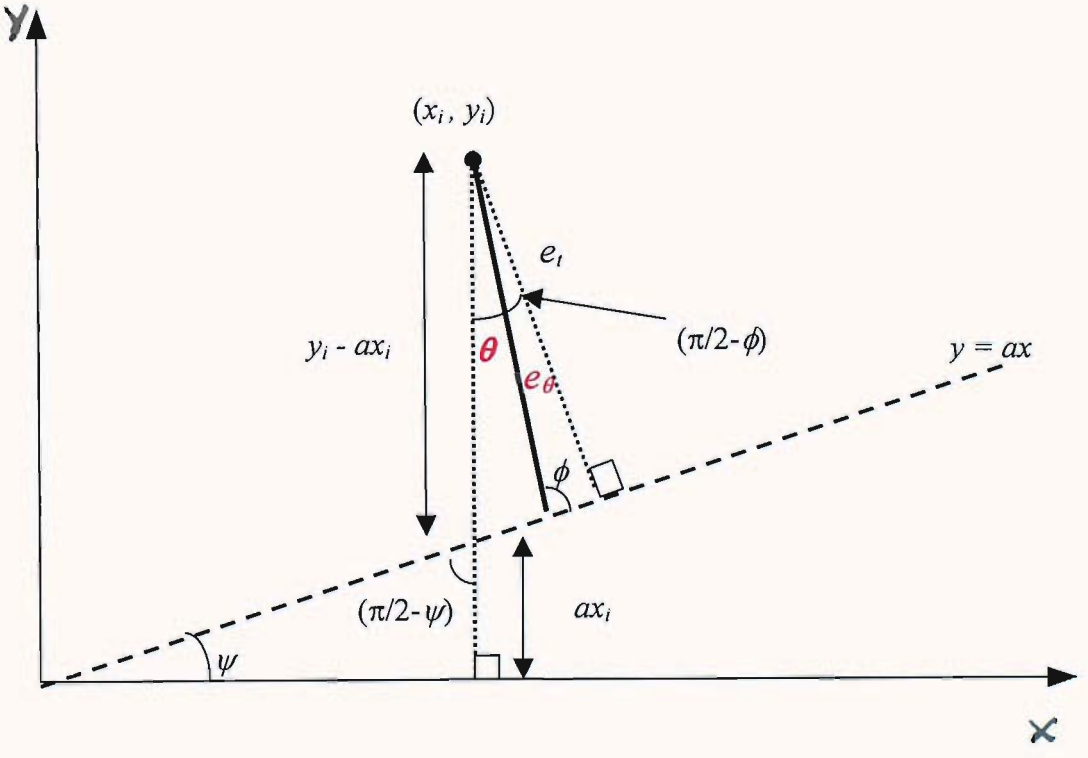


**Figure 3.6** Generalisation of TLS.

Therefore,

$$\sin\phi = \sin[\pi/2 + (\theta - \psi)] = \cos(\theta - \psi) = \cos\theta\cos\psi + \sin\theta\sin\psi \tag{3.34}$$

and since

$$\sin\psi = \frac{a}{\sqrt{1+a^2}} \quad \& \quad \cos\psi = \frac{1}{\sqrt{1+a^2}} \tag{3.35a,b}$$

(3.34) can be rewritten as

$$\sin\phi = \frac{\cos\theta + a\sin\theta}{\sqrt{1+a^2}} \tag{3.36}$$

and the new error distance is given by

$$e_\theta = \frac{y_i - ax_i}{\cos\theta + a\sin\theta} \tag{3.37}$$

Using the expression (3.37), we can obtain the standard error distances $e_y$, $e_x$ and $e_t$ corresponding to the three basic least squares estimators $a_1$, $a_2$ and $a_{TLS}$ respectively, as follows:

i. If $\theta = 0$ then $e_\theta = y_i - ax_i \Rightarrow e_y$ hence $a \to a_1$ (3.37a)

ii. If $\theta = \pi/2$ then $e_\theta = \frac{y_i}{a} - x_i \Rightarrow e_x$ hence $a \to a_2$ (3.37b)

iii. If $\theta = \psi$ then $e_\theta = \frac{y_i - ax_i}{\sqrt{1+a^2}} \Rightarrow e_t$ hence $a \to a_{TLS}$ (3.37c)

As can be seen from the three cases above, by spanning the angle $\theta$ between 0 and $\pi/2$ we get the error criteria for the standard least squares estimators.

### 3.3.1 Computational Expression

Now, let $\theta$ be some other angle that is fixed and independent of $a$ (note that in the third case given above where the error criterion leads to the TLS solution, $\theta$ is not independent of $a$ since the error minimisation criterion is based on $\theta = \psi$). Then from (3.37) we get

$$e_\theta = \frac{y_i - ax_i}{\cos\theta(1 + a\tan\theta)} \tag{3.38}$$

and forming the corresponding cost function as

$$J_\theta = \frac{1}{N}\sum_{i=1}^{N}(e_\theta^{\,i})^2 = \frac{1}{N}\sum_{i=1}^{N}\frac{(y_i - ax_i)^2}{\cos^2\theta(1 + a\tan\theta)^2} \tag{3.39}$$

the value of $a$ can be obtained from the solution of

$$\frac{dJ_\theta}{da} = \frac{2}{N}\sum_{i=1}^{N}\frac{(y_i - ax_i)(-x_i)}{\cos^2\theta(1 + a\tan\theta)^2} - \frac{2}{N}\sum_{i=1}^{N}\frac{(y_i - ax_i)^2\tan\theta}{\cos^2\theta(1 + a\tan\theta)^3} = 0 \tag{3.40}$$

from which using $\sigma$ as appropriate and after some algebra $a_\theta$ is given by

$$a_\theta = \frac{\sigma_{xy} + \sigma_y^2\tan\theta}{\sigma_x^2 + \sigma_{xy}\tan\theta} \tag{3.41}$$

In accordance with (3.37a,b,c), when we consider some specific values for the angle $\theta$, the gain estimator given by (3.41) leads us to the following cases

i. If $\theta = 0$ then $a_\theta = \dfrac{\sigma_{xy}}{\sigma_x^2} \Rightarrow a_1$ (3.41a)

ii. If $\theta = \pi/2$ then $a_\theta = \dfrac{\sigma_y^2}{\sigma_{xy}} \Rightarrow a_2$ (3.41b)

iii. If $\theta = \pi/4$ then $a_\theta = \dfrac{\sigma_{xy} + \sigma_y^2}{\sigma_x^2 + \sigma_{xy}}$ (3.41c)

Therefore, we can see that the third case corresponding to the angle $\theta = \pi/4$ leads to an estimator between the least squares estimators, $a_1$ and $a_2$, that is algebraically much simpler than the standard TLS gain estimator given by (3.26). We would expect this estimator to be equally optimal with the TLS estimator in the special case of equal input-output measurement errors with the true gain factor being unity for which the distance $e_\theta$ would be geometrically dividing two equal right-angle triangle. However when either of these errors were dominant than the result obtained using the above expression would be biased whose degree would depend on the ratio of the input-output noise powers.

Figure 3.7 gives a direct numerical comparison between $a_{TLS}$ and $a_\theta$ over 1 million-sample noisy zero-mean stationary random input-output data for a true gain factor of 3 and $\theta = \pi/4$. (3.37c) describes the TLS optimisation landscape as based on $\theta = \psi$ and hence in this case the tangent of both will be equal to 3 whereas for $a_\theta$ the angle $\theta$ is effectively considered $\pi/4$. Input variance is 64 and both noise variances are 16 corresponding to Case 3 of Section 3.2.4. As can be clearly seen from the direction of the corresponding arrows indicating the slope of each estimator, there is a difference between the two results by a factor of $10^{-1}$. $a_{TLS}$ is computed as 2.92 and $a_\theta$ is 2.82. This is due to the fact that, despite noise variances being approximately equal over the data samples, the fitted line has a larger slope than 1 and hence $\theta = \pi/4$ does not lead to the optimal error distance to be minimised for $a_\theta$.

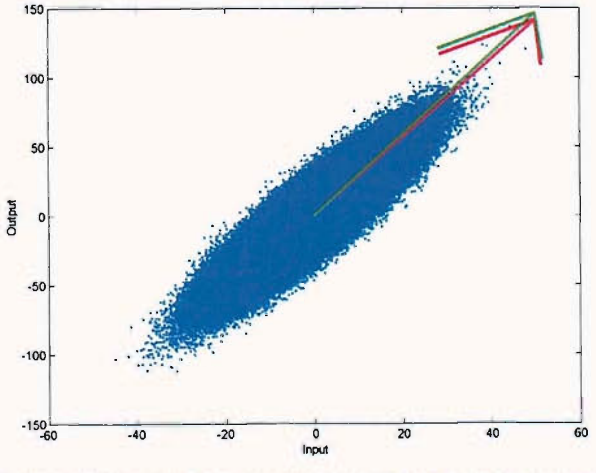


**Figure 3.7** Comparison of standard and the generalised (3.41c) TLS gain estimators for equal input-output noise. Dots: Noisy input-output scatter points; Red Arrow: $a_\theta$; Green Arrow: $a_{TLS}$.

### 3.3.2 Theoretical Analysis

In order to further investigate the significance of our approach to the TLS input-output problem described above, consider the cost function given by (3.39), this time analytically, by including noise terms on both the measured input and the output as

$$J_\theta = \frac{\left(\sigma_y^2 + \sigma_{n_y}^2\right) + a_\theta^2\left(\sigma_x^2 + \sigma_{n_x}^2\right) - 2a_\theta\sigma_{xy}}{\cos^2\theta\left(1 + a_\theta \tan\theta\right)^2} \tag{3.42}$$

where

$$\sigma_y^2 = a^2\sigma_x^2 \quad \& \quad \sigma_{xy} = a\sigma_x^2$$

and therefore

$$J_\theta = \frac{\left(a^2\sigma_x^2 + \sigma_{n_y}^2\right) + a_\theta^2\left(\sigma_x^2 + \sigma_{n_x}^2\right) - 2a_\theta a\sigma_x^2}{\cos^2\theta\left(1 + a_\theta \tan\theta\right)^2} \tag{3.43}$$

which shows that $J_\theta$ is a function of $\sigma_x$ , $\sigma_{n_x}$, $\sigma_{n_y}$, $a$ and $\theta$. Furthermore, if we modify the expression for the estimator $a_\theta$ accordingly accounting for noise, we get the corresponding theoretical expression

$$a_\theta = \frac{a\sigma_x^2\left(1 + a\tan\theta\right) + \sigma_{n_y}^2 \tan\theta}{\sigma_x^2\left(1 + a\tan\theta\right) + \sigma_{n_x}^2} \tag{3.44}$$

that can be rewritten as

$$a_\theta = \frac{a\frac{\sigma_x^2}{\sigma_{n_x}^2}\left(1 + a\tan\theta\right) + \frac{\sigma_{n_y}^2}{\sigma_{n_x}^2}\tan\theta}{\frac{\sigma_x^2}{\sigma_{n_x}^2}\left(1 + a\tan\theta\right) + 1} \tag{3.45}$$

If we let

$$\text{Input SNR, } \frac{\sigma_x^2}{\sigma_{n_x}^2} = \rho \quad \& \quad \text{Noise Ratio, } \frac{\sigma_{n_y}^2}{\sigma_{n_x}^2} = r \tag{3.46a,b}$$

Substituting (3.46a,b) into (3.45) we obtain

$$a_\theta = \frac{a\rho(1+a\tan\theta)+r\tan\theta}{\rho(1+a\tan\theta)+1} \tag{3.47}$$

Furthermore, the theoretical expression given by (3.47) can be appropriately manipulated in order to verify the performances of three standard least squares estimators. With reference to Figure 3.6 and the relationship given by (3.37c) when $\theta=\psi$, $\tan\theta$ is simply equal to the true gain $a$, describing the standard TLS solution representing the case of input-output noise. Therefore if we let $r=1$, (3.47) can be rewritten as

$$a_\theta = \frac{a\rho(1+a^2)+a}{\rho(1+a^2)+1} = \frac{a\{\rho(1+a^2)+1\}}{\rho(1+a^2)+1} \to a \tag{3.48}$$

showing that the TLS estimator is equal to the true gain factor for equal input-output noise. In order to represent the case of input noise only, we let $r=0$ and $\theta=\pi/2$, leading to

$$a_\theta = \frac{a\rho(1+a\tan\theta)}{\rho(1+a\tan\theta)+1} = \frac{a^2\rho}{a\rho} \to a \tag{3.49}$$

Similarly, for the case of output noise only, we let $\rho=r=\infty$ and $\theta=0$ to give

$$a_\theta = \frac{a\rho}{\rho+1} = \frac{a}{1+\frac{1}{\rho}} \to a \tag{3.50}$$

Now, let us look at a special case in an attempt to examine the behaviour of (3.47) for varying the angle $\theta$. We consider the true gain factor and the output noise to input noise ratio are equal to unity i.e.

$$a=1 \quad \& \quad r=1$$

Substituting the above into (3.47) and after some algebra we get

$$a_\theta = \frac{\rho(1+\tan\theta)+\tan\theta}{\rho(1+\tan\theta)+1} \tag{3.51}$$

Figure 3.8 illustrates the relationship between the estimator (3.51) and the input SNR $\rho$ for $\theta$ equal to 0, $\pi/2$ and $\pi/4$ respectively. When $\theta$ is 0, (3.51) reduces to

$$a_\theta \to \frac{\rho}{1+\rho}$$

and hence as the input SNR is improved it converges towards the true gain factor 1 (see top-left plot of Figure 3.8) although it will remain biased as there is always some noise on both input and output (recall (3.37a) and (3.41a)). Note that starting from around 0.5 associated with the 0 dB input SNR, it always gives underestimated results for the true gain factor. If we select $\theta$ as $\pi/2$ then the estimator (3.51) can be rewritten as

$$a_\theta \to \frac{\rho+1}{\rho} = 1+\frac{1}{\rho}$$

corresponding to the input noise optimal case (recall (3.37b) and (3.41b)). As can be seen from the top-right plot of Figure 3.8, in this case the estimator has a similar exponential behaviour but in a decreasing fashion. Again, it converges towards the true gain factor asymptotically although the overall performance is less accurate with higher biasing effect compared to that of the previous case. Finally, when we look at the case of $\theta$ is equal to $\pi/4$ (recall (3.37c) and (3.41c)), the expression (3.51) reduces to

$$a_\theta \to \frac{2\rho+1}{2\rho+1} = 1$$

indicating that using $\theta = \pi/4$ is sensible as it will coincide with the standard TLS scheme for the case of equal input-output noise and hence is unity for all $\rho$ (Figure 3.8, bottom plot).

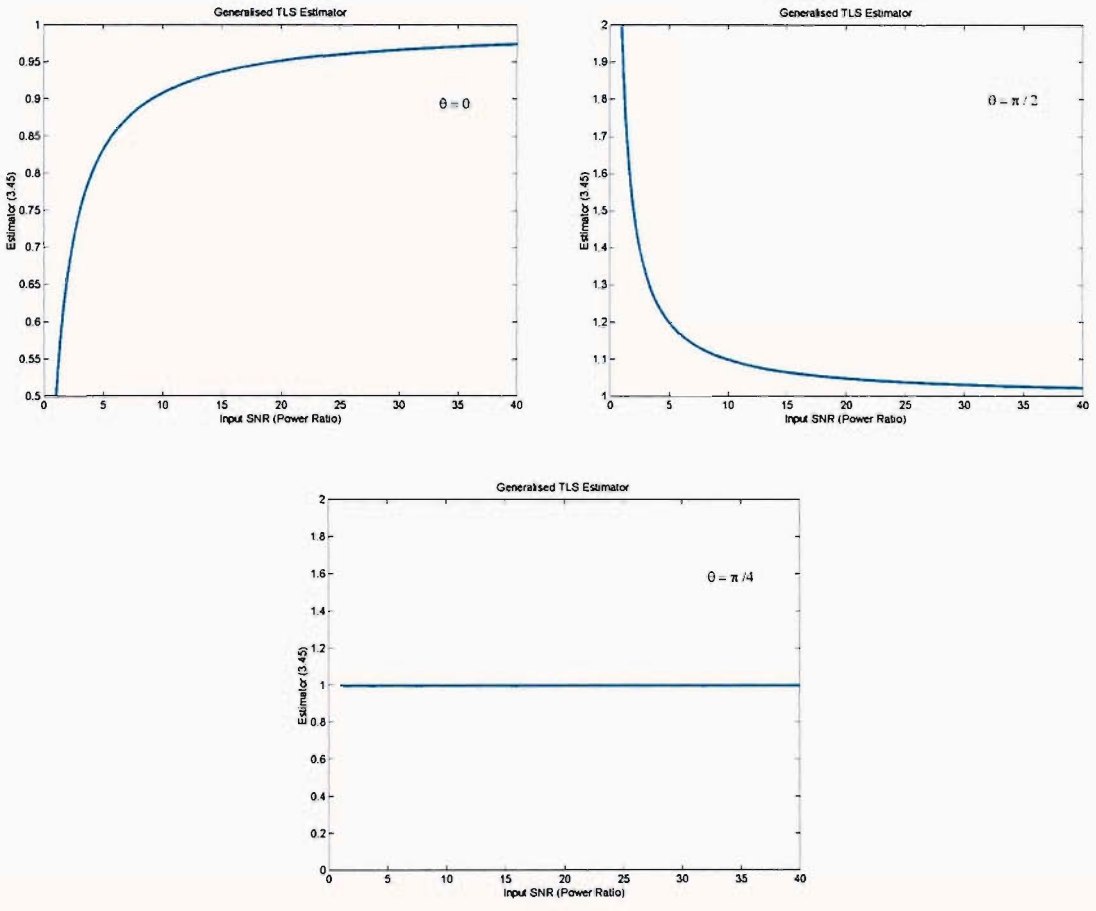


**Figure 3.8** Theoretical expression for the generalised TLS Estimator (3.45) for the special case of (3.51) plotted versus Input SNR (i.e. for $a = r = 1$). Top-Left: $\theta = 0$; Top-Right: $\theta = \pi/2$; Bottom: $\theta = \pi/4$.

It is also possible to generalise the estimator $a_\theta$ with respect to certain conditions of the parameters $r$, $\rho$ and $\theta$ under which its estimate gives the exact value of the true gain factor *a*. Simply, substituting $a$ for $a_\theta$ in (3.47) we get

$$a = r \tan\theta \tag{3.52}$$

which shows that when the product "$r\tan\theta$" equals the true gain factor, this estimator always gives the exact result. This means that for specific values of the true gain factor there is no better estimator than $a_\theta$. This can be demonstrated through a simple example as follows:

Let us assume that the true gain factor and the noise ratio are given as

$$a = 2 \quad \& \quad r = 2$$

If we consider the case corresponding to estimator $a_1$, we let $\theta = 0$ from which (3.47) takes the form

$$a_\theta = a_1 = \frac{2\rho}{\rho+1} = \frac{2(\rho+1)-2}{\rho+1} \to 2 - \frac{2}{\rho+1} \tag{3.53}$$

which shows that $a_1$ is biased for low input SNR although it converges towards the true gain factor as $\rho$ is increased. Secondly, let us consider the case corresponding to estimator $a_2$ in which we let $\theta = \pi/2$ and subsequently (3.47) becomes

$$a_\theta = a_2 = \frac{4\rho+2}{2\rho} \to 2 + \frac{1}{\rho} \tag{3.54}$$

Also in this case the estimate is biased for low input SNR and approaches the true value as $\rho$ tends to infinity. The corresponding standard TLS estimator is based on the criterion $\tan\theta = 2$ using which the expression (3.47) is rewritten as

$$a_\theta = a_{TLS} = \frac{2\rho(1+4)+4}{\rho(1+4)+1} \to 2 + \frac{4}{5\rho+1} \tag{3.55}$$

verifying the biasing effect. Finally, if we look at the case of $\theta = \pi/4$, (3.47) takes the form

$$a_\theta = \frac{2\rho(1+2)+2}{\rho(1+2)+1} = \frac{2\{\rho(1+2)+1\}}{\rho(1+2)+1} \to 2 \tag{3.56}$$

from which it can be seen that the estimator $a_\theta$ is unbiased for all $\rho$ and therefore is the best estimator for this specific case.

### 3.3.3 Summary

Above analysis is based on the geometrical interpretation of the newly defined error distance (3.37) in terms of the measured input-output data position vector and a fixed angle $\theta$ that is also a function of the transfer characteristics of the data point. It has been shown that by choosing the angle $\theta$ according to the signal and noise characteristics, the generalised TLS estimator (3.41) can be appropriately manipulated in order to obtain an accurate estimate of the true gain factor. For the special cases of the angle $\theta$ being equal to 0, $\pi/2$ and $\psi$ (see Figure 3.6); the equivalent least squares estimators $a_1$, $a_2$ and $a_{TLS}$ (for equal input-output noise) can be derived respectively. Under certain conditions, the generalised TLS estimation scheme gives the exact true gain factor for all input and output SNRs unlike the corresponding standard least squares forms. Although this is of no practical use as its verification relies upon a priori knowledge of the true gain factor, it is an interesting observation revealing the superior behaviour of the proposed estimation scheme.

In the next section we cover the corresponding frequency domain versions of the standard least squares estimators given above.

## 3.4 Least Squares FRF Estimators

### 3.4.1 FRF Estimators $H_1$ and $H_2$

$H_1$ and $H_2$ are the two classical transfer function estimators based on the least squares approach for additive output measurement noise and for additive input measurement noise, respectively, whose derivations in the time domain (using real valued data in order for easy visualisation) are given in Sections 3.2.1 and 3.2.2, in relation to the estimation of the transfer characteristics of a gain system. With reference to Figure 2.4 these can be defined as [2, 7]

$$H_1(f) = \frac{\hat{S}_{x_m y_m}(f)}{\hat{S}_{x_m x_m}(f)} \tag{3.57}$$

and

$$H_2(f) = \frac{\hat{S}_{y_m y_m}(f)}{\hat{S}_{y_m x_m}(f)} \tag{3.58}$$

where $\hat{S}_{ab}(f)$ is an estimator for the cross-spectral density between $a(t)$ and $b(t)$ and if $a(t)=b(t)$ then this spectrum is referred to as an auto-spectral density or a power spectrum (see Appendix A for the methodology of corresponding derivations using complex valued data in the frequency domain). Assuming the system under investigation is truly linear and the two additive measurement noises $n_x(t)$ and $n_y(t)$ are mutually uncorrelated and uncorrelated with the input signal, the statistical behaviour of these two FRF estimators in the presence of additive measurement noise is well established. The important results can be summarized as for the case of measurements with only output noise, estimator $H_1(f)$ is unbiased; whereas for the case of measurements with only input noise, estimator $H_2(f)$ is unbiased; and when noise is present on both the input and output both $H_1(f)$ and $H_2(f)$ are biased (see computational results in Section 3.2.4). In the latter case one can further show that [2]

$$E[H_1(f)] \le H(f) \le E[H_2(f)] \tag{3.59}$$

where $E[\ ]$ denotes the expectation operator. This result allows one to approximately bracket the correct result by computing both transfer function estimators. It should be noted that (3.59) is developed using the theoretical values for $H_1$ and $H_2$ and there is no guarantee that for finite data lengths it will hold true. A more correct fashion by which to bound estimates of the transfer function is, to use the concept of a confidence interval. For example, it can be shown [2,7] that the confidence interval for the magnitude of a transfer function estimated via $H_1$ is given by

$$|H_1(f)|^2 \cdot \left\{1 \pm \frac{4}{N-2} \cdot \left(\frac{1}{\gamma^2_{x_m y_m}(f)} - 1\right) f_{2,N-2}(1-\beta)\right\} \tag{3.60}$$

where $f_{2,N-2}(\beta)$ is the inverse cumulative distribution of the $F$-Distribution with "2, $N$-2" degrees of freedom (for large $N$ $f_{2,N-2}(\beta) \approx -\log(1-\beta)$) and $\gamma^2_{x_m y_m}(f)$ is the ordinary coherence function between the measured variables which is given in its most general form by (2.10).

### 3.4.2 FRF Estimator $H_S$ (or $H_V$) and $H_W$

Besides the above most commonly used transfer function estimators $H_1$ and $H_2$ there exists an alternative estimator based upon the concept of Total Least Squares (TLS) whose time domain version has been given in Section 3.2.3 in the context of gain estimation with reference to $a_{TLS}$. Although it has various derivations in the literature that are slightly different from each other [8,9,10,11] in its most widely used form the TLS Estimator $H_s$ is defined as

$$H_s(f)=\frac{\hat{S}_{y_m y_m}(f)-s\hat{S}_{x_m x_m}(f)+\sqrt{\left\{s\hat{S}_{x_m x_m}(f)-\hat{S}_{y_m y_m}(f)\right\}^2+4s\left|\hat{S}_{x_m y_m}(f)\right|^2}}{2\hat{S}_{y_m x_m}(f)} \tag{3.61}$$

and $s$ is a scale factor that allows one to manipulate the FRF estimates. By letting $s=0$ one obtains $H_2(f)$ and the case where

$$s \to \infty$$

is best addressed by defining

$$\varepsilon = 1/s$$

by writing (3.61) in terms of $\varepsilon(f)$ and letting

$$\varepsilon \to 0$$

then after some algebra it can be easily shown that

$$H_s(f) \to H_1(f)$$

Hence, if one varies $s$ over the range $[0,\infty]$ the estimator $H_s(f)$ takes values in the range

$$[H_1(f), H_2(f)]$$

whereas the case of $s$=1 defines an additional FRF estimator, namely $H_v(f)$ [8,9,11,12].

An alternative approach to FRF estimation that has been considered by White, Tan and Hammond is that of statistical inference [13] where the principle of Maximum Likelihood has been applied to derive optimal estimators for the FRF (see Chapter 5 for details). The resulting algorithm corresponds to the established $H_s(f)$ FRF estimator, with the parameter $s$ equated to the ratio of the measurement noise spectra and the estimator $H_W$ is given by

$$H_W(f) = \frac{\hat{S}_{y_m y_m}(f) - \kappa(f)\hat{S}_{x_m x_m}(f) + \sqrt{\left\{\hat{S}_{x_m x_m}(f)\kappa(f) - \hat{S}_{y_m y_m}(f)\right\}^2 + 4\left|\hat{S}_{x_m y_m}(f)\right|^2 \kappa(f)}}{2\hat{S}_{y_m x_m}(f)} \quad (3.62)$$

in which $\kappa(f)$ represents the ratio $S_{n_y n_y}(f) \Big/ S_{n_x n_x}(f)$.

The primary outcome of the methodology adopted in the above paper is that ML estimators are guaranteed to be unbiased and asymptotically efficient [14,15]. Therefore, this estimator is unbiased in the presences of both input and output noise and for large data sets one can be confident that the ML estimator approximately satisfies the Cramer-Rao Lower Bound (CRLB) ensuring that, asymptotically, no unbiased estimator will achieve a better performance than an ML estimator. The analysis of the ML approach for FRF estimation will be seen in detail in Chapter 5.

### 3.4.3 Statistical Assessment of Least Squares FRF Estimators

In an attempt to investigate the performances of the FRF estimators covered in this chapter, computational statistical behaviour assessment procedures at a single frequency for a fixed gain factor have been carried out computing the *estimator means* and *estimator variances*. These quantities have been plotted at each value of the ratio of the standard deviation of the output noise to the standard deviation of the input noise from 0 to 2 using 801 sample points (0.0025 step size) whose sequence is given by

$$\frac{\sigma_{n_y}}{\sigma_{n_x}} = \left[\frac{0}{4}, \frac{0.01}{4}, \ldots, \frac{7.99}{4}, \frac{8}{4}\right] = [0, 0.0025, 0.005, \ldots, 1.9975, 2.0]$$

This means that there is always additive measurement noise on the system input with a variance of 16 which is kept constant as the standard deviation of the noise on the system output varies from 0 to 8. For each FRF estimator, 100 realisations each consisting of 100 samples have been computed and averaged for the corresponding noise ratio.

In Figure 3.9 the means of the FRF estimators $H_1(f)$, $H_2(f)$, $H_V(f)$ and $H_W(f)$ are shown. Since the input noise level is kept constant for each computation, estimator $H_1(f)$ is severely biased throughout the whole range of the noise ratio. Estimator $H_2(f)$ is equal to the true gain factor when there is only input noise and gets biased gradually as the output noise is introduced and its level is increased. $H_v(f)$ starts slightly biased when there is only input noise and it meets the estimator $H_W(f)$ where the noise ratio becomes 1 i.e. equal amount of input and output noise. The ML estimator $H_W(f)$ appears to be the most optimal and hence unbiased for any noise ratio having the closest values to the true gain factor throughout.

Figure 3.10 shows the results of the computations for the comparison between the variances of each FRF estimator. It is clear to see that $H_W(f)$ has a relatively high variance with $H_2(f)$ and $H_v(f)$ compared to $H_1(f)$. All of the four estimators tend to have increasing variances as the level of the output noise is increased. Starting from the region where there is only input noise $H_W(f)$, $II_2(f)$ and $H_v(f)$ demonstrate almost identical behaviours although $H_2(f)$ gets more erroneous than the other two with increasing variability as the effect of output noise becomes dominant. For the highest levels of output noise $H_2(f)$ has the maximum variance followed by $H_v(f)$ whose value gradually deviates from $H_W(f)$ starting from the equal input-output noise region.

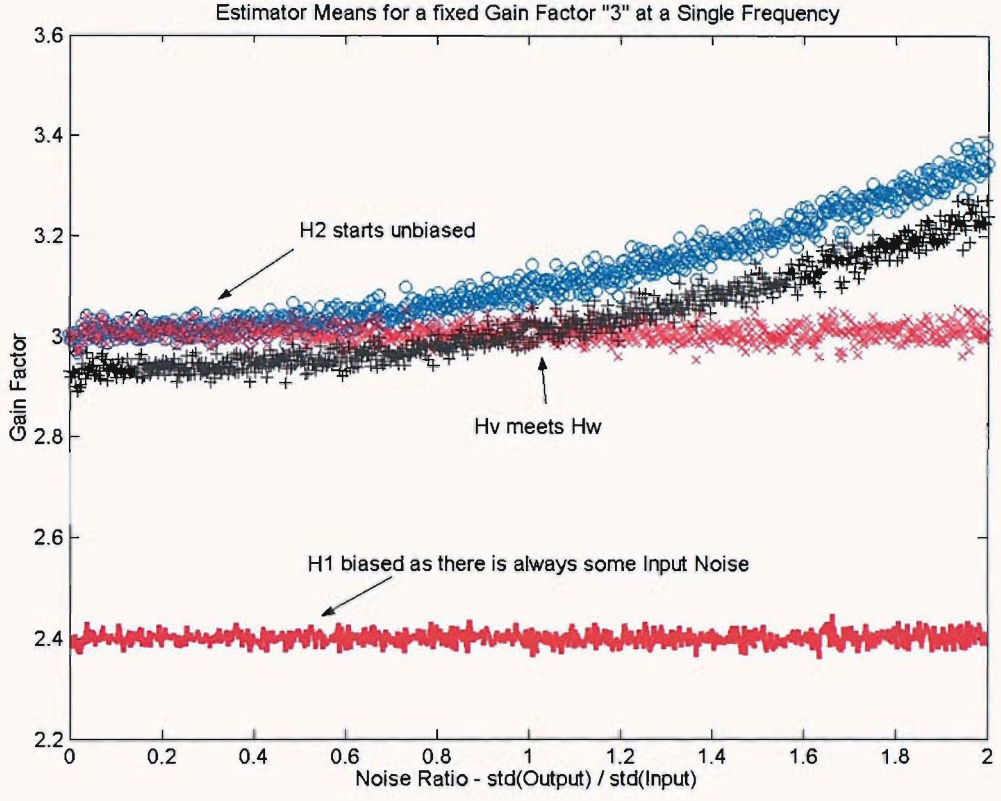


**Figure 3.9** Means of FRF estimators computed at each noise ratio for a fixed gain factor of 3 at a single frequency. Red/Solid line - $H_1(f)$, Blue/o - $H_2(f)$, Black/+ - $H_v(f)$, Red/x – $H_w(f)$.

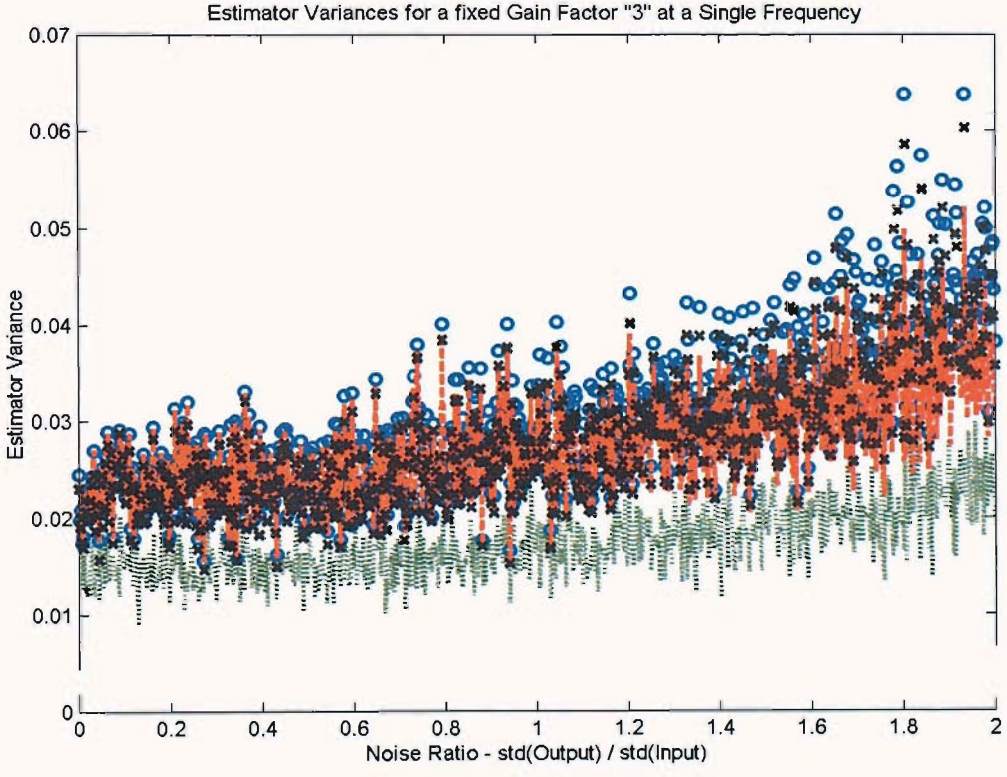


**Figure 3.10** Variances of FRF estimators computed at each noise ratio for a fixed gain factor of 3 at a single frequency. Green/Dotted line - $H_1(f)$, Blue/o - $H_2(f)$, Black/x - $H_v(f)$, Orange/Dotted line - $H_w(f)$.

## 3.5 Summary

This chapter has covered the estimators already in use for the transfer function of a system with stationary random inputs and additive measurement noise. Conventional FRF Estimators based on the least squares approach have been presented and their specific noise sensitivities have been analysed in order to form a solid background for the introduction of the new work and its comparison with the existing methods which are given in the Chapters 4 and 5 of this thesis.

With reference to Figure 2.5, which shows a set of measured data (representing the input-output scatter points) and various error measures that can be adopted, if one minimises the sum of the squared vertical errors ($e_y$) between the fitted line and the data points then the estimator $H_1(f)$ is obtained, whereas if the sum of the squared horizontal errors ($e_x$) is the quantity to be minimised then the estimator $H_2(f)$ results. In addition, if it is the sum of the perpendicular errors ($e_\perp$) that is minimised then the TLS estimator $H_v(f)$ is realised.

The important results can be summarised as: for the case of measurements with only output noise, estimator $H_1(f)$ is unbiased; whereas for the case of measurements with only input noise, estimator $H_2(f)$ is unbiased; and when an equal amount of noise is present on both the input and output both $H_1(f)$ and $H_2(f)$ are biased but $H_v(f)$ is unbiased. A generalised TLS scheme has been introduced from a geometric viewpoint allowing one to readily interpret the relationships of the existing least squares estimators in the time domain. The proposed approach utilizes the minimization of an error distance dependant on an angle that may be appropriately varied in order to suit the relevant measurement/analysis conditions on the basis of a priori knowledge of the noise/system characteristics. It has been shown that the generalised TLS estimator $a_\theta$ gives completely unbiased results for the true gain factor for all input and output SNRs under certain conditions.

Chapters 4 and 5 further discusses the transfer function estimation problem and explains how PCA can be used as a tool to solve this problem in the time and frequency domains respectively, including extensive computational simulations to provide comparisons with the existing techniques.

# Chapter Four

# GAIN ESTIMATION USING PCA

## 4.1 Introduction

It has been shown in the previous chapter that the conventional FRF estimators for SISO systems based on the least squares approach can be derived from a geometric standpoint, relying upon the fact that in the frequency domain the problem of estimating a transfer function is a linear regression problem. These interpretations are powerful intuitive tools allowing one to readily identify the merits of the corresponding algorithms. The drawback of such an interpretation is that it adds little to the mathematical underpinning.

The aim of this chapter in conjunction with Chapter 5 is to demonstrate that one of the most effective multivariate data analysis techniques, the so called Principal Component Analysis (PCA), can be employed to solve transfer function estimation problems providing a novel mathematical viewpoint and that the result from this approach can also be generalised to MIMO systems.

In essence, this chapter forms the theoretical background of our PCA FRF estimation approach introducing the fundamental mathematical procedures on the relatively simple gain estimation problem in the time domain in order to provide a comprehensive reference for the concepts covered in the next chapter where the results presented here will be extended to the frequency domain applications with slight modifications and the corresponding verifications will also be given through extensive computational simulations.

## 4.2 Gain Estimation in Memoryless SISO Systems

This section aims to discuss how PCA can be used to estimate gains of SISO measurement systems. The application of the method of principal components to the problem of gain estimation of a memoryless SISO System is based on carrying out the analysis on the covariance matrix of the measurement vector which contains information on second-order statistics of the measured input and the measured output data. By this technique, a set of correlated measured variables are linearly transformed into a new set of uncorrelated (virtual) variables, the so called principal components, which in total exhibit the same variability as the original variables (recall (2.26)). These components are ordered according to the proportion of the total variance they account for. This approach also allows one to identify components of low power that may be removed from the data set without significantly affecting the data, thus producing a dimensionally reduced form of the original data. The aim of the method is to introduce *parsimony* to the analysis. The analysis is carried out on the covariance matrix of the observed variables in the form of an Eigen-Value Decomposition (EVD) in which the direction of each eigenvector represents the direction of each component and these are weighted according to the values of the corresponding eigenvalues.

In order for the above technique to be applied to SISO system identification, the procedure is required to be carried out on the input-output covariance matrix. Physical interpretation and the details of the mathematical procedures on which our approach is based are given in the upcoming subsections

### 4.2.1 Physical Interpretation of PCA Gain Estimation

With reference to a SISO gain system we first define the vector transformation from the correlated observed variables **x** (input $x_m$ and output $y_m$) into the uncorrelated principal components **z** ($z_1$ and $z_2$) through the transformation matrix **T** as

$$\mathbf{z}=\mathbf{T}\mathbf{x} \tag{4.1}$$

which can be rewritten as (recall (2.21) )

$$\mathbf{x}=\mathbf{T}^{-1}\mathbf{z} \tag{4.2}$$

From the above relationships, one can effectively consider representing the system input-output relationship in two different ways and these can be described as the actual SISO process involving the original variables (Figure 4.1) and the virtual Two-Input-Two-Output (TITO) process involving both the original variables and the new uncorrelated variables (Figure 4.2). In this virtual system the principal components are the inputs and the original signals are the outputs. PCA solves the inverse problem by finding the transformation that maps the two correlated variables into two uncorrelated variables in the following way:

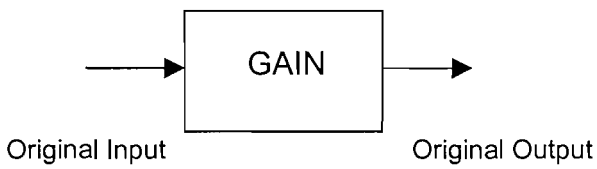


**Figure 4.1** Actual SISO Gain Process involving 2 variables.

Using the form given by (2.22) we can extend (4.2) and define the input-output covariance matrix leading to its corresponding EVD solution as

$$\mathbf{R}_{xx}=\mathbf{T}^{T}\mathbf{R}_{zz}\mathbf{T} \tag{4.3}$$

where $\mathbf{R}_{zz}$ is a diagonal matrix containing the ranked eigenvalues of $\mathbf{R}_{xx}$ and the orthonormal transformation matrix $\mathbf{T}^T$ is the matrix containing the corresponding eigenvectors as its columns i.e. $\mathbf{T}^T = \mathbf{T}^{-1} = \begin{bmatrix} t_{11} & t_{12} \\ t_{21} & t_{22} \end{bmatrix}$. Expanding (4.2) we obtain

$$\begin{bmatrix} x_m \\ y_m \end{bmatrix} = \begin{bmatrix} t_{11} & t_{12} \\ t_{21} & t_{22} \end{bmatrix} \cdot \begin{bmatrix} z_1 \\ z_2 \end{bmatrix} = \begin{bmatrix} t_{11}z_1 + t_{12}z_2 \\ t_{21}z_1 + t_{22}z_2 \end{bmatrix} \tag{4.4}$$

and it can be easily seen that both input and the output are made up of parts of the uncorrelated virtual variables. For the measured input, the part due to $z_1$ is $t_{11}z_1$ whereas for the measured output, the part due to $z_1$ is $t_{21}z_1$. Since $z_1$ is the first principal component representing the total or the majority of the total variance (depending on the degree of linear association between the original variables) it is logical to use the ratio of its corresponding eigenvector as the estimate of the transfer function linking the original (actual) variables $x$ and $y$ and hence the gain related to $z_1$ is given by the ratio $t_{21}/t_{11}$.

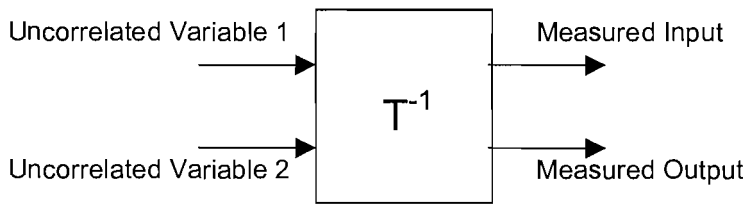


**Figure 4.2** Virtual TITO Process involving 4 variables which illustrates the inverse problem through which the principal components are transformed into the measured variables.

Therefore, it is proposed that the PCA is carried out on the input-output covariance matrix and the values of its eigenvalues are observed. If the system is purely linear and the measured variables are noise-free, one would expect only one non-zero eigenvalue whose value is equal to the sum of the powers of the measured variables. The ratio of the two values in the associated eigenvector determines the gain factor i.e. the slope of the eigenvector corresponding to this eigenvalue would give information about the system's transfer characteristics.

However it should also be noted that for the cases where the measurements are noise contaminated and/or the input-output relationship is not completely linear then both eigenvalues will be non-zero as some part of the total variance contained in the measured variables will be represented by the weighting factor of the second principal component. In this case, if the noise power and/or the effect of potential non-linearity is low compared to the variance of the original signals and the input-output linear association respectively there will be a great difference between the numerical values of the eigenvalues and we can still consider the gain factor obtained by PCA from the eigenvector corresponding to the larger eigenvalue as a realistic approximation to the transfer characteristics of the system.

In the next subsection the derivation of the generalised theoretical expression for the SISO PCA gain estimator is presented.

### 4.2.2 Derivation of SISO PCA Gain Estimator

The general theoretical expression defining the PCA gain estimator for the above SISO gain system with uncorrelated additive measurement noise on both input and output can be derived as follows:

The input-output covariance matrix between the measured input and the measured output is given using (2.20) as

$$\mathbf{R}_{xx} = E\left[\begin{bmatrix} x_{m_i} \\ y_{m_i} \end{bmatrix} \cdot \begin{bmatrix} x_{m_i} & y_{m_i} \end{bmatrix}\right] = \begin{bmatrix} E[x_m^2] & E[x_m y_m] \\ E[y_m x_m] & E[y_m^2] \end{bmatrix} \tag{4.5}$$

in which the time domain measurement vector for each sample is given by

$$\mathbf{x}_i = \begin{bmatrix} x_{m_i} \\ y_{m_i} \end{bmatrix}, \text{ for } i=1,2,\ldots,N$$

over $N$ samples and the measured system input and output are defined by (3.1a,b). Assuming that the system is a pure gain of the true value $a$, we can use the relationships (3.2) to (3.6) and substituting the symbol $\sigma^2$ as appropriate to denote the signal variance, in the case of noise on both input and the output, the matrix given by (4.5) can be rewritten as

$$\mathbf{R}_{xx} = \begin{bmatrix} \sigma_x^{\,2} + \sigma_{nx}^{\,2} & a\sigma_x^{\,2} \\ a\sigma_x^{\,2} & a^2\sigma_x^{\,2} + \sigma_{ny}^{\,2} \end{bmatrix} \tag{4.6}$$

In order to find the eigenvalues and the eigenvectors of the matrix $\mathbf{R}_{xx}$ one solves the equation

$$\mathbf{R}_{xx} \cdot \mathbf{t}_i = \lambda_i \cdot \mathbf{t}_i \tag{4.7}$$

i.e

$$\begin{bmatrix} \sigma_x^{\,2} + \sigma_{nx}^{\,2} & a\sigma_x^{\,2} \\ a\sigma_x^{\,2} & a^2\sigma_x^{\,2} + \sigma_{ny}^{\,2} \end{bmatrix} \cdot \begin{bmatrix} t_{1i} \\ t_{2i} \end{bmatrix} = \lambda_i \cdot \begin{bmatrix} t_{1i} \\ t_{2i} \end{bmatrix} \tag{4.8}$$

for $i$=1,2; where $i$ is the eigenvalue index and $\mathbf{t}_i$ is the eigenvector corresponding to the $i^{th}$ eigenvalue $\lambda_i$. The above gives the simultaneous equations

$$(\sigma_x^2 + \sigma_{n_x}^2) \cdot t_{1i} + (a\sigma_x^2) \cdot t_{2i} = \lambda_i t_{1i} \tag{4.9a}$$

$$(a\sigma_x^2) \cdot t_{1i} + (a^2\sigma_x^2 + \sigma_{n_y}^2) \cdot t_{2i} = \lambda_i t_{2i} \tag{4.9b}$$

In order to solve for the eigenvectors, we need the eigenvalues $\lambda_i$. These follow from 4.7 and written as

$$(\mathbf{R}_{xx} - \lambda\mathbf{I}).\mathbf{T}=0 \tag{4.10}$$

By Cramer's Theorem this has a non-trivial solution if and only if its coefficient determinant is zero i.e. the characteristic equation of the system is

$$\det(\mathbf{R}_{xx} - \lambda\mathbf{I}) = 0 \tag{4.11}$$

This can be written as

$$\det\begin{bmatrix} \sigma_x^2 + \sigma_{n_x}^2 - \lambda & a\sigma_x^2 \\ a\sigma_x^2 & a^2\sigma_x^2 + \sigma_{n_y}^2 - \lambda \end{bmatrix} = 0 \tag{4.12}$$

which can be expanded

$$\lambda^2 + \left(-\sigma_x^2 - \sigma_{n_x}^2 - a^2\sigma_x^2 - \sigma_{n_y}^2\right)\lambda + \sigma_x^2\sigma_{n_y}^2 + a^2\sigma_x^2\sigma_{n_x}^2 + \sigma_{n_x}^2\sigma_{n_y}^2 = 0 \tag{4.13}$$

The roots of this quadratic equation are

$$\lambda_{1,2} = \frac{1}{2}\cdot\left\{\left(\sigma_x^2 + \sigma_{n_x}^2 + a^2\sigma_x^2 + \sigma_{n_y}^2\right) \pm \sqrt{\left[\left(-\sigma_x^2 - a^2\sigma_x^2\right) + \left(-\sigma_{n_x}^2 - \sigma_{n_y}^2\right)\right]^2 - 4\sigma_x^2\sigma_{n_y}^2 - 4a^2\sigma_x^2\sigma_{n_x}^2 - 4\sigma_{n_x}^2\sigma_{n_y}^2}\right\} \tag{4.14}$$

and after some algebra the ratio of the components of the theoretical expression for the eigenvector corresponding to the largest eigenvalue, say $\lambda_1$ which corresponds to the addition case in (4.15) describes the estimate for the system gain obtained by using the method of Principal Components i.e

$$a_{PCA} = {}^{t_{21}}\!/_{t_{11}} = \frac{-\left(\sigma_x^2 - a^2\sigma_x^2 + \sigma_{n_x}^2 - \sigma_{n_y}^2 - \sqrt{\sigma_x^4(1+a^4) + 2a^2\sigma_x^2 + \sigma_{n_x}^4 + \sigma_{n_y}^4 - 2\sigma_{n_x}^2\sigma_{n_y}^2 + 2\left(\sigma_x^2\sigma_{n_x}^2\right)\left(1-a^2\right) + 2\left(\sigma_x^2\sigma_{n_y}^2\right)\left(a^2-1\right)}\right)}{2a\sigma_x^2} \tag{4.15}$$

which in practice can be simply computed from the EVD of the correlation matrix between the measured variables given by 4.5.

In an attempt to give a clearer mathematical insight to the above described gain factor estimation procedure and in order to form a solid foundation for the extension of the method to MIMO cases, in the next section, we will consider a particular case for the analysis of the system under investigation.

### 4.2.3 Zero Eigenvalue and PCA

With reference to the SISO gain system given in the previous section, let us assume that the measurements are noise-free. Then the input-output covariance matrix between the correlated variables given by (4.6) takes the form

$$\mathbf{R}_{xx} = \begin{bmatrix} \sigma_x^{\,2} & a\sigma_x^{\,2} \\ a\sigma_x^{\,2} & a^2\sigma_x^{\,2} \end{bmatrix} \tag{4.16}$$

and the simultaneous equations given by (4.9) are replaced by

$$(\sigma_x^2)\cdot t_{1i} + (a\sigma_x^2)\cdot t_{2i} = \lambda_i t_{i1} \tag{4.17a}$$

and

$$(a\sigma_x^2)\cdot t_{1i} + (a^2\sigma_x^2)\cdot t_{2i} = \lambda_i t_{2i} \tag{4.17b}$$

In accordance with the procedure described from (4.10) to (4.12) and after some algebra we get the eigenvalues

$$\lambda_1 = \left(a^2+1\right)\cdot\sigma_x^2 \quad \text{and} \quad \lambda_2 = 0 \tag{4.18}$$

from which the corresponding eigenvectors can be simply derived as

$$\mathbf{t}_1 = \begin{bmatrix} 1 \\ a \end{bmatrix} \quad \text{and} \quad \mathbf{t}_2 = \begin{bmatrix} -a \\ 1 \end{bmatrix} \tag{4.19}$$

(Note that the above forms of the eigenvectors emphasize the ratio of their components symbolically and hence in practice they would be normalized)

As it has already been explained in Section 4.2.1, the results (4.18) and (4.19) clearly indicate that if the correlated signals contained in the input-output covariance matrix are related through a purely linear process and are completely noise-free, it is possible to obtain the exact value of the system's gain factor from the ratio

$$t_{2i}/t_{1i}$$

of the components of its eigenvector corresponding to the non-zero eigenvalue whereas the remaining eigenvalue must be zero.

The zero eigenvalue has an important interpretation in terms of PCA. It can be easily seen that the components of the eigenvector corresponding to the zero eigenvalue may also be used in order to derive the exact value of the gain factor using the ratio

$$-t_{1i}/t_{2i}$$

If there is an eigenvalue equal to zero then this means that the variance of the projections on the corresponding eigenvector is zero and the corresponding principal component is reduced to zero. In the case of the analysis having carried out on the covariance matrix then the data to be analysed have been centred and the zero eigenvalue creates an opportunity in order to form linear combinations of the original variables with the components of the corresponding eigenvector as its coefficients. This indicates that the input is a perfect linear function of the output and hence they are perfectly correlated.

This implication can be simply illustrated for the above bivariate case as follows: Equation (4.7) can be expanded (assuming sample by sample eigen-decomposition of the covariance between the variables) using the notation for the measured input and the output as

$$\begin{bmatrix} x_m \\ y_m \end{bmatrix} \cdot [x_m \quad y_m] \cdot \begin{bmatrix} t_{1i} \\ t_{2i} \end{bmatrix} = \lambda_i \cdot \begin{bmatrix} t_{1i} \\ t_{2i} \end{bmatrix} \tag{4.20}$$

where $\lambda_i$ is the $i^{th}$ eigenvalue and

$$\mathbf{t}_i = \begin{bmatrix} t_{1i} \\ t_{2i} \end{bmatrix}$$

is its corresponding eigenvector. If $\lambda_i$=0 then (4.20) becomes

$$\begin{bmatrix} x_m \\ y_m \end{bmatrix} \cdot [x_m \quad y_m] \cdot \begin{bmatrix} t_{1i} \\ t_{2i} \end{bmatrix} = \mathbf{0} \tag{4.21}$$

and since it is assumed that

$$\begin{bmatrix} x_m \\ y_m \end{bmatrix} \neq \mathbf{0}$$

then this has a non-trivial solution

$$[x_m \quad y_m] \cdot \begin{bmatrix} t_{1i} \\ t_{2i} \end{bmatrix} = 0 \tag{4.22}$$

which can be expanded as

$$x_m t_{1i} + y_m t_{2i} = 0 \tag{4.23}$$

forming a homogeneous linear system with the coefficients $t_{1i}$ and $t_{2i}$. Therefore we can conclude that if the values of these coefficients can be determined from the EVD of the SISO input-output covariance matrix then one can also simply derive each potential gain factor relating *pairs* of *correlated* input-output variables from the ratio of the components of the eigenvector corresponding to the zero eigenvalue using (4.23) such as

$$\frac{y_m}{x_m} = -\frac{t_{1i}}{t_{2i}} \tag{4.24}$$

The analysis given from (4.16) to (4.24) shows that if one of the eigenvalues of the covariance matrix is equal to zero then this is an indication of the existence of a collinearity condition between the original variables and the corresponding eigenvector can also be used in order to obtain the associated relationship in accordance with the procedure given above. We will use this result for the application to the time domain multi-variate cases in Section 4.3 and to the frequency domain multi-variate cases in Chapter 5. It is noted that the above conclusion can also be justified starting from the equation (4.1) and assuming $z_2$ to be zero corresponding to the zero eigenvalue.

### 4.2.4 PCA and the TLS Solution

In the previous subsections we have shown that PCA can be employed to solve problems involving gain estimation of SISO systems through an approach providing a more solid mathematical foundation compared to that of the standard methods based on linear regression. As a matter of fact the application of PCA leading to the solution for the above problem given by the theoretical expression (4.15) is equivalent to the methods based on the concept of Total Least Squares (TLS). This is not a surprising result since the TLS solution can be obtained from an eigenvalue decomposition of the spectral correlation matrix [16], which is exactly the same mechanism used to compute the PCA estimate i.e. evidently this estimator is exactly that associated with the TLS solution, namely $a_{TLS}$ (see equation (3.26) ). The interesting observation is the novel viewpoint that this result provides, the advantage being that it allows one to simply obtain the same result from the EVD of the input-output covariance matrix rather than using the TLS algebra. The mathematical verification of the above result can be easily obtained as follows:

The estimate of the input-output covariance matrix defined by (4.5) can be given without expanding the measured variables and using summation operator over $N$ samples ($i$=1,...,$N$) as

$$\hat{\mathbf{R}}_{xx} = \frac{1}{N}\begin{bmatrix} \sum_{i=1}^{N} x_{m_i}^2 & \sum_{i=1}^{N} x_{m_i} y_{m_i} \\ \sum_{i=1}^{N} y_{m_i} x_{m_i} & \sum_{i=1}^{N} y_{m_i}^2 \end{bmatrix} \tag{4.25}$$

Now, let us rewrite (4.25) in terms of $b$, $c$ and $d$ representing the corresponding averaged coefficients for simplicity

$$\hat{\mathbf{R}}_{xx} = \begin{bmatrix} b & c \\ c & d \end{bmatrix} \tag{4.26}$$

where

$$b = \frac{1}{N}\sum_{i=1}^{N} x_{m_i}^2 \tag{4.26a}$$

$$d = \frac{1}{N}\sum_{i=1}^{N} y_{m_i}^2 \tag{4.26b}$$

$$c = \frac{1}{N}\sum_{i=1}^{N} x_{m_i} y_{m_i} = \frac{1}{N}\sum_{i=1}^{N} y_{m_i} x_{m_i} \tag{4.26c}$$

This time from (4.7) we get the simultaneous equations in the form

$$bt_{1k} + ct_{2k} = \lambda_k t_{1k} \tag{4.27a}$$

and

$$ct_{1k} + dt_{2k} = \lambda_k t_{2k} \tag{4.27b}$$

for $k$=1,2 ; where $k$ is the eigenvalue index and $\mathbf{t}_k$ is the eigenvector corresponding to the $k^{\text{th}}$ eigenvalue $\lambda_k$. In accordance with the procedure given by (4.10) and (4.11) the characteristic equation associated with (4.26) can be written as

$$\det\begin{bmatrix} b-\lambda & c \\ c & d-\lambda \end{bmatrix} = 0 \tag{4.28}$$

from which the eigenvalues are obtained

$$\lambda_{1,2} = \frac{1}{2}\left[(b+d) \pm \sqrt{(b+d)^2 - 4(bd-c^2)}\right] \tag{4.29}$$

and the eigenvector corresponding to the largest eigenvalue, say $\lambda_1$ which corresponds to the addition case in (4.29) gives the estimate for the system gain

$$a_{PCA} = {}^{t_{21}}\!/_{t_{11}} = \frac{(d-b)+\sqrt{(d-b)^2+4c^2}}{2c} \tag{4.30}$$

Substituting (4.26a,b,c) into (4.30) we get

$$a_{PCA} = \frac{\sum_i (y_{m_i}^2 - x_{m_i}^2) + \sqrt{\left[\sum_i \left(y_{m_i}^2 - x_{m_i}^2\right)^2 + 4\sum_i \left(x_{m_i} y_{m_i}\right)^2\right]}}{2\sum_i x_{m_i} y_{m_i}} \tag{4.31}$$

and hence comparing (4.31) with (3.26) it can be concluded that

$$a_{TLS} = a_{PCA} \tag{4.32}$$

## 4.3 Gain Estimation in Memoryless MIMO Systems

In this section we extend the above described application of PCA for the SISO system gain estimation to the linear time-invariant memoryless MIMO systems whose general schematic diagram is shown in Figure 4.3. Our theoretical analyses here are based on the noise-free cases in order to emphasize the significance of the zero-eigenvalue although as will be seen in the upcoming subsections as long as the system under investigation is assumed to be linear and time-invariant the estimation procedures for the MIMO systems can also be simply carried out in the same way for the relatively low power input and/or output noise cases relying upon the selection of the most appropriate eigenvector.

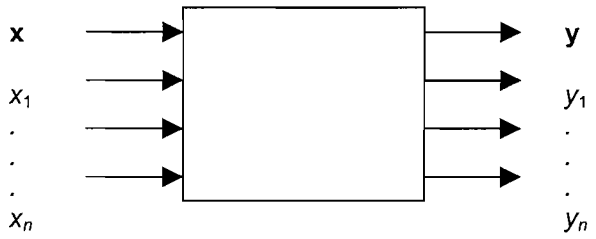


**Figure 4.3** Multi-Input-Multi-Output System with input vector **x** and output vector **y**.

In order to illustrate the presentation and for easy visualisation we shall consider a Two-Input-Single-Output (TISO) system although the corresponding mathematical procedures followed can be readily extended to multi-channel systems with more complex structures in the similar form by considering each of the outputs in turn within the associated analysis.

### 4.3.1 Multi-Input-Single-Output Systems

Figure 4.4 shows the noise-free TISO measurement system on which our investigations are based. This is a memoryless system relating the input $x_1$ to output $y$ through the gain $a$ and relating the input $x_2$ to output $y$ through the gain $b$ in the form

$$y = ax_1 + bx_2 \tag{4.33}$$

Assuming the system inputs to be stationary random signals, the analysis proceeds in the same way as in the SISO system covered in the previous section based on the EVD of the measurement covariance matrix which in this case will be of the size 3x3.

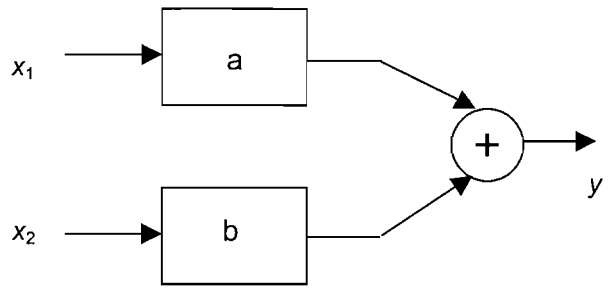


**Figure 4.4** Memoryless TISO system with the gain 'a' between $x_1$ & $y$ and the gain 'b' between $x_2$ & $y$.

This time the measurement vector contains three components and given by

$$\mathbf{m} = \begin{bmatrix} x_1 \\ x_2 \\ y \end{bmatrix} \tag{4.34}$$

and using the form (4.5) the corresponding covariance matrix is derived as

$$\mathbf{R}_{mm} = \begin{bmatrix} \overline{x_1^2} & \overline{x_2 x_1} & \overline{y x_1} \\ \overline{x_1 x_2} & \overline{x_2^2} & \overline{y x_2} \\ \overline{x_1 y} & \overline{x_2 y} & \overline{y^2} \end{bmatrix} \tag{4.35}$$

Expanding (4.2), defining the transformation of principal components to the measured variables, for the above TISO system we get

$$\begin{bmatrix} x_1 \\ x_2 \\ y \end{bmatrix} = \begin{bmatrix} t_{11} & t_{12} & t_{13} \\ t_{21} & t_{22} & t_{23} \\ t_{31} & t_{32} & t_{33} \end{bmatrix} \cdot \begin{bmatrix} z_1 \\ z_2 \\ z_3 \end{bmatrix} = \begin{bmatrix} t_{11}z_1 + t_{12}z_2 + t_{13}z_3 \\ t_{21}z_1 + t_{22}z_2 + t_{23}z_3 \\ t_{31}z_1 + t_{32}z_2 + t_{33}z_3 \end{bmatrix} \tag{4.36}$$

If we now associate the relationships between the measured signals and the virtual signals in accordance with our interpretation for the SISO PCA gain estimation presented in Section 4.2.1, we can easily see that the corresponding gain factors relating the output $y$ to the input $x_1$ and to the input $x_2$ would be defined as

$$t_{31}/t_{11} \quad \& \quad t_{31}/t_{21}$$

respectively (using the components of the eigenvector corresponding to the non-zero eigenvalue for the purely linear system with noise-free signals or corresponding to the largest eigenvalue for the linear system with some parasitic effects on the measured signals). However from the relationship (4.33) we know that the output $y$ is made of weighted sums of the inputs $x_1$ and $x_2$ and if we express $y$ in terms of the proportions of the original signals represented by the principal virtual signal we obtain

$$t_{31}z_1 = at_{11}z_1 + bt_{21}z_1 \tag{4.37}$$

Hence the above ratios are equal to

$$\frac{t_{31}}{t_{11}} = a + b\frac{t_{21}}{t_{11}} \qquad \& \qquad \frac{t_{31}}{t_{21}} = a\frac{t_{21}}{t_{11}} + b \tag{4.38a,b}$$

showing that for such a system, the separate gain factors cannot be derived without biasing effects from the relationships between the components of the eigenvector corresponding to the largest eigenvalue.

Also it is important to note that as the number of original variables increase, the total variance are distributed over the principal virtual signals with different weights according to the degree of correlation between the original variables and thus one principal component may not always be enough to describe the actual process. For the bivariate case, however, there is only one main component representing the total power shared by the input and the output which is effectively originating from the original process associated with the first principal component i.e. the input signal and thus the above approach is appropriate.

The EVD of the multivariate case given above can be carried out using the matrix (4.35) which substituting the symbol $\sigma$ as appropriate to denote the signal auto- and cross-correlation estimates and after some algebra takes the form

$$\mathbf{R}_{mm} = \begin{bmatrix} \sigma_{x_1}^2 & \sigma_{x_1x_2} & a\sigma_{x_1}^2 + b\sigma_{x_1x_2} \\ \sigma_{x_1x_2} & \sigma_{x_2}^2 & a\sigma_{x_1x_2} + b\sigma_{x_2}^2 \\ a\sigma_{x_1}^2 + b\sigma_{x_1x_2} & a\sigma_{x_1x_2} + b\sigma_{x_2}^2 & a^2\sigma_{x_1}^2 + b^2\sigma_{x_2}^2 + 2ab\sigma_{x_1x_2} \end{bmatrix} \tag{4.39}$$

and from

$$\det\begin{bmatrix} \sigma_{x_1}^2 - \lambda & \sigma_{x_1x_2} & a\sigma_{x_1}^2 + b\sigma_{x_1x_2} \\ \sigma_{x_1x_2} & \sigma_{x_2}^2 - \lambda & a\sigma_{x_1x_2} + b\sigma_{x_2}^2 \\ a\sigma_{x_1}^2 + b\sigma_{x_1x_2} & a\sigma_{x_1x_2} + b\sigma_{x_2}^2 & a^2\sigma_{x_1}^2 + b^2\sigma_{x_2}^2 + 2ab\sigma_{x_1x_2} - \lambda \end{bmatrix} = 0 \tag{4.40}$$

the eigenvalues of (4.39) are given by the roots of the cubic equation

$$\lambda\left\{\lambda^2 - \left\{\left(a^2+1\right)\sigma_{x_1}^2 + \left(b^2+1\right)\sigma_{x_2}^2 + 2ab\sigma_{x_1x_2}\right\}\lambda + \left(a^2+b^2+1\right)\sigma_{x_1}^2\sigma_{x_2}^2 - \left(a^2+b^2+1\right)\sigma_{x_1x_2}^2\right\} = 0 \tag{4.41}$$

and the corresponding eigenvectors can be computed accordingly. Note that for the special case of uncorrelated inputs, (4.41) reduces to

$$\lambda\left\{\lambda^2 - \left\{\left(a^2+1\right)\sigma_{x_1}^2 + \left(b^2+1\right)\sigma_{x_2}^2\right\}\lambda + \left(a^2+b^2+1\right)\sigma_{x_1}^2\sigma_{x_2}^2\right\} = 0 \tag{4.42}$$

As it can be clearly seen from (4.41) and (4.42), the EVD of the multi-input covariance matrix of a general system described by the linear form (4.33), results with one of the eigenvalues equal to zero.

Therefore in view of our previous comments regarding the eigenvector corresponding to the largest eigenvalue being inappropriate for MIMO transfer characteristics estimation, we may as an alternative, consider using the components of the eigenvector corresponding to the zero eigenvalue to derive the separate gain factors in accordance with the result of the bivariate case given by (4.24). In accordance with the form given by (4.20), we can modify (4.22) for the three-variable case which seeks the linear combinations of the original variables as,

$$[x_1 \quad x_2 \quad y]\cdot\begin{bmatrix} t_{i1} \\ t_{i2} \\ t_{i3} \end{bmatrix} = 0 \tag{4.43}$$

and expanding we get

$$x_1 t_{i1} + x_2 t_{i2} + y t_{i3} = 0 \tag{4.44}$$

from which it can be easily seen that the ratio of each pair of coefficients $t_i$ will result in each scale factor and hence the input-output gain factor relating the two dimensions of the corresponding eigenvector such as

$$\frac{y}{x_1} = -\frac{t_{i1}}{t_{i3}} \rightarrow a \quad \& \quad \frac{y}{x_2} = -\frac{t_{i2}}{t_{i3}} \rightarrow b \tag{4.45}$$

From the above theoretical analysis we can see that for a memoryless noise-free TISO system the use of PCA provides accurate estimates of the gain factors relating the corresponding parts of the output to each input through the ratios of the components of the eigenvector corresponding to the zero eigenvalue. In practice, these estimators can be derived using the form (4.7) for the above system

$$\begin{bmatrix} \overline{x_1^2} & \overline{x_2 x_1} & \overline{y x_1} \\ \overline{x_1 x_2} & \overline{x_2^2} & \overline{y x_2} \\ \overline{x_1 y} & \overline{x_2 y} & \overline{y^2} \end{bmatrix}\cdot\begin{bmatrix} t_{1i} \\ t_{2i} \\ t_{3i} \end{bmatrix} = \lambda_i \cdot \begin{bmatrix} t_{1i} \\ t_{2i} \\ t_{3i} \end{bmatrix} \tag{4.46}$$

and thus for $\lambda_i = 0$, we get the computational expressions

$$-\frac{t_{i1}}{t_{i3}} = \frac{\overline{x_2 x_1}\cdot\overline{y x_2} - \overline{x_2^2}\cdot\overline{y x_1}}{\left(\overline{x_1 x_2}\right)^2 - \overline{x_1^2}\cdot\overline{x_2^2}} \quad \& \quad -\frac{t_{i2}}{t_{i3}} = \frac{\overline{x_1^2}\cdot\overline{y x_2} - \overline{x_1 x_2}\cdot\overline{y x_1}}{\overline{x_1^2}\cdot\overline{x_2^2} - \left(\overline{x_1 x_2}\right)^2} \tag{4.47a,b}$$

It is immediately obvious from (4.47a,b) that, when both inputs are *truly* uncorrelated with each other, the multi-channel PCA estimators reduce to the least squares estimator $a_1$ between each input-output pair as

$$-\frac{t_{i1}}{t_{i3}} = \frac{\overline{yx_1}}{\overline{x_1^2}} \quad \& \quad -\frac{t_{i2}}{t_{i3}} = \frac{\overline{yx_2}}{\overline{x_2^2}} \tag{4.48a,b}$$

which can also simply be derived by forming the input-output pair cross-correlation e.g.

$$\overline{x_1 y} = a\overline{x_1^2} + b\overline{x_1 x_2} \Rightarrow a = \frac{\overline{x_1 y}}{\overline{x_1^2}}$$

Therefore we conclude that, in essence, $a_1$ can also be used as the optimal estimator in order to determine the individual gain factors of the *uncorrelated-multi-input* system configuration, if applied as in the SISO-based form. However as we shall see in the next chapter in the context of the corresponding FRF estimation scheme, when finite data are involved the use of the computational PCA expression is superior to the equivalent least squares estimators. This is due to some form of scaling influence of the non-zero input-input cross-correlation terms when measured/generated data sample populations are used for their estimations.

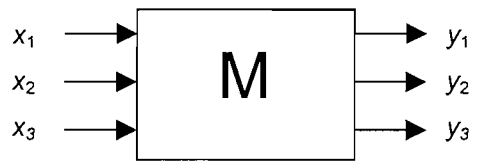


**Figure 4.5** Multi-Input-Multi-Output mixing process.

The above result can be readily extended to any memoryless linear time-invariant MIMO system e.g. for a Three-Input-Three-Output system such as that shown in Figure 4.5 where the inputs $x_1$, $x_2$ and $x_3$ and the outputs $y_1$, $y_2$ and $y_3$ are related to the inputs through a mixing matrix

$$\mathbf{M} = \begin{bmatrix} a & b & c \\ d & e & f \\ g & h & k \end{bmatrix} \tag{4.49}$$

such as

$$\mathbf{y} = \mathbf{M}\mathbf{x} \tag{4.50}$$

which can be expanded as

$$\begin{bmatrix} y_1 \\ y_2 \\ y_3 \end{bmatrix} = \begin{bmatrix} a & b & c \\ d & e & f \\ g & h & k \end{bmatrix} \cdot \begin{bmatrix} x_1 \\ x_2 \\ x_3 \end{bmatrix} \tag{4.51}$$

and

$$\begin{aligned} y_1 &= ax_1 + bx_2 + cx_3 \\ y_2 &= dx_1 + ex_2 + fx_3 \\ y_3 &= gx_1 + hx_2 + kx_3 \end{aligned} \tag{4.52}$$

i.e. each coefficient of the mixing matrix **M** being equal to the gain factor relating a proportion of each output to one of the inputs. In this case if we are to analyse the input-output relationship according to the procedure described above then we simply form the covariance matrix by using all the inputs and only one of the outputs at a time e.g.

$$\mathbf{R}_{\mathrm{mm}} = \begin{bmatrix} x_1 \\ x_2 \\ x_3 \\ y_i \end{bmatrix} \cdot \begin{bmatrix} x_1 & x_2 & x_3 & y_i \end{bmatrix} \tag{4.53}$$

By taking the outputs in turn and proceeding the analysis in the same way as before we obtain the coefficients of the mixing matrix and hence each gain factor between relevant signal pairs. In fact the estimation of the coefficients of the mixing matrix of a MIMO process such as that described above is a widely known Blind Analysis problem in Signal Processing when the only measurable signals are the outputs and under certain conditions has a solution by the well-established technique of Blind Source Separation (BSS) using Independent Component Analysis (ICA) [4]. The fundamental assumption in ICA-based source separation is that the original signals to be estimated are statistically independent. Statistical independence which requires the joint probability density function of the associated random variables to be factorizable is a much stronger condition than uncorrelatedness (recall (2.12)). An intuitive and important estimation principle of ICA is to exploit non-Gaussianity in the components to be estimated. This relies on the fact that according to Central Limit Theorem [17] the mixtures (i.e. linear combinations of the original variables) are closer to Gaussian than the original variables.

## 4.4 Concluding Remarks

The analytical results presented in this chapter form the fundamental mathematical and physical concepts of the application of PCA to the problem of estimating the transfer characteristics of SISO/MIMO systems in the frequency domain which will be covered in detail in Chapter 5.

We have shown that PCA provides a unique approach through the interpretation of the eigenvalues and the eigenvectors of the input-output covariance matrix to solve the gain estimation problem in memoryless systems and the resulting gain estimator $a_{PCA}$ defined for the basic linear time-invariant SISO system is equivalent to the Total Least Squares estimator $a_{TLS}$. It has also been demonstrated analytically that our approach originating from the basic SISO case can be appropriately extended to a specific form of MIMO systems in which the output is a linear combination of a number of independent inputs. To summarise, if the system under investigation is assumed to be linear and time-invariant:

i. for the case of noise-free measurements, the components of the eigenvectors corresponding to the distinct and/or the zero eigenvalue;
ii. for the case of noisy measurements, the components of the eigenvectors corresponding to the largest and/or the smallest eigenvalue;

can be used in order to calculate the transfer characteristics of the system between associated input-output pairs in accordance with the procedures described for the SISO and MIMO processes in the relevant sections above respectively. In the next chapter the PCA FRF estimation problem will be covered in detail using the same methodology as in this chapter with slight modifications in order to suit the mathematical procedures to complex-valued data in the frequency domain.

# Chapter Five

# FREQUENCY RESPONSE FUNCTION ESTIMATION USING PCA

## 5.1 Introduction

In this chapter we investigate the applications of Principal Component Analysis (PCA) for Frequency Response Function (FRF) estimation in Linear Time-Invariant (LTI) dynamical systems. The mathematical procedures for the transfer characteristic estimation scheme are based on the extensions of our approach introduced in the previous chapter for the gain estimation problem since the associated concepts can be readily considered appropriate for the analysis of complex-valued signals in the frequency domain obtained through Fourier transformations.

In the next section, the PCA FRF estimation approach for the basic linear time-invariant SISO measurement system in the presence of additive measurement noise on both input and output measurements is presented. It is shown that the PCA based FRF estimator $H_{\mathrm{PCA}}$ is equivalent to the TLS FRF estimator $H_{\mathrm{S}}$ (for the special case of measurement noise with equal variance on both input and output and hence $H_{\mathrm{v}}$). Following this result, FRF estimation is also cast as a problem in statistical inference and it shown that the use of the principle of Maximum Likelihood (ML) leads to a novel development of a generalised TLS scheme. Performance assessment and comparison of the proposed estimator with the existing estimators based on the least squares approach are also given through computational simulations on an artificial system.

Section 5.3 presents the generalised applications of the same technique for dynamical MIMO systems whose fundamental principles have also been covered in Chapter 4. The procedure is described for a basic form of Two-Input-Single-Output (TISO) system on which the direct comparison between the existing and the proposed methods are demonstrated. Computational simulations have also been carried out on artificial systems for both noise-free and noisy cases, the results of which verify that the use of PCA for multi-channel FRF estimation in general provides more accurate estimates of both magnitude and phase responses relative to the methods based on the least squares approach.

Section 5.4 gives a brief summary of the results presented in this chapter, pointing out the concluding remarks with relation to our work in the upcoming chapters of this thesis.

## 5.2 FRF Estimation in Dynamical SISO Systems

The problem of estimating the dynamic characteristics of a linear time-invariant SISO system (e.g. its transfer function or impulse response) from measurements of its input and output is of long standing interest in many areas of engineering. In most real-life applications the solution to this problem is realised in the frequency domain, leading to the estimation of the system's Frequency Response Function (FRF). It is crucial to the problem of FRF estimation that the most appropriate statistical estimation procedure is followed in order to obtain an accurate estimate for the transfer characteristics of the system under investigation.

In Chapter 3 the details of the most familiar FRF estimators based on the least squares method, the so called $H_1(f)$, $H_2(f)$ and $H_s(f)$ (or $H_V(f)$), have been covered. The most significant statistical behaviours of these estimators can be summarised as: for the case of measurements with only output noise, estimator $H_1(f)$ is unbiased; whereas for the case of measurements with only input noise, estimator $H_2(f)$ is unbiased; and when noise is present on both the input and output both $H_1(f)$ and $H_2(f)$ are biased but $H_V(f)$ is unbiased. It has also been shown in Chapter 3 that the above FRF estimators can be derived from a geometric standpoint, relying upon the fact that in the frequency domain the problem of estimating a transfer function is a linear regression problem.

In Chapter 4 we have described in detail how PCA can be used as a tool to solve the transfer function (gain) estimation problem in the time domain and in this section we further reconsider the problem of FRF estimation for a SISO system using PCA in accordance with the mathematical procedures described in the previous chapter. In the next subsection we seek to demonstrate how PCA can be employed to obtain a FRF estimate.

### 5.2.1 PCA and Transfer Function Estimation

As has already been explained in Chapter 2 the problem of transfer function estimation relies on the analysis of the input-output measurements of the system under investigation and the traditional experimental response testing procedures are subject to several potential confounding factors. In particular the measurements can often be undermined by various factors including non-linear system behaviour, change of system characteristics with time, instability and, most commonly, the contamination of the data by additive measurement noise. Figure 2.4 depicts the generic problem of FRF estimation in the presence of uncorrelated additive measurement noise in block diagram form which forms the focus for this section. Note that in this figure Fourier transform pairs are indicated by the symbol $\leftrightarrow$.

The application of the method of principal components to the problem of gain estimation of a memoryless SISO System whose input-output relationship is of the from $y(t) = ax(t)$ in the time domain is based on carrying out the analysis on the covariance matrix of the measurement vector (see Chapter 4 for details) which contains information on second-order statistics (time domain descriptors) of the measured input and the measured output data. When we move on to the frequency domain in order to use the same technique for the FRF estimation of a dynamical SISO measurement system, the time domain convolution of the impulse response function with the system input is mapped to multiplication by the Fourier transform leading to the input-output relationship $Y(f) = H(f)X(f)$ and hence the original variables to be analysed becomes complex and the gain $a$ is now replaced by the FRF of the system. In this case the complex-valued signals involved are required to be described by means of the relevant spectra (frequency domain descriptors) and the analysis is to be carried out on the spectral correlation matrix which again contains information on second-order statistics of the measured signals this time in the frequency domain. Therefore in order to describe the PCA estimation procedure in the frequency domain one first needs to consider the estimation of the spectra involved. One can employ a variety of spectral estimation techniques, but for the purposes of this analysis we shall assume the use of a direct (segment averaging) technique.

In direct spectral estimation algorithms the measured signals $x_m(t)$ and $y_m(t)$, such as that shown in Figure 2.4, are first partitioned into overlapping segments of equal length, a window is then applied and the estimate of, say the cross-spectrum, is defined as

$$\hat{S}_{x_m y_m}(f) = \frac{1}{N} \sum_{n=1}^{N} X^*_{m_n}(f) Y_{m_n}(f) \tag{5.1}$$

in which $X_{m_n}(f)$ and $Y_{m_n}(f)$ are the Fourier Transforms (FTs) of the $n^{th}$ (windowed) segment of $x_m(t)$ and $y_m(t)$ respectively, $N$ is the total number of segments. From hereon, it is tacitly assumed that the length of each window is sufficiently large so that the biasing effects of the window can be neglected. The next section presents the derivation of SISO PCA FRF estimator on the basis of the above principles.

### 5.2.2 Derivation of SISO PCA FRF Estimator

The derivation of principal components for such processes in the frequency domain can be given as follows: Form an array of measurement vectors $\boldsymbol{\theta}_n(f)$ containing the FTs of the input and output data

$$\boldsymbol{\theta}_n(f) = \begin{bmatrix} X_{m_n}(f) \\ Y_{m_n}(f) \end{bmatrix}_{n=1,\ldots N} \tag{5.2}$$

The spectral correlation matrix $\mathbf{R}(f)$ is defined as

$$\mathbf{R}(f) = E[\boldsymbol{\theta}_n(f)\boldsymbol{\theta}_n(f)^H] = \mathbf{Q}^H \boldsymbol{\Lambda} \mathbf{Q} \tag{5.3}$$

where $\boldsymbol{\Lambda}$ is a diagonal matrix containing the ranked eigenvalues of $\mathbf{R}(f)$ and the orthonormal transformation matrix $\mathbf{Q}$ is the matrix containing the corresponding eigenvectors as its columns and $^H$ denotes the conjugate transpose (Hermitian). The principle components $\mathbf{z}_n$ of the data $\boldsymbol{\theta}_n(f)$ are defined through a transformation matrix $\mathbf{T}$ as

$$\mathbf{z}_n(f) = \mathbf{T}\boldsymbol{\theta}_n(f) = \mathbf{Q}^H \boldsymbol{\theta}_n(f) \tag{5.4}$$

If PCA is carried out on the noise-free input-output data then in addition to the actual SISO process involving $X_{m_n}(f)$ and $Y_{m_n}(f)$ (as shown in Figure 2.4) one can also consider representing the system by a virtual Two-Input-Two-Output (TITO) process, depicted in Figure 5.1.

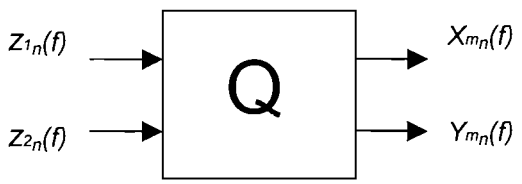


**Figure 5.1** Virtual Two-Input-Two-Output system representing the inverse transformation from principal components to the measured variables.

In this virtual system the principal components $z_1(f)$ and $z_2(f)$ are the inputs and the original signals $X_{m_n}(f)$ and $Y_{m_n}(f)$ are the outputs. PCA solves the inverse problem by finding the transformation that interprets the two correlated variables as having come from two uncorrelated variables. If the system is linear, so that

$$Y_{m_n}(f) = \beta X_{m_n}(f)$$

then only one non-zero eigenvalue exists whose value is equal to the sum of the powers of the inputs. The ratio of the two values in the associated eigenvector determines the scale factor β. To estimate a transfer function, this procedure is applied frequency bin by frequency bin. The spectral correlation matrix is estimated using

$$\hat{\mathbf{R}}(f) = \begin{bmatrix} \hat{S}_{x_m x_m}(f) & \hat{S}_{y_m x_m}(f) \\ \hat{S}_{x_m y_m}(f) & \hat{S}_{y_m y_m}(f) \end{bmatrix} \tag{5.5}$$

The eigenvalues and the eigenvectors of the above given matrix can be computed leading to

$$\lambda_{1,2} = \frac{\hat{S}_{x_m x_m}(f) + \hat{S}_{y_m y_m}(f) \pm \sqrt{\left(\hat{S}_{x_m x_m}(f) - \hat{S}_{y_m y_m}(f)\right)^2 + 4\left|\hat{S}_{x_m y_m}(f)\right|^2}}{2} \tag{5.6}$$

and

$$\left\{\frac{t_{1,k}}{t_{2,k}}\right\}_{k=1,2} = \frac{\hat{S}_{y_m y_m}(f) - \hat{S}_{x_m x_m}(f) \pm \sqrt{\left(\hat{S}_{x_m x_m}(f) - \hat{S}_{y_m y_m}(f)\right)^2 + 4\left|\hat{S}_{x_m y_m}(f)\right|^2}}{2\hat{S}_{y_m x_m}(f)} \tag{5.7}$$

where $\{t_{i,j}\}$ are the elements of the transformation matrix **T**. The eigenvector associated with the largest eigenvalues corresponds to the addition case in (5.6) and it is this ratio that represents an estimate of the transfer function, $H_{PCA}(f)$.

$$H_{PCA}(f) = \frac{\hat{S}_{y_m y_m}(f) - \hat{S}_{x_m x_m}(f) + \sqrt{\left(\hat{S}_{x_m x_m}(f) - \hat{S}_{y_m y_m}(f)\right)^2 + 4\left|\hat{S}_{x_m y_m}(f)\right|^2}}{2\hat{S}_{y_m x_m}(f)} \tag{5.8}$$

Evidently this estimator is exactly that associated with the TLS solution, namely $H_v(f)$, see equation (3.33) with $s$=1. As it has already been mentioned in Chapter 4 this is not a surprising result since the TLS solution can be obtained from an Eigen-Value-Decomposition (EVD) of the spectral correlation matrix [16], which is the same mechanism used to compute the PCA estimate.

In order to verify the physical significance of the above result mathematically one can consider the basic case of noise-free measurements which leads to the spectral correlation matrix given by (5.5) to be rewritten as

$$\hat{\mathbf{R}}(f)=\begin{bmatrix} \hat{S}_{xx}(f) & H^*(f)\hat{S}_{xx}(f) \\ H(f)\hat{S}_{xx}(f) & |H(f)|^2\hat{S}_{xx}(f) \end{bmatrix} \tag{5.9}$$

in terms of the input auto-spectral density and the FRF estimates whose eigenvalues can be easily calculated as

$$\lambda_1=\hat{S}_{xx}(f)\left\{1+|H(f)|^2\right\} \quad \text{and} \quad \lambda_2=0 \tag{5.10a,b}$$

If we now derive the corresponding eigenvectors (see Appendix B) we get the forms (which in practice would be normalised as for the case of (4.19))

$$\mathbf{t}_1=\begin{bmatrix} a \\ H(f)\cdot a \end{bmatrix} \quad \text{and} \quad \mathbf{t}_2=\begin{bmatrix} -H^*(f)\cdot b \\ b \end{bmatrix} \tag{5.11a,b}$$

respectively, from which it can be easily seen that the ratio of the components of both eigenvectors (corresponding to zero/non-zero eigenvalues) can be used in order to determine the scale factor (or FRF) relating the input-output pairs. Again it should be noted that here the important observation is the novel approach and physical interpretation leading to this result.

### 5.2.3 Statistical Interpretation of PCA Transfer Function Estimation

In this section we shall present a statistical inference based approach to FRF estimation leading to the estimator $H_w(f)$ [13] that has been considered by White, Tan and Hammond. The methodology adopted is that of an ML estimator; the primary reason for this is that ML estimators are guaranteed to be unbiased and asymptotically efficient [14,15]. Therefore, for large data sets one can be confident that the ML estimator approximately satisfies the Cramer-Rao Lower Bound (CRLB) ensuring that, asymptotically, no unbiased estimator will achieve a better performance than a ML estimator.

With reference to Figure 2.4 let us assume that the spectra of noise processes $S_{n_x n_x}(f)$ and $S_{n_y n_y}(f)$ are known for the purposes of the initial discussion. In this case the problem of estimating the transfer function from input-output data involves only two unknown variables and these are the FRF $H(f)$ and the input spectrum $S_{xx}(f)$ since the output spectrum $S_{yy}(f)$ can be inferred from the knowledge of $H(f)$ and $S_{xx}(f)$. It is assumed that all the signals are Gaussian and that $X(f)$, $N_x(f)$ and $N_y(f)$ are mutually uncorrelated. The assumption of Gaussianity is not very restrictive, since even if the time series $x(t)$ is non-Gaussian, then the act of taking a Fourier transform involves linear combinations of the data, which, by virtue of the Central Limit Theorem, tends to make the Fourier coefficients closer to Gaussian [17].

In our probabilistic framework the data vector is represented as a bivariate complex Gaussian whose Probability Density Function (PDF) is

$$\Pr\{\boldsymbol{\theta}_n(f)\} = \frac{1}{\pi|\mathbf{R}(f)|} \cdot e^{-\boldsymbol{\theta}_n(f)^H \mathbf{R}(f)^{-1} \boldsymbol{\theta}_n(f)} \tag{5.12}$$

The spectral correlation matrix can be expressed in terms of the two unknowns, the true FRF and the input spectrum, as

$$\mathbf{R}(f) = \begin{bmatrix} S_{xx}(f) + S_{n_x n_x}(f) & H(f)^* S_{xx}(f) \\ H(f) S_{xx}(f) & |H(f)|^2 S_{xx}(f) + S_{n_y n_y}(f) \end{bmatrix} \tag{5.13}$$

If one has a set of $N$ measurement vectors, denoted by $\boldsymbol{\Theta}_n(f)$, and assuming the individual measurement vectors to be uncorrelated then the PDF of $\boldsymbol{\Theta}_n(f)$ is given by

$$\Pr\{\boldsymbol{\Theta}_n(f)\} = \frac{1}{\pi^N |\mathbf{R}(f)|^N} \cdot e^{-\sum_{n=1}^{N} \boldsymbol{\theta}_n(f)^H \mathbf{R}(f)^{-1} \boldsymbol{\theta}_n(f)} \tag{5.14}$$

In the Maximum Likelihood approach probability density function $\Pr\{\boldsymbol{\Theta}_n(f)\}$ is regarded as a function of the unknown parameters and is maximised with respect to those unknowns. Since the logarithmic function is monotonic then one can equivalently maximise $L = \log\{\Pr\{\boldsymbol{\Theta}_n(f)\}\}$. Therefore the problem is to solve the following equations to obtain the two unknown parameters,

$$\frac{\partial L}{\partial H(f)} = 0 \quad \text{and} \quad \frac{\partial L}{\partial S_{xx}(f)} = 0 \tag{5.15}$$

Taking logarithms of (5.14) leads to the log likelihood function $L$ being written as

$$L = -N\log(\pi) - N\log\left(|\mathbf{R}(f)|\right) - \frac{1}{|\mathbf{R}(f)|} \cdot \sum_{n=1}^{N} \boldsymbol{\theta}_n(f)^H \tilde{\mathbf{R}} \boldsymbol{\theta}_n(f) \tag{5.16}$$

where $\tilde{\mathbf{R}}$ is the adjoint of $\mathbf{R}(f)$. The derivative of this function with respect to an arbitrary parameter, denoted here as $\alpha$, can be written as

$$\frac{\partial L}{\partial \alpha} = \frac{1}{|\mathbf{R}(f)|^2} \frac{\partial |\mathbf{R}(f)|}{\partial \alpha} \left\{ \sum_{n=1}^{N} \boldsymbol{\theta}_n(f)^H \tilde{\mathbf{R}} \boldsymbol{\theta}_n(f) - N|\mathbf{R}(f)| \right\} - \frac{1}{|\mathbf{R}(f)|} \sum_{n=1}^{N} \boldsymbol{\theta}_n(f)^H \frac{\partial \tilde{\mathbf{R}}}{\partial \alpha} \boldsymbol{\theta}_n(f) \tag{5.17}$$

The ML estimate of $\alpha$ is given by the value that renders this derivative zero, implying that

$$\left( \frac{\partial |\mathbf{R}(f)|}{\partial \alpha} \right)^{-1} \sum_{n=1}^{N} \boldsymbol{\theta}_n(f)^H \frac{\partial \tilde{\mathbf{R}}}{\partial \alpha} \boldsymbol{\theta}_n(f) = \sum_{n=1}^{N} \boldsymbol{\theta}_n(f)^H \mathbf{R}(f)^{-1} \boldsymbol{\theta}_n(f) - N \tag{5.18}$$

In this problem where there are a pair of unknown parameters one needs to solve a pair of equations of the form (5.19). These two equations have identical right hand sides so the following equation must be satisfied

$$\frac{\partial|\mathbf{R}(f)|}{\partial S_{xx}(f)}\sum_{n=1}^{N}\boldsymbol{\theta}_n(f)^H\frac{\partial\tilde{\mathbf{R}}}{\partial H(f)}\boldsymbol{\theta}_n(f)=\frac{\partial|\mathbf{R}(f)|}{\partial H(f)}\sum_{n=1}^{N}\boldsymbol{\theta}_n(f)^H\frac{\partial\tilde{\mathbf{R}}}{\partial S_{xx}(f)}\boldsymbol{\theta}_n(f) \tag{5.19}$$

After some algebra this equation reduces to

$$H(f)^2\hat{S}_{y_m x_m}(f)+H(f)\left\{\hat{S}_{x_m x_m}(f)\kappa(f)-\hat{S}_{y_m y_m}(f)\right\}-\hat{S}_{x_m y_m}(f)\kappa(f)=0 \tag{5.20}$$

in which $\kappa(f)$ represents the ratio $S_{n_y n_y}(f)\big/S_{n_x n_x}(f)$. The solutions of this quadratic equation are

$$H(f)=\frac{\hat{S}_{y_m y_m}(f)-\kappa(f)\hat{S}_{x_m x_m}(f)\pm\sqrt{\left\{\hat{S}_{x_m x_m}(f)\kappa(f)-\hat{S}_{y_m y_m}(f)\right\}^2+4\left|\hat{S}_{x_m y_m}(f)\right|^2\kappa(f)}}{2\hat{S}_{y_m x_m}(f)} \tag{5.21}$$

In order to address the question of which sign to take in (5.21) one needs only to consider the limiting cases for $\kappa(f)$. The choice of the positive sign corresponds to the TLS solution and represents the solution where $L$ is maximised whereas the negative sign indicates a worst case solution, i.e. least likelihood solution. This indicates that the ML estimator $H_w(f)$ is equivalent to the $H_s(f)$ estimator with the parameter $s$ equal to $\kappa(f)$.

Note that whilst the problem was originally defined obtaining estimates for two unknowns, $H(f)$ and $S_{xx}(f)$, in fact these two elements decouple, so that the problem of estimating the true FRF does not require one to estimate the true input spectrum. Such a decoupling is extremely useful but could not be readily justified prior to the above analysis. The noise spectra, knowledge of which has been assumed throughout this derivation, only enter the solution through the parameter $\kappa(f)$. Thus it is necessary to know the ratio of the noise spectra in order to select appropriate value of the parameter $s$, but it is not necessary to estimate the absolute levels of the noises.

The observation that the FRF estimators based on TLS and PCA are equivalent to ML solutions of appropriate problems is not only of academic interest. The wealth of available knowledge pertaining to ML estimators also applies to the TLS and PCA estimators in this case. More specifically, it is well known that ML estimators are [14]

*i.* Unbiased.

*ii.* Asymptotically efficient, that is to say that for large $N$ the ML estimators achieve the CRLB.

*iii.* Are distributed according to Gaussian statistics.

Combining these properties one can conclude that the error associated with the ML estimators are approximately distributed as $N(0,\sigma^2)$, where $\sigma^2$ is the CRLB. Therefore this analysis also provides a framework within which one can compute asymptotic expressions for the variance of such estimators i.e. in addition to the above, it can be shown that (see Appendix C) by exploiting the general properties of ML estimators an expression for the variance of the $H_s(f)$ estimator is given by

$$Var\left\{\left|H_s(f)\right|^2\right\} = \frac{4\left|H(f)\right|^4}{N}\left\{\frac{S_{n_y n_y}(f)}{S_{yy}(f)} + \frac{S_{n_x n_x}(f)}{S_{xx}(f)}\right\}^2 \tag{5.22}$$

### 5.2.4 Performance Assessment of SISO PCA FRF Estimator

A series of simulation studies have been undertaken to illustrate the results of the theoretical analyses presented. These simulations have all been based on estimating the FRF of a simple digital system containing two poles and two zeros. In particular the poles and zeros were all located at a radius of 0.95, with the poles being located at angle of $\pm\pi/4$ and zeros at $\pm 3\pi/4$. The system was excited by Gaussian white noise (with unit variance) and the simulated input and output measurements were corrupted using independent, additive Gaussian noise. In each trial 1000 realisations of the processes were constructed, with the FRF magnitudes being estimated using various methods and the means and variances being computed across these realisations. Each realisation consisted of 1 million samples and the spectra were estimated using segment averaging based on FFTs of 256 samples and employing a Hann window. This regime allowed us to compute the mean and variances of the FRF estimators with a high degree of accuracy. It should be noted that the phase information contained in the existing and the proposed estimators is identical and hence we have not included here any simulations for the phase estimates of the FRF.

Figure 5.2 illustrates the mean of the three FRF estimators: $H_1(f)$, $H_2(f)$ and $H_V(f)$. The measurement noises were unit variance, white and Gaussian. The estimator $H_1(f)$ yields a biased estimator of the true FRF. Since the input SNR is constant the bias in $H_1(f)$ is a constant multiplicative factor, which appears as a constant offset on a decibel scale. The behaviour of the $H_2(f)$ estimator is more complex because the SNR of the output measurement varies as a function of frequency, due to shaping effects of the system. Consequently when the output signal level is low, e.g. at frequencies near the zeros (like the anti-resonance in the high frequency region of our example FRF), the SNR is correspondingly low and the bias is large. Conversely where the output signal's amplitude is large, e.g. at frequencies near the poles (like the resonance in the low frequency region of the example FRF), the SNR is large and the bias is small. In this case the estimator $H_V(f)$ yields an (almost) unbiased estimate of the FRF. Note $H_V(f)$ corresponds to $H_{PCA}(f)$ or $H_S(f)$ with $\kappa(f)$ set to unity, which is the appropriate value for this simulation. The small disparities between the theoretical FRF and mean of the estimator $H_V(f)$ are due to the effect of the window.

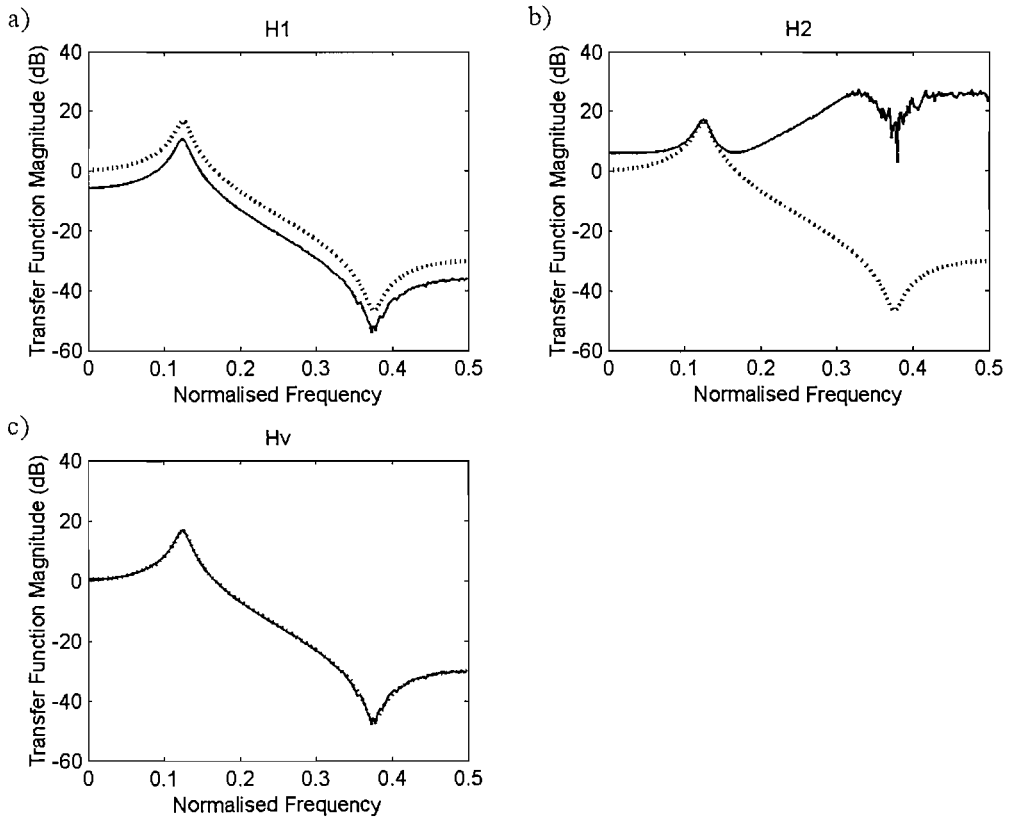


**Figure 5.2** Mean of the FRF estimators; computed using white measurement noise. a)Estimator $H_1(f)$, b) Estimator $H_2(f)$ c) Estimator $H_V(f)$ or $H_{PCA}(f)$ - Theoretical FRF shown as a dotted line, estimator shown as the solid line (White, Tan and Hammond).

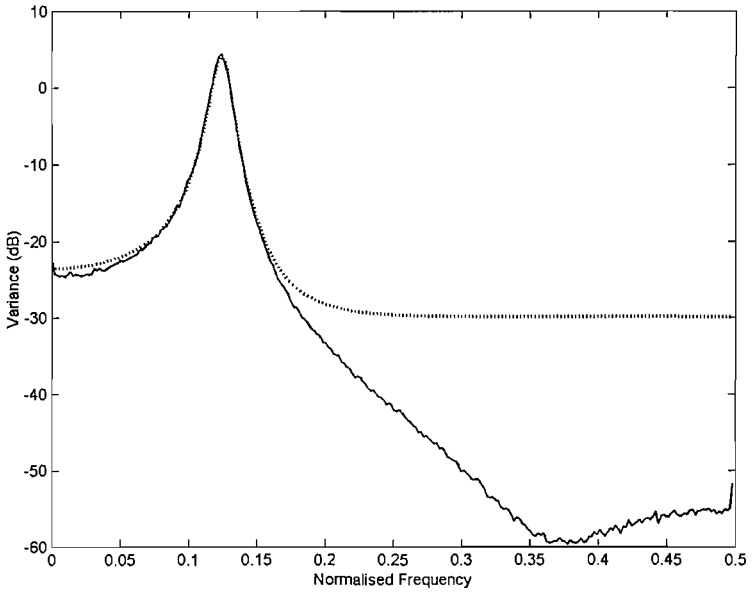


**Figure 5.3** Variance of ML spectral estimator for equal input-output noise. (Solid line - measured variance, dotted line – theoretical prediction of the variance, see (5.22)) (White, Tan and Hammond).

Figure 5.3 depicts the variance of the estimator $H_1(f)$ and $H_{PCA}(f)$ computed across the 1000 realisations of the processes and as predicted by equation (5.22). The theoretical prediction can be seen to be good in the region where the SNR is large, but the variance is poorly predicted in the high frequency region, where the SNR is low. This is a consequence of the approximation for the evaluation of CRLB (Appendix C) used in deriving (5.22) becoming invalid.

The final simulation study used coloured measurement noises, the colouration being realised by filtering with low order FIR filters. The spectra of the two noise processes are shown in Figure 5.4. Figure 5.5 illustrates the behaviour of the three FRF estimators $H_1(f)$ with $s \to \kappa(f)$, $H_2(f)$ and $H_S(f)$ whereas the comparison between the theoretical and measured variances of the ML estimator is shown in Figure 5.6. In this case it is necessary to use the estimator $H_S(f)$ (or $H_W(f)$) since $\kappa(f) \neq 1$. The general behaviour of $H_1(f)$ and $H_2(f)$ remains consistent, so that $H_1(f)$ has a large bias when the input SNR is low and $H_2(f)$ has a large bias when the output SNR is low. Clearly the estimator $H_S(f)$ remains very nearly unbiased. Once again small deviations from the theoretical predictions are due to the finite window size. The theoretical prediction of the variance is quite inaccurate almost over the whole frequency range except for the vicinity of the resonance in the low frequency region where the SNR is relatively large.

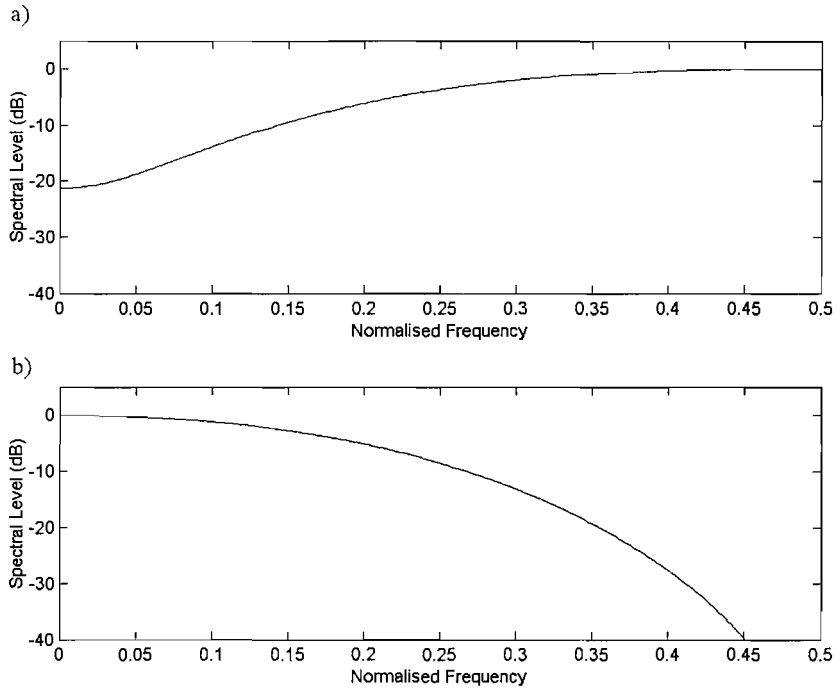


**Figure 5.4** Measurement noise spectra. a) Input noise, b) Output noise (White, Tan and Hammond).

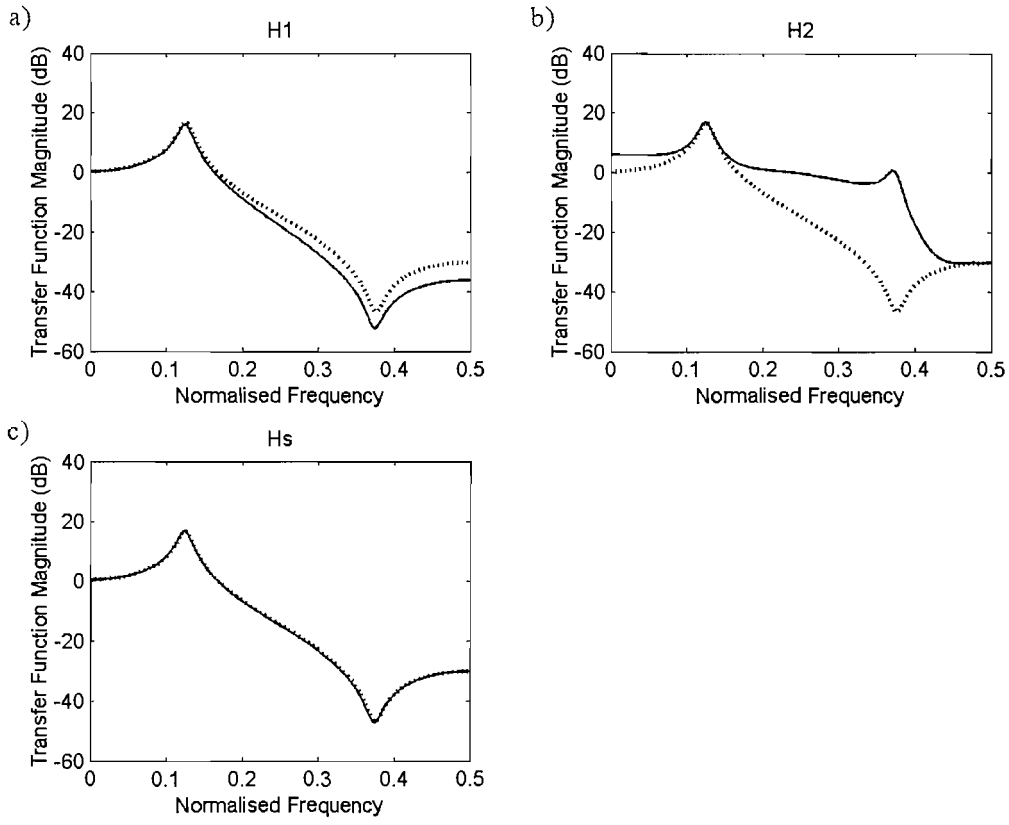


**Figure 5.5** Means of FRF estimators; computed using coloured measurement noise. a) Estimator $H_1(f)$, b) Estimator $H_2(f)$ c) Estimator $H_s(f)$ - Theoretical FRF shown as a dotted line, estimator shown as the solid line (White, Tan and Hammond).

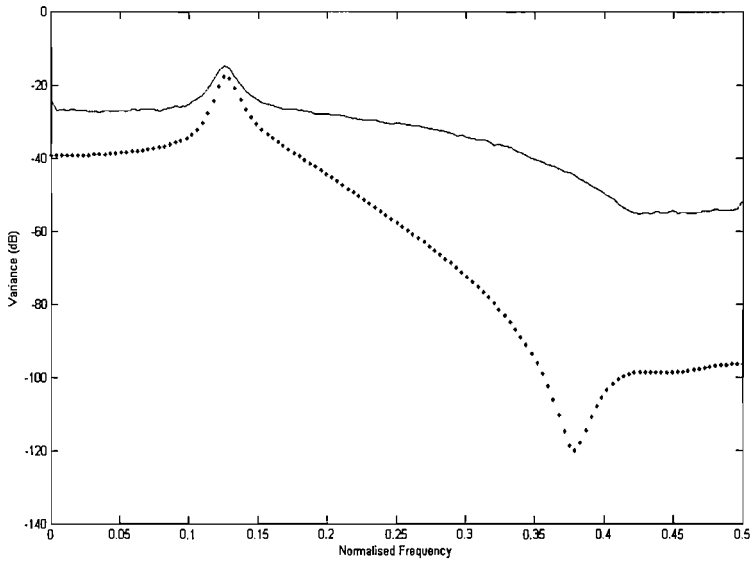


**Figure 5.6** Variance of ML spectral estimator for coloured input-output noise. (Solid line - measured variance, dotted line – theoretical prediction of the variance, see (5.22)).

## 5.3 FRF Estimation in Dynamical MIMO Systems

In this section we extend the application of the PCA FRF estimation scheme to LTI dynamical MIMO measurement systems. The basic form of multi-channel case which has been considered as for the PCA gain estimation problem covered in Chapter 4 comprises a Two-Input-Single-Output (TISO) system with an output in the form of a weighted sum of the inputs, each of which is filtered through a LTI system. Investigations take into account the potential presence of additive measurement noise on all signals. The theoretical procedure is developed through a generalised model in the form of an EVD of the input-output spectral correlation matrix, the results of which have been validated by computational simulations using artificially generated signals and systems. The components of the eigenvector corresponding to the zero eigenvalue are used for estimating the associated FRFs as for the gain estimation procedure detailed in the previous chapter.

For the initial derivations of the eigenvalues, the measured signals are considered to be noise-free in order to point-out the existence of a zero eigenvalue. Subsequently, it is shown that general computational parameters developed can be appropriately used for the cases where measured signals are noise contaminated. This is based on the fact that, although parasitic effects lead to the values of the eigenvalues to converge, we can still use the dimensions of the relevant eigenvector (associated with the smallest eigenvalue) for our proposed transfer function estimation scheme.

The performance assessments of the proposed method has also been provided through direct comparisons with the standard FRF estimators based on the least squares approach. The methods introduced in this section can be easily extended to cases where the identification of more complex linear time-invariant dynamical systems with similar forms of input-output structures is involved.

### 5.3.1 Multi-Input-Single-Output Systems

Figure 5.7 shows the block diagram of a dynamical TISO measurement system which forms the basis for the examination of the multi-channel system in this section. Based on the corresponding multi-channel PCA gain estimation scheme presented in the previous chapter, the model we shall use consists of two stationary random time histories representing the original inputs $x_1$ and $x_2$ filtered through the FRFs $H_a(f)$ and $H_b(f)$ leading to an original output $y$ which is the sum of both above filters' individual outputs. In the generic model all the measured signals ($x_{m1}$, $x_{m2}$ and $y_m$) are assumed to be contaminated by additive measurement noise ($n_{x1}$, $n_{x2}$ and $n_y$) which are uncorrelated with the input-output signals and each other.

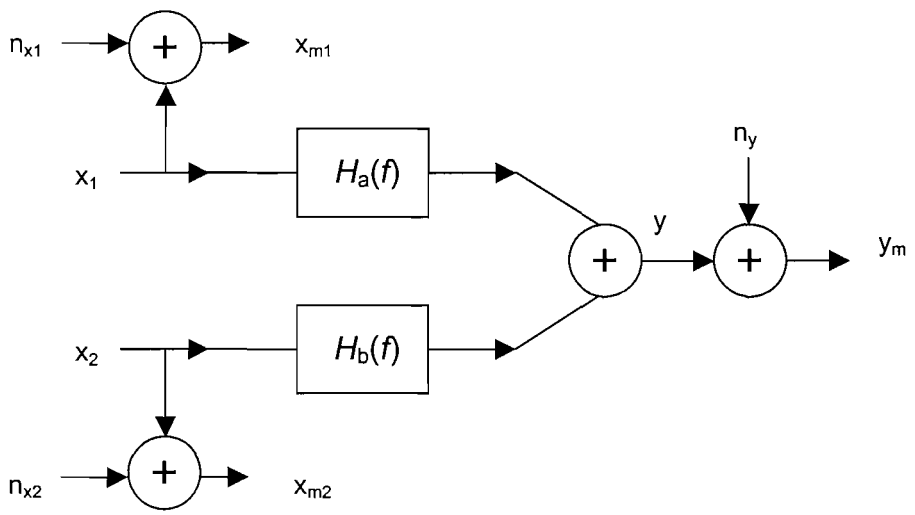


**Figure 5.7** Dynamical Two-Input-Single-Output system with uncorrelated inputs and uncorrelated additive measurement noise.

In order to derive the PCA FRF estimator for the above case the spectral correlation matrix we shall use to describe the system based on the measured signals will be formed similarly to the one of Section 5.2.2 but this time using three variables (2 inputs and 1 output) and hence will be of the size 3x3 and given by

$$\hat{\mathbf{R}}(f)=\begin{bmatrix} \hat{S}_{x_{m1}x_{m1}}(f) & \hat{S}_{x_{m2}x_{m1}}(f) & \hat{S}_{y_m x_{m1}}(f) \\ \hat{S}_{x_{m1}x_{m2}}(f) & \hat{S}_{x_{m2}x_{m2}}(f) & \hat{S}_{y_m x_{m2}}(f) \\ \hat{S}_{x_{m1}y_m}(f) & \hat{S}_{x_{m2}y_m}(f) & \hat{S}_{y_m y_m}(f) \end{bmatrix} \tag{5.23}$$

The analysis proceeds in the same way as described in Section 4.3.1 which is based on the EVD of the measurement covariance matrix although this time the statistical information matrix we use is complex owing to the fact that all signals are now represented by their Fourier Transforms (FTs). If it is assumed that the measurements are noise-free i.e.

$$n_{x1} = n_{x2} = n_y = 0 \tag{5.24a}$$

and thus

$$\begin{aligned} x_{m1} &= x_1 \\ x_{m2} &= x_2 \\ y_m &= y \end{aligned} \tag{5.24b}$$

then it can be shown after some algebra (see Appendix D) that the eigenvalues of the above spectral correlation matrix are given by the roots of the cubic equation

$$\lambda\left\{\lambda^2 - \left\{\left(|H_a|^2+1\right)S_{x_1x_1} + \left(|H_b|^2+1\right)S_{x_2x_2} + 2\,\mathrm{Re}\left(H_a^* H_b S_{x_1x_2}\right)\right\}\lambda + \left(|H_a|^2+|H_b|^2+1\right)S_{x_1x_1}S_{x_2x_2} - \left(|H_a|^2+|H_b|^2+1\right)\left|S_{x_1x_2}\right|^2\right\} = 0 \tag{5.25}$$

which reduces to

$$\lambda\left\{\lambda^2 - \left\{\left(|H_a|^2+1\right)S_{x_1x_1} + \left(|H_b|^2+1\right)S_{x_2x_2}\right\}\lambda + \left(|H_a|^2+|H_b|^2+1\right)S_{x_1x_1}S_{x_2x_2}\right\} = 0 \tag{5.26}$$

for the special case of uncorrelated inputs. In accordance with the corresponding results given in the previous chapter (see (4.41) and (4.42)), it can be clearly seen that for the above system input-output configuration there is one zero eigenalue whose corresponding eigenvector can be used for deriving the FRF's, relating each input with the corresponding part of the output, which follows from the description of the proposed SISO FRF estimation scheme given in Section 5.2.2. Therefore we seek to define the eigenvector corresponding to the zero eigenvalue, and use the associated ratios of its components describing each FRF. In accordance with the frequency domain version of (4.46) we get

$$\begin{bmatrix} \hat{S}_{x_{m1}x_{m1}}(f) & \hat{S}_{x_{m2}x_{m1}}(f) & \hat{S}_{y_m x_{m1}}(f) \\ \hat{S}_{x_{m1}x_{m2}}(f) & \hat{S}_{x_{m2}x_{m2}}(f) & \hat{S}_{y_m x_{m2}}(f) \\ \hat{S}_{x_{m1}y_m}(f) & \hat{S}_{x_{m2}y_m}(f) & \hat{S}_{y_m y_m}(f) \end{bmatrix} \cdot \begin{bmatrix} t_{1i} \\ t_{2i} \\ t_{3i} \end{bmatrix} = \lambda_i \cdot \begin{bmatrix} t_{1i} \\ t_{2i} \\ t_{3i} \end{bmatrix} \tag{5.27}$$

which leads to the estimators

$$-\frac{t_{i1}}{t_{i3}} \rightarrow H_a(f) = \frac{S_{x_{m2}x_{m1}} S_{y_m x_{m2}} - S_{x_{m2}x_{m2}} S_{y_m x_{m1}}}{\left|S_{x_{m1}x_{m2}}\right|^2 - S_{x_{m2}x_{m2}} S_{x_{m1}x_{m1}}} \tag{5.28a}$$

and

$$-\frac{t_{i2}}{t_{i3}} \rightarrow H_b(f) = \frac{S_{x_{m1}x_{m1}} S_{y_m x_{m2}} - S_{x_{m1}x_{m2}} S_{y_m x_{m1}}}{S_{x_{m1}x_{m1}} S_{x_{m2}x_{m2}} - \left|S_{x_{m1}x_{m2}}\right|^2} \tag{5.28b}$$

Although the above FRF estimators for the Two-Input-Single-Output system have been derived on the basis of the assumption that all measurements are noise-free, as described in the previous chapter, these forms can be readily used for the cases where measurements are also noise contaminated as long as the corresponding signal-to-noise-ratios are not too poor i.e. for the cases where noise power is low compared to the signal power. This means that for the cases of noise-free measurements, the components of the eigenvector corresponding to the zero eigenvalue whereas for the cases of noisy measurements, the components of the eigenvector corresponding to the smallest eigenvalue is used in the above described forms to derive the FRF's.

As has already been mentioned in the previous chapter, the least squares estimator $H_1(f)$ (or its time domain equivalent $a_1$) can be considered as the optimal estimator for uncorrelated-multi-input system configuration when derived on the basis of single input-output pairs. Also from (5.28a,b) we can clearly see that for truly uncorrelated inputs their cross spectra is effectively zero and thus the PCA estimators reduce to the corresponding least squares version. In the next section performance assessment of the above estimators is presented through computational simulations on artificial systems providing a direct comparison with the standard estimators based on the least squares approach. The results verify that even if the inputs are uncorrelated when finite lengths of data are involved, the input-input cross spectral estimates are not exactly zero and the PCA estimators in general give better results relative to $H_1(f)$.

### 5.3.2 Performance Assessment of TISO PCA FRF Estimator

Computational simulations have been undertaken in order to assess the performance of the TISO PCA FRF Estimator $H_{PCA}(f)$ whose theoretical analysis has been presented in the previous section. System FRF's $H_a(f)$ and $H_b(f)$ such as that illustrated in Figure 5.7 have been simulated using simple digital systems one of which is identical to that used for the statistical assessment study in Section 5.2.4. The second artificial model, a low-pass filter, has been chosen to represent a lightly damped system in order to allow one to be able to clearly visualise/compare the potential bias errors on the computed FRF estimates. Figures 5.8 and 5.9 illustrate the zero-pole locations of these systems on the z-plane.

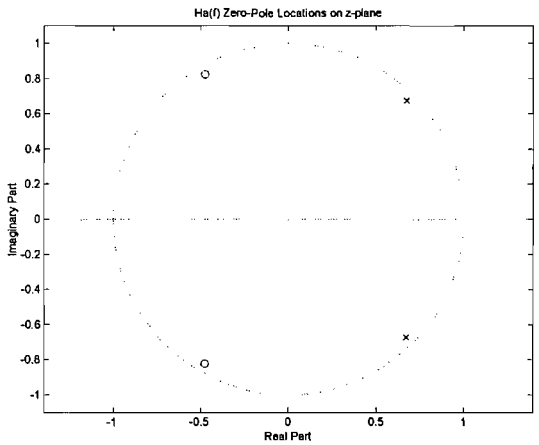


**Figure 5.8** Zero-Pole locations of the system representing the FRF $H_a(f)$ in the TISO system shown in Figure 5.7.

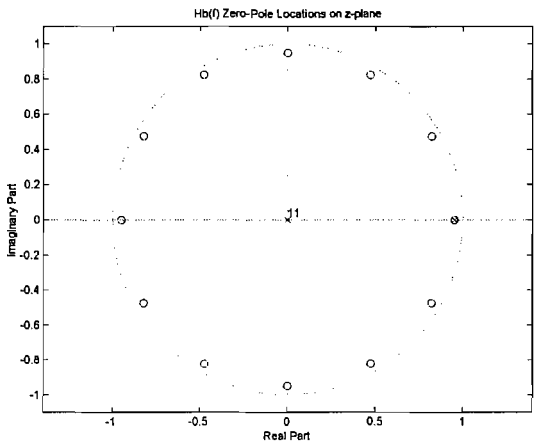


**Figure 5.9** Zero-Pole locations of the system representing the FRF $H_b(f)$ in the TISO system shown in Figure 5.7.

The model system under investigation has been excited by independent Gaussian white noise input signals with variances of 64 and 36 respectively. Two particular cases of trials have been considered and these are the noise-free and noise on both input and output cases. For the noisy case input and output signals have been corrupted using independent, additive Gaussian noise. The corresponding power and cross spectra have been estimated using segment averaging based on FFT's of 1024 samples and a Hann window of 512 points with no overlapping segments with each realisation consisting of 1 hundred thousand samples. FRF magnitude and phase responses for the estimators $H_{PCA}(f)$, $H_1(f)$, $H_2(f)$ and $H_W(f)$ have been computed following the above regime. Here it should be noted that the PCA estimator used is in the form (5.28a,b) described above whereas the least squares estimators computed for the comparisons have been based on measured input-output pairs and hence represent the SISO equivalent case i.e. in their standard forms but considering each pair of input-output signals associated with the corresponding part of the system at a time.

Figures 5.10 and 5.12 illustrate the magnitude estimates of the FRF's $H_a(f)$ and $H_b(f)$, respectively, for the noise-free case obtained using the four estimators. Despite zero noise levels on the measured signals $H_2(f)$ gives extremely inaccurate results over almost the whole frequency range for both filters. The main reason for this is due to the fact that this estimator is strongly dependent on the output power spectral density (see (3.30)) which in the case of the system under investigation is a function of the outputs from each digital filter and hence both inputs. Therefore if we compute $H_2(f)$ using the first input and the total output, the influence of the second input on the measured output will cause a strong parasitic effect as additive output noise and large deviations on the estimate compared to the true FRF and vice versa when computed using the second input and the total output. In Figure 5.10 this negative effect gets reinforced by the lower SNR towards the mid to high frequency region due to the decreasing gain factor of the first filter whereas for the FRF estimate of the second filter such as that shown in Figure 5.12 $H_2(f)$ is strongly affected by the shaping characteristics of the first filter which is most noticeable in the low frequency region.

The behaviour of the estimator $H_W(f)$ is also quite complex with inaccurate behaviour over the whole frequency range but this being less severe compared to that of $H_2(f)$ in the first filter's estimates although in the case of the second filter $H_2(f)$ and $H_W(f)$ give similar results in the low frequency region. Despite being optimal for both input and

output noise for the SISO FRF estimation problem as shown in Section 5.2, when applied to the multi-input-single-output case of the above form, $H_W(f)$ results in highly biased estimates of the FRF's. Again this estimator is dependent on the power spectral density of the output (see (3.34)) and although the magnitude estimate obtained using this estimator such as that shown in Figure 5.10 can be considered as slightly improved compared to that of $H_2(f)$ around the anti-resonance region, there is severe biasing effects in the low frequency region of both Figures 5.10 and 5.12 due to the high gain characteristics of each FRF in these regions.

Both $H_2(f)$ and $H_W(f)$ reveal fluctuating bias errors rather than constant offset effects, which is related to the variations in the gain factors of the FRF's $H_a(f)$ and $H_b(f)$ and hence causing irregular changes in the corresponding SNR's. The magnitude estimate of $H_a(f)$ calculated using the estimator $H_1(f)$ is relatively good and hence is almost unbiased. This is a result of this estimator being a function of both input-output cross-spectral density and the input power spectral density (see (3.29)). Theoretically, in the case of uncorrelated noise-free inputs the cross spectrum is not affected by the second input although the slight variability that can be observed by eye on the $H_1(f)$ estimator in the high frequency region of Figure 5.10 is mainly due to the input signals not being truly uncorrelated as a result of windowing effects and secondarily due to the limitation of using finite length data and hence a limited number of windows. The estimate of the FRF $H_b(f)$ derived using $H_1(f)$ as shown in Figure 5.12 has more irregular behaviour in the region corresponding to the resonance frequency of the first filter which is again a consequence of the above effects but this time to a higher degree as the larger gain factor of the first system in this region makes the input-output cross spectrum slightly more dominant on the input power spectral density. In this case it can be clearly seen from the Figures 5.10 and 5.12 that the estimator $H_{PCA}(f)$ yields unbiased estimates of the FRF's. Note that the PCA estimator is not a function of the output power spectrum and consequently its computation is not influenced by the parasitic effect induced by the second input.

Although, theoretically, for uncorrelated inputs the expressions (5.26a,b) defining the PCA estimators effectively reduce to $H_1(f)$, as it has been mentioned above the estimates obtained using these two estimators are not identical as the result of the input signals being slightly correlated due to windowing effects in the computations. We can conclude that the extra terms contained in $H_{PCA}(f)$ reduces the random variability errors

on the estimate as a smoothing operator and hence are beneficial. It should be noted that if the input signals are truly uncorrelated these two estimators give exactly the same results.

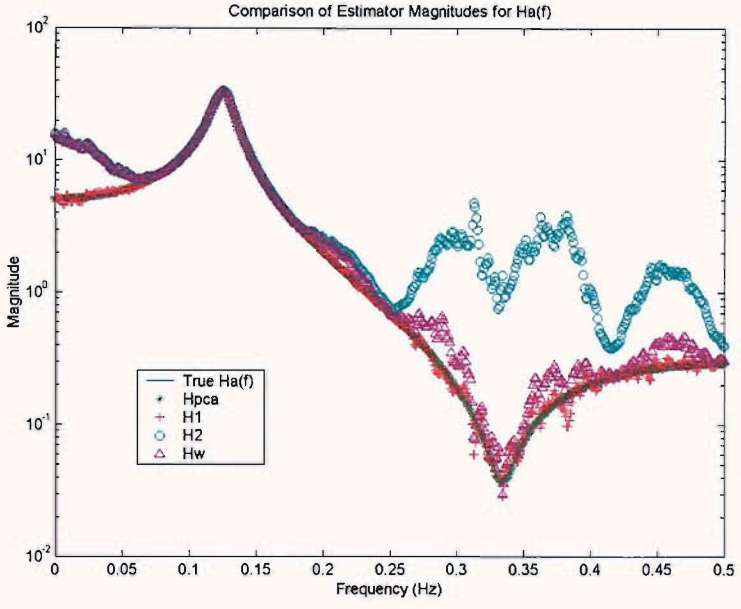


**Figure 5.10** Comparison of various estimator magnitudes of the FRF $H_a(f)$ of the TISO system illustrated in Figure 5.7 for noise-free measurements.

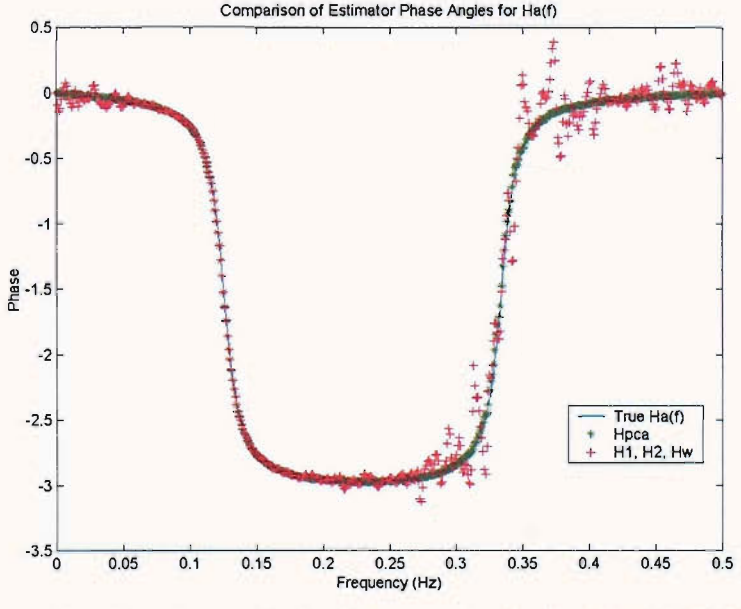


**Figure 5.11** Comparison of various estimator phase angles for the FRF $H_a(f)$ of the TISO system illustrated in Figure 5.7 for noise-free measurements.

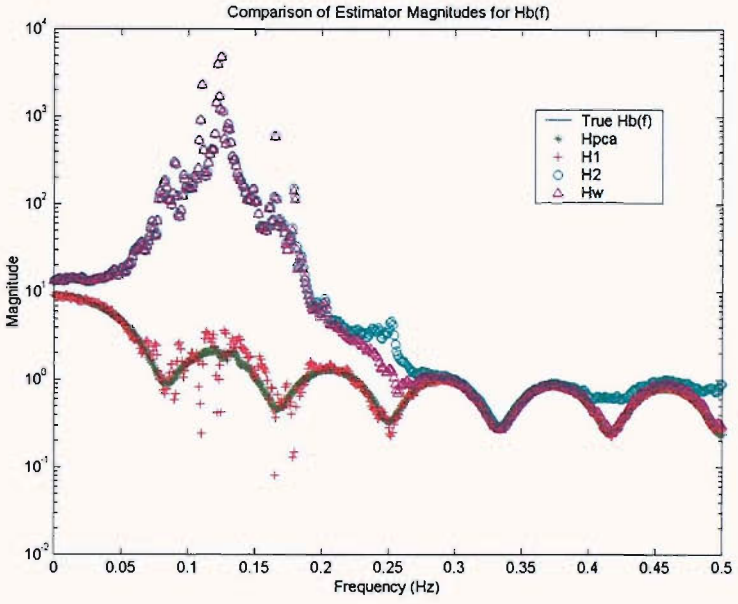


**Figure 5.12** Comparison of various estimator magnitudes for the FRF $H_b(f)$ of the TISO system illustrated in Figure 5.7 for noise-free measurements.

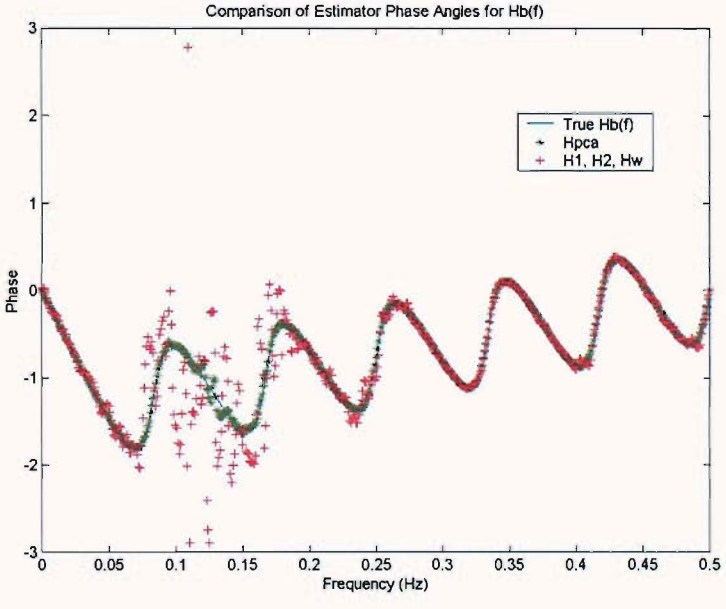


**Figure 5.13** Comparison of various estimator phase angles for the FRF $H_b(f)$ of the TISO system illustrated in Figure 5.7 for noise-free measurements.

Figures 5.11 and 5.13 illustrate the phase estimates of the FRF's $H_a(f)$ and $H_b(f)$, respectively, obtained using four estimators for the noise-free case as defined in the above paragraph. We have mentioned in Section 5.2.4 that for the SISO case the phase information contained in the least squares estimators and the PCA estimator is identical. However for the TISO case if there exists some amount of correlation between the input signals, phase estimate from the PCA estimator may well be different from that of the least squares estimators again due to the extra information contained within the terms relating to the cross-spectra between both inputs and between the output and the remaining input respectively (see (5.26a,b)). Furthermore this behaviour can be easily observed with the least squares estimators having a significantly high variability both in the low and high frequency regions for the second and the first filter estimates respectively whereas the PCA estimator being completely unbiased overlapping the true FRFs.

Figures 5.14 to 5.17 show the results of our second simulation study for the case of noisy measurement with SNR's of 6 dB for the inputs and 10 dB for the output. It can be seen from Figure 5.14 that the magnitude estimates obtained for the first filter using $H_1(f)$ and $H_{PCA}(f)$ are both biased in the form of a constant multiplicative factor in the low to mid frequency region with the $H_1(f)$ having higher variability particularly in the high frequency region as in the noise-free case. $H_2(f)$ reveals the most inaccurate behaviour among the four estimators with the biasing effect reaching high values over the whole frequency range except for around the first resonance whereas $H_W(f)$ also yields a severely biased estimate but with relatively consistent results particularly in the anti-resonance region compared to that of $H_2(f)$. The above observed behaviours of the four estimators become more significant for the magnitude estimates of the second filter for the noisy case such as that shown in Figure 5.16, this time $H_W(f)$ and $H_2(f)$ giving almost identical results with slight differences in the low frequency region. $H_1(f)$ and $H_{PCA}(f)$ are again biased which appears as a constant offset on a logarithmic scale. As in the previous case $H_{PCA}(f)$ has less variability and hence gives more accurate results compared to $H_1(f)$. Figures 5.15 and 5.17 show the phase estimates obtained for the filters in the case of noisy measurements from which it can be easily seen that all four estimators reveal similar behaviour with slight variations in their random errors that become more noticeable in the regions where corresponding SNRs are low.

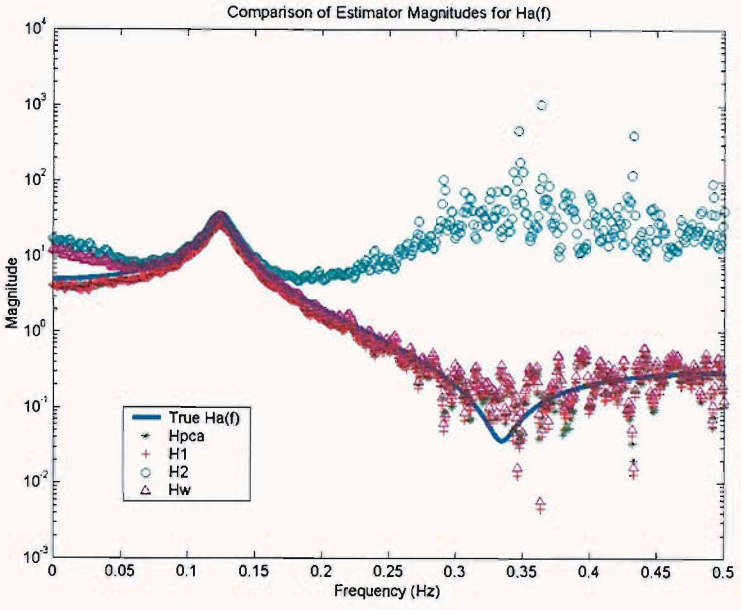


**Figure 5.14** Comparison of various estimator magnitudes of the FRF $H_a(f)$ of the TISO system illustrated in Figure 5.7 for noisy measurements ($SNRx_{m1}$=$SNRx_{m2}$=6dB, $SNRy_m$=10dB).

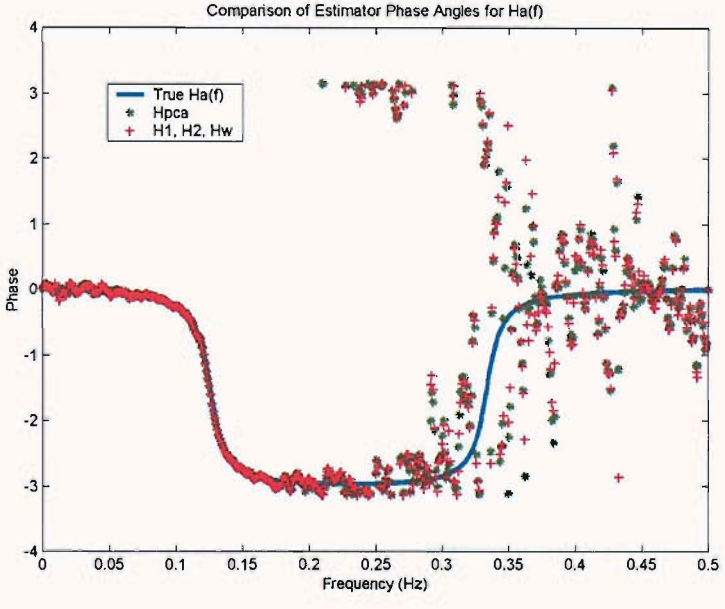


**Figure 5.15** Comparison of various estimator phase angles of the FRF $H_a(f)$ of the TISO system illustrated in Figure 5.7 for noisy measurements ($SNRx_{m1}$=$SNRx_{m2}$=6dB, $SNRy_m$=10dB).

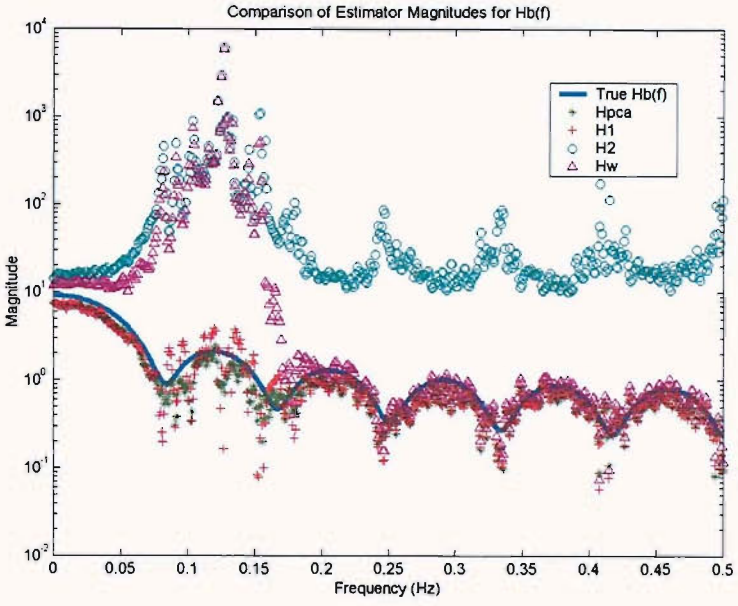


**Figure 5.16** Comparison of various estimator magnitudes of the FRF $H_b(f)$ of the TISO system illustrated in Figure 5.7 for noisy measurements ($SNRx_{m1}$=$SNRx_{m2}$=6dB, $SNRy_m$=10dB).

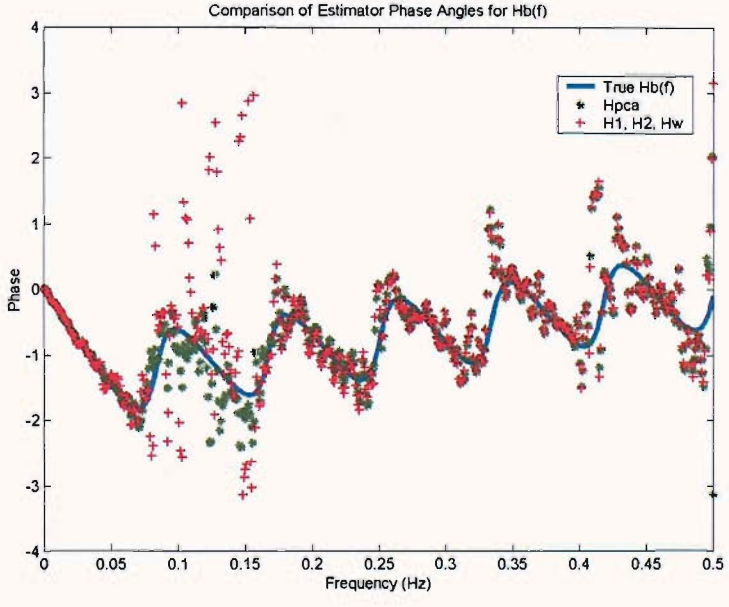


**Figure 5.17** Comparison of various estimator phase angles of the FRF $H_b(f)$ of the TISO system illustrated in Figure 5.7 for noisy measurements($SNRx_{m1}$=$SNRx_{m2}$=6dB, $SNRy_m$=10dB) .

## 5.4 Concluding Remarks

Applications of PCA for the estimation of FRF's of linear time-invariant dynamical systems have been presented in detail which follows our proposed technique introduced through the gain estimation problem in Chapter 4. The first part of this chapter has covered the PCA FRF estimation problem on a basic linear time-invariant SISO measurement system whereas in the second part the application has been extended to a generic form of uncorrelated-multi-input system. Both investigations have been verified through computational simulations on artificial system for noise-free and noisy measured signal cases.

It has been shown that the use of PCA FRF estimation scheme for a SISO measurement system is equivalent to the solution based on the Total Least Squares (TLS) approach for the special case of the scale factor $s$ being equal to unity and hence equal variance measurement noise on both input and output. Furthermore, it has also been shown in the same context that the use of principle of Maximum Likelihood (ML) results in a generalised TLS procedure in which the scale factor $s$ is replaced by the ratio of the power spectra of the measurement noises. When both input and output measurements are noise contaminated the use of estimators $H_{PCA}(f)$ (or $H_v(f)$) and $H_w(f)$ (or $H_S(f)$) are unbiased for the cases of equal variance noise on measured signals and different variance noise on measured signals respectively.

The extension of the proposed PCA FRF estimation procedure to multi-input systems works relatively well and demonstrates a significant improvement on the FRF estimates compared to that of obtained through the standard methods based on the least squares approach. Although the multi-channel PCA estimator is also biased to a certain degree for the noisy case, especially the shape of the FRF magnitude is estimated with high accuracy and very low variability. Analytical and computational procedures carried out has been based on a basic form of Two-Input-Single-Output (TISO) system with which in practice can be readily extended to multi channel systems with more complex structures of similar form. If the input signals are truly uncorrelated the computational expression for multi-channel $H_{PCA}(f)$ reduces to the corresponding $H_1(f)$ although the extra terms contained in the PCA estimator has a smoothing effect on both magnitude and phase estimates compared to that of $H_1(f)$ when there is some amount of correlation

between the inputs due to computational errors. Multi-channel FRF estimates obtained using the estimators $H_2(f)$ and $H_w(f)$ are severely biased over the whole frequency range and can be of no practical use for this purpose.

In the next chapter we introduce the application of PCA for the detection and interpretation of non-linearities in measurement systems. In essence, also the upcoming application follows the concepts introduced here and in the previous chapter for linear systems, however, this time our approach leads us to a form of linearisation of the potentially non-linear system under investigation and hence estimating the linear equivalent transfer characteristics by analysing the relationships between the eigenvalues of the measurement covariance or spectral correlation matrix in the time or frequency domains respectively.

# Chapter Six

# PCA FOR NON-LINEAR SYSTEMS

## 6.1 Introduction

In Chapters 4 and 5, the use of PCA in the problem of estimating the transfer characteristics of linear time-invariant SISO/MIMO systems has been investigated in detail both in the time and frequency domains. It has been shown that in the case of uncorrelated additive noise on measured signals, the PCA transfer function estimator gives results which make it a useful alternate to the standard estimators originating from the least squares approach.

The aim of this chapter is to investigate the use of PCA for the detection and interpretation of system non-linearities with a view to introduce an approximation procedure for determining the linear equivalent transfer characteristics. The method proposed is assessed both theoretically and through examples involving numerical simulations on both memoryless and dynamical non-linearity. In addition, experimental investigations have been carried out for the fault diagnosis of a rotating machine in order to assess the performance of the proposed non-linearity detection technique on real data.

In the next section, methods that are proposed for linear equivalent transfer function estimation in both time and the frequency domains are presented respectively. Section 6.3 introduces the derivation of the Virtual Coherence Function from a different viewpoint than that of the conventional approach in the form of a Non-Linearity Detection Ratio and referred to as NDR whereas Section 6.4 covers an experimental study for the performance assessment of this parameter. Section 6.5 gives a summary of this chapter and outlines the concluding remarks.

## 6.2 Linear Equivalent Transfer Function Estimation

Our main motivation for seeking to develop a linear equivalent transfer function estimation scheme using PCA is based on the need to analyze the behaviour of non-linear systems, which may be come across in various forms in many engineering applications, in a generalised and relatively simple way. This originates from the fact that every system is non-linear except for some limited operation ranges. The well-established linear system theory allows one to understand the behaviours of all linear (time-invariant) systems although no such unified results exist to aid the analysis of non-linear systems. Unlike the linear case, in general different types of non-linear behaviour require different methods some of which may be exact and some may be approximate.

One commonly used approximate method to deal with a non-linear system is based on *linearisation*. This involves using the gain factor of the non-linear term(s) in the vicinity of an operation point as the gain of a linear term. Our proposed approach based on PCA also leads to a form of linearisation of the system in the above form through the EVD of the input-output covariance (or spectral correlation) matrix when the input is stationary random. This is carried out by using the components of the eigenvector corresponding to the principal component leading to a system's transfer characteristics in accordance with the procedures presented in Chapters 4 and 5.

It has been shown in our analysis for the SISO linear gain estimation problem covered in Chapter 4 that PCA provides an effective approach to its solution through the interpretation of the eigenvalues and the eigenvectors of the input-output covariance matrix. More specifically, in the cases where the system input-output relationship is purely linear and the measured signals are noise-free, there is only one non-zero eigenvalue whose value is equal to the sum of the powers of the measured variables and the ratio of the components of the corresponding eigenvector determines the associated gain factor. Following this result we have also come to the conclusion that for the cases where measurements are noise contaminated and/or the input-output relationship is not completely linear then both eigenvalues will be non-zero as the result of some part of the total variance of the process being contained within the second principal component which is orthogonal to the first one by definition. If this potential parasitic effect is not dominant over the undistorted/linear behaviour of the system under investigation, then

one would expect a great difference between the numerical values of the eigenvalues and the gain estimate obtained using PCA through the above procedure will be a good approximation to the system's transfer characteristics. This result has been verified by simulations for the FRF estimation problem presented in Chapter 5 where the potential parasitic effects were assumed to be caused by uncorrelated additive measurement noise on the signals. Here, we extend the application of the same result to systems where the above parasitic effects are caused by non-linearity.

In the first part of this section the method proposed has been applied to a system with memoryless cubic non-linearity. In the second part, a dynamical system has been considered with a well-established form of non-linearity (Duffing's Form) leading us to the use of the method in the frequency domain through Fourier based transformations. In each case the theoretical results have been verified through computational simulations for the estimation of the transfer characteristics of the associated system for varying some key parameters such as the variance of the input excitation and the coefficient of the non-linear term.

### 6.2.1 Memoryless Non-Linearity

In this subsection we consider the problem of estimating the linear equivalent gain of the system whose input-output relationship is of the form

$$y=ax+bx^3 \tag{6.1}$$

With reference to the SISO PCA gain estimation procedure presented in Chapter 4, let us recall the form (4.2) defining the linear transformation of the principal components to the measured variables but this time substituting the noise-free input-output measurement vector $\mathbf{x}=\begin{bmatrix} x & y \end{bmatrix}^T$ for the original variables. If we expand this transformation in accordance with (4.3) and (4.4) we get

$$x = t_{11}z_1 + t_{12}z_2 \tag{6.2a}$$

$$y = t_{21}z_1 + t_{22}z_2 \tag{6.2b}$$

and hence for the equivalent linear system the gain relating the output to the input through the principal component is given by the ratio

$$t_{21}/t_{11}$$

From this result it is logical to conclude that if a large proportion of the total power of the whole process is represented by the principal component the ratio given above can be considered, in some sense, as a good approximation to the system's *actual* gain characteristics. This form of linearisation applied to the memoryless non-linear SISO system given above allows us to reduce the dimensionality by transforming the measurement vector $\mathbf{x}$ representing the set of original variables, into each one dimensional index $\mathbf{z}_i$ (each principal component) i.e. by multiplying both sides of (4.2.) with $\mathbf{T}=\mathbf{T}^T$ from left and expanding we obtain

$$z_1 = t_{11}x + t_{21}y \tag{6.3a}$$

$$z_2 = t_{12}x + t_{22}y \tag{6.3b}$$

So that each component is a linear combination of those parts of the original variables weighted according to the variability in each original axis. As before, the solution to the problem of determining the principal components of the measured variables can be obtained analytically from the EVD of the measurement covariance matrix as follows:

The computation of the noise-free variance-covariance matrix,

$$\mathbf{R}_{xx} = \begin{bmatrix} E[x^2] & E[x\ y\ ] \\ E[y\ x\ ] & E[y^2] \end{bmatrix}$$

for the input-output form given by (6.1), involves the fourth and the sixth moments of the input signal. Note that the central moments for the Gaussian probability distribution are given by [2]

$$m_n = 0 \qquad \text{if } n \text{ is an odd integer} \quad (6.4a)$$

$$m_{2n} = 1 \times 3 \times 5 \times \ldots \times (2n-1) \cdot \sigma^{2n} \qquad \text{for } n = 0, 1, 2, 3, \ldots \quad (6.4b)$$

where $\sigma$ denotes the standard deviation of the variable. Therefore if it is assumed that the input signal of the above system is a zero-mean Gaussian random variable then from the relationships (6.4a,b) one can easily obtain

$$E[x^4] = 3\sigma_x^4 \quad \& \quad E[x^6] = 15\sigma_x^6 \qquad (6.4c,d)$$

Using (6.4c,d), the theoretical noise-free input-output covariance matrix can be derived as

$$\mathbf{R}_{xx} = \begin{bmatrix} \sigma_x^2 & a\sigma_x^2 + 3b\sigma_x^4 \\ a\sigma_x^2 + 3b\sigma_x^4 & a^2\sigma_x^2 + 15b^2\sigma_x^6 + 6ab\sigma_x^4 \end{bmatrix} \qquad (6.5)$$

and it can be shown after some algebra that its eigenvalues are

$$\lambda_{1,2} = \frac{1}{2}\left\{15b^2\sigma_x^6 + 6ab\sigma_x^4 + a^2\sigma_x^2 + \sigma_x^2 \pm \sqrt{\left(-15b^2\sigma_x^6 - 6ab\sigma_x^4 - a^2\sigma_x^2 - \sigma_x^2\right)^2 - 12b\sigma_x^8(5b-3)}\right\} \qquad (6.6)$$

whose corresponding eigenvectors can be computed accordingly.

In an attempt to assess the performance of the method numerically, theoretical curves derived from (6.1) have been plotted against the gain estimates obtained from the EVD of the input-output covariance matrix estimate using a stationary random (Gaussian white) excitation for varying input variance and the coefficient of the non-linear term, *b*. The LHS plot in Figure 6.1 shows the curve (6.1) for the case of $a$=3 and $b$=0.1 with the gain estimates for the input variances 0.1 and 9, respectively. As can be seen, when the input variance is low the system is completely dominated by its linear behaviour and the PCA gain estimate gives the result equivalent to the slope of the linear part of the theoretical curve i.e. the coefficient of the linear term being approximately equal to 3 which can also be verified from the eigenvalues and the eigenvectors calculated as

$$\lambda_1 = 1.01 \quad \& \quad \lambda_2 = 0$$

and

$$\mathbf{t}_1 = \begin{bmatrix} 0.31 \\ 0.94 \end{bmatrix} \quad \& \quad \mathbf{t}_2 = \begin{bmatrix} 0.94 \\ -0.31 \end{bmatrix}$$

However when the input variance is increased to 9, despite the coefficient $b$ still being relatively small compared to the coefficient $a$, the non-linear effect within the system becomes more significant and the PCA gain estimate also increases to around 6.5, tending towards a linear equivalent slope describing the behaviour of the part of the curve for large $x$ in which case the eigenvalues and the eigenvectors have been computed as

$$\lambda_1 = 344 \quad \& \quad \lambda_2 = 1.14$$

and

$$\mathbf{t}_1 = \begin{bmatrix} 0.15 \\ 0.98 \end{bmatrix} \quad \& \quad \mathbf{t}_2 = \begin{bmatrix} 0.98 \\ -0.15 \end{bmatrix}$$

Figure 6.1 RHS illustrates the corresponding results for the case of $a$=3 and $b$=1 with the gain estimates for the input variances 0.1, 1 and 9. Again, as can be clearly seen, the influence of increasing the input variance results in the increase of the gain estimate obtained using PCA due to the non-linear effect being less dominated by the linear part and hence the slope of the eigenvector corresponding to the principal component tending towards the behaviour of the theoretical curve in the asymptotic region.

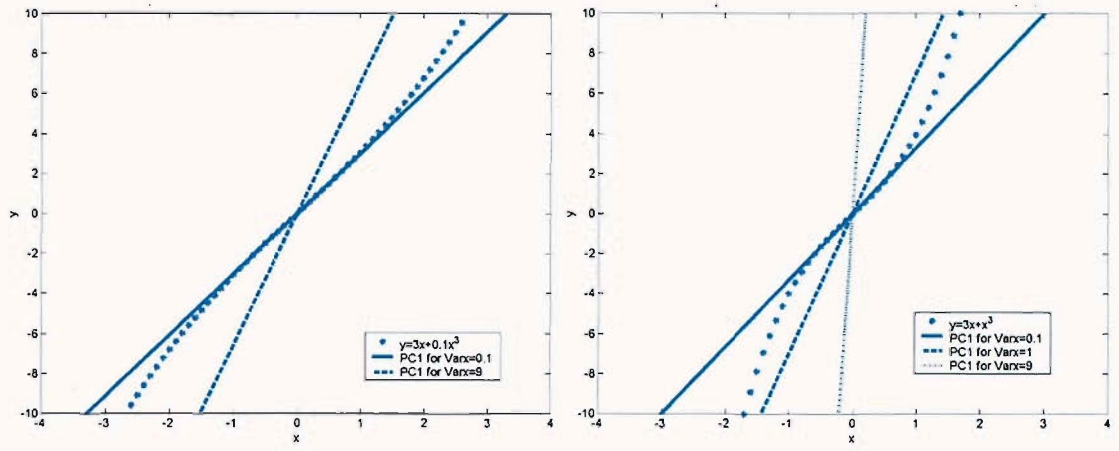


**Figure 6.1** Comparison of (6.1) for $a$=3, $b$=0.1 and input variances 0.1 & 9 (LHS plot) and for $a$=3, $b$=1 and input variances 0.1, 1 & 9 (RHS plot) with the corresponding PCA gain estimates.

As covered in detail in Chapters 2 and 3, the principle which is widely used in problems that are involved with error minimisation and/or statistical estimation is known as the method of least squares. In order to apply this technique to the above problem in terms of determining the optimum equivalent linear gain (in the least squares sense) one can define a cost function for the error distance between the actual output of the system given by (6.1) and its least squares estimate (LSE), to be minimised in accordance with the standard procedures described in Chapter 3.

The optimisation landscape for this procedure is depicted in block diagram form in Figure 6.2 where $x$ is the original input, $y$ is the original output, $\hat{y}$ is the LSE of the system output and $e$ is the deviation between the actual output and the estimate that is to be minimised. It can be clearly seen from this diagram that the error distance is given by

$$e = y - \hat{y} \tag{6.7}$$

where $\hat{y} = G_{LSE}x$ and $G_{LSE}$ is the gain obtained from least squares method. Substituting $ax+bx^3$ and $G_{LSE}$ into (6.7) we get

$$e = ax+bx^3-G_{LSE}x \tag{6.8}$$

and form a cost function such that

$$J = E[e^2] \approx \frac{1}{N}\sum_{i=1}^{N}(e\ )^2 = \frac{1}{N}\sum_{i=1}^{N}\left(ax+bx^3-G_{LSE}x\right)^2 \tag{6.9}$$

which can be expanded and rewritten as

$$J = a^2\overline{x^2} + b^2\overline{x^6} + {G_{LSE}}^2\overline{x^2} - 2bG_{LSE}\overline{x^4} + 2ab\overline{x^4} - 2aG_{LSE}\overline{x^2} \tag{6.10}$$

and after some algebra it can be shown that (assuming Gaussianity of $x$)

$$J = a^2\sigma_x^2 + 15b^2\sigma_x^6 + {G_{LSE}}^2\sigma_x^2 - 6bG_{LSE}\sigma_x^4 + 6ab\sigma_x^4 - 2aG_{LSE}\sigma_x^2 \tag{6.11}$$

Above expression is a quadratic function of the parameter $G_{LSE}$, and its minimisation can be obtained from the solution of

$$\frac{dJ}{dG_{LSE}} = 0$$

and after some algebra one can obtain (6.12) as the least squares linear approximation to the system gain i.e.

$$G_{LSE} = 3b\sigma_x^2 + a \tag{6.12}$$

In order to compare the theoretical results obtained using PCA and LSE techniques we have calculated the gain estimates using the matrix given by (6.4) and the expression given by (6.12) respectively for the values of the input variance in the range 0.1 to 10 and plotted against each other such as that shown in Figure 6.3 for the cases of $b$ is 0.1 (LHS plot) and 1 (RHS plot) respectively. Within the [0.1,1.0] variance range of the input excitation, i.e. when the influence of the non-linear term is much smaller compared to the influence of the linear term contained in the system descriptor function, PCA and LSE gives almost exactly the same results. However the results obtained for the [1,10] variance range of the input excitation show that if the effect of non-linearity is increased the two methods start to give significantly different results with the noticeably lower values of the LSE method compared to that of PCA.

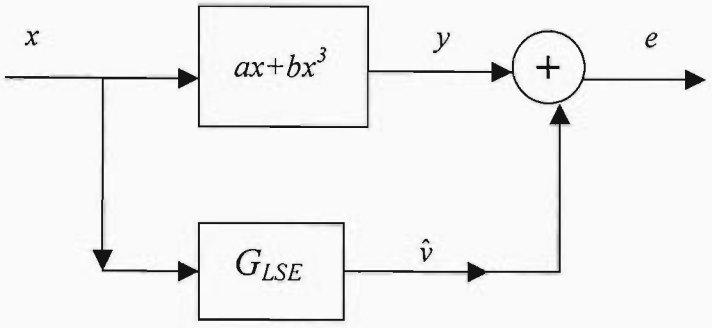


**Figure 6.2** Schematic diagram of the optimisation landscape for linear equivalent gain estimation using LSE.

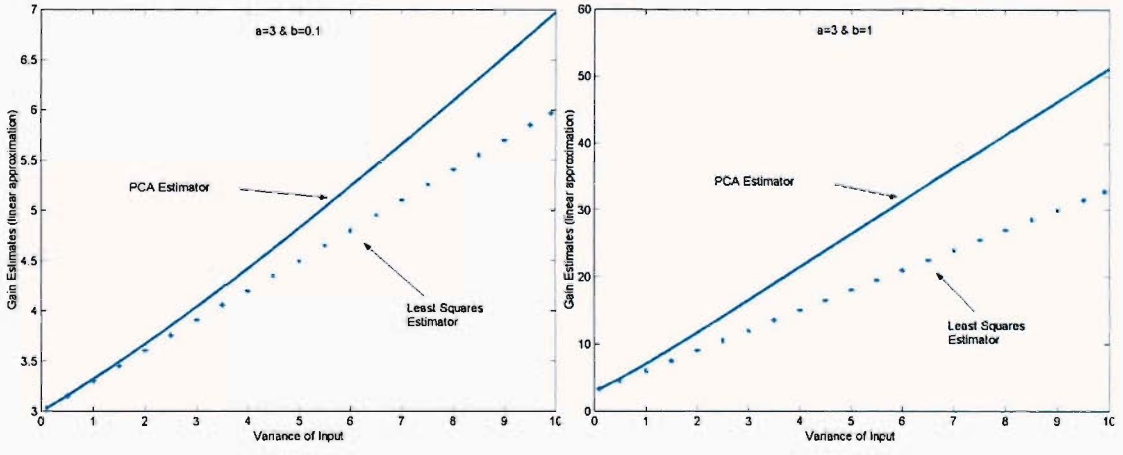


**Figure 6.3** Comparison between the slopes representing the gain estimates using PCA and LSE for varying input variance for $a$=3 & $b$=0.1 (LHS plot) and for $a$=3 & $b$=1 (RHS plot).

### 6.2.2 Dynamical Non-Linearity

Here, we extend the application of our proposed approach presented in the previous section to the frequency domain for the analysis of a dynamical non-linear system. The equation of motion for a single-degree-of-freedom (SDOF) system that exhibits a classical non-linear behaviour is the modified form of the Duffing's Oscillator

$$\ddot{x} + 2\xi\omega_0\dot{x} + (\omega_0^2 + \varepsilon x^2)x = \omega_0^2 F(t) \tag{6.13}$$

with cubic non-linearity contained in the stiffness term, which will be used in this part of our study in order to represent the characteristics of the model system whose Simulink block diagram is given in Figure 6.4. In the above expression, $x$ is the displacement, $\xi$ is the viscous damping coefficient, $\omega_0$ is the undamped natural frequency (for the linear equivalent form) and $F(t)$ is the excitation force. Our motivation is, as in the case of the linear equivalent gain estimation problem, to try to establish a method for the identification of the system characteristics statistically, using the relationship between the measured input and the measured output data when the system is excited by a Gaussian stationary random process. The SISO PCA linear equivalent FRF estimation procedure which we will follow is based on the EVD of the input-output spectral correlation matrix such as that described in Chapter 5 leading to the estimator $H_{PCA}(f)$ given by (5.8). The effects of non-linearity on the FRF computations of the above typical system have been investigated using the existing and the proposed estimators through simulations by varying some key parameters such as the variance of the excitation force and the strength of the nonlinearity through the constant factor $\varepsilon$. In essence, three extreme cases involving various combinations of noise and non-linearity effects have been considered for the performance assessment procedures and for each case magnitude and phase responses of the FRF estimators $H_1(f)$, $H_2(f)$, $H_W(f)$ and $H_{PCA}(f)$ have been calculated. Power and cross spectral densities have been estimated using 200 seconds long input (force) and output (acceleration) data sampled at 100 sps (samples per second) with 512 point Hann window zero padded to 1024 points and Fourier transformed. The undamped natural frequency of the system has been set to 5 Hz and the damping coefficient has been set to 0.05 to ensure that the resolution at the resonance frequency is sufficiently fine.

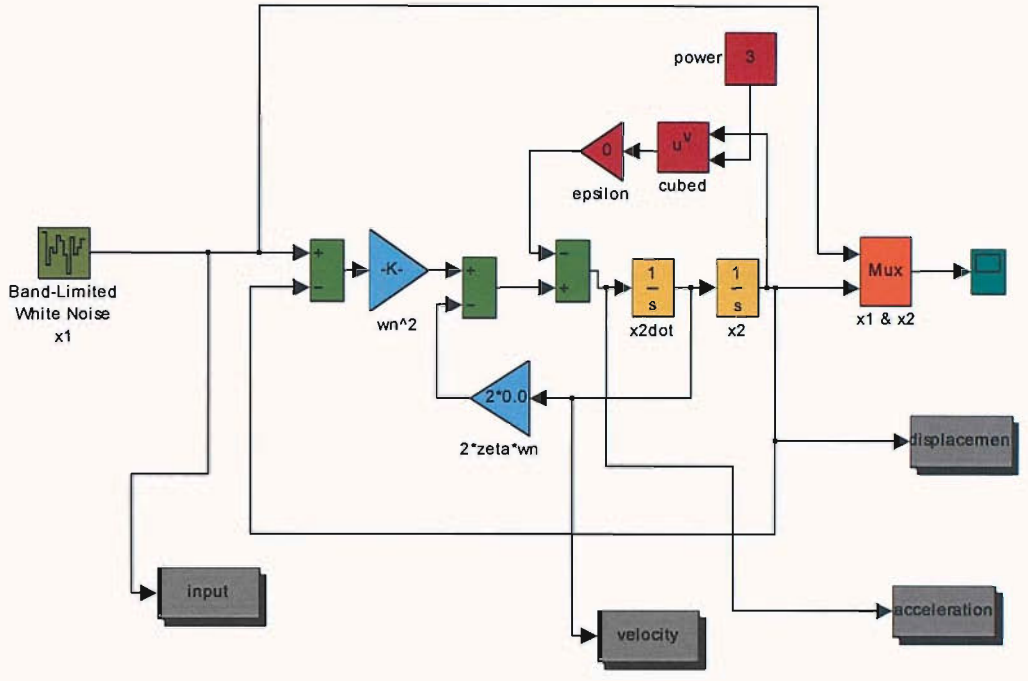


**Figure 6.4** Simulink block diagram of the Duffing's Oscillator given by equation (6.13).

Figure 6.5 shows the results obtained for the case of zero non-linearity and noise-free case. Clearly, FRF magnitude and phase estimates obtained using $H_1$, $H_2$, $H_{PCA}$ and $H_W$ give the same results over the whole frequency range as expected in accordance with the results from the simulations presented in Chapter 5 for the comparison of these estimators on a linear time-invariant (LTI) system. System response is typical of a linear time-invariant SDOF behaviour with resonance around the undamped natural frequency.

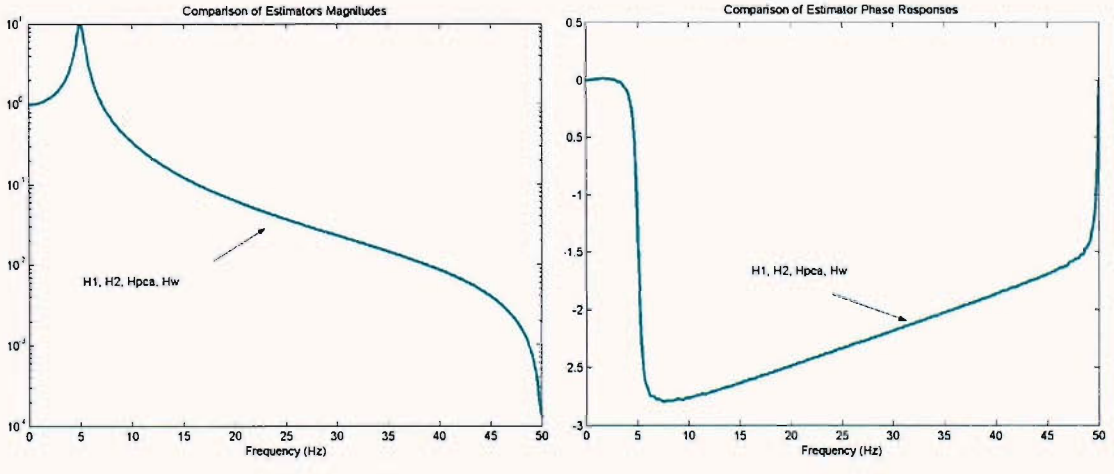


**Figure 6.5** Comparison of various FRF estimator magnitude (LHS plot) and phase (RHS plot) responses of the system described by (6.13) for zero non-linearity and noise-free case.

The second case we have considered is a high level of non-linearity with noise-free measurements. Note that, also an increase in the system excitation reinforces the significance of any potential non-linearity in the system response as well as the increase in the coefficient of the non-linear term itself. When both the non-linear coefficient ($\varepsilon$=10) and the input variance is high (equal to 100), the estimates of the equivalent FRF magnitudes obtained using various estimators give noticeably different results such as those shown in Figure 6.6. As has already been mentioned previously all of the above estimators contain identical phase information and hence it is the magnitude estimates that are of primary interest in order to give a direct comparison between their behaviours.

The estimators $H_1$ and $H_2$ are significantly different relative to the other estimators in the low and the high frequency regions respectively. The behaviour of $H_{PCA}$ and $H_W$ can be considered *most accurate* over the whole frequency range *if* we take the FRF curve of the equivalent linear system (Figure 6.5) as a reference. Also it is interesting to observe that all of the estimators indicate some systematic irregularity on both the magnitude and the phase responses at a frequency that is approximately a multiple of the first resonance i.e. possibly a harmonic of the non-linear resonance. Assuming that the actual system response tends to increase and/or change around this frequency, the magnitude estimate derived from $H_2$ reflects this behaviour most clearly. Considering its robustness for LTI transfer function estimation, the performance of $H_1$ in the low frequency region, in particular around the first resonance, is surprisingly poor again with reference to the linear equivalent FRF given in Figure 6.5.

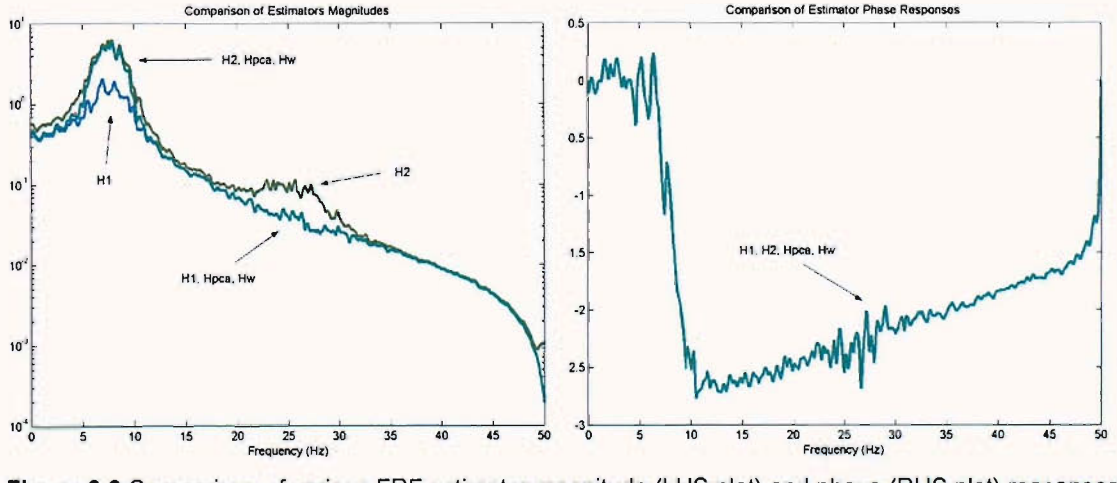


**Figure 6.6** Comparison of various FRF estimator magnitude (LHS plot) and phase (RHS plot) responses of the system described by (6.13) for high non-linearity, high input variance and noise-free case.

For the case of high non-linearity, high input variance and noise (input variance=4 and output variance=1) on both input and output (Input SNR=14 dB and Output SNR=18dB), the FRF magnitude estimate curves derived in Figure 6.7 using various estimators reveal major differences. At low frequencies especially around the resonance, the magnitude estimate obtained using $H_1$ is much lower compared to those of $H_{PCA}$, $H_W$ and $H_2$ whereas in the mid and high frequency region $H_2$ gives overestimated results compared to $H_{PCA}$, $H_1$ and $H_W$ as in the previous case but in a more amplified fashion. Despite this we have some amount of additive measurement noise on both the input and the output, due to the gain characteristics of this system especially in the mid to high frequency region output noise becomes dominant and hence the behaviour of $H_2$ is understandably poor in this region. However compared to the previous case (high non-linearity & noise-free) the magnitude estimate obtained from $H_1$ is almost identical except with higher variability over the whole frequency range. Considering the overall results from the three extreme cases, the behaviour of $H_{PCA}$ and $H_W$ may be interpreted as more consistent in terms of statistical reliability when the measurements are violated by noise contamination and the system is highly non-linear.

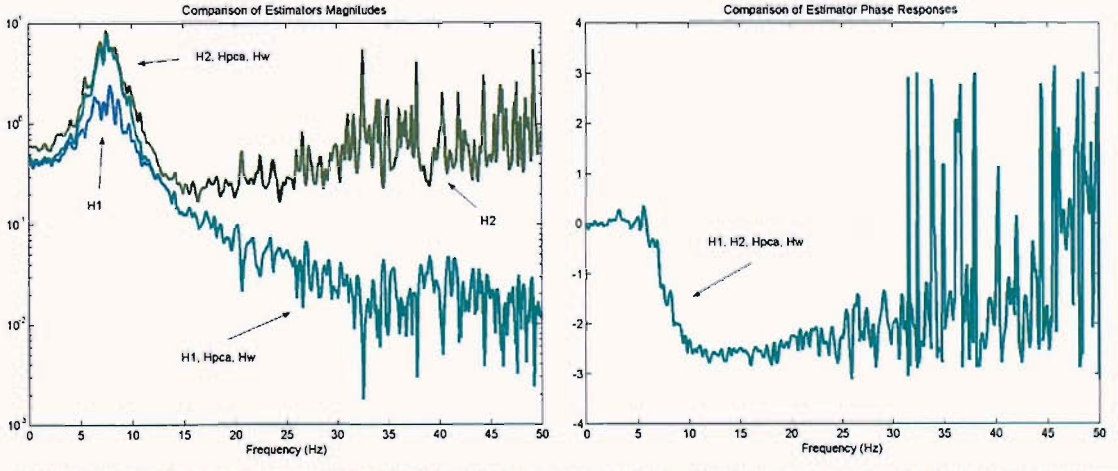


**Figure 6.7** Comparison of various FRF estimator magnitude (LHS plot) and phase (RHS plot) responses of the system described by (6.13) for high non-linearity, high input variance and noisy case.

### 6.2.3 Discussion of Results

In view of the analytical and numerical results presented in this section we can conclude that PCA linear equivalent gain/transfer function estimation regime offers a logical and consistent interpretation to the above problem and leads to a form of linearisation of the system. This regime gives results that differ from those obtained by the standard least squares optimisation technique especially for the cases of noisy measurements with high non-linearity. For the memoryless non-linear system, in the case of the amount of the non-linear effect in the system descriptor function being much smaller than that of the linear effect, the PCA gain estimates obtained results in an approximation to the slope of the linear region in the input-output curve of the system whereas if the amount of the non-linear effect is increased the estimates tend to give the line with a slope best-fitting the associated asymptotical part of the same function. The increasing trend of the slope of the first principal component as the non-linear effect is increased is an indicator of the consistency of this estimator showing that its results lead us to reliable approximations to the system's linear equivalent behaviour not only within a locally limited input excitation region but over the whole potential operation range. For the dynamical non-linear system, FRF estimates obtained using the PCA approach give consistent results with reference to the FRF of the equivalent linear system over the whole frequency range, being more robust to additive measurement noise compared to the estimators $H_1$ and $H_2$. In contrast with the conventional describing function approach, the main advantage of this approximate signal-based method can be considered to be its flexibility in terms of being able to be applied simply to any input-output data pairs without the requirement of prior knowledge/assumption of the form of the non-linearity/input excitation of the system.

## 6.3 Non-Linearity Detection

In this section we will extend the linear equivalent transfer function estimation procedures described above based on PCA to develop a virtual coherence function which can be used to detect potential non-linearities within a system and/or between signal pairs.

As has already been mentioned in Chapter 2, the ordinary coherence function (OCF) given by the expression (2.10), is a measure of the degree of linear association between two signals. It is a function of frequency with values between 0 and 1 that indicates how well a signal (which may be the input) corresponds to another signal (which may be the output) at each frequency. With reference to Figure 2.4 given $x_m$ and $y_m$ as the measured input and the measured output time histories respectively, expanding the transformation of principal components to the measured variables defined (6.2a,b) we obtain

$$x_m = t_{11}z_1 + t_{12}z_2 = x_m^1 + x_m^2 \tag{6.14a}$$

$$y_m = t_{21}z_1 + t_{22}z_2 = y_m^1 + y_m^2 \tag{6.14b}$$

where $x_m^1$ is that part of $x_m$ that is linearly related to $z_1$;

$x_m^2$ is that part of $x_m$ that is linearly related to $z_2$;

$y_m^1$ is that part of $y_m$ that is linearly related to $z_1$;

$y_m^2$ is that part of $y_m$ that is linearly related to $z_2$,

leading to the virtual TITO process in the time domain illustrated in Figure 4.2. From the above relationships, the variance of the PCA interpretations of the measured signals can be simply written as

$$Var[x_m] = Var[x_m^1] + Var[x_m^2] = t_{11}^2 Var[z_1] + t_{12}^2 Var[z_2] \tag{6.15a}$$

$$Var[y_m] = Var[y_m^1] + Var[y_m^2] = t_{21}^2 Var[z_1] + t_{22}^2 Var[z_2] \tag{6.15b}$$

i.e. in terms of the sum of the variances of those parts of each signal related to the first and the second principal components. In Chapter 2, it has been shown that with the use of PCA an original set of correlated variables are linearly transformed into a set of uncorrelated variables, the so called, principal components where the first components accounts for the maximum proportion of the total variance, second component accounts for the maximum proportion of the remaining variance and so on. It has also been shown that the sum of the eigenvalues of the measurement covariance matrix of interest is equal to the total variance (power) contained in these original variables and each corresponding eigenvector represent the direction of the variability of each component. Therefore in accordance with the procedures introduced in Sections 5.2.1 and 5.2.2, the frequency domain version of the above relationships can be logically derived as

$$S_{\underset{x_m}{1}} + S_{\underset{x_m}{2}} = |t_{11}|^2 \cdot S_{z_1} + |t_{12}|^2 \cdot S_{z_2} \tag{6.16a}$$

$$S_{\underset{y_m}{1}} + S_{\underset{y_m}{2}} = |t_{21}|^2 \cdot S_{z_1} + |t_{22}|^2 \cdot S_{z_2} \tag{6.16b}$$

in terms of the parts of the actual signal power spectral densities, virtual signal power spectral densities and the magnitudes of associated components of complex eigenvectors where $S_{z_1}$ and $S_{z_2}$ are effectively the first and the second eigenvalues of the spectral correlation matrix given by (5.5). Furthermore, in view of the interpretations given above we can conclude that the output power of the actual non-linear process consists of two main parts which can be defined as

i. Output Power due to the Primary Virtual Input,

$$S_{\underset{y_m}{1}} = |t_{21}|^2 \cdot S_{z_1} \tag{6.17a}$$

ii. Output Power due to the Secondary Virtual Input,

$$S_{\underset{y_m}{2}} = |t_{22}|^2 \cdot S_{z_2} \tag{6.17b}$$

This means that the linear association between the output power due to the primary virtual input and the output power due to the secondary virtual input can also be considered as a coherence function linking these signals through the fraction of $y_m$ that is linearly related to $x_m$. More specifically, the ratio between the primary output power and the total output power is effectively the virtual coherence function linking the measured system output $y_m$ and the primary virtual signal $z_1$, the so called first principal component.

Here this parameter forms an alternative notion in terms of the detection of potential non-linearity which can be appropriately interpreted as a Non-Linear Detection Ratio (NDR) and is given by

$$NDR = \frac{Var\left[y_m^1\right]}{Var\left[y_m\right]} = \frac{|t_{21}|^2 \cdot S_{z_1}}{|t_{21}|^2 \cdot S_{z_1} + |t_{22}|^2 \cdot S_{z_2}} = \frac{|t_{21}|^2 \cdot \lambda_1}{|t_{21}|^2 \cdot \lambda_1 + |t_{22}|^2 \cdot \lambda_2} \tag{6.18}$$

It should also be mentioned that when the effect of potential non-linearity is low compared to that of linearity in the original process the difference between the eigenvalues will be high whereas for the cases in which non-linearity becomes less dominated by the linear effect this difference will tend to decrease and hence the two virtual processes will be required to be treated as contributing to equivalent amount of the total power rather than being considered as primary and secondary. It is clear to see that although the above result has been obtained considering the measurement data as input-output pair of a system, the form of NDR given by (6.18) can be readily used to investigate the linear association between any signal pairs since the relative values of the eigenvalues and the eigenvectors of the spectral correlation matrix of interest will lead to a direct indication of the significance of non-linearity between these signals. In fact application of this result is shown through our experimental study presented in Section 6.4 demonstrating that the use of NDR on the output signal pairs of a rotating machine for fault diagnosis is useful in terms of the detection of fault induced non-linearity.

For the performance assessment of the proposed parameter relative to the conventional OCF, computational simulations have been undertaken on the SDOF Duffing system covered in Section 6.2 whose input-output relationship is given by (6.13). As before, stationary random signals have been used to represent the input excitation and additive measurement noise. Power and cross spectral densities have been estimated using the exact procedure described in Section 6.2.2. OCF curves have been derived from the expression (2.10) whereas for NDR the corresponding spectral correlation matrix have been formed using the input-output power/cross spectra and the expression (6.18) have been derived from the EVD of this matrix.

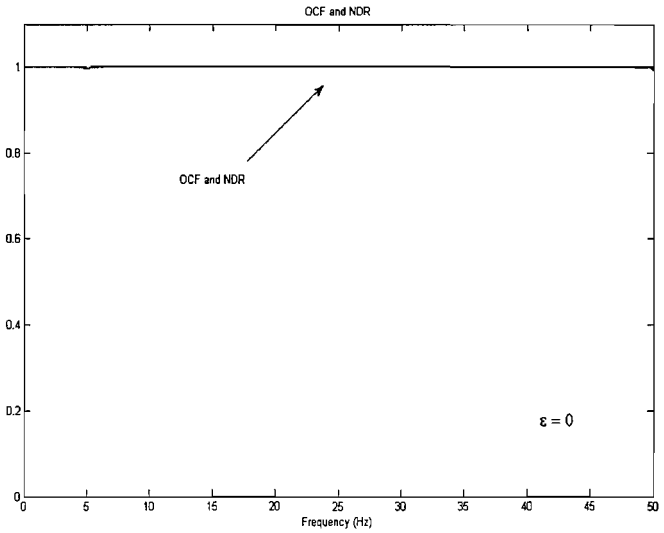


**Figure 6.8** Comparison of NDR and OCF for the case of purely linear noise-free measurements.

Figure 6.8 illustrates the comparison between the NDR and the OCF for the purely linear case (i.e. the non-linearity coefficient $\varepsilon$ is set to zero with the input variance set to 10) and noise-free measurements. NDR and OCF curves give almost exactly the same results overlapping each other, both being equal to unity over the whole frequency range.

The results of the second case is given by Figure 6.9 for which the measurements are still noise-free but this time non-linearity is introduced by setting $\varepsilon$ to 10 and input variance to 100. NDR and OCF curves have similar behaviour although they are not identical. In the low frequency region especially around the resonance of the system, NDR's dip gets much narrower compared to that of OCF. Below the resonance frequency OCF gives noticeably lower results than NDR, which appears like a biasing effect increasing towards the resonance frequency. In the mid frequency region there is a significant dip in both curves which coincides with a frequency that is approximately equivalent to the multiple (harmonic) of the first resonance frequency and is associated with a second non-linear resonance region. As can be remembered from the linear equivalent transfer function estimation results given in Section 6.2.2, this harmonic of the resonance frequency was also detected by various FRF estimators.

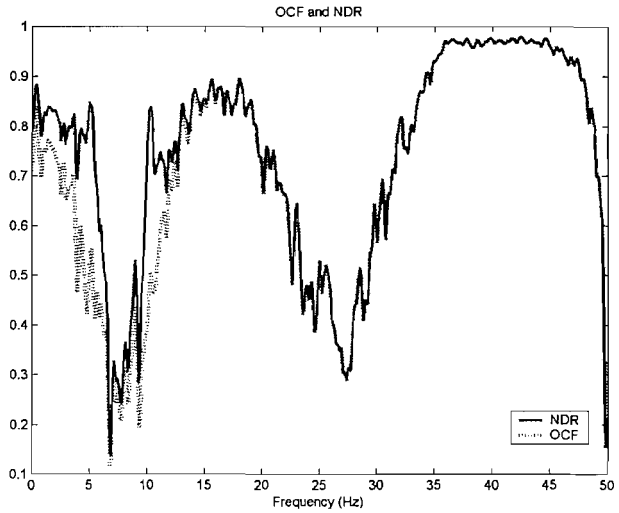


**Figure 6.9** OCF and NDR for the case of high non-linearity and noise-free measurements.

Figure 6.10 shows the NDR and OCF curves derived for the case of noisy measurements (input and output SNRs 20 dB and 18 dB respectively) and the same amount of non-linearity (with $\varepsilon$ equal to 10 and the input variance equal to 100). Due to the shaping effects of the system causing noticeably different SNR's in the low and the high frequency regions, results obtained for this case vary dramatically compared to those of the previous equivalent non-linear case with no noise. Although in the low frequency region the narrow behaviour of NDR is still obvious, towards the high frequency region, as the gain characteristics of the system decreases estimates for both parameters are severely affected by the noise with results approaching nearly zero. In addition, NDR has less variability in the low frequency region compared to OCF.

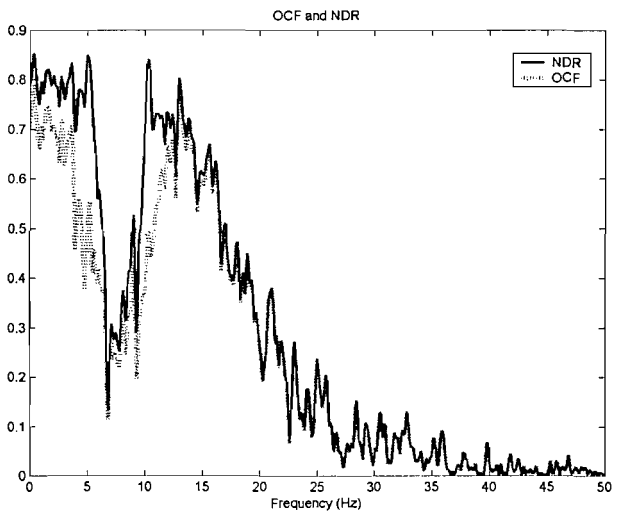


**Figure 6.10** OCF and NDR for the case of high non-linearity and noisy measurements.

The above results show that the EVD of the measured input-output spectral correlation matrix of a non-linear system leads to the direct indication of the existence of non-linearity. In particular the proposed ratio NDR is useful for measuring the degree of linear association between the input and the output and it can be considered as an effective alternative to the OCF although its performance is degraded in the presence of measurement noise. In the next section the application of the above procedure to signal-based fault diagnosis of rotating machinery is studied experimentally through the use of output signal pairs.

## 6.4 Fault Detection in Rotating Machinery

It is inevitable that faults occur during operation of rotating machinery that may damage or totally destroy the system. One of the most important areas of interest in condition monitoring of rotating machinery is that of vibration. Non-linear distortions of a vibrational signal can be used as a very sensitive indicator of damage and/or faults occurring within a rotating system. Despite the fact that, even in the absence of any form of faulty condition, signals from such machinery exhibit inherent quadratic non-linearity due to unbalance of the rotating part(s), the overall effects of nonlinear distortions on the measured signals get even more complex when faults exist.

It is possible to detect and locate major faults such as cracked shafts, shaft bow, rub condition and mass unbalance by the measurement and analysis of the vibration of rotating machinery. Today, signal-based monitoring systems for *fault diagnosis* are widely used as the result of recent developments in condition monitoring technologies. These techniques are most useful when it is impossible to model the transfer characteristics between the input(s) and output(s) of the system under investigation.

The aim of this section is to assess the practical applicability of our proposed method based on a non-parametric fault diagnosis approach using PCA whose detailed description has been given in the previous section. More specifically, the use of NDR on a real-world blind fault detection problem has been studied on a multi-output measurement system. Experimental investigations have been carried out on a compact model of a rotating machine, such as that shown in Figure 6.11, which simulates a number of categories of lateral shaft vibration. The rotor kit could be set up in various configurations in order to simulate a variety of machinery conditions e.g. mass unbalance, preload, shaft rub etc. although our measurements and analyses have focused on the detection and interpretation of shaft rub condition.

In an attempt to detect the existence of non-linearity induced by rub condition introduced within the rotor kit, PCA has been carried out on the measured XY Probe outputs data in accordance with the procedure described in the previous section. NDR curves have been computed for various cases and compared to the curves derived using the OCF method.

Our motivation here is that by analysing the degree of linear association between *output pairs* over a certain frequency range for various cases we can establish an indicative knowledge on the faulty condition of the machinery operation. The experimental layout is given in Appendix E. The model kit measures the vibration characteristics with proximity transducers positioned in purpose-built sensor mountings. The two probes (X and Y) are used in order to monitor the relative displacements in the $x$ and $y$ axes. The motor speed control of the rotating machine is a feedback controller which uses pulses from a probe observing a 20-notch wheel mounted on the rotor kit. The speed control compares this signal to the set-point signal and the difference is used for the adjustment of the motor voltage in order to maintain the set speed. A rub condition of the desired degree can be obtained by adjusting the screw in the rub housing until the screw is in contact with the shaft. Four different pairs (X and Y probes) of data sets, each being 10 seconds long, have been acquired by a frequency analyzer at a sampling rate of 16384 sps in order to represent various operational speeds and faults combinations and used for further post-measurement analysis and these are:

i. 250 RPM with no Rub Condition
ii. 250 RPM with moderate Rub condition
iii. 2500 RPM with no Rub Condition
iv. 2500 RPM with moderate Rub Condition

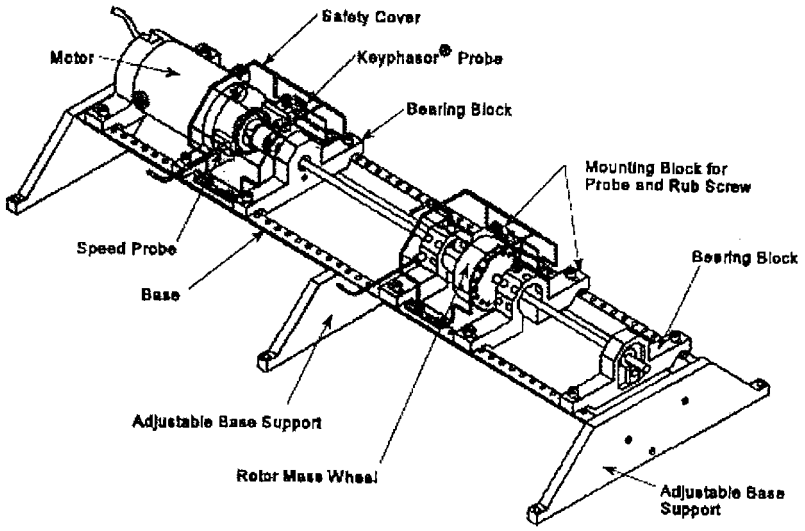


**Figure 6.11** Main components of the rotor kit (Bently Nevada).

Spectral densities of the acquired time histories have been estimated using segment averaging technique based on 8192 point Hann window zero padded to 16384 points and Fourier transformed subsequently. In Figure 6.12 each single window size of time records from the XY Proximity Probe outputs are given for the case of 250 RPM rotational speed and no fault condition whilst their corresponding PSDs are shown in Figure 6.13. As it can be clearly seen, time domain signals representing the relative displacements are periodic and the majority their energy is concentrated below around 200 Hz. Closer examination on the PSD plots reveal that the peak amplitudes of the frequency components occur at approximately every 4 Hz i.e. the fundamental frequency and it harmonics corresponding to the 250 RPM rotational speed. OCF and NDR curves (Figures 6.14) have almost exactly the same behaviour for the lowest frequency region up to 25 Hz where the signal levels are highest. Within this region there is an almost completely linear association between the signals that suddenly starts decaying and reaches its minimum values from 100 Hz onwards at irregular intervals in both curves although in the OCF plot these dips are more noticeable. This significantly low degree of linearity between signals over the major proportion of the frequency range, even for the case of no rub condition, is due the inherent non-linearity in the vibrational characteristics of rotating machinery. Both plots reveal different results in the mid to high frequency region. In general, the OCF curve has a higher variability and demonstrates a lower linear association between signals whereas for the NDR the variability is relatively low and linearity is higher. This less pessimistic behaviour of NDR can be interpreted as a more realistic representation of the non-faulty condition.

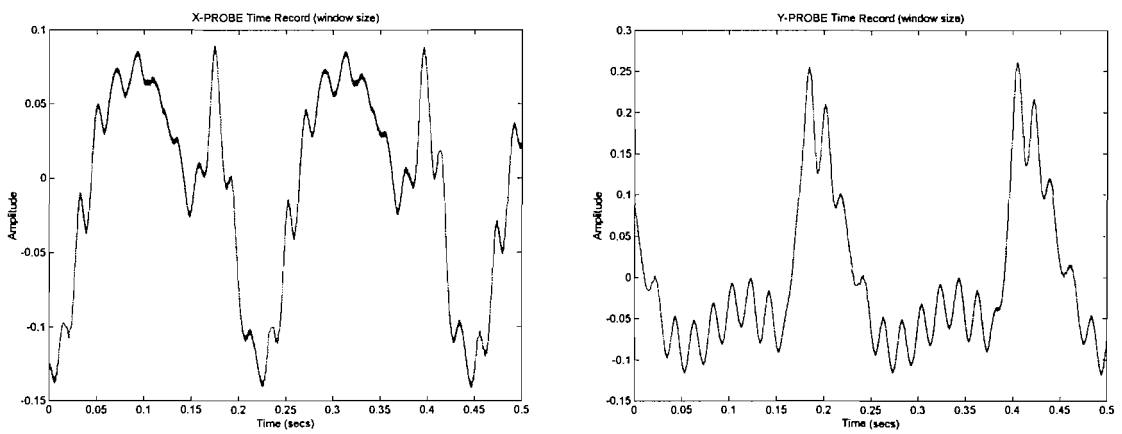


**Figure 6.12** X-Probe (LHS) and Y-Probe (RHS) output time histories for slow speed and no rub condition.

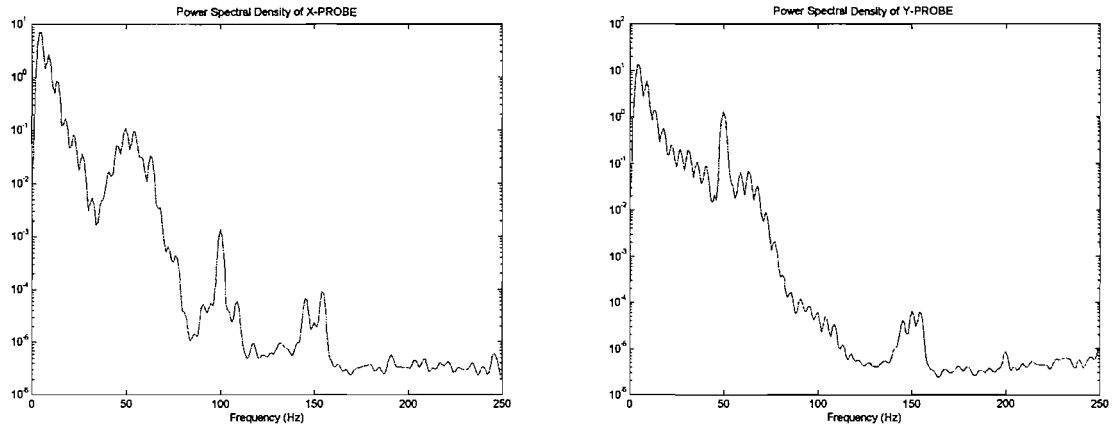


**Figure 6.13** PSD estimates of the X-Probe (LHS) and Y-Probe (RHS) output time histories shown in Figure 6.12.

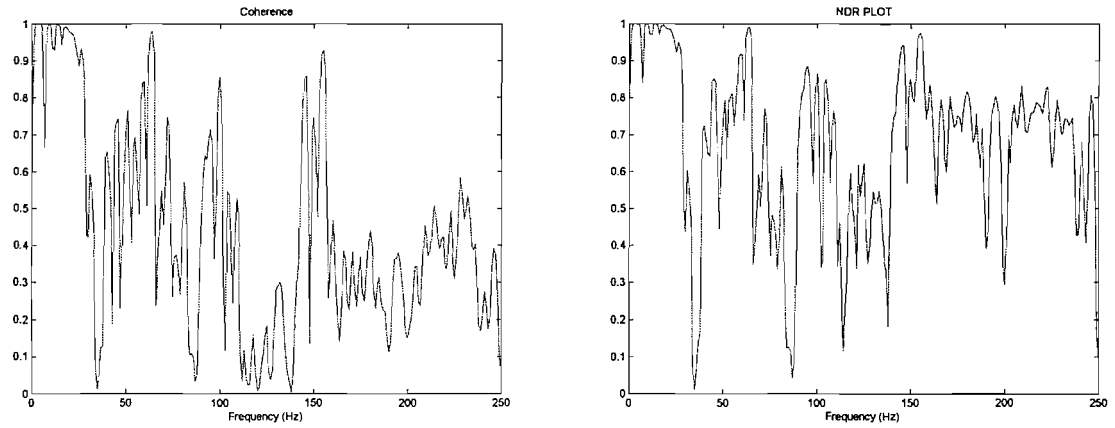


**Figure 6.14** OCF and NDR plots for slow speed and no rub condition.

Figure 6.15 shows the signals for the case of 250 RPM and moderate rub condition. Signals are still periodic but this time with significant non-linear distortions. Again, the main proportion of the energy is approximately between 0-200 Hz region (see Figure 6.16). Due to the introduction of rub condition, the overall linear association between the signals is lower compared to the previous case for both OCF and NDR such as that shown in Figure 6.17. Curves show different behaviours over the whole frequency range other than very low frequencies. Most significantly, with the introduction of the fault there is an isolated highly linear region appearing somewhere around 180-200 Hz which is broader and of larger magnitude in the NDR plot. This linear region corresponds to the relatively low energy section of the spectra. OCF seems to be severely biased in general but this time with slightly lower variability. Also for this case NDR shows relatively lower non-linear effect compared to OCF although overall it is highly non-linear considering its corresponding non-faulty case.

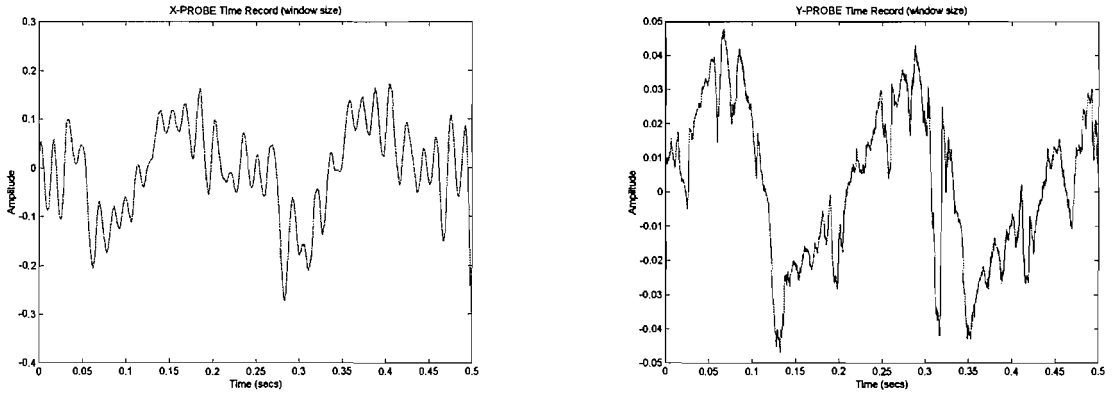


**Figure 6.15** X-Probe (LHS) and Y-Probe (RHS) output time histories for slow speed and moderate rub condition.

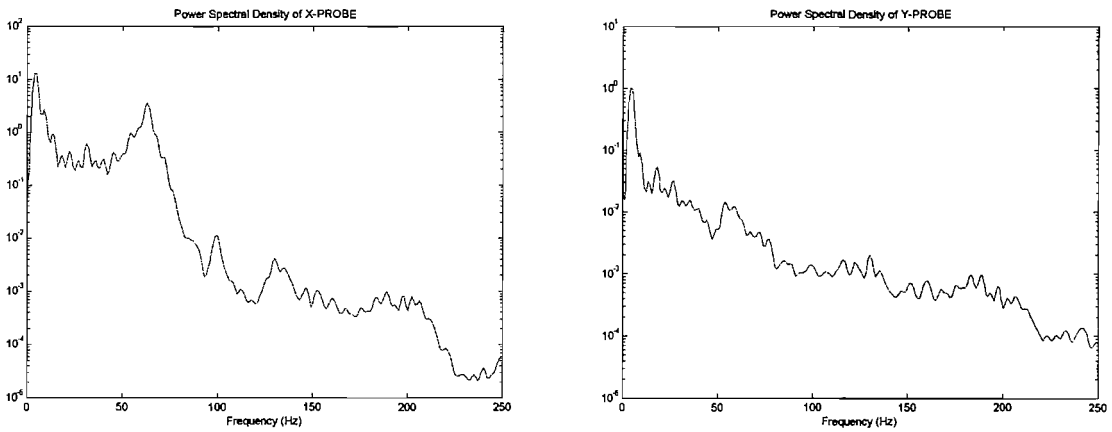


**Figure 6.16** PSD estimates of the X-Probe (LHS) and Y-Probe (RHS) output time histories shown in Figure 6.15.

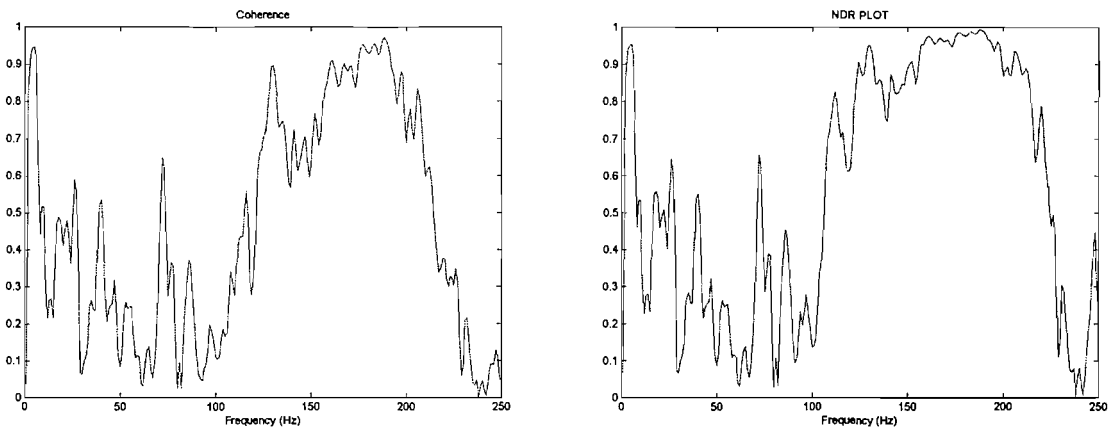


**Figure 6.17** OCF and NDR plots for slow speed and moderate rub condition.

In Figure 6.18, the outputs are given for the case of 2500 RPM rotational speed and no rub condition, and their PSDs are shown in Figure 6.19. Frequency contents of the signals have slightly increased showing spiky periodic behaviour. High amplitudes in the PSD plots appear around every 40 Hz corresponding to the fundamental frequency and the harmonics associated with the rotational speed. Time histories reveal a low-frequency amplitude-modulated almost periodic waveform with minor non-linear distortions. OCF and NDR (Figure 6.20) have similar fluctuations although OCF gives lower results over the whole frequency range. In contradiction with Cases 1 and 2, there is no almost continuous completely linear region however at discrete frequencies associated with the harmonics coherence clearly reaches maximum values for both parameters. From 100-200 Hz region upwards curves get significantly different with the NDR revealing much less non-linear behaviour. Also the variability of NDR is considerably higher in the mid to high frequency region.

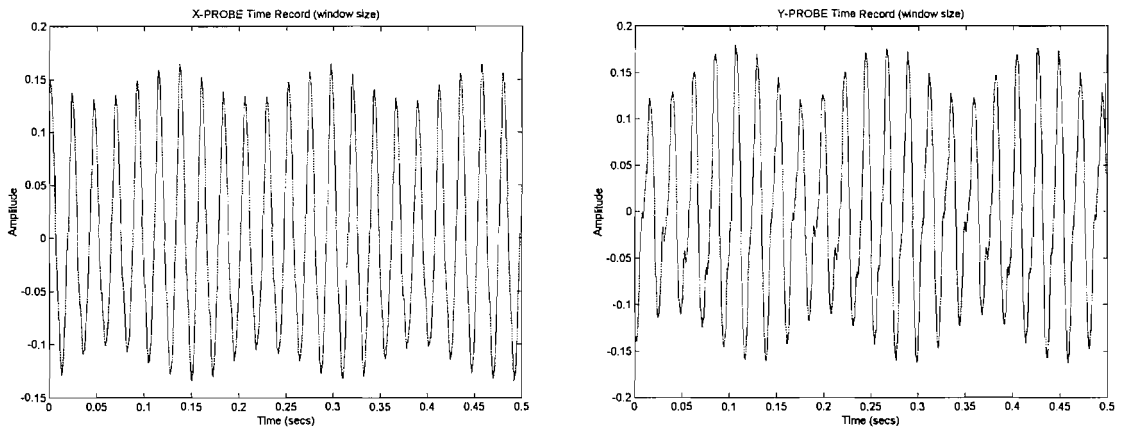


**Figure 6.18** X-Probe (LHS) and Y-Probe (RHS) output time histories for fast speed and no rub condition.

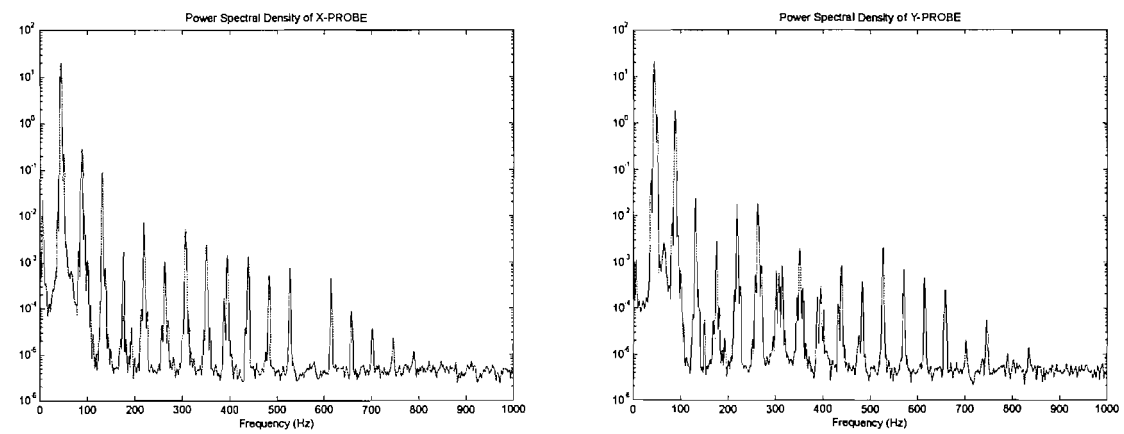


**Figure 6.19** PSD estimates of the X-Probe (LHS) and Y-Probe (RHS) output time histories shown in Figure 6.18.

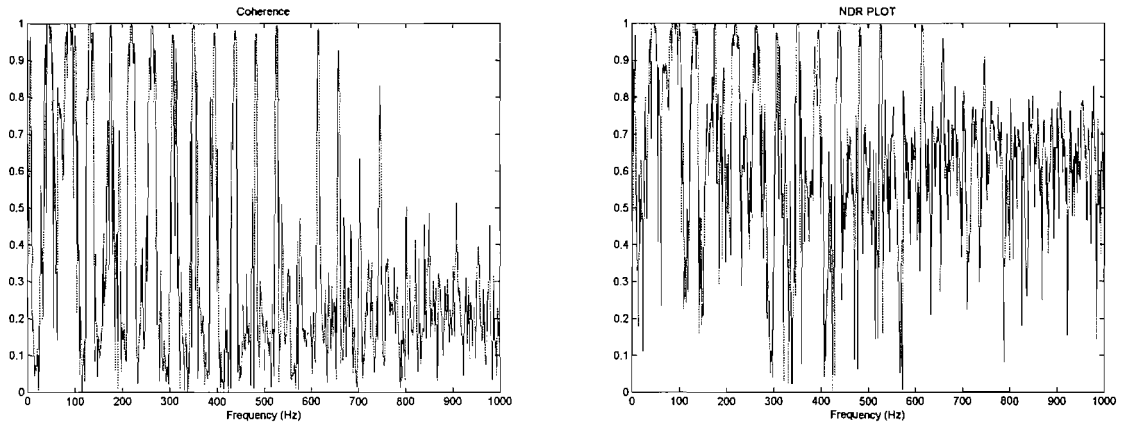


**Figure 6.20** OCF and NDR plots for fast speed and no rub condition.

Time histories from the proximity probe outputs for the case of 2500 RPM rotational speed and moderate rub condition are shown in Figure 6.21. Time domain signals representing the relative displacements reveal the same low-frequency amplitude-modulated almost periodic waveforms with much higher non-linear distortions compared to the corresponding non-faulty case. The significance of these non-linear distortions are more noticeable in the time record obtained from the Y-Probe output whereas the low-frequency modulation behaviour is more noticeable in the time record obtained from the X-Probe output. In this case, the coherence at the harmonics has decreased dramatically for both NDR and OCF (Figure 6.23). The behaviour of the computed parameters can be investigated in two separate distinctive regions which are 0 Hz to 200 Hz and 200 Hz to 1 kHz. Over the whole frequency range the OCF has a slight downward shift which can be considered a biasing effect although not as significant as in the previous cases. In the low frequency region the linear association between two measured outputs and the variability is lower except for the 180-200 Hz bandwidth as for the corresponding results of Case 2. This behaviour is believed to be rather surprising to occur only when there is a faulty condition and can be used as the main indicator of a problematical operation. Note that NDR is broader and higher at this linear region as it was for Case 2. In the mid to high frequency region both curves are very low down to values within the range 0 to 0.3 with densely packed fluctuations and high variability although OCF again gives lower results.

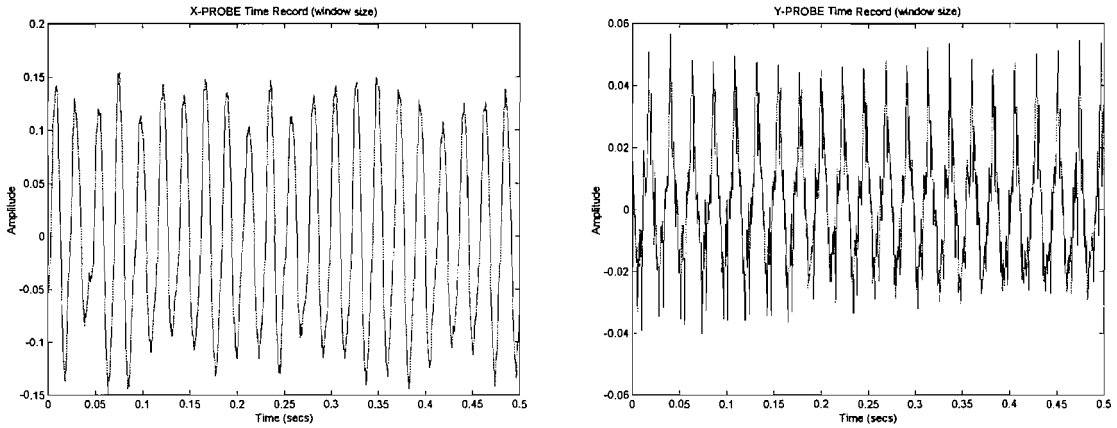


**Figure 6.21** X-Probe (LHS) and Y-Probe (RHS) output time histories for fast speed and moderate rub condition.

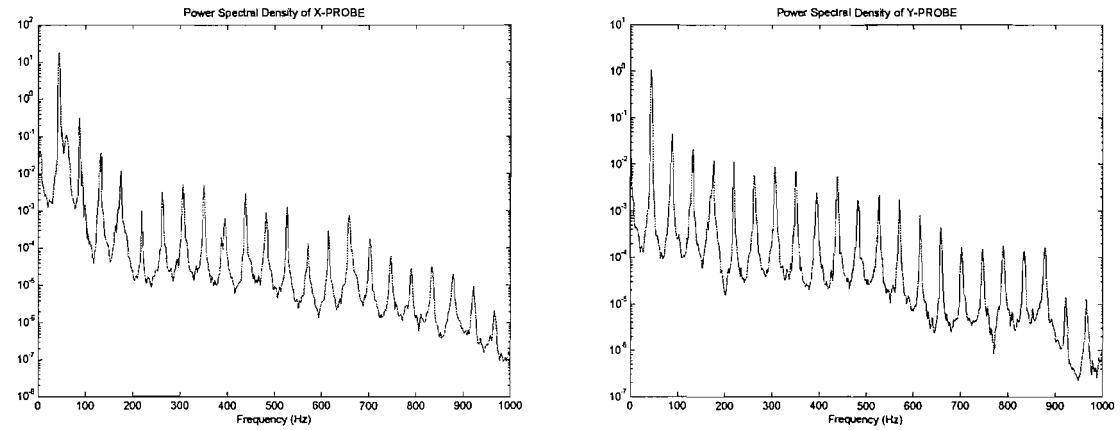


**Figure 6.22** PSD estimates of the X-Probe (LHS) and Y-Probe (RHS) output time histories shown in Figure 6.21.

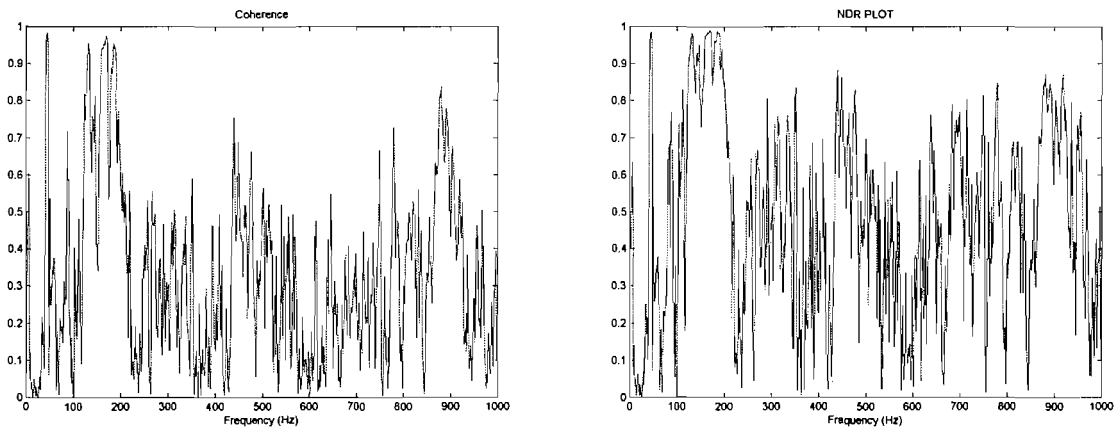


**Figure 6.23** OCF and NDR plots for fast speed and moderate rub condition.

## 6.5 Concluding Remarks

It has been shown that the use of PCA offers a simple and unified approach to SISO equivalent linear FRF estimation. The eigenvalues and the eigenvectors of the input-output spectral correlation matrix give a direct indication of the existence of non-linearity within the system. When the input-output relationship is non-linear the proposed method leads to a form of linearisation of the system which differs from the conventional *describing function* approach conceptually, but offers a logical and consistent interpretation. The relative strengths (eigenvalues) of the *principal* components is a direct indicator of the significance of the non-linearity and the eigenvectors give the features of the equivalent linear system following from the results presented in Chapters 4 and 5. Simulations show that NDR is useful in terms of measuring the degree of linear association between signal pairs, however, its performance is degraded in the presence of measurement noise and further work is required in order to eliminate the noise masking effects.

An experimental investigation has been carried out for fault (rub condition) diagnosis in rotating machinery in order to assess the applicability of the proposed method for non-linearity detection through the analysis of outputs only. Results show that OCF and NDR curves vary significantly in various frequency regions for several operating conditions and the latter has proved to be an alternate notion in terms of revealing the degree of linear association between pairs of data sets obtained from real applications. Analysis of the measured output time history pairs show that, when there is a faulty condition both OCF and NDR gives a continuous almost linear region between 180-200 Hz which is broader and higher in the EVD based technique. This interesting result can be used as an indicator of the existence of rub condition in rotating machinery following further research for its generalisation.

# Chapter Seven

# DELAY DETECTION USING PCA

## 7.1 Introduction

So far in this thesis, the applications of the principal component method to the identification of the transfer characteristics based on the gain or frequency response of various forms of linear/non-linear time-invariant systems in the time or the frequency domains have been considered through the analysis of the zero-lag covariance (or spectral correlation) matrix of input-output signals respectively.

Our objective in this chapter is focused on the detection of a non-dispersive time delay relationship between the two signals using PCA. The method proposed in this chapter may also be considered as an extension of the previous procedures in terms of generalised linear characterization for input-output relationships although this time instead of utilizing the statistical relationships between the measured signals using their zero-lag covariance (or spectral correlation) matrix only, we propose an extended time domain based approach which considers the EVD of the array of covariance matrices for a number of negative and positive time-lag (shift) values.

It is shown for both noise-free and noisy cases that, PCA, when carried out on the array of measurement covariance matrices for a sufficient number of positive and negative time-lag values of the corresponding non-dispersive single/multi path time delay system, the amount of the delay between the signals can be successfully detected by simply observing the behaviour of the series of associated eigenvalues. In the case of noise-free measurements the detection procedure gives the exact value of the time delay whereas for the cases in which the measurements are corrupted even by very high

amount of additive noise only slight deviations of the detection from the actual value occur.

Our work presented here can also be used as a reference by investigators who have been using PCA for a variety of applications, by means of interpreting their results by taking into account the influence of the potential time delay relationship within their data sets on the eigenvalues/eigenvectors and/or the principal components.

In the next section the basis of our approach and its associated mathematical derivation are presented showing the fundamental difference between the time and the frequency domain analysis in terms of the applicability of the proposed procedure whose description is given in Section 7.3 in the context of time delay detection for both single and multi path problems. In Section 7.4 a series of computational simulations are presented which has been undertaken in order to validate the analytical results and to give a direct comparison between the proposed technique and the conventional cross-correlation method for time delay detection. In the last section a summary of this chapter is given with concluding remarks.

## 7.2 Signals with Pure Delay and PCA

We have presented in our previous analyses (see Chapters 4 and 5) that when the EVD is carried out on the measurement covariance (or spectral correlation) matrix of a linear time-invariant SISO or uncorrelated-multi-input system, if the observations are noise-free then there must be at least one zero-eigenvalue. If all eigenvalues are non-zero then this is associated with the existence of various parasitic elements such as additive measurement noise or non-linear system behaviour (see Chapter 6). It has also been shown that in terms of the estimation of transfer characteristics (gain or FRF) the effect of relatively low power noise or low non-linearity could be eliminated by choosing the components of the eigenvector corresponding to the larger eigenvalue in order to approximate the system's gain/FRF characteristics. More specifically, EVD has been carried out on the zero-lag covariance (or spectral correlation) matrix of the measured variables resulting in the new uncorrelated virtual variables, the so called principal components which are ordered according to the amount of their variances. It has been shown on the SISO application that for the noise-free and purely linear case when one of the eigenvalues is zero, the non-zero eigenvalue gives the strength of its corresponding eigenvector which is interpreted as a representation of the transfer characteristics of the system under investigation whereas for the noisy and/or non-linear case the eigenvector corresponding to the largest eigenvalue can be used accordingly. Subsequently the extension of the above procedure to uncorrelated-multi-input systems have led us to the use of the components of the eigenvector corresponding to the zero-eigenvalue appropriately in order to derive the transfer characteristics.

Although the derivations and fundamental principles were introduced in the time domain for simplicity, the main part of the above analysis was considered in the frequency domain in an attempt to relate our generalised approach to practical measurement situations of various engineering applications. In neither of the transfer function analysis work mentioned above, the existence of potential time delay between the input(s) and output(s) of the corresponding system under investigation was considered. It should be noted that even if two signals are identical i.e. completely linearly related to each other with the only exception that one of them is a delayed/shifted version of the other, then the above linear characterization will result in

misleading results where the EVD of the time domain input-output measurement covariance matrix is carried out. This is because the estimate of the covariance matrix obtained from the sample populations of an original signal and its delayed version would give *false* information on the second order statistics of the data set which is fundamental to PCA. Consequently, this would result in two non-zero eigenvalues whose numerical values are relatively close to each other and hence confusing the actual linear association between the associated segments of the signals.

Therefore once again we emphasize that if two signals exhibit a completely linear association with each other the only time we get one of the eigenvalues of their covariance matrix equal to zero is when this matrix is formed for zero time lag. However this shortcoming of the above approach is of no concern if the data is stationary random and that the analysis is carried out on the spectral correlation matrix formed through Fourier-based transformations in order to estimate the system FRF. This is because once the data is linearly transformed into the frequency domain, despite its statistical properties are preserved, its shift in time becomes no longer significant in terms of correlations between its coherent parts. This is due to the fact that its power (variance) representation in the frequency domain is obtained using segments or ensembles that are ergodic.

Mathematically, the above observation can be simply verified on a linear time-invariant single path pure delay system with input $x(t)$ and output $y(t)=x(t-\Delta)$ where $\Delta$ denotes the amount of the delay introduced by the system such as that shown in Figure 7.1. The EVD of the time domain and frequency domain measurement covariance matrix can be obtained as follows: In the time domain the measurement vector over $N$ samples is given by

$$\mathbf{x}=\begin{bmatrix} x(t) \\ y(t) \end{bmatrix}_{n=1,\ldots,N}=\begin{bmatrix} x(t) \\ x(t-\Delta) \end{bmatrix}_{n=1,\ldots,N} \tag{7.1}$$

whose corresponding zero-lag (i.e. $\tau=0$ where $\tau$ denotes time/shift lag) covariance matrix will be

$$\mathbf{R}=\frac{1}{N}\sum_{n=1}^{N}\begin{bmatrix} x(t) \\ x(t-\Delta) \end{bmatrix}\cdot\begin{bmatrix} x(t) & x(t-\Delta) \end{bmatrix} \tag{7.2}$$

which can be expanded using averaging operator for computations over a sample population as

$$\mathbf{R} = \begin{bmatrix} \overline{x^2(t)} & \overline{x(t)x(t-\Delta)} \\ \overline{x(t-\Delta)x(t)} & \overline{x^2(t)} \end{bmatrix} \tag{7.3}$$

and rewritten as

$$\mathbf{R} = \begin{bmatrix} \sigma_x^2 & R_{xx}(\Delta) \\ R_{xx}(\Delta) & \sigma_x^2 \end{bmatrix} \tag{7.4}$$

where $\sigma_x^2$ denotes the input variance and $R_{xx}(\Delta)$ is effectively the auto-correlation function of the input for a time delay of $\Delta$. In order to calculate the eigenvalues of (7.4) we need to solve

$$\det\begin{bmatrix} \sigma_x^2 - \lambda & R_{xx}(\Delta) \\ R_{xx}(\Delta) & \sigma_x^2 - \lambda \end{bmatrix} = 0 \tag{7.5}$$

which can be expanded as

$$(\sigma_x^2 - \lambda)^2 - R_{xx}^2(\Delta) = 0 \tag{7.6}$$

and

$$\lambda^2 - 2\lambda\sigma_x^2 + \sigma_x^4 - R_{xx}^2(\Delta) = 0 \tag{7.7}$$

Hence we can expect the two non-zero eigenvalues

$$\lambda_{1,2} = \frac{2\sigma_x^2 \pm \sqrt{4\sigma_x^2 - 4\left(\sigma_x^4 - R_{xx}^2(\Delta)\right)}}{2} \Rightarrow \sigma_x^2 \pm R_{xx}(\Delta) \tag{7.8}$$

from which it can be seen that in general there are two non-zero eigenvalues except when $\Delta = 0$ in which case one of the eigenvalues is zero.

If we carry out the same procedure this time in the frequency domain the measurement vector takes the form (7.9) over the sample realisation index $K$ using the Fourier transform (FT) versions of the input and the output given by (7.1)

$$\Theta_k(f) = \begin{bmatrix} X(f) \\ Y(f) \end{bmatrix}_{k=1,\ldots,K} = \begin{bmatrix} X(f) \\ X_\Delta(f) \end{bmatrix}_{k=1,\ldots,K} \tag{7.9}$$

where $X(f)$ is the FT of input and $Y(f)$ is the FT of output being equal to $X_\Delta(f)$ indicating that the input has been delayed by $\Delta$ and transformed into the frequency domain. Since the relationship between the input and the output in the frequency can be written as (7.10) including the phase factor in polar form

$$Y(f) = e^{-j2\pi f\Delta} \cdot X(f) \tag{7.10}$$

then the estimation of the spectral correlation matrix

$$\hat{\mathbf{R}}(f) = \begin{bmatrix} \hat{S}_{xx}(f) & \hat{S}_{yx}(f) \\ \hat{S}_{xy}(f) & \hat{S}_{yy}(f) \end{bmatrix} \tag{7.11}$$

can be expanded in accordance with (5.9) to give

$$\hat{\mathbf{R}}(f) = \begin{bmatrix} \hat{S}_{xx}(f) & e^{-j2\pi f\Delta}\hat{S}_{xx}(f) \\ e^{j2\pi f\Delta}\hat{S}_{xx}(f) & \hat{S}_{xx}(f) \end{bmatrix} \tag{7.12}$$

Similarly, the eigenvalues of (7.12) can be obtained from the solution of

$$\det\begin{bmatrix} \hat{S}_{xx}(f) - \lambda & e^{-j2\pi f\Delta}\hat{S}_{xx}(f) \\ e^{j2\pi f\Delta}\hat{S}_{xx}(f) & \hat{S}_{xx}(f) - \lambda \end{bmatrix} = 0 \tag{7.13}$$

which can be rewritten as

$$\left(\hat{S}_{xx}(f) - \lambda\right)^2 - \hat{S}_{xx}^2 = 0 \tag{7.14}$$

and after some algebra the eigenvalues are computed as

$$\lambda_1 = 0 \text{ and } \lambda_2 = 2\hat{S}_{xx} \tag{7.15}$$

(7.15) shows that as opposed to carrying out the eigen-analysis in the time domain, if we seek to use the same strategy on the spectral correlation matrix, the resulting eigenvalues do not give any useful information on the existence of a delay relationship between the signals. Therefore, from the comparison of (7.8) to (7.15) we can conclude that for a pure delay system if the input-output data is transformed into the frequency domain we would have one zero eigenvalue from EVD of the spectral correlation matrix verifying the system's linearity whereas if the same procedure is carried out on the zero-lag covariance matrix in the time domain then we would expect to have two non-zero eigenvalues although the system is purely linear. However it should be noted that if we continue the above procedure for estimating the FRF of the input-output in accordance with the procedure described from (5.9) to (5.11) in Chapter 5, the ratio of the components of the corresponding eigenvectors leads us to the time delay information as contained in the phase factor of the transfer function.

In the upcoming section we show the exact procedure for time (shift) delay detection based on this observation.

## 7.3 Method Described

From the analyses presented in the previous section we can clearly see that if the linear time-invariant system under investigation is a pure delay with stationary random input, the EVD carried out on the covariance matrix (i.e. using time histories) and the spectral correlation matrix (i.e. using FTs of the time histories) would give two different results one of which would be misleading in terms of linear characterisation. In view of this result we propose that the former case would be utilized in order to apply PCA for the detection of potential time delay(s) introduced by the system under investigation.

In an attempt to illustrate the basic form of proposed method let us first consider the simple pure delay system with no noise contamination in any of the measured signals such as that shown in Figure 7.1 where for a time-lag $\tau$ the relationship between the input and the output can be rewritten as

$$y(t) = x(t+\tau-\Delta) \tag{7.16}$$

and the covariance matrix on which the eigenvalue-eigenvector decomposition will be carried can be modified accordingly including the time-lag such that

$$\mathbf{R}=\begin{bmatrix} R_{xx}(0) & R_{xx}(\tau-\Delta) \\ R_{xx}(\tau-\Delta) & R_{yy}(0) \end{bmatrix} \tag{7.17}$$

where $R_{xx}(0) = E[x^2(t)]$ i.e the auto-correlation function of the input which is also equal to its variance and can be denoted by $\sigma^2$;

$R_{xx}(\tau-\Delta) = R_{xy}(\tau) = E[x(t)y(t+\tau)] = E[x(t)x(t+\tau-\Delta)]$ i.e. the cross-correlation function between the input and the output for lag $\tau$.

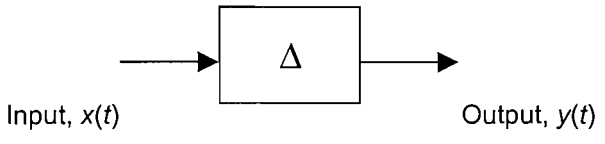


**Figure 7.1** Linear time-invariant single-path-pure-delay system where Δ is the time delay introduced to the input.

Based on (7.8), we can study the behaviour of the eigenvalues of the input-output covariance matrix for the system given in Figure 7.1, analytically. Suppose, $x(t)$ has an auto-correlation function of the form

$$R_{xx}(\tau) = \sigma_x^2 \cdot e^{-\alpha|\tau|} \tag{7.18}$$

where $\sigma_x^2$ is the signal variance and $\alpha$ is a constant scale factor. Then the input-output cross-correlation function of the above system for time lag $\tau$ is

$$R_{xy}(\tau) = \sigma_x^2 \cdot e^{-\alpha|\tau-\Delta|} \tag{7.19}$$

The corresponding eigenvalues of the pure delay covariance matrix between the original signal and its delayed version are given by

$$\lambda_1 = \sigma_x^2\left(1 + e^{-\alpha|\tau-\Delta|}\right) \rightarrow 2\sigma_x^2 \quad \text{for} \quad \Delta = \tau$$
$$\rightarrow \sigma_x^2 \quad \text{for} \quad \Delta \rightarrow \infty \tag{7.20a}$$

$$\lambda_2 = \sigma_x^2\left(1 - e^{-\alpha|\tau-\Delta|}\right) \rightarrow 0 \quad \text{for} \quad \Delta = \tau$$
$$\rightarrow \sigma_x^2 \quad \text{for} \quad \Delta \rightarrow \infty \tag{7.20b}$$

from which we can clearly see that when the time delay is equal to the time-lag one of the eigenvalues is zero whereas when the delay tends to infinity both eigenvalues converge towards each other. This means that, if the ratio $\dfrac{1+e^{-|\tau-\Delta|}}{1-e^{-|\tau-\Delta|}}$ of the eigenvalues are plotted for a series of negative and positive time lags the behaviour of the resultant curve is in the form such as that shown in Figure 7.2, indicating the value of the time delay at $\Delta = \tau$.

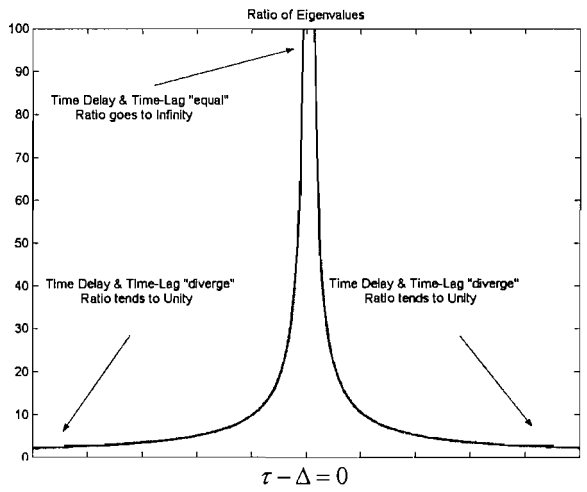


**Figure 7.2** Theoretical eigenvalue ratio of SISO pure delay system.

Therefore the delay detection procedure can simply be undertaken by forming the input-output covariance matrix in the time domain and computing its eigenvalues for a series of positive and negative lags such as that shown in Figure 7.3. We can then observe the lag value at which a zero eigenvalue is obtained which would be considered as the delay introduced to the input signal. In addition, if the signals are noise contaminated then the time lag at which the numerical difference between the eigenvalues is largest will give the delay accordingly.

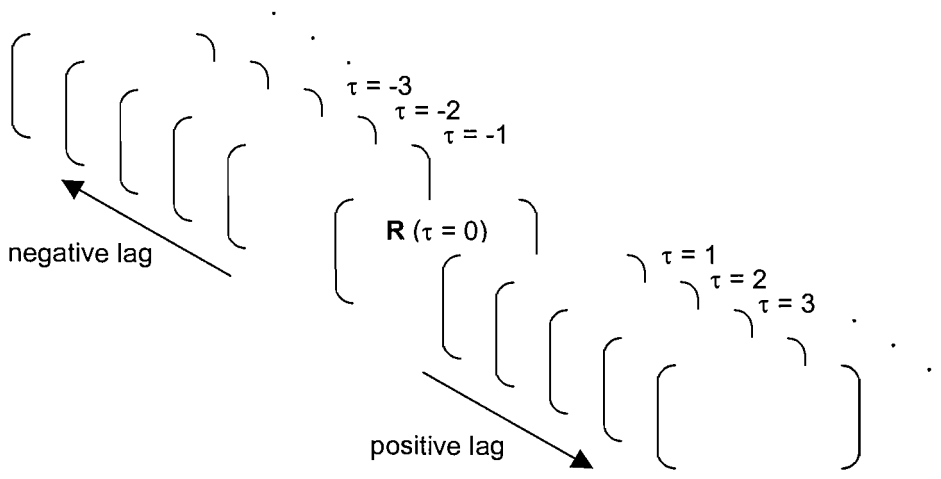


**Figure 7.3** Array of positive and negative lag input-output covariance matrices to be computed for PCA Delay Detection Technique. Egienvalues are to be observed in order identify the lag value corresponding to the amount of delay introduced on the input signal.

This application can also be generalised to various forms of multi-path systems such as that shown in Figures 7.4 and 7.5. In the first case a single input is filtered through two separate pure delay systems $\Delta_1$ and $\Delta_2$ to produce the two outputs *y(t)* and *z(t)*. Similar to the bivariate case presented in the previous paragraph also for this single-input multi-path system the EVD is to be carried out on the array of 3x3 negative and positive lag input-ouptut covariance matrices whose eigenvalues can be observed and this time two of the eigenvalues are expected to have one zero-crossing each of which are equal to the time delays $\Delta_1$ and $\Delta_2$ at the corresponding lag values respectively. The multi-path input-output covariance matrix for the case in Figure 7.4 can be obtained as follows: Forming the measurement covariance matrix for three signals as

$$\mathbf{R} = \frac{1}{N}\sum_{n=1}^{N}\begin{bmatrix} x(t) \\ y(t) \\ z(t) \end{bmatrix}\begin{bmatrix} x(t) & y(t) & z(t) \end{bmatrix} \tag{7.21}$$

and

$$\mathbf{R} = \frac{1}{N}\sum_{n=1}^{N}\begin{bmatrix} x(t) \\ x(t-\Delta_1) \\ x(t-\Delta_2) \end{bmatrix}\cdot\begin{bmatrix} x(t) & x(t-\Delta_1) & x(t-\Delta_2) \end{bmatrix} \tag{7.22}$$

which can be expanded

$$\mathbf{R} = \begin{bmatrix} \overline{x^2(t)} & \overline{x(t)x(t-\Delta_1)} & \overline{x(t)x(t-\Delta_2)} \\ \overline{x(t-\Delta_1)x(t)} & \overline{x^2(t)} & \overline{x(t-\Delta_1)x(t-\Delta_2)} \\ \overline{x(t-\Delta_2)x(t)} & \overline{x(t-\Delta_2)x(t-\Delta_1)} & \overline{x^2(t)} \end{bmatrix} \tag{7.23}$$

and rewritten as

$$\mathbf{R} = \begin{bmatrix} \sigma_x^2 & R_{xx}(\Delta_1) & R_{xx}(\Delta_2) \\ R_{xx}(\Delta_1) & \sigma_x^2 & R_{xx}(\Delta_1-\Delta_2) \\ R_{xx}(\Delta_2) & R_{xx}(\Delta_1-\Delta_2) & \sigma_x^2 \end{bmatrix} \tag{7.24}$$

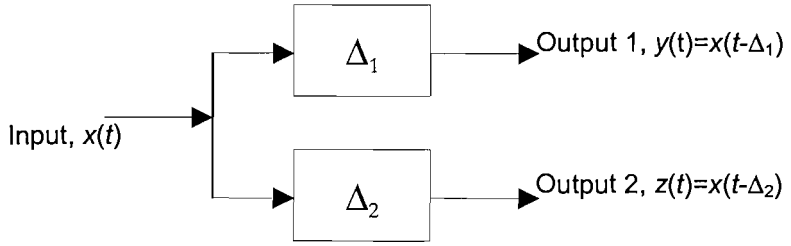


**Figure 7.4** Linear time-invariant multi-path single-input-two-output pure-delay system where $\Delta_1$ and $\Delta_2$ are the time delays introduced to Input *x(t)* to produce Output 1 and Output 2.

In Figure 7.5, a variation of the above single-input-two-output multi-path system is illustrated where a single output is produced as the sum of the two pure delay filters $\Delta_1$ and $\Delta_2$ and hence a convolutive mixture of the original input is obtained with no amplitude weighting (gain) factor. This model can be considered as a simple simulation of signal propagation in a dispersive medium. In this case the input-output covariance matrix can be derived from

$$\mathbf{R} = \frac{1}{N}\sum_{n=1}^{N}\begin{bmatrix} x(t) \\ y(t) \end{bmatrix}\begin{bmatrix} x(t) & y(t) \end{bmatrix} \tag{7.25}$$

and

$$\mathbf{R} = \frac{1}{N}\sum_{n=1}^{N}\begin{bmatrix} x(t) \\ x(t-\Delta_1)+x(t-\Delta_2) \end{bmatrix}\begin{bmatrix} x(t) & x(t-\Delta_1)+x(t-\Delta_2) \end{bmatrix} \tag{7.26}$$

which can be expanded as

$$\mathbf{R} = \begin{bmatrix} \overline{x^2(t)} & \overline{x(t)\cdot\{x(t-\Delta_1)+x(t-\Delta_2)\}} \\ \overline{\{x(t-\Delta_1)+x(t-\Delta_2)\}\cdot x(t)} & \overline{\{x(t-\Delta_1)+x(t-\Delta_2)\}^2} \end{bmatrix} \tag{7.27}$$

and the array of 2x2 input-output covariance matrices will be based on the form

$$\mathbf{R} = \begin{bmatrix} \sigma_x^2 & R_{xx}(\Delta_1)+R_{xx}(\Delta_2) \\ R_{xx}(\Delta_1)+R_{xx}(\Delta_2) & 2\sigma_x^2+2R_{xx}(\Delta_1-\Delta_2) \end{bmatrix} \tag{7.28}$$

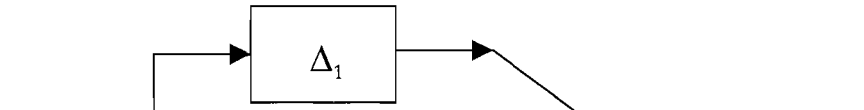


**Figure 7.5** Linear time-invariant multi-path-pure-delay system where $\Delta_1$ and $\Delta_2$ are the time delays introduced to the input.

In the next section, computational simulations for the performance assessment of the above described technique are presented. Both single path and multi path systems have been considered for noise-free and noisy measurements and the delay detection results obtained using the eigenvalues of the array of covariance matrices such as that defined above have been compared to those from the conventional input-output cross-correlation technique.

## 7.4 Performance of PCA Delay Detector

In an attempt to assess the performance of principal components method for the detection of a potential time delay relationship between signal pairs a number of simulation studies have been undertaken. The schematic diagram of the signal generation mechanism used is given in Figure 7.6 where a stationary random input is first low-pass filtered in order to form a band-limited signal $x(t)$ and zero padded at both ends increasing the total sample to allow a shift (time delay) to be introduced and then passed through a single or multi path delay system of one of the forms such as that described in the previous section (see Figures 7.1, 7.4 and 7.5) producing the corresponding output(s).

Zero-pole map, impulse response and frequency response functions of the AR(1) low-pass filter is given in Figure 7.7. Figure 7.8 shows a typical stationary random time history and its corresponding auto-correlation function. Signals within the boundaries of the model systems under investigation have been considered for both noise-free and noisy cases. Noisy cases have been particularly chosen to have very poor signal to noise ratios (SNRs) in order to examine the robustness of the method under conditions with extreme measurement errors.

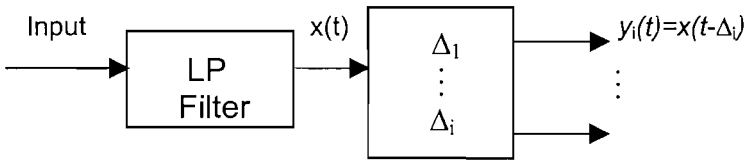


**Figure 7.6** Schematic diagram of low-pass filtered and delayed signal for delay detection computations.

The first simulation study involves a noise-free single-path problem where the output signal being delayed by 50 sample points relative to its corresponding input. Figure 7.9 LHS shows the signals and their cross-correlation function from which it can be clearly seen that the maximum of the correlation function occurs exactly at the time lag equal to the delay of 50 points. In Figure 7.9 RHS the eigenvalues of the array of covariance matrices and their ratios are plotted against the corresponding time lag values verifying that for the covariance matrix computed for the time lag equal to the delay the difference between the two eigenvalues reaches a maximum where one of them equals to zero and hence the ratio of the larger one to the smaller one at that point goes to infinity.

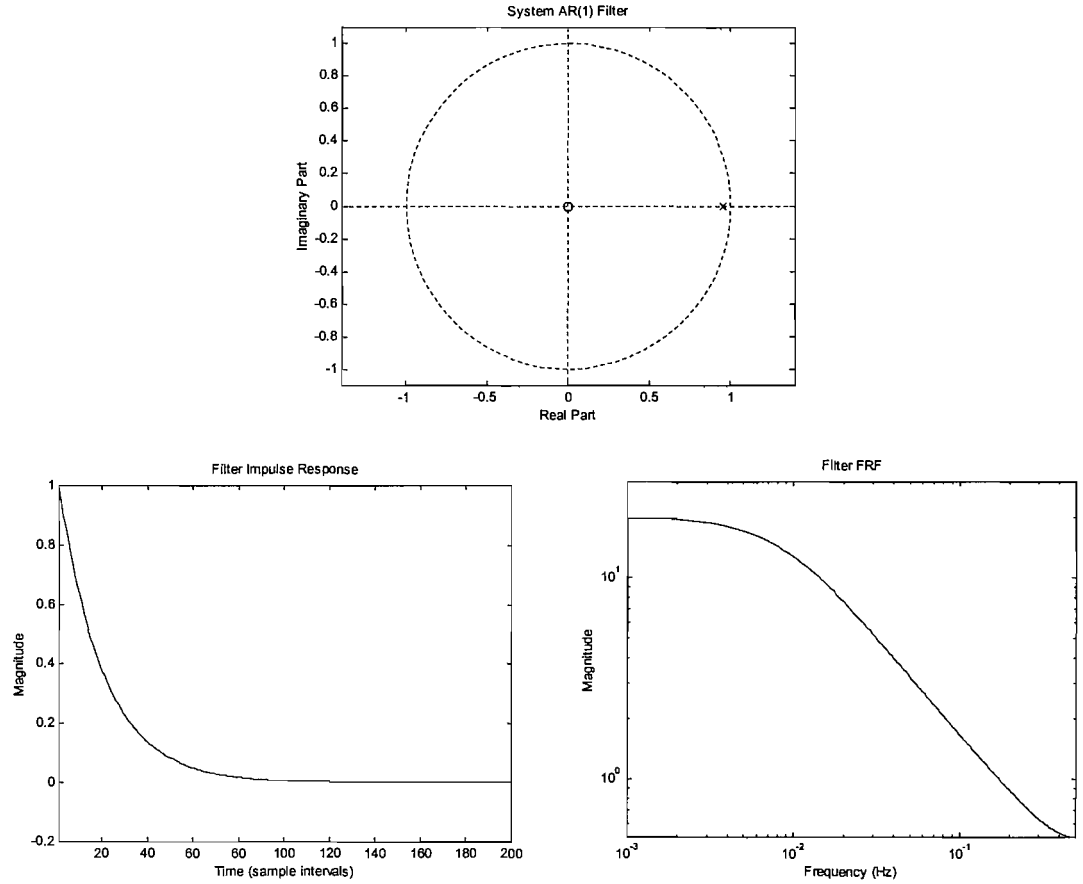


**Figure 7.7** Zero-Pole Map (top), Impulse Response (bottom-left) and the Frequency Response (bottom-right) of the AR(1) digital low-pass filter.

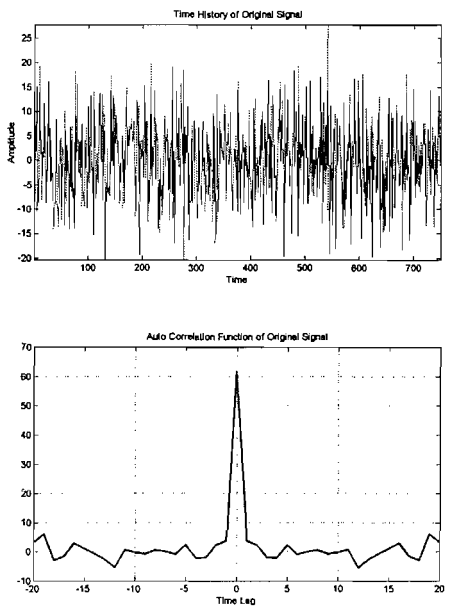


**Figure 7.8** Time history and auto-correlation function of typical stationary random data used as original signal for computations.

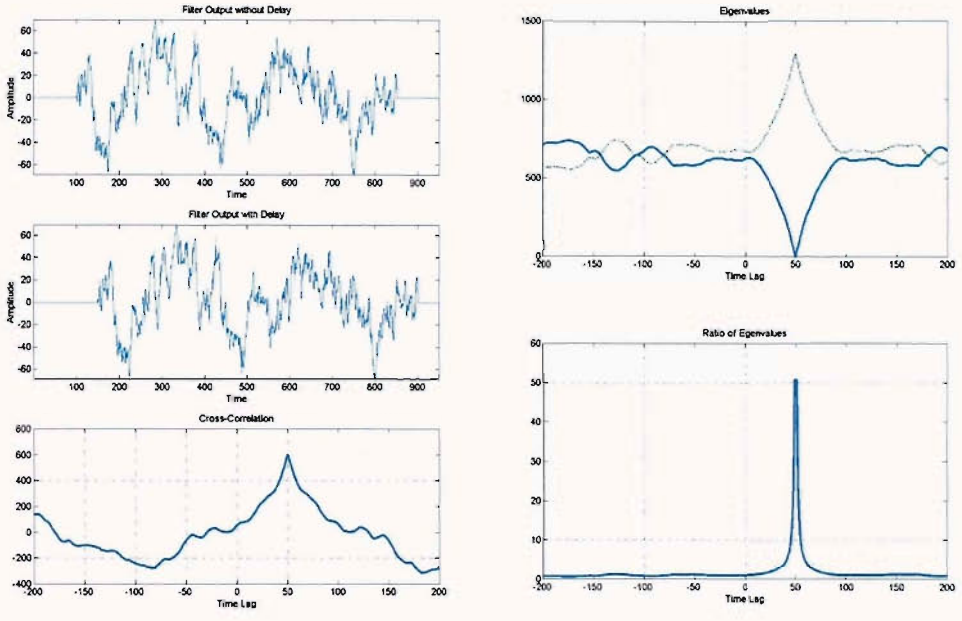


**Figure 7.9** LHS: Noise-free original and delayed (50 points) signals and their cross-correlation. RHS: Eigenvalues of the array of covariance matrices and their ratios for corresponding time lag values. In the top figure, solid and dotted curves illustrate each of the eigenvalues respectively.

In addition to the above noise-free case Figure 7.10 LHS shows the input-output signals of the same single-path system (i.e. output delayed by 50 points) and their cross-correlation function estimate this time for the case of both signals with high amount of noise contamination with SNRs of approximately -5dB. Also for this case the maximum of the cross-correlation function detects the time delay with considerable accuracy occurring at the time lag value only slightly lower than 50. The eigenvalues of the array of input-output covariance matrices and their ratios are illustrated in Figure 7.10 RHS. It can be clearly seen from this figure that although both eigenvalues are non-zero at the time lag value of around 50 due to parasitic effects induced by severe noise, the difference between the eigenvalues reaches its maximum value and hence the time delay has been detected using our PCA-based approach as accurately as the cross-correlation method.

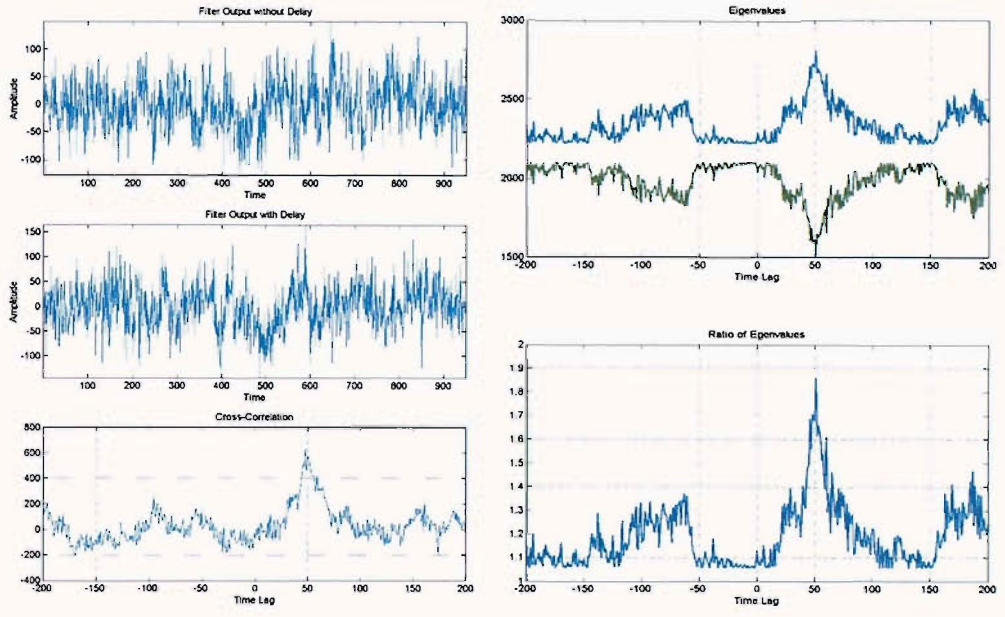


**Figure 7.10** LHS: Noisy version of the signals and their cross-correlation given in Figure 7.9. RHS: Eigenvalues of the array of covariance matrices and their ratios for corresponding time lag values. In the top figure, blue and green curves illustrate each of the eigenvalues respectively.

The second set of simulation studies we have considered are for a single-input multi-path system such as that illustrated in Figure 7.4, i.e. the output index shown in Figure 7.6 is 2. The outputs of the above low-pass filter have been delayed by 50 and 125 points respectively and the PCA-based delay detection technique applied this time on the array of 3x3 input-output covariance matrices formed using the three signals in accordance with the form given by (7.21) to (7.23). Figure 7.11 LHS shows the input-output signals and the cross-correlation estimates of each delayed output with the original input signal for the noise-free case. Maximum values of the cross-correlation estimates occur exactly at the time lag values 50 and 125 respectively corresponding to the time delays introduced on each signal. From Figure 7.11 RHS, it can be easily seen that, as expected from our analytical results given in the previous section, this time one of the eigenvalues is equal to zero for the time lag values of 50 and another eigenvalue is equal to zero for the time lag value of 125. When each of these eigenvalues have zero values in turn, one of the other two remaining eigenvalues reaches the overall maximum value and hence verifying that the associated input-output pair has a total collinearity.

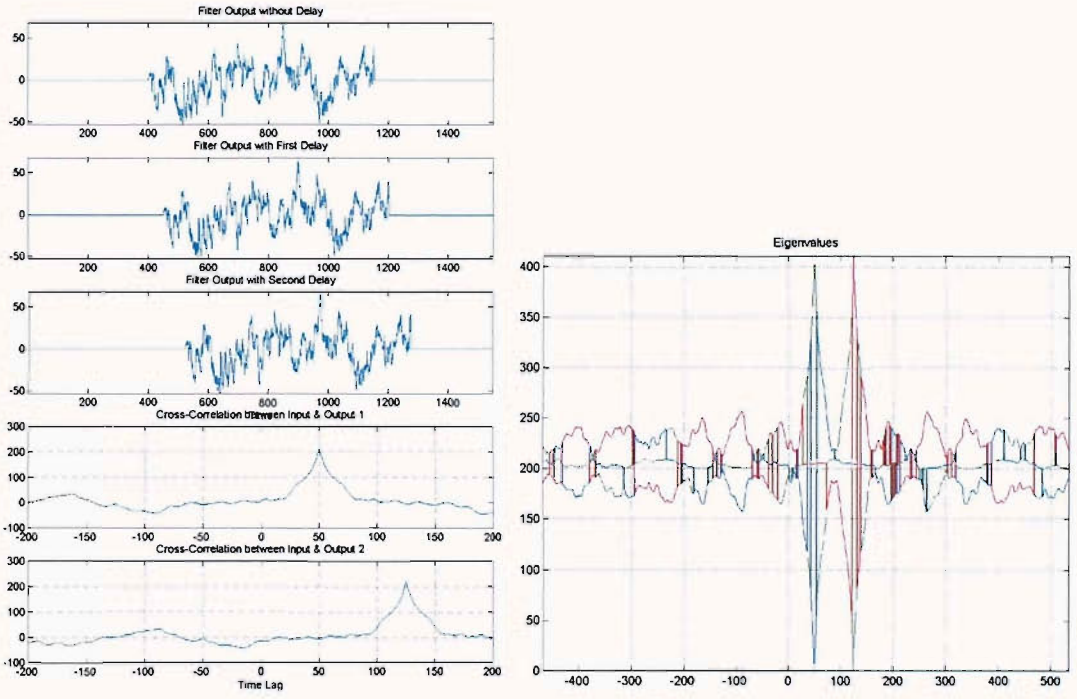


**Figure 7.11** LHS: Noise-free original and delayed (50 and 125 points) signals and their cross-correlation based on the system given by Figure 7.4. RHS: Eigenvalues of the array of covariance matrices for corresponding time lag (*x*-axis) values. Each of red, blue and green solid lines represent one of the eigenvalues.

Further investigations on the same system are carried out for the case of high noise on all three signals with SNRs around 1dB. Figure 7.12 LHS shows the noisy signals and the corresponding cross-correlation estimates. As for the noise-free case the maxima of the correlation functions indicate the amount of the time delays introduced to the corresponding signals with substantial accuracy. From the eigenvalue plots of the corresponding covariance matrix array (Figure 7.12 RHS) one can see the considerable irregularity on their behaviour compared to the corresponding noise-free case although both time delay values can be easily detected observing the time lag values at which the maximum difference between eigenvalue pairs occur.

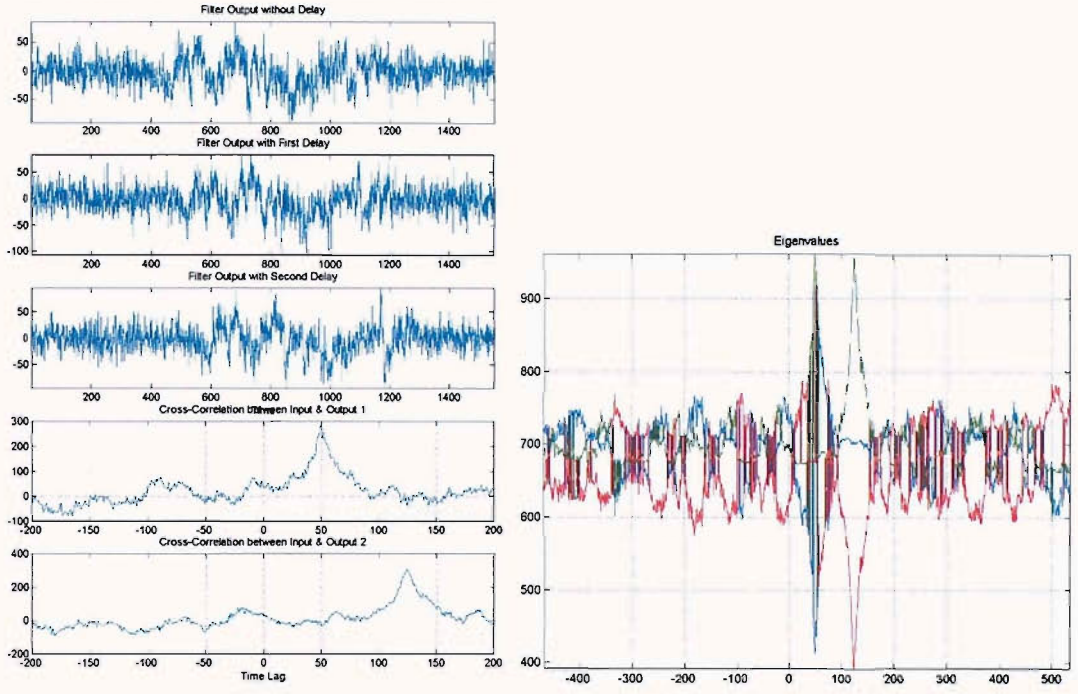


**Figure 7.12** LHS: Noisy version of the signals and their cross-correlation given in Figure 7.11. RHS: Eigenvalues of the array of covariance matrices for corresponding time lag (*x*-axis) values. Each of red, blue and green solid lines represent one of the eigenvalues.

The final set of simulations is based on the system model shown in Figure 7.5 where a single-input multi-path system gives a single-output as the sum of two separately delayed signals (50 and 125 points respectively). Figure 7.13 LHS shows the noise-free input and the output signals and their cross-correlation. The eigenvalues of the input-output covariance matrices and their ratios for the noise-free case of the mixing system shown in Figure 7.13 RHS indicate that unlike the previous noise-free cases there is no zero-eigenvalue due to the corruption of the original waveform by the summation of the individual outputs. Consequently this leads to less-correlated signals contained in the measurement vector although at the lag values equal to the individual delays the difference between two eigenvalues reach their highest values. The corresponding noisy case is illustrated in Figure 7.14. Despite low SNRs, also in this case the greatest difference between the eigenvalues occur at the exact values of the delays showing that the proposed method is also suitable for additive multi-path delay detection as described by the form (7.25) to (7.27).

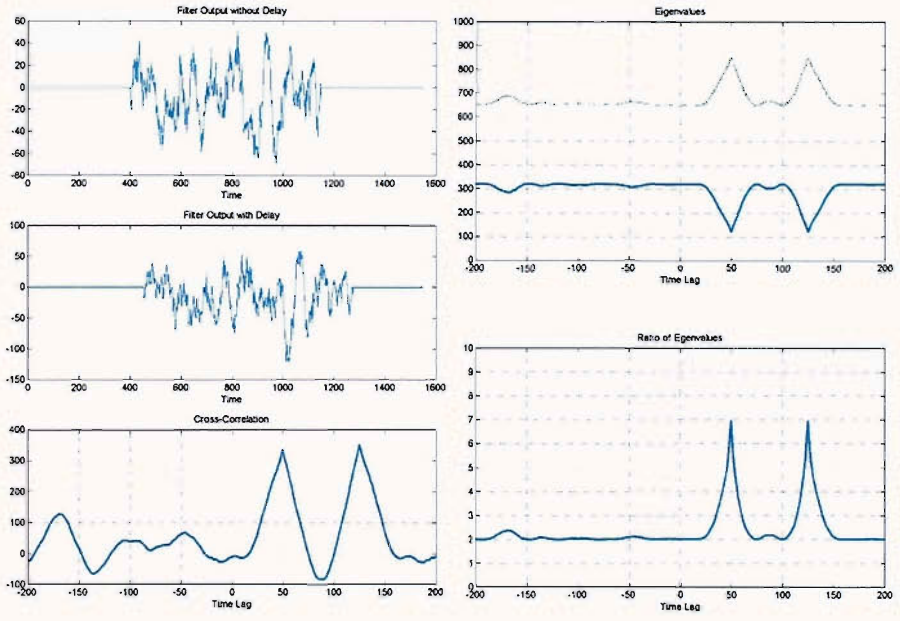


**Figure 7.13** LHS: Noise-free original and delayed (50 and 125 points) signals and their cross-correlation based on the system given by Figure 7.5. RHS: Eigenvalues of the array of covariance matrices and their ratios for corresponding time lag values. In the top figure, solid and dotted curves illustrate each of the eigenvalues respectively.

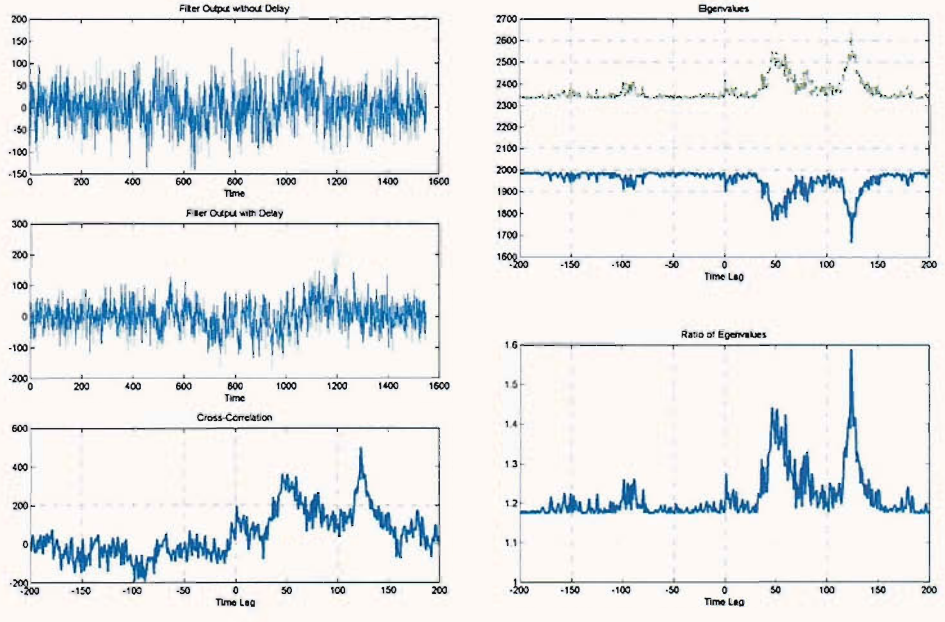


**Figure 7.14** LHS: Noisy version of the signals and their cross-correlation given in Figure 7.13. RHS: Eigenvalues of the array of covariance matrices and their ratios for corresponding time lag values. In the top figure, solid and dotted curves illustrate each of the eigenvalues respectively.

## 7.5 Concluding Remarks

In this chapter the use of the linear transformation technique of PCA as a delay detector has been investigated through a novel approach in terms of the use of the technique over an array of covariance matrices for a series of time lags between the signals within the data set under investigation which can be bivariate or multivariate of various forms.

Our motivation for the work presented above originates from the basic fact that if the data set to be analysed using PCA-based EVD exhibits simply mutual pure delay relationship, then in the time domain one would get the maximum difference between the associated eigenvalues only for the covariance matrix which is formed for the time lag value equal to the amount of the delay by which the signals are related to each other. Otherwise, for all other time lag covariance matrices, the low cross-correlations between the signals would lead to relatively close-valued eigenvalues and hence the consequent information based on low degree of linear association between the signals would be obtained from the analysis.

We have also shown that if the above analysis is carried out in the frequency domain, the cross-correlation information between the coherent parts of the signals is lost as a result of Fourier transformation based on segmentation or ensemble techniques and subsequently the potential time delay(s) cannot be detected through the observation of the corresponding eigenvalues.

This chapter is considered to be extremely useful in terms of introducing an application of PCA to a form of input-output relationship of linear time-invariant systems from a different viewpoint compared to the rest of the thesis.

# Chapter Eight

# PCA FOR TIME-VARYING PROCESSES

## 8.1 Introduction

The use of PCA for signal-based system identification has been investigated by means of several forms in the previous part of this thesis. Applications have included gain/FRF estimation of linear time-invariant systems, linear equivalent transfer function estimation of non-linear systems as well as detection of time delay introduced by various pure delay systems. In all cases mentioned above we have considered the system inputs as stationary random time histories and most importantly the system characteristics as not changing with time, leading us to the corresponding outputs that are also stationary random.

The basis of our analysis has comprised the EVD of the input-output covariance matrix and the observation of the associated eigenvalues and eigenvectors in order to establish the degree of linear association between these signals. This procedure and its variations (originating from the same basic approach) provided us with the opportunity to interpret the relevant results in different ways with the restriction that the system properties were constant.

In real life, however, especially in many engineering applications one may come across a variety of data whose statistical structure change with time, the so called non-stationary processes. Regardless of the statistical properties of their input(s), the output(s) of time-variant systems always exhibit non-stationary behaviour of some form. Non-stationary processes may arise from linear or non-linear time variant systems as well as non-linear time-invariant systems.

A set of common methods used for the investigation of non-stationary processes are based on *time-frequency analysis* such as the short-time Fourier transform (STFT), Wigner-Ville distribution, wavelet transform etc. These subjects are beyond the scope of this thesis except for the STFT which will be briefly described and used in several signal spectrogram computations for comparison purposes.

In this last part of our study we introduce a procedure for the preliminary detection of non-stationary signals/systems through the use of PCA in a view to provide useful information for further analysis. The method proposed is based on a conceptually different approach from the rest of the thesis in terms of the formation of the pairs of bivariate data sets on which the EVD is carried out although the basic principle remains the same i.e. the extraction of the degree of collinearity between data sets using second order statistical information.

Section 8.2 gives an overview to the problem of non-stationarity detection using PCA in terms of the analysis principles on which our approach is based on. In Section 8.3, the short-term PCA for time-varying gain detection in the time domain is introduced whereas Section 8.4 presents the details of the extension of this method for the estimation of non-stationary dynamics using moving segment EVD of spectral correlation matrices, the so called short-term spectral PCA (STSPCA). Both sections also include results from a number of computational simulations for the performance and applicability assessments of the methods. Concluding remarks are summarised in Section 8.5.

## 8.2 Non-Stationarity and PCA

A stochastic signal is said to be non-stationary if its statistical structure changes as a function of time e.g. the mean, variance, correlation etc. may vary with time and consequently the joint probability density relating the values of signal $x(t)$ at times $t_1$, $t_2$, $t_3$, ..., also varies under a shift in time. Signals which may not be considered strictly random can also display a structure that can also be described as non-stationary e.g. chirp signal which has a changing frequency. Either deterministic or stochastic, non-stationary processes with numerous forms of varying structures such as that described in the first paragraph, often arise in the physical world. Examples include birdsong, speech, noise and vibration signals from accelerating traffic, Doppler shifted sound, vibration response of machinery undergoing operational changes and so on. It has long been an interest for the analysis of non-stationary signals in statistical signal processing since it is crucial for many fields of engineering being able to detect, interpret and model potential non-stationarities within measurement systems and/or hidden in observed data sets in order to identify the system characteristics and/or for further prediction/analysis purposes.

The main proportion of our research has been involved with the application of PCA for linear characterisation of multivariate data. This has been carried out through the observation of the eigenvalues and eigenvectors of the corresponding input-output measurement covariance (or spectral correlation) matrix which allowed one to readily identify components of low power (or one component whose power is represented by a zero eigenvalue for the ideal linear time-invariant system) that may be removed from the data set without significantly affecting the data. Subsequently the *principal* components have been related to the original variables via a virtual process in order for the linear (equivalent) transfer characteristics to be derived. We have shown that this procedure could be used as an effective tool for the estimation and/or detection of gain, FRF, delay or non-linearity when the data sets forming the covariance matrix to be analysed consist of system input(s) and output(s).

The basic principle of our previous system input-output relationship analyses for the above given cases was based on the EVD of the ensemble (or segment) averaged measurement correlation matrix directly i.e. with no pre-processing perhaps only except for standardisation (centring and scaling). This measurement matrix was assumed to be

formed between data sets that are assumed to be related through a *constant scale factor* and hence having time-invariant statistical structure. Therefore increasing the sample size of each segment would reduce any biasing and/or variability effects consistently resulting in the assumption that for two stationary random signals whose time domain measurement vector for each ensemble (segment) realisation given by

$$\mathbf{x}_k = \begin{bmatrix} x_{m_k} \\ y_{m_k} \end{bmatrix}, \text{ for } k=1,2,\ldots,K;$$

the covariance matrix (for zero-mean variables) can be simply estimated from

$$R_{xx} = \begin{bmatrix} E[x_{m_k}^2] & E[x_{m_k} y_{m_k}] \\ E[y_{m_k} x_{m_k}] & E[y_{m_k}^2] \end{bmatrix}_{k=1,\ldots,K} \approx \frac{1}{N} \begin{bmatrix} \sum_{i=1}^{N} x_{m_i}^2 & \sum_{i=1}^{N} x_{m_i} y_{m_i} \\ \sum_{i=1}^{N} y_{m_i} x_{m_i} & \sum_{i=1}^{N} y_{m_i}^2 \end{bmatrix} \tag{8.1}$$

where $E[\ ]$ denotes the expectation operation and the sample index is defined by $i=1,\ldots,N$. Above procedure relies on the assessment of the degree of linear association between signal pairs using the eigenvalues and their corresponding eigenvectors. Here we propose to extend this approach to extract some useful information about the time-varying structure of the data set with particular reference to varying mean and/or variance in the time domain and varying frequency content and/or energy distribution in the frequency domain by applying a modified PCA procedure. If we assume that a non-stationary system is excited by a stationary random input then the output signal will be non-stationary. Therefore, in this case, using the procedure for the computation of the measurement correlation matrix such as that described by (8.1) would be *conceptually incorrect* because the input and the output would have different statistical properties being related through a *varying scale factor* and hence the second order statistical information contained in the covariance matrix would be useless. Note that the covariance matrix estimator given by (8.1) is valid if the variables have constant probability densities i.e. which do not vary under a shift in time. However we would of course still get some results from the EVD of the covariance matrix in question above although the direction of the principal component would lead us to a form of averaged gain factor relating the input and the output rather than extracting any potential time varying characteristics within the corresponding parts of the signals. The mathematical verification of this restriction is as follows:

Consider the specific example where the memoryless SISO system given in Figure 8.1 is assumed to be linear and *time-variant* with gain $a(t)$ which varies in a *deterministic* fashion with the input-output relationship of the form (8.2) so that one can expect the system output to be a stochastic non-stationary process.

$$y(t) = a(t).x(t) \tag{8.2}$$

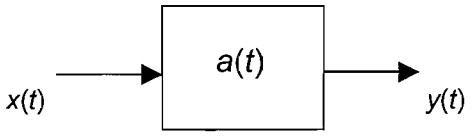


**Figure 8.1** Linear Time Varying Memoryless SISO Gain System.

Using the expectation operator for the estimation of a local input-output covariance matrix for the segment $k$ we get

$$\mathbf{R}_{xx}(t) = E\begin{bmatrix} x^2(t) & a(t)x^2(t) \\ a(t)x^2(t) & a^2(t)x^2(t) \end{bmatrix}_k \tag{8.3}$$

and expanding (8.3) by substituting the symbol $\sigma^2$ as appropriate to denote the signal variance, we obtain

$$\mathbf{R}_{xx}(t) = \begin{bmatrix} \sigma_x^2 & a(t)\sigma_x^2 \\ a(t)\sigma_x^2 & a^2(t)\sigma_x^2 \end{bmatrix}_k \tag{8.4}$$

whose eigenvalues can be derived from the solution of

$$\det\begin{bmatrix} \sigma_x^2 - \lambda & a(t)\sigma_x^2 \\ a(t)\sigma_x^2 & a^2(t)\sigma_x^2 - \lambda \end{bmatrix} = 0 \tag{8.5}$$

from which

$$\lambda_1 = \sigma_x^2[1 + a^2(t)] \text{ and } \lambda_2 = 0 \tag{8.6}$$

which shows that despite the fact that the gain is time-varying in the global sense if it's local value is assumed to be constant within the limits of the segment $k$, one of the eigenvalues will be zero and the principal component power will be contained within the non-zero eigenvalue whose corresponding eigenvector's direction after some algebra can be derived as

$$\frac{t_2}{t_1} = a(t) \tag{8.7}$$

Note that (8.7) represents the slope of the *instantaneous* gain between the input and the output. However if we now consider carrying out the EVD on the covariance matrix formed using the summation operator, $\Sigma$, rather than the expectation operator then this matrix would be of the form (also including the time (or sample) index $i = 0, 1, 2, \ldots, N$)

$$\mathbf{R}_{xx}(t) = \frac{1}{N}\begin{bmatrix} \sum_{i=1}^{N} x^2(t_i) & \sum_{i=1}^{N} a(t_i)x^2(t_i) \\ \sum_{i=1}^{N} a(t_i)x^2(t_i) & \sum_{i=1}^{N} a^2(t_i)x^2(t_i) \end{bmatrix} \tag{8.8}$$

from which it can be clearly seen that the time-varying term $a(t)$ which has a deterministic non-stationary nature would be contained within the averaging process over the data length $N$ and we would expect from the EVD of the above matrix that both of the eigenvalues to be non-zero as a result of the parasitic effect caused by the variation of the probability density function of the elements of the matrix and the gain factor obtained from the direction of the eigenvector corresponding to the larger eigenvalue would be equal to the mean (average) value of the varying gain.

The above mathematical manipulations and our interpretations have also been verified computationally. We have generated a zero-mean white Gaussian process of 1000 samples with a variance of 64 representing the input of the system given in Figure 8.1 and filtered this input through a time-varying gain in the form of

$$a(t) = c + \sin\Omega \cdot t \tag{8.9}$$

where $\Omega$ is set to 0.016 and the constant $c$ is 2, in order to generate an amplitude-modulated stationary random process which would effectively be non-stationary (with fluctuating variance) such as that shown in Figure 8.2 (LHS).

The EVD of the input-output covariance matrix of the form (8.8) has been carried out and the *averaged* gain factor has been derived using the eigenvector corresponding to the larger eigenvalue. The values of the eigenvalues have been calculated as 331.4 and 4.6 verifying that there are two non-zero eigenvalues. In the RHS of Figure 8.2, the comparison between the computational and theoretical first eigenvalues is given revealing the significance of using different covariance matrix EVD procedures i.e. ensemble averaging vs time (or sample) averaging whereas Figure 8.3 shows the input-output scatter plot and the equivalent gain estimates derived using these two different techniques.

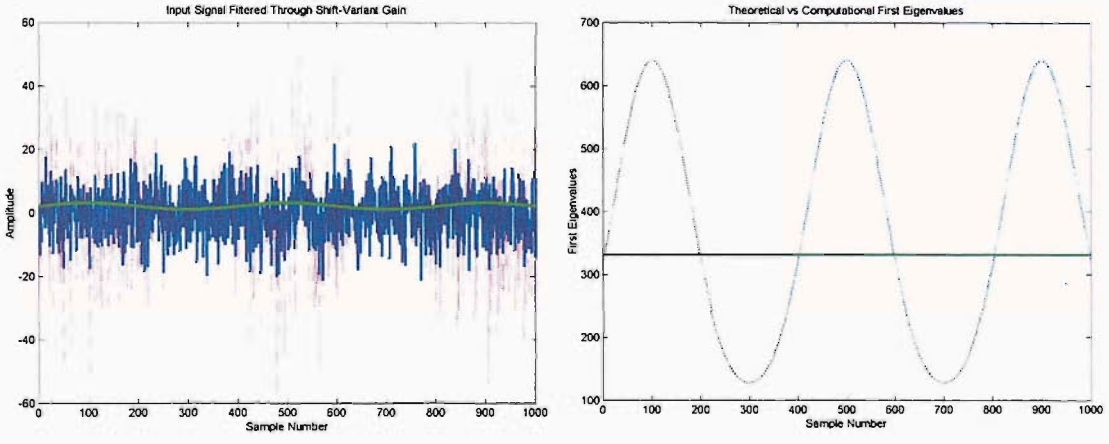


**Figure 8.2** LHS: Stationary random input (blue solid line) filtered through a deterministic non-stationary gain (green solid line) forming the random non-stationary output (red dotted line); RHS: Comparison between the theoretical and computational versions of the first eigenvalues of the covariance matrix between the signals whose scatter plot is given in Figure 8.3. Dotted line shows the theoretical varying eigenvalue whereas the solid line shows the computational averaged eigenvalue.

It is clear from the above eigenvalue plots that if the analysis carried out is based on the covariance matrix of the form (8.8), we would end up with a *single* gain factor whose direction is shown by the red arrow, that is the arithmetic average value of the original time varying *a(t)* which in fact has a sinusoidal behaviour. Here it should be noted that the direction of the principal component is given by the average slope of the input-output correlation behaviour whose gain spans the values between 1 and 3. Furthermore, the theoretical time-varying eigenvectors corresponding to the first eigenvalues such as that plotted in Figure 8.2 (RHS) would lead us to the time-varying slopes. A number of direction representations of the actual gain factors have also been illustrated by the green arrows in Figure 8.3 shown below.

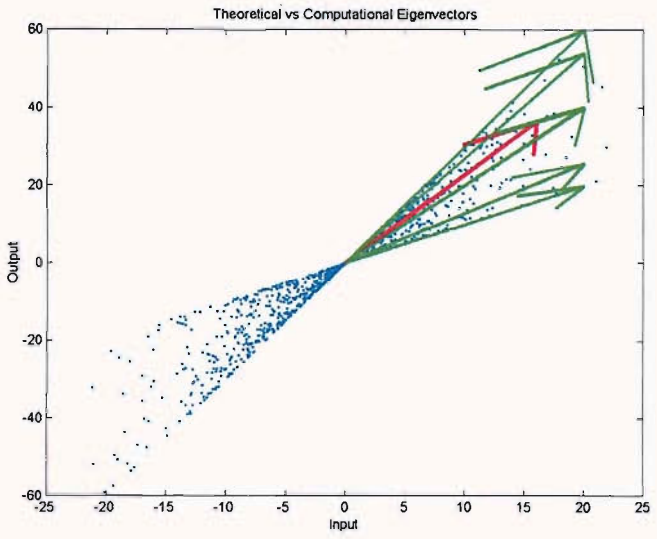


**Figure 8.3** Input-Output Scatter plot (dots) of the system given in Figure 8.1, the gain estimate (red arrow) obtained using PCA based on simplified covariance matrix computation as defined by (8.1) and the theoretical gain estimates (green arrows) obtained using the eigenvectors defined by (8.7).

In the next two sections we present the details of our proposed non-stationary system identification techniques based on the modified versions of the measured covariance matrix EVD in the time and the frequency domains respectively. The first case considers the analysis of short-term input-output segments in order for the estimation of potentially time-varying gain characteristics. The second case will look at the extension of this procedure using short-term adjacent input-output spectral correlation matrices of a dynamical system with oscillating natural frequency. The applicability and performance of each method has also been examined by computational simulations.

## 8.3 Short-Term PCA for Non-Stationary Gain Estimation

In view of our comments on the applicability of the standard form of PCA to the time-varying processes as presented in the previous section, here we seek to develop an EVD procedure such that when carried out on a set of input-output data with a varying gain relationship we can determine the transfer characteristics from the interpretation of the principal component(s) of their covariance matrix.

From our above analysis it is obvious that even if the system input-output relationship is completely linear, the existence of a time-varying filtering results in two non-zero eigenvalues from the EVD of their covariance matrix which is misleading with respect to the accurate estimation of the true transfer characteristics of the system under investigation. Considering the implications of this limitation, we propose to analyse the short-term covariance matrices of an input-output data pair, the output of which has a non-stationary time structure and thus the direction of the principal components of each covariance matrix can be used in order to identify the gain characteristics along the whole time history.

If we employ short-term averaging when forming the associated input-output covariance matrix of a pair of long time histories with potentially time varying transfer relationship, depending on the window length of the averaging operation relative to the rate of change of the system's gain characteristics, it would be possible to obtain small-range estimates for the actual gain factor and hence repeating this operation as a moving average EVD process for a series of covariance matrices along the whole available time series we can determine the varying structure of the gain factor. This procedure is illustrated in Figure 8.4 where

$$[\mathbf{R}_{xx}]_{k=1,2,3,\ldots,K}$$

represents the array of short-term input-output covariance matrices for successive segment pairs. From the PCA of each matrix we can simply obtain the local gain factor of the corresponding segment in accordance with the procedures introduced in Chapter 4 i.e. using the slope of the principal component associated with the largest eigenvalue.

Consequently, combining the values obtained from the EVD of each covariance matrix results in the overall gain curve linking the input-output time histories along the data length. It should be noted that, instead of using adjacent segments without common sample points such as that shown in this figure, which is mainly for visual simplicity, it would also be appropriate to carry out the analysis on a series of overlapping consecutive segments which could also lead us to accurate results for the gain estimates depending on the fluctuation nature of the time history. As can be clearly seen, the selection of the length of each segment is crucial in order to obtain a good estimate for the associated transfer characteristics. If the gain factor is a slowly varying function of time then relatively long segments with zero-overlap would be sufficient to describe its approximate behaviour although for the cases where this gain changes rapidly then too long segments would result in average values within the window range of each segment that are not very useful.

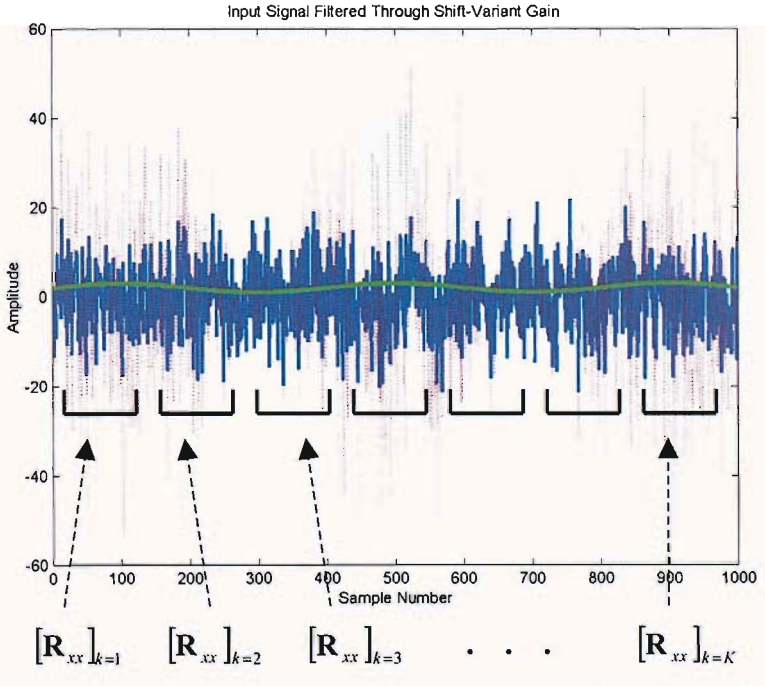


**Figure 8.4** Illustration of short-term moving average EVD in order to estimate the local gain factors from a non-stationary input-output relationship through a time-varying gain (of Figure 8.2 LHS) over the segments $k$=1,2,3...,$K$.

In an attempt to provide a clear illustration and to assess the performance of this technique, a number of simulation studies have been undertaken the results of which are presented in Figure 8.5. We have analysed the same artificial input-output signals as introduced in Section 8.2 by using the above technique. Four different lengths of overlapping segments of 10, 50, 100 and 150 sample points have been considered for simultaneous covariance matrix computations over the whole input-output time histories whose total sample numbers are 1000 each.

Estimates of the computed gain curves and the system's true gain are plotted on the same axes as shown in the LHS of Figure 8.5. It can be easily seen from this figure that using different segment lengths lead to dramatically different results for the time-variant gain estimates. For the shortest segment length (10 sample points) used the accuracy of the gain estimate is extremely high having almost identical values with the true gain verifying the consistency of our approach introduced above although as the number of points used for each covariance matrix window is increased the gain estimate becomes severely biased tending towards an average value as described in detail in Section 8.2. From the curves derived from the first and the second eigenvalues for the shortest segment estimates as illustrated in the RHS of Figure 8.5, we can see that due to the use of sufficiently small-range covariance matrices, the input-output pairs behave as if their relationship is completely free from any parasitic effects and hence one of the eigenvalues is always zero whereas the non-zero eigenvalue has an irregular fluctuating nature.

From the results of the above numerical procedure we can see that by the EVD of local input-output covariance matrix of a memoryless non-stationary system it is possible to obtain accurate estimates of the small-range transfer characteristics. In addition, it has also been shown that by computing a series of local scale factors from the array of these local covariance matrices, one can build the global structure of changing system characteristics. In the next section we extend the above procedure to a more general case of time-varying transfer function estimation of dynamical systems through the application of a modified version of our data processing technique in the frequency domain.

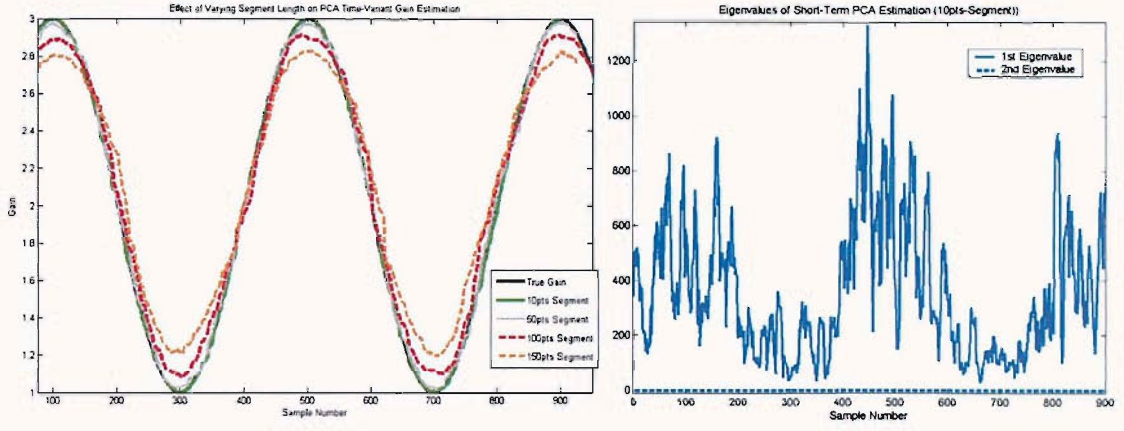


**Figure 8.5** LHS: Effect of varying segment length on short-term moving average EVD procedure for the local gain factor estimation from a non-stationary input-output relationship. RHS: Eigenvalues of the 10-point segment short-term PCA.

## 8.4 Short-Term Spectral PCA for Input-Output Analysis

Investigating the inherent non-stationarity of the dynamics of physical systems and/or exploring the internal structure of non-stationary processes using time-frequency descriptions has been commonplace to the engineering world for a long time. The fundamental requirements of signal-based non-stationary system analysis are to be able to determine the spectral components contained in measured signal(s) within the boundary of such systems and/or to obtain information about the time intervals at which certain frequencies occur i.e. when specific frequency components make their dominant contribution to the measured time history.

Conventional Fourier transforms do not assign spectral components to time and hence only partly solves the above problem by giving an *indicative* estimate of the average power/cross spectra of the whole signal analysed. The most commonly used classical method of time-frequency analysis is the short-time Fourier transform (STFT) whose basic concept is very simple. The time record is multiplied by a sliding window (which suppresses the signal outside a certain region) and the Fourier transform of the consecutive windowed segments are computed resulting in a series of *local spectra*. STFT of a continuous-time signal is obtained from,

$$S(t,\omega) = \int_{-\infty}^{\infty} x(t')w(t-t')e^{-j\omega t'}\,\mathrm{d}t' \tag{8.10}$$

where $t$ is the time, $\omega$ is the angular frequency and $x(t')$ & $w(t-t')$ are the truncated signal and the corresponding window centred at time $t'$ respectively. A widely used method for displaying the STFT is called the *spectrogram* (or *periodogram*) and is derived from the squared magnitude of (8.10) to give

$$\left|S(t,\omega)\right|^2 \tag{8.11}$$

This quantity is plotted as a function of $t$ and $\omega$, forming a three-dimensional representation of the signal which *crudely* illustrates the distribution of its energy over

time and frequency. Despite being empirical in terms of providing estimates of potentially changing spectra from window to window, it has been established as a very useful preliminary analysis tool for time-varying signals.

As detailed in Chapter 2, a Linear Time-Invariant (LTI) system is characterised by its *time-invariant impulse response function* $h(t)$, leading to the theoretical relationship between the input $x(t)$ and the output $y(t)$ in the form of a convolution (2.3) which is also very much simplified when an integral transform (Fourier or Laplace) is taken. Note that when the system is LTI, the impulse response function is defined as the output of the system at any time to a unit impulse input applied a time $t$ before. This relationship can be used to construct the time-invariant response to an arbitrary input at, say $t_1$, through the convolution integral as

$$y(t) = \int_{-\infty}^{t} h(t - t_1)x(t_1)dt_1 \tag{8.12}$$

by using the substitution, $t - t_1 = \tau$, (8.12) can be written in an alternative form, i.e.

$$y(t) = \int_{0}^{\infty} h(\tau)x(t - \tau)d\tau \tag{8.13}$$

However, if the system is time-varying then the above relationship based on a constant impulse response function is no longer valid since the system characteristics change with time and hence for a fixed input the corresponding output also varies with time.

In order to represent the time-varying characteristics theoretically, we can modify the above relationship considering the impulse response function as changing with time in the form

$$y(t) = \int_{0}^{\infty} h(t, \tau)x(t - \tau)d\tau \tag{8.14}$$

with a view to describe a time variable transfer function. Since the input (assumed to be stationary random) can be written using the Fourier integral (in the frequency domain) as

$$x(t - \tau) = \int_{-\infty}^{\infty} X(\omega)e^{j\omega(t-\tau)}d\omega \tag{8.15}$$

then substituting (8.15) into (8.14) we get

$$y(t) = \int_{\tau=0}^{\infty} h(t,\tau) \int_{\omega=-\infty}^{\infty} e^{j\omega(t-\tau)} X(\omega) d\omega d\tau \tag{816}$$

which can be rewritten as

$$y(t) = \int_{\omega=-\infty}^{\infty} e^{j\omega t} \cdot \int_{\tau=0}^{\infty} h(t,\tau) e^{-j\omega\tau} d\tau \cdot X(\omega) d\omega \tag{8.17}$$

and

$$y(t) = \int_{\omega=-\infty}^{\infty} e^{j\omega t} \cdot H(t,\omega) \cdot X(\omega) d\omega \tag{8.18}$$

From (8.17) and (8.18) it can be seen that the *time-varying transfer function (or FRF)* i.e. the system's approximate response to frequency $\omega$ at time $t$, is embodied in the expression

$$H(t,\omega) = \int_{0}^{\infty} h(t,\tau) e^{-j\omega\tau} d\tau \tag{8.19}$$

Therefore, the input-output relationship in the frequency domain can be given by

$$Y(t,\omega) = H(t,\omega) X(\omega) \tag{8.20}$$

from which one can also derive the corresponding pair

$$S_{yy}(t,\omega) = |H(t,\omega)|^2 S_{xx}(\omega) \tag{8.21a}$$

$$S_{xy}(t,\omega) = H(t,\omega) S_{xx}(\omega) \tag{8.21b}$$

defining the time-varying FRF in terms of the power and cross spectral densities of the input and the output.

Following from the methodology introduced in the previous section, here we consider the frequency domain extension of our approach, the so called short-term spectral PCA (STSPCA) in order to estimate the time-varying transfer characteristics of a dynamical non-stationary system. The above analysis given from (8.12) to (8.21) justifies that the problem of approximating the time-varying transfer function can be considered on the basis of estimating the time-varying output power and input-output cross spectral densities as accurately as possible. The calculation of $H(t,\omega)$ is difficult because obtaining $h(t,\tau)$ is difficult. However we might conceive of some *approximate* approach to this when the time variation is *slow*. In this case we may conceive of a *frozen* time dependant transfer function as parameters of the system vary. The use of short-time Fourier analysis essentially builds on this idea. Accordingly, we can consider using short-time Fourier-based methods to derive approximations to $H(t,\omega)$. Our proposed input-output analysis procedure is based on the moving segment EVD of the signal pair as depicted in Figure 8.2, but this time through the adjacent spectral correlation matrices i.e. the array of matrices to be analysed will be replaced by

$$\left[\hat{\mathbf{R}}(f)\right]_{k=1,2,3,\ldots,K} = \left[\begin{matrix} \hat{S}_{x_m x_m}(f) & \hat{S}_{y_m x_m}(f) \\ \hat{S}_{x_m y_m}(f) & \hat{S}_{y_m y_m}(f) \end{matrix}\right]_{k=1,2,3,\ldots,K} \tag{8.22}$$

for each segment pair $k$ of which will contain the power and cross spectral density estimates of the measured signals. In accordance with the standard procedure described for the time-varying gain estimation problem, the slope of the eigenvector corresponding to the largest eigenvalue of each matrix will give a local transfer function estimate (see Chapter 5 for the details of SISO PCA FRF estimation). Furthermore, by undertaking the exact procedure over the whole length of the time record one can obtain a series of transfer functions which can be defined as

$$H(t,f) = \lim_{|k|\to 0}\left\{H(k,f)_{k=1,2,3\ldots,K}\right\} \tag{8.23}$$

i.e. is a function of both frequency $f$ and the segment index $k$.

Therefore, from (8.23) it can also be seen that in principle it is possible obtain the true time-varying transfer function as the segment length $|k|$ tends to zero i.e. as segments get smaller, intuitively we are closer to $H(t,f)$. Note that by using the same segment length for different types of non-stationary systems, depending on the rate of change in each system's characteristics with time, one may end up with transfer function estimates exhibiting various degrees of accuracy from system to system. In this context we have two fundamental assumptions on which our frequency domain approach for the above problem is based on and these are:

i. in terms of the statistical reliability (or consistency) of the spectral estimates obtained from truncated parts of the time records: the duration of each segment is sufficiently long with a high sampling rate that will allow the necessary averaging operations over a number of Fourier transformed windows so that each estimate will have a *converging* behaviour (reducing variability) with good frequency resolution (low bias);

ii. in terms of accurate time dependant representations of the frequency content of adjacent signal segments: the non-stationarity in each truncated part of the time record is a slowly varying function of time for each frequency that will result in *largely* accurate averaged spectral estimates and hence will allow one to observe the *true* variations in the energy distributions from segment to segment.

In essence, the above assumptions suggest that for each input-output segment pair the system under investigation will be considered as having *almost stationary* transfer characteristics. Although this seems to be a strong (and hence restrictive) condition, it can be appropriately met *to a certain extent* for the vast majority of non-stationary data one may come across in real-life engineering applications.

However it should be noted that, considering the input excitation to be stationary random, for the cases in which the rate of variation in the system's non-stationarity is relatively high, shorter segments will be required in order to represent a minimum amount of fluctuations of the energy components contained in the output power and the input-output cross spectra. This will help to obtain improved time resolution but at the expense of poor frequency resolution and hence increased bias on the spectral estimates. Therefore, the overall accuracy of the analysis will heavily rely on the *trade-off* between the choices of better *time* and *frequency* information for which the signal analyst will need to make a decision according to the application and/or the available data.

In an attempt to demonstrate the applicabilitiy of the proposed STSPCA time-varying transfer function estimation technique, a series of computational simulations have been undertaken. The non-stationary dynamical SDOF system we consider is a second order oscillator given by the form

$$\ddot{y}(t) + 2\xi\omega_0(t)\dot{y}(t) + \omega_0^2(t)y(t) = \omega_0^2(t)x(t) \tag{8.24}$$

where $y(t)$ is the displacement, $\xi$ is the viscous damping coefficient, $x(t)$ is the excitation force and $\omega_0(t)$ is the time-varying undamped natural frequency in the form of a frequency modulated (FM) signal oscillating between 100 Hz and 900 Hz (completing one full cycle in 1 second) i.e. is centred on 500 Hz with a 400 Hz sinusoidal FM. The approximate *frozen* (local) transfer function of the above system can be defined using the Laplace transformation as

$$H(t,s) \approx \frac{\omega_0^2(t)}{s^2 + 2\xi\omega_0(t)s + \omega_0^2(t)} \tag{8.25}$$

where $s$ is the Laplace variable. The model system is excited by a zero-mean broad-band stationary random (Gaussian white) process for 20 seconds at a sampling rate of $10^5$sps and the resulting displacement is recorded as the system output to be analysed. The damping coefficient $\xi$ has been set to $10^{-5}$.

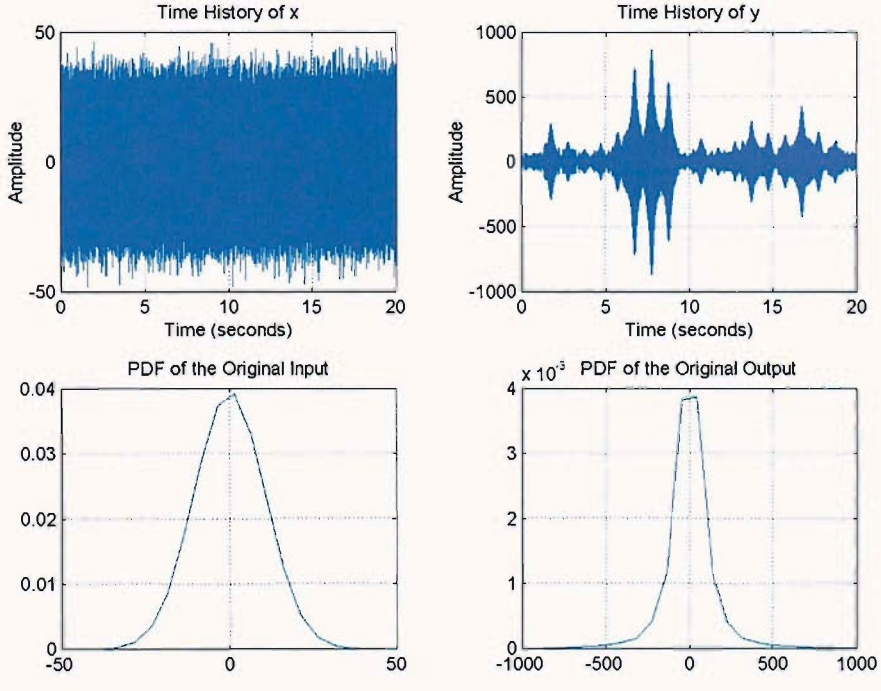


**Figure 8.6** Input-Output time histories of the system described by (8.14) and their corresponding probability density function estimates.

Figure 8.6 shows the input and output time histories and their computed probability density function (PDF) estimates from the recorded data sets each of which consists of 2 million sample points. Clearly, the output signal reveals significant time-varying structure with non-stationary variance whose fluctuations are not systematic. It is also interesting to observe the major difference between the two PDF estimates as the output signal has a super-Gaussian distribution with a kurtosis of around 9.5. Note that we have used the whole signal to come up with this answer i.e. treating the output as stationary.

In order to explore the internal structures of the measured signals in the time-frequency plane, their spectrograms are calculated initially, using Hann windows with no overlapping. In Figure 8.7 is shown the spectrograms of the input and the output, with the output signal image plotted within various frequency ranges for visualisation purposes. The amplitudes of the signals are displayed by using a typical colour-map scale, hot colours reflecting higher values.

The input spectrogram (top-left) is not of much interest as the signal is white Gaussian and hence contains all the frequencies up to the half of the sampling rate with a homogeneous distribution along the both axes. The output spectrogram plotted within the full frequency range (top-right) shows that the main proportion of the signal energy is concentrated at the low frequencies from which we can conclude that the system is acting like a typical time-varying narrow-band filter. As the axis ranges of the plot is reduced (centre and bottom figures) the time-frequency varying patterns on the output signal becomes more noticeable with sinusoid high energy regions (indicating the oscillating resonance frequencies) progressing along the time axis.

Note that the window size used for the spectrogram calculations is 2048 points which is also zero-padded to the length of 4096 points FFT. This means that each segment covers approximately 0.02 seconds of data which gives a reasonably good time resolution allowing one to visualise the complete cycle of resonance frequencies in 1 second centred at 500 Hz, spanning between 100 Hz and 900 Hz. However the frequency resolution is approximately 25 Hz and consequently the vertical spreading of the dominant energy in the frequency axis causes the extended spiky display of the resonant regions towards the minimum and maximum values. This spreading behaviour becomes more significant towards the higher frequencies as with a fixed damping coefficient the resonance bandwidth increases with frequency.

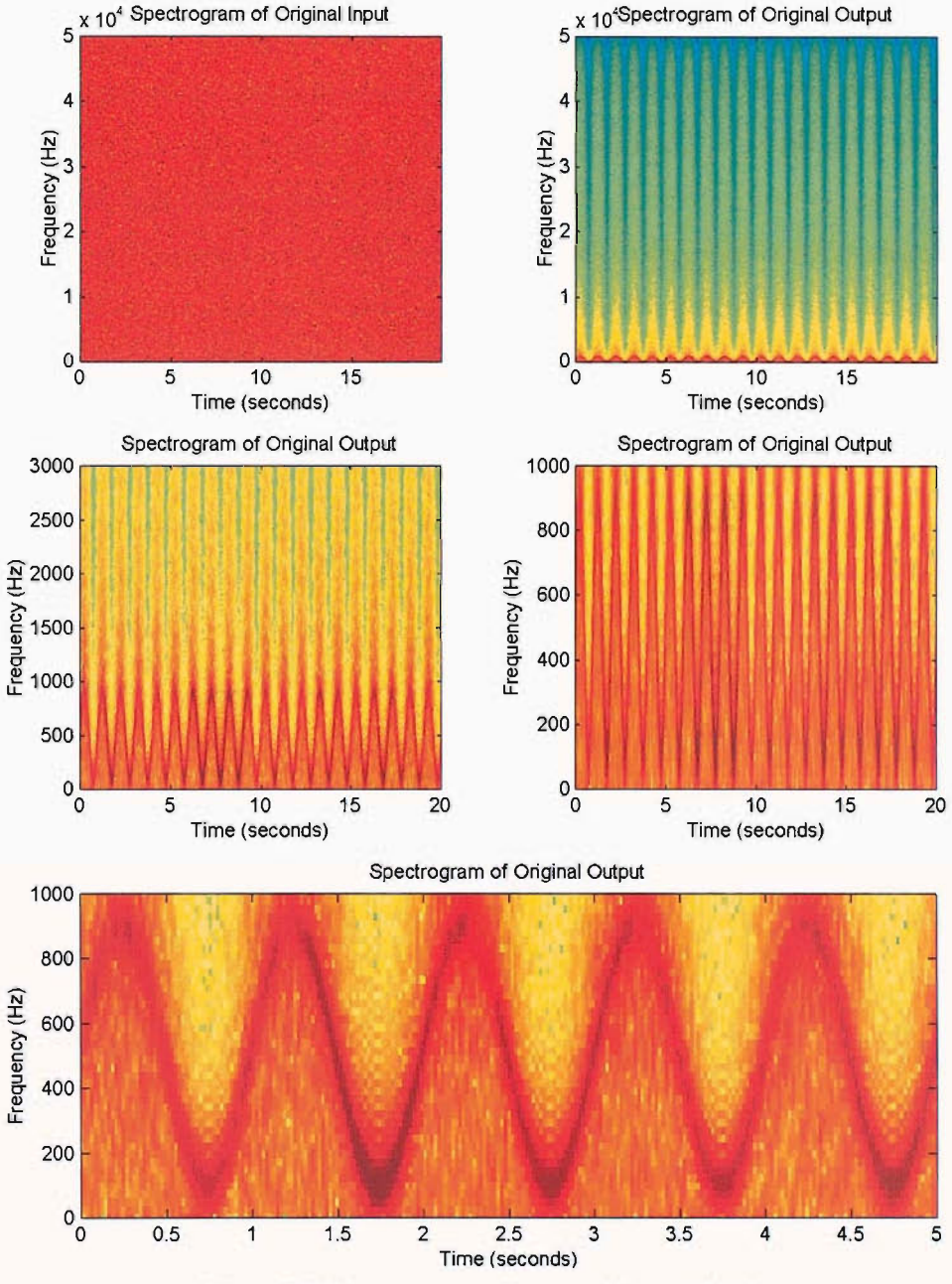


**Figure 8.7** Spectrograms of Input and Output signals.

In Figures 8.8 and 8.9 are shown the striking results of STSPCA-based time-varying transfer function estimation. Moving segment EVD procedure is carried out on adjacent spectral correlation matrices formed between $10^4$ point input-output signal pairs with no overlapping i.e. each matrix containing statistical information on 0.1 second data. Power and cross spectral estimates are calculated using standard segment averaging technique based on 2048 point windows (Hann) zero-padded to 4096 point FFT. The magnitude of the slope of the eigenvector corresponding to the largest eigenvalue of each spectral correlation matrix is used to form a series of adjacent local FRF gain factors.

Top plots of this figure illustrate the input-output relationship using spectrogram-like display, based on colour-map scale magnitude representations. In the bottom figures the corresponding results are displayed using three-dimensional waterfall plots in order to further explore the internal structure of the transfer functions and hence significant variations on its changing characteristics from segment to segment. Both representations are plotted for several frequency/time ranges. From STSPCA Map plots it can be clearly seen that the patterns formed by high and low energy regions is almost identical to that of the output spectrogram concentrated within the 0Hz-1kHz band. LHS waterfall plot of Figure 8.8 shows that the varying resonant frequencies are distributed over this frequency range with densely packed amplitude variations. Closer examination of the adjacent local FRFs reveals that (RHS waterfall plots of Figures 8.8 and 8.9) there is a distinguishable peak amplitude for each local transfer function where the maximum response between the input-output pair occurs. In comparison to the spectrogram plots given above, here the time resolution is lower although reasonably sufficient to give a clear picture of the variation in the energy distribution.

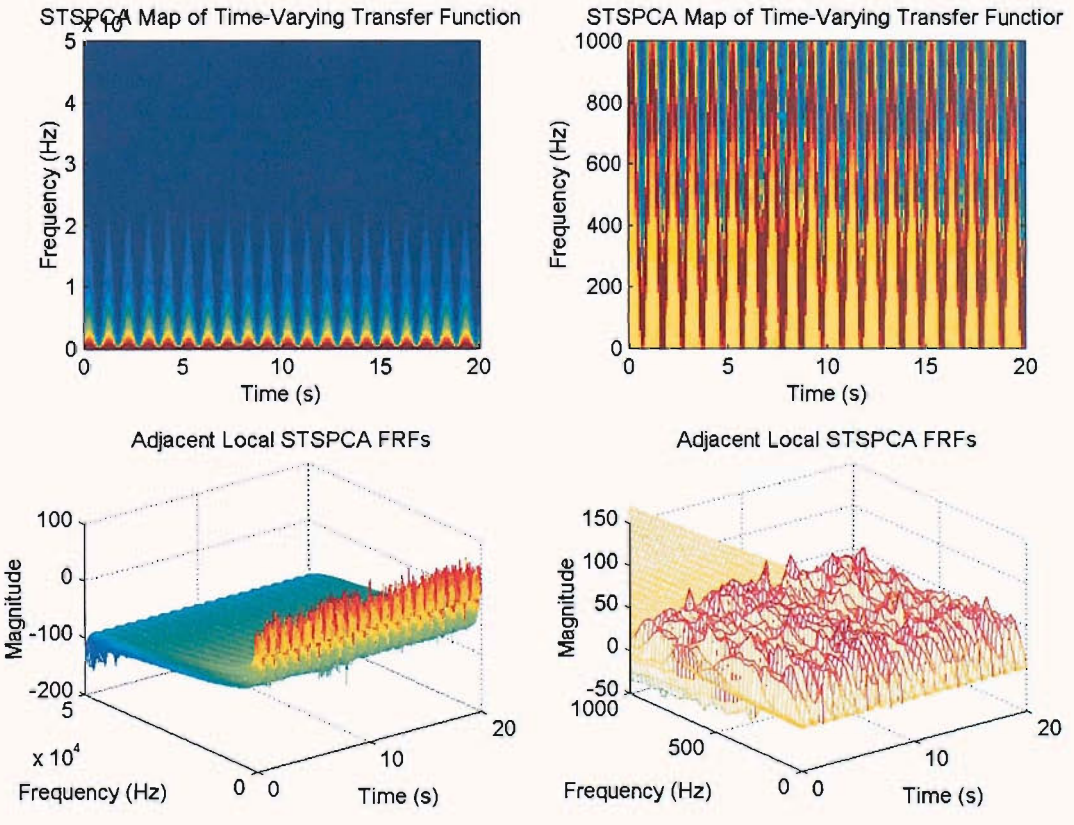


**Figure 8.8** STSPCA Map and Waterfall Plots of the time-varying transfer function. LHS Top: 0Hz-50kHz STSPCA Map; LHS Bottom: 0Hz-50kHz STSPCA Waterfall Plot; RHS Top: 0Hz-1kHz STSPCA Map; RHS Bottom: 0Hz-1kHz STSPCA Waterfall Plot.

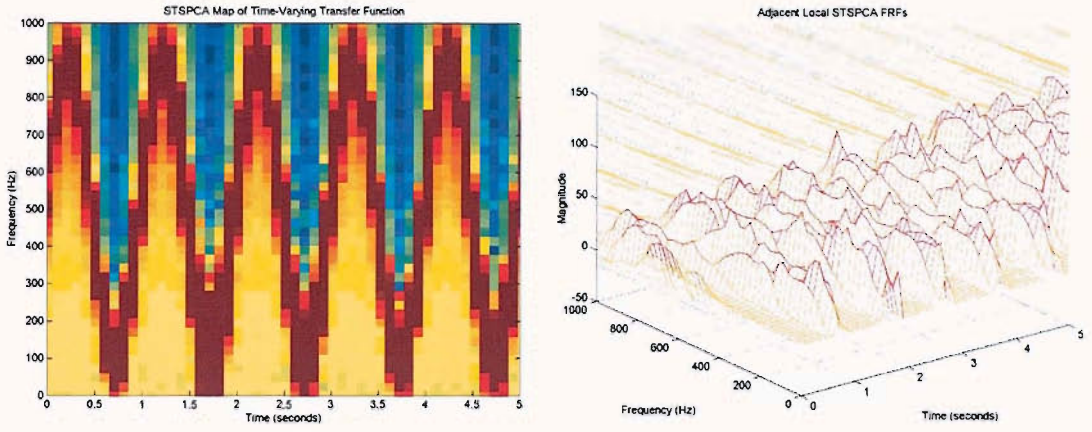


**Figure 8.9** Magnified versions of STSPCA Map and Waterfall Plots of time-varying transfer function.

Originating from the above described processing strategy based on segment-wise power/cross spectral estimation, one can also consider visualising a time-varying coherence (OCF) between the input and the output signals. Figure 8.10 illustrates this concept using three-dimensional shaded surface (LHS) and two-dimensional colour-map (RHS), representing the z-axis coherence values between 0 and 1 across the time-frequency plane. The most interesting feature of the LHS plot is its almost flat high linearity platforms corresponding to the low energy regions of the STSPCA map given in Figure 8.9. In the valleys between these flat surfaces there are regions of very low linearity associated with the concentration of resonant energy. Towards the higher frequencies (from 900 Hz upwards) the degree of linear association tends to increase. This is due to the signals having very low energy resulting in the spectral estimates being dominated by the windowing effects and subsequently the computed quantity effectively starts to reflect the coherence between the window functions rather than the signals.

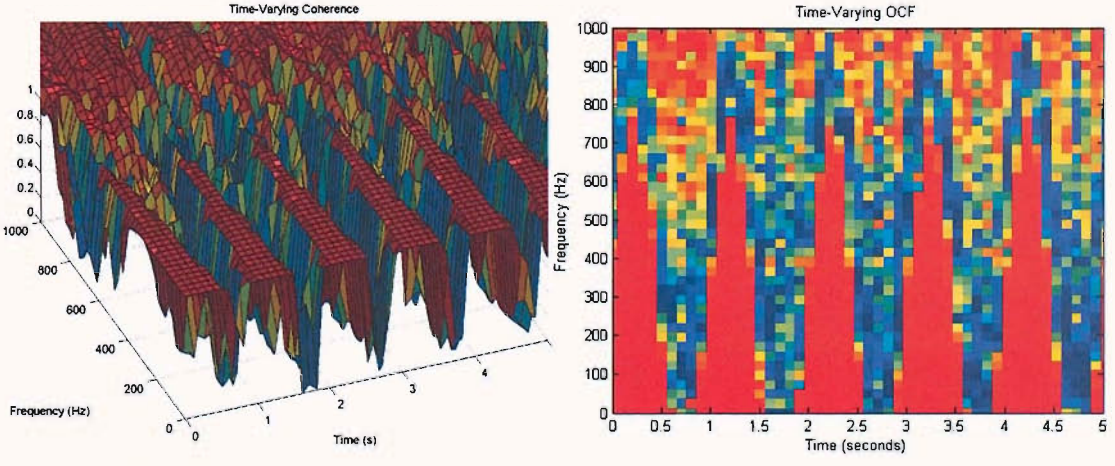


**Figure 8.10** Time-varying ordinary coherence function (OCF) between the input and the output.

## 8.5 Conclusion

In this chapter, PCA-based moving segment EVD techniques have been introduced for the input-output analysis of time-varying systems in the time and the frequency domains. Proposed methods provide very useful background both theoretically and computationally with reference to the application of EVD to Non-Stationary Data Analysis.

The results obtained from the short-term PCA method in the time domain demonstrate that by the use of optimal length segments with respect to the dynamic structure of the data set in order to ensure that both time and frequency resolutions are sufficiently fine, one can obtain accurate estimates of the time-variant gain introduced by a non-stationary system. The application of the STSPCA technique for time-varying transfer function estimation proves to be a logical and reliable alternate to the classical STFT spectrogram in terms of its practicality and input-output feature extraction property. However, care has to be taken to choose the duration of the segments in order to best represent the structure of the time-varying transfer function on the time-frequency plane. The exact procedures can be easily applied to any form of input-output data from a variety of applications.

# Chapter Nine

# CONCLUDING REMARKS

## 9.1 Summary of Results

In essence, this research introduces a new approach for the use of the statistical multivariate data analysis technique Principal Component Analysis (PCA). The standard Eigen-Value Decomposition (EVD) procedure is applied to the covariance or spectral correlation matrix constructed from the input(s) and the output(s) of a physical system in the time or the frequency domain. Subsequent observation and interpretation of the eigenvalue-eigenvector behaviour provide various forms of linear characterisation of the system under investigation, with a view to extract the unknown transfer features. Originating from this core principle, it is demonstrated that the analysis strategy leads to an expansion of the proposed methodology to several subgroups of signal-based system identification applications. Original contributions of this thesis can be summarised as follows:

- In the context of analytical and numerical review of the existing transfer function estimators based on the least squares approach (Chapter 3), a generalisation scheme for the Total Least Squares (TLS) estimation in the time domain is introduced from a geometric viewpoint. The input-output relationship is established by the minimisation of an error distance that is defined with respect to a variable angle. The main benefit of this result is to allow one to readily interpret the relationships between the three standard least squares estimators and hence verify analytically that the value of $a_{TLS}$ is bound by the estimators $a_1$

and $a_2$. It is also shown that the resulting estimator gives the exact true gain factor for all input and output SNRs under certain conditions. Despite the fact that this is not of immediate practical use as its verification relies upon the prior knowledge of the true gain factor, it is an interesting observation revealing the superior behaviour of the proposed scheme.

- Single-Input-Single-Output (SISO) Linear Time-Invariant (LTI) system Frequency Response Function (FRF) estimation problem is formulated using PCA through the EVD of bivariate input-output spectral correlation matrix (Chapters 4 and 5). The proposed approach leads to the development of a SISO PCA FRF estimator that is equivalent to the SISO TLS FRF estimator for the special case of equal input-output additive measurement noise. The fact that PCA can be employed to solve such transfer function estimation problems provides an important fundamental background for the physical interpretation of eigen-analysis.

- The Multi-Input-Single-Output (MISO) LTI system FRF estimation problem is formulated using PCA through the EVD of multivariate input-output spectral correlation matrix (Chapters 4 and 5). The proposed approach leads to the development of a MISO PCA FRF estimation scheme. Computational simulations undertaken using uncorrelated input signals verify that the proposed estimator gives results with substantial accuracy in the presence of additive measurement noise on all signals in comparison to the SISO-based least squares estimators.

- With reference to the application of PCA-based linearization to SISO non-linear time-invariant (NLTI) systems (Chapter 6): The derivation of a non-linearity detection ratio (NDR), as a function of the eigenvalues and the components of the eigenvectors of the bivariate input-output covariance (or spectral correlation) matrix, is introduced. This quantity is equivalent to the virtual coherence function. In addition to the above, following from the results introduced in the context of SISO PCA FRF estimation, the same approach provides a logical

approximation procedure for linear equivalent transfer function estimation of memoryless / dynamical non-linear systems;

- A PCA-based delay detection method for non-dispersive single- and multi-path systems is developed (Chapter 7) in the time domain. Multi-path systems considered include both single- and multi-output configurations. Utilising the relationship between the eigenvalues of each matrix in the array of positive and negative lag input-output covariance matrices, forms the basis of the processing strategy. This approach originates from the fact that, if the data set to be analysed exhibits a pure delay relationship, then in the time domain one would get the maximum difference between the associated eigenvalues only for the covariance matrix for the time lag value equal to the time delay. Work presented here introduces an application of PCA to a form of input-output relationship of linear time-invariant systems from a different viewpoint compared to the rest of the thesis.

- Time-varying transfer function estimation problem is considered adopting a moving segment EVD process on a series of adjacent spectral correlation matrices. Proposed Short-Term Spectral PCA (STSPCA) technique for input-output analysis proves to be a logical and consistent procedure which is also a superior alternate to the conventional non-stationary signal analysis tool, Short-Time Fourier Transform (STFT) spectrogram. Results provide very useful background both theoretically and computationally with reference to the application of EVD to non-stationary data analysis.

## 9.2 Future Research

MISO LTI system gain/FRF estimation is considered in Chapters 4 and 5 for the special case of uncorrelated input signals. The comparisons between the results from the multi channel PCA technique and the existing methods are limited with the corresponding SISO bivariate-based forms of the least squares estimators. In an attempt to give a more objective performance assessment of the proposed estimator, it would be useful to consider the optimisation landscape for the least squares estimation scheme in a multi-dimensional space and hence to develop the associated estimators with respect to the modified error criteria.

The work presented in Chapter 6 forms an important background for the application of PCA to non-linear systems in the form of a linear approximation procedure. With respect to the multi-output fault detection problem, one may consider an extension of the procedure by using Independent Component Analysis (ICA) and further research may lead to the generalisation of the method to be applied for various mechanical and/or structural condition monitoring and/or fault diagnostic systems.

Chapter 7 introduces the concept of *PCA as a function of time lag* between the variables. Our approach is based on the observation that, the results of the conventional EVD procedure is strongly dependant on the potential time delay relationship involving the signals to be analysed. Extending from this fundamental nature of the signal-based eigen-analysis, it would be interesting to see whether or not there would be any inherent implications on the interpretation of the results from PCA-based investigations that have been undertaken in other fields.

STSPCA for the estimation of time-varying transfer functions is considered in Chapter 8, with reference to SISO systems. Another interesting investigation would be based on combining the idea of multi-channel PCA (Chapters 4 and 5) with the moving segment EVD processing strategy in a view to develop a generalised Multi-Input-Multi-Output (MIMO) time-varying transfer function estimation scheme.

# APPENDIX A

## Methodology for Derivations of SISO Least Squares FRF Estimators

In the context of gain estimation of memoryless SISO systems, the methodology for deriving the least squares estimators in the time domain is detailed in Section 3.2 from a geometric viewpoint involving real bivariate data. To summarise, with reference to Figure 2.5 we define an error distance between the measured data and a regression line in the form

$$y = ax \tag{A.1}$$

which reflects the assumed linear relationship between input $x$ and output $y$ through the gain $a$, and furthermore form a cost function that is the sum of the squared errors over a number of samples. Then this cost function is minimised with respect to the unknown gain factor in an attempt to obtain an optimal estimate. However when we consider using the same optimisation procedure for the Frequency Response Function (FRF) estimation of dynamical SISO systems the corresponding input-output relationship given above becomes

$$Y(f) \approx H(f)X(f) \tag{A.2}$$

through Fourier-based transformations of finite length signals. Consequently the original variables to be analysed becomes complex and the gain $a$ is now replaced by the FRF of the system with real and imaginary parts corresponding to its gain and phase factors respectively.

Note that in the time domain the linear gain relationship we are based on is between sample pairs whereas in the frequency domain the equivalent relationship is obtained over sets of stationary random data pairs at a single frequency i.e. segments (or ensembles) of input-output pairs. This effectively means that for each segment pair we will have an approximate complex transfer function with real and imaginary parts. In accordance with the procedure used in the gain estimation problem, this time we define a complex error distance expressed at a single frequency based on the required criteria e.g. Case 1, 2 or 3 in Section 2.3 (Chapter 2). Say, we are looking at Case 1, then the associated frequency domain error criterion for an input-output segment pair is given by

$$E_k(f) = Y_k(f) - H_1(f)X_k(f) \tag{A.3}$$

in which $X_n(f)$ and $Y_n(f)$ are the Fourier Transforms (FTs) of the $k^{th}$ (windowed) segment of $x(t)$ and $y(t)$ respectively, over a total number of $K$ segments. Therefore the corresponding cost function equivalent to the magnitude of the error criterion (A.3) to be minimised will be of the form

$$J_1(f) = \frac{1}{K}\sum_{k=1}^{K} E_k^*(f)E_k(f) \tag{A.4}$$

where ' * ' denotes complex conjugate. Note that the expectation operator E[ ] indicating the theoretical average is replaced by the summation operator $\Sigma$ as appropriate in practice. (A.4) can be expanded as

$$J_1(f) = \frac{1}{K}\sum_{k=1}^{K}\left(Y_k(f) - H_1(f)X_k(f)\right)^*\left(Y_k(f) - H_1(f)X_k(f)\right) \tag{A.5}$$

and minimising (A.5) with respect to $H_1(f)$ can be obtained from the solution of

$$\frac{dJ_1(f)}{dH_1(f)} = 0 \tag{A.6}$$

Since the above cost function is now complex its differentiation must be carried out with respect to both the real and the imaginary parts of the FRF. Expanding (A.5) we get

$$J_1(f) = \frac{1}{K}\sum_{k=1}^{K}\left(Y_k^* Y_k - H_1 Y_k^* X_k - H_1^* X_k^* Y_k + H_1^* H_1 X_k^* X_k\right) \tag{A.7}$$

(where $f$'s in brackets indicating the frequency domain have been omitted for brevity) which can be rewritten in terms of the real and the imaginary parts of the FRF as

$$J_1(f) = \frac{1}{K}\sum_{k=1}^{K}\left(Y_k^* Y_k - (\mathrm{Re}[H_1] + j\,\mathrm{Im}[H_1])Y_k^* X_k - (\mathrm{Re}[H_1] - j\,\mathrm{Im}[H_1])X_k^* Y_k + (\mathrm{Re}[H_1]^2 + \mathrm{Im}[H_1]^2)X_k^* X_k\right) \tag{A.8}$$

assuming

$$H_1 = \mathrm{Re}[H_1] + j\,\mathrm{Im}[H_1] \tag{A.9a}$$

$$H_1^* = \mathrm{Re}[H_1] - j\,\mathrm{Im}[H_1] \tag{A.9b}$$

Therefore by equating the partial derivatives of (A.8) with respect to the real and the imaginary parts of the FRF to zero, one can simply obtain

$$\frac{\partial J_1(f)}{\partial \mathrm{Re}[H_1(f)]} = 0 \Rightarrow \mathrm{Re}[H_1(f)] = \frac{1}{K}\sum_{k=1}^{K}\frac{Y_k^*(f)X_k(f) + X_k^*(f)Y_k(f)}{2X_k^*(f)X_k(f)} \tag{A.10a}$$

$$\frac{\partial J_1(f)}{\partial \mathrm{Im}[H_1(f)]} = 0 \Rightarrow \mathrm{Im}[H_1(f)] = \frac{1}{K}\sum_{k=1}^{K}\frac{j\left(Y_k^*(f)X_k(f) - X_k^*(f)Y_k(f)\right)}{2X_k^*(f)X_k(f)} \tag{A.10b}$$

and substituting (A.10a,b) into (A.9a) the FRF estimator $H_1(f)$ is given by

$$H_1(f) = \frac{1}{K}\sum_{k=1}^{K}\frac{X_k^*(f)Y_k(f)}{X_k^*(f)X_k(f)} \tag{A.11}$$

which can be rewritten in terms of the relevant auto and cross spectra estimates as

$$H_1(f) = \frac{\hat{S}_{xy}(f)}{\hat{S}_{xx}(f)} \tag{A.12}$$

The exact procedure described above can be undertaken for the error criteria defined by Cases 2 and 3 in Section 2.3 (Chapter 2) and the corresponding FRF estimators $H_2(f)$ and $H_V(f)$ can be easily derived respectively.

# APPENDIX B

## Eigen-Value Decomposition of the SISO System Spectral Correlation Matrix

The eigenvalues ( $\lambda_i$ ) and eigenvectors ( $\mathbf{t}_i$ ) of the noise-free spectral correlation matrix (5.9) are obtained (for $i$=1, 2) from the solution of

$$\hat{\mathbf{R}}(f) \cdot \mathbf{t}_i = \lambda_i \cdot \mathbf{t}_i \tag{B.1}$$

which can be expanded as

$$\begin{bmatrix} \hat{S}_{xx}(f) & H^*(f)\hat{S}_{xx}(f) \\ H(f)\hat{S}_{xx}(f) & |H(f)|^2 \hat{S}_{xx}(f) \end{bmatrix} \begin{bmatrix} t_{1i} \\ t_{2i} \end{bmatrix} = \lambda_i \cdot \begin{bmatrix} t_{1i} \\ t_{2i} \end{bmatrix} \tag{B.2}$$

leading to the simultaneous equations

$$\left\{\hat{S}_{xx}(f)\right\} \cdot t_{1i} + \left\{H^*(f) \cdot \hat{S}_{xx}(f)\right\} \cdot t_{2i} = \lambda_i \cdot t_{1i} \tag{B.3a}$$

$$\left\{H(f) \cdot \hat{S}_{xx}(f)\right\} \cdot t_{1i} + \left\{|H(f)|^2 \cdot \hat{S}_{xx}(f)\right\} \cdot t_{2i} = \lambda_i \cdot t_{2i} \tag{B.3b}$$

Using Cramer's Theorem in order to solve for the eigenvalues

$$\det\left\{\hat{\mathbf{R}}(f) - \lambda \cdot \mathbf{I}\right\} = 0 \tag{B.4}$$

we get

$$\det \begin{bmatrix} \hat{S}_{xx}(f) - \lambda & H^*(f)\hat{S}_{xx}(f) \\ H(f)\hat{S}_{xx}(f) & |H(f)|^2 \hat{S}_{xx}(f) - \lambda \end{bmatrix} = 0 \qquad \text{(B.5)}$$

This can be expanded as

$$\left\{\hat{S}_{xx}(f) - \lambda\right\} \cdot \left\{|H(f)|^2 \hat{S}_{xx}(f) - \lambda\right\} - \left\{H(f)\hat{S}_{xx}(f)\right\} \cdot \left\{H^*(f)\hat{S}_{xx}(f)\right\} = 0 \qquad \text{(B.6)}$$

and after some algebra the eigenvalues are given by (5.10a,b) from which substituting into (B.3) we get

$$\left\{\hat{S}_{xx}(f)\right\} \cdot t_{1i} + \left\{H^*(f) \cdot \hat{S}_{xx}(f)\right\} \cdot t_{2i} = 0 \qquad \text{(B.7a)}$$

$$\left\{\hat{S}_{xx}(f)\right\} \cdot t_{1i} + \left\{H^*(f) \cdot \hat{S}_{xx}(f)\right\} \cdot t_{2i} = \left\{\hat{S}_{xx}(f) + |H(f)|^2 \hat{S}_{xx}(f)\right\} \cdot t_{1i} \qquad \text{(B.7b)}$$

and the corresponding eigenvectors are given by the forms (5.11a,b).

# APPENDIX C

## Variance of the Maximum Likelihood FRF Estimator

Following from (5.21) with the corresponding properties of the Maximum Likelihood (ML) estimators it is concluded that the error associated with the ML estimators are approximately distributed as $N(0,\sigma^2)$, where $\sigma^2$ is the CRLB. This observation can be exploited to allow one in order to define the confidence intervals for the ML estimator by computing the Cramer-Rao Lower Bound (CRLB). Since estimation of $H(f)$ and $S_{xx}(f)$ decouple then one is essentially dealing with a single (complex valued) parameter estimation problem. Furthermore, rather than treating the problem as one of estimating a single complex parameter, $H(f)$, we can consider it as a problem in two real valued parameters, namely

$$H_R(f) = \mathrm{Re}\{H(f)\} \text{ and } H_I(f) = \mathrm{Im}\{H(f)\} \qquad \text{(C.1a,b)}$$

It is well known that the CRLBs for multi-parameter problems are given by the diagonal elements of the $\mathbf{J}^{-1}$, where $\mathbf{J}$ is the Fisher information matrix defined by

$$J_{p,q} = E\left[-\frac{\partial^2 L}{\partial\alpha_p \partial\alpha_q}\right] = E\left[\frac{\partial L}{\partial\alpha_p}\frac{\partial L}{\partial\alpha_q}\right] \qquad \text{(C.2)}$$

where $\alpha_p$ and $\alpha_q$ are the parameters being estimated. For Gaussian problems, like the one we consider, it can be shown that [19]

$$J_{p,q} = E\left[\frac{\partial L}{\partial \alpha_p}\frac{\partial L}{\partial \alpha_q}\right] = N\,Tr\left\{\mathbf{R}(f)^{-1}\frac{\partial \mathbf{R}(f)}{\partial \alpha_p}\mathbf{R}(f)^{-1}\frac{\partial \mathbf{R}(f)}{\partial \alpha_q}\right\} \quad (p,q)\in(1,2) \qquad \text{(C.3)}$$

where $\alpha_1 = H_R(f)$ and $\alpha_2 = H_I(f)$. From the definition of spectral correlation matrix it is simple to show that

$$\frac{\partial \mathbf{R}(f)}{\partial H_R(f)} = S_{xx}(f)\begin{bmatrix}0 & 1\\ 1 & 2H_R(f)\end{bmatrix} \qquad \text{(C.4a)}$$

$$\frac{\partial \mathbf{R}(f)}{\partial H_I(f)} = S_{xx}(f)\begin{bmatrix}0 & -i\\ i & 2H_I(f)\end{bmatrix} \qquad \text{(C.4b)}$$

Substituting these expressions into (C.3) and after some algebra one can show that

$$\mathbf{J} = \frac{2NS_{xx}(f)^2}{\left|\mathbf{R}(f)\right|^2}\left\{\left|\mathbf{R}(f)\right|I + 2S_{n_xn_x}(f)^2\,\underline{H}\underline{H}^T\right\} \qquad \text{(C.5)}$$

and

$$\left|\mathbf{R}(f)\right| = S_{xx}(f)S_{n_yn_y}(f) + S_{n_xn_x}(f)S_{n_yn_y}(f) + S_{n_xn_x}S_{yy}(f) \qquad \text{(C.6)}$$

in which $\underline{H} = \left[H_R(f)H_I(f)\right]^T$ and CRLBs can be evaluated, with the aid of the matrix inversion lemma (Woodbury's Identity) [20], one can show that

$$CRLB\left\{H_R(f)\right\} = \frac{\left|\mathbf{R}(f)\right|}{NS_{xx}(f)^2}\left(1 - \frac{S_{n_xn_x}(f)^2 H_R(f)^2}{2S_{n_xn_x}(f)^2\left|H(f)\right|^2 + \left|\mathbf{R}(f)\right|}\right) \qquad \text{(C.7a)}$$

$$CRLB\left\{H_I(f)\right\} = \frac{\left|\mathbf{R}(f)\right|}{NS_{xx}(f)^2}\left(1 - \frac{S_{n_xn_x}(f)^2 H_I(f)^2}{2S_{n_xn_x}(f)^2\left|H(f)\right|^2 + \left|\mathbf{R}(f)\right|}\right) \qquad \text{(C.7b)}$$

For large Signal to Noise Ratios (SNRs), i.e. $S_{xx}(f), S_{yy}(f) >> S_{n_xn_x}(f), S_{n_yn_y}(f)$; (C.7a,b) can be significantly simplified by neglecting quadratic terms in the noise spectra, so that

$$|\mathbf{R}(f)| \approx S_{xx}(f)S_{n_y n_y}(f) + S_{yy}(f)S_{n_x n_x}(f) >> 2S_{n_x n_x}(f)^2 |H(f)|^2 \tag{C.8}$$

in which case the CRLBs become

$$CRLB\{H_R(f)\} = CRLB\{H_I(f)\} \approx \frac{|H(f)|^2}{N}\left\{\frac{S_{n_y n_y}(f)}{S_{yy}(f)} + \frac{S_{n_x n_x}(f)}{S_{xx}(f)}\right\} \tag{C.9}$$

Therefore, the approximate CRLBs are proportional to the sum of the inverse SNRs on the input and the output. It should also be noted that the $1/N$ factor in (C.9) indicates that the ML estimator is consistent. The assumption invoked in approximating (C.7a,b) by (C.9) also imposes the independence of $H_R(f)$ and $H_I(f)$. It has already been mentioned in Section 5.2.3 that ML estimators are distributed according to Gaussian statistics. By virtue of this property, then the random variable

$$\frac{N|H_s(f)|^2}{|H(f)|^2\left\{\frac{S_{n_y n_y}(f)}{S_{yy}(f)} + \frac{S_{n_x n_x}(f)}{S_{xx}(f)}\right\}} = \frac{N\left\{H_R(f)^2 + H_I(f)^2\right\}}{|H(f)|^2\left\{\frac{S_{n_y n_y}(f)}{S_{yy}(f)} + \frac{S_{n_x n_x}(f)}{S_{xx}(f)}\right\}} \tag{C.10}$$

is a chi-squared random variable with 2 degrees of freedom and hence the variance of the estimator $H_s(f)$ is given by (5.22). This allows one to write the confidence interval for the squared magnitude of $H_s(f)$ as

$$|H_s(f)|^2\left[1 \pm \log(\beta)\frac{4}{N}\left\{\frac{S_{n_y n_y}(f)}{S_{yy}(f)} + \frac{S_{n_x n_x}(f)}{S_{xx}(f)}\right\}^2\right] \tag{C.11}$$

where the fact that the $100\beta$ percentile of a chi-squared distribution, with 2 degrees of freedom is given by $\log(\beta)$ has been exploited. The equivalence between (C.11) and (3.60) can be shown by assuming large $N$ (so that $N\text{-}2 \approx N$) and noting that for the case of output noise only then $S_{n_x n_x}(f) = 1 - \gamma^2_{x_m y_m}(f)$.

In order that (C.11) can be used in practice one needs to first estimate the input power spectrum $S_{xx}(f)$, from which $S_{yy}(f)$ can simply be obtained. This could be approached in various ad hoc fashions, herein we retain the philosophy of ML and solve (5.17), with $\alpha = S_{xx}(f)$, and replacing $H(f)$ by its ML estimate (5.21). Again after some algebra one can obtain the optimal estimator of $S_{xx}(f)$ as

$$S_{xx}(f) = \frac{S_{x_m x_m}(f)\kappa(f) + S_{y_m y_m}(f)}{\kappa(f) + |H_s(f)|^2} \tag{C.12}$$

This estimate of the input spectrum only depends upon the ratio $\kappa(f)$ and not on the absolute levels of the noise spectra.

By using (C.11) and (C.12) in conjunction one can obtain confidence intervals for the squared magnitude of the transfer function estimator $H_s(f)$. Notice how, whilst the estimators of $H(f)$ and $S_{xx}(f)$, (5.21) and (C.12) respectively, only require the knowledge of the ratio of the noise spectra, in order to compute the confidence intervals one requires the absolute levels of the noise spectra, i.e. values for $S_{n_x n_x}(f)$ and $S_{n_y n_y}(f)$.

# APPENDIX D

## Eigen-Value Decomposition of the TISO System Spectral Correlation Matrix

The eigenvalues ( $\lambda_i$ ) and eigenvectors ( $\mathbf{t}_i$ ) of the noise-free spectral correlation matrix (5.23) are obtained (for $i$=1, 2,3) from the solution of (5.27) which can be expanded as (omitting $f$'s in brackets for brevity)

$$\begin{bmatrix} \hat{S}_{x_1x_1} & \hat{S}_{x_2x_1} & H_a^*\hat{S}_{x_1x_1} + H_b^*\hat{S}_{x_2x_1} \\ \hat{S}_{x_1x_2} & \hat{S}_{x_2x_2} & H_a^*\hat{S}_{x_1x_2} + H_b^*S_{x_2x_2} \\ H_a\hat{S}_{x_1x_1} + H_bS_{x_2x_2} & H_a\hat{S}_{x_2x_1} + H_bS_{x_2x_2} & |H_a|^2S_{x_1x_1} + |H_b|^2S_{x_2x_2} + H_a^*H_bS_{x_1x_2} + H_b^*H_aS_{x_2x_1} \end{bmatrix} \begin{bmatrix} t_{1i} \\ t_{2i} \\ t_{3i} \end{bmatrix} = \lambda_i \begin{bmatrix} t_{1i} \\ t_{2i} \\ t_{3i} \end{bmatrix} \quad \text{(D.1)}$$

Using Cramer's Theorem in order to solve for the eigenvalues

$$\det\left\{\hat{\mathbf{R}}(f) - \lambda \cdot \mathbf{I}\right\} = 0 \quad \text{(D.2)}$$

we get

$$\det\begin{bmatrix} \lambda - \hat{S}_{x_1x_1} & -\hat{S}_{x_2x_1} & -(H_a^*\hat{S}_{x_1x_1} + H_b^*\hat{S}_{x_2x_1}) \\ -\hat{S}_{x_1x_2} & \lambda - \hat{S}_{x_2x_2} & -(H_a^*\hat{S}_{x_1x_2} + H_b^*S_{x_2x_2}) \\ -(H_a\hat{S}_{x_1x_1} + H_bS_{x_2x_2}) & -(H_a\hat{S}_{x_2x_1} + H_bS_{x_2x_2}) & \lambda - (|H_a|^2S_{x_1x_1} + |H_b|^2S_{x_2x_2} + H_a^*H_bS_{x_1x_2} + H_b^*H_aS_{x_2x_1}) \end{bmatrix} = 0 \quad \text{(D.3)}$$

Expanding (D.3) and after some algebra we get the expressions (5.25) and (5.26) defining the eigenvalues for the cases of correlated and uncorrelated inputs, respectively. Note that, in both cases there a two non-zero eigenvalues and one zero eigenvalue.

# APPENDIX E

## Experimental Layout – Fault Detection in Rotating Machinery

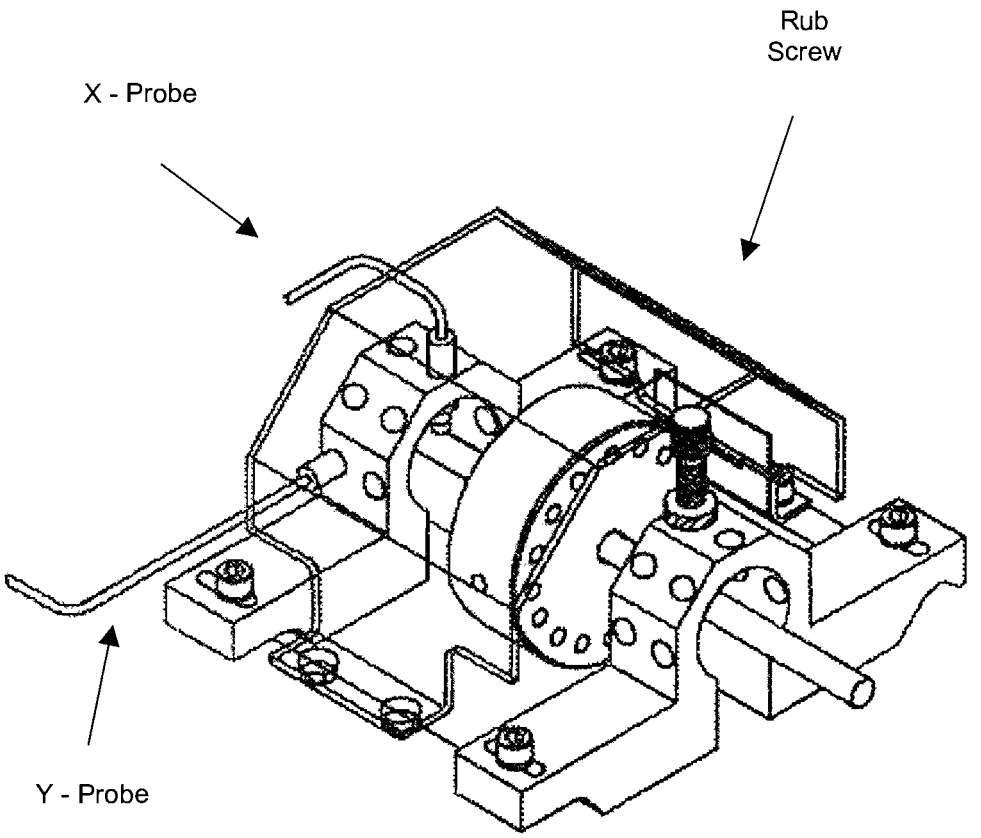


**Figure E.1** XY Probe mount and the typical rub screw set up (Bently Nevada).

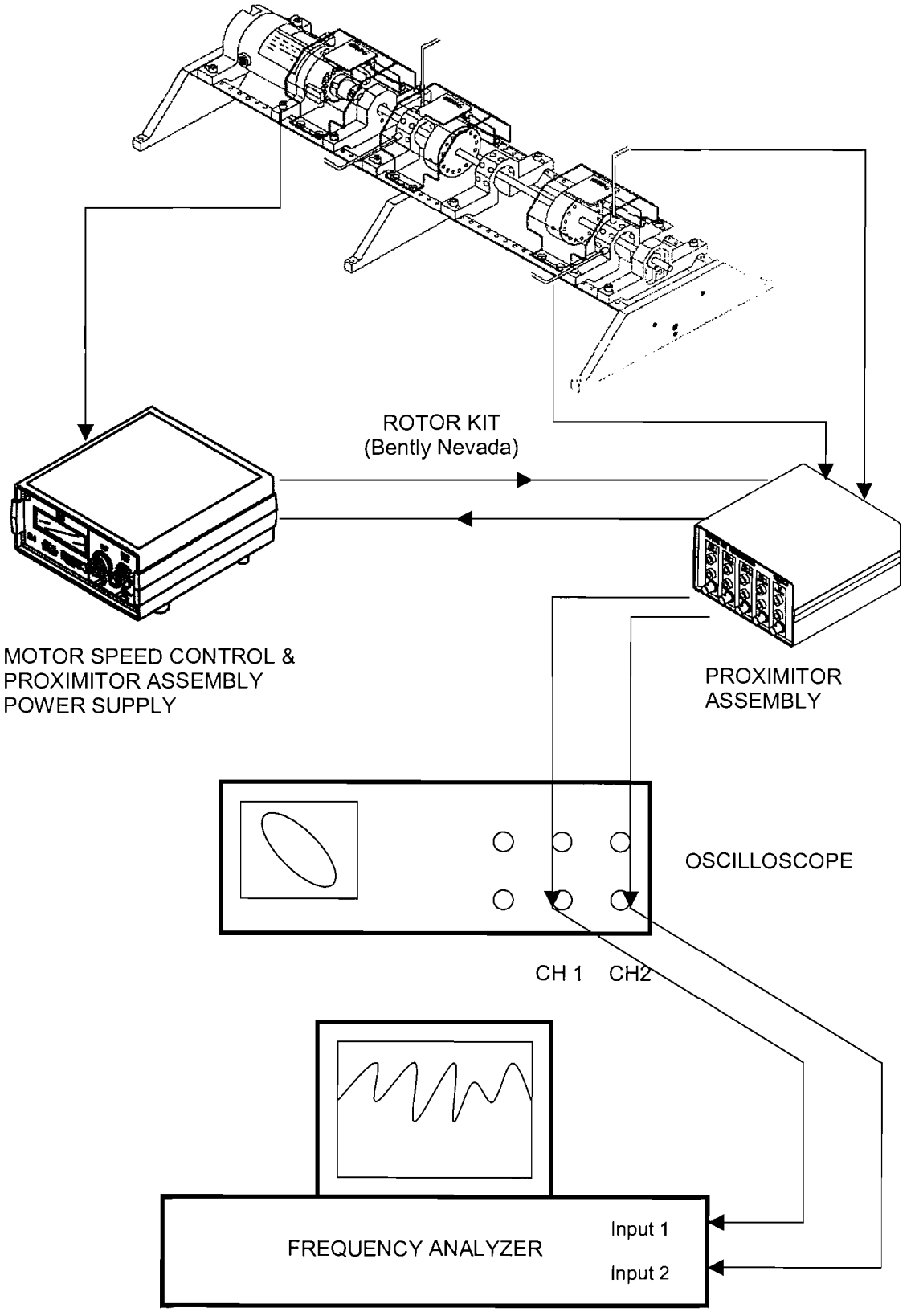


**Figure E.2** Equipment and the experimental layout.

# References


[1] J.S. Bendat and A.G. Piersol, "Engineering Applications of Correlation and Spectral Analysis," John Wiley & Sons, New York, 1980.

[2] J.S. Bendat and A.G. Piersol, "Random Data – Measurement & Analysis Procedures," John Wiley & Sons, New York, 1986.

[3] A.V. Oppenheim and A.S. Willsky , "Signals and Systems," Prentice-Hall, Englewood Cliffs, 1983.

[4] A. Hyvarinen, J. Karhunen and E. Oja, "Independent Component Analysis: A Volume in the Wiley Series on Adaptive nad Learning Systems for Signal Processing, Communications and Control," Simon Haykin, John Wiley & Sons, New York, 2001.

[5] G.H. Dunteman, "Principal Component Analysis Series: Quantitative Applications in Social Sciences," Sage, Newbury Park, 1987.

[6] E. Kreyszig "Advanced Engineering Mathematics," 7th Edition, John Wiley & Sons, New York, 1993.

[7] G.M. Jenkins and D.G. Watts, "Spectral Analysis and Its Applications," Holden Day, 1968.

[8] H. Vold, J.R. Crowley and T.G Rocklin, "New Ways of Estimating Frequency Response Functions," Sound and Vibration, Vol. 18(11), pp. 34-38, 1984.

[9] T.G Rocklin, J.R. Crowley and H. Vold, "A Comparison of $H_1$, $H_2$ and $H_v$ Frequency Response Function Estimators," Proceedings of the 3rd International Modal Analysis Conference, IMAC, Orlando-Florida, pp. 272-278, 1985.

[10] A. L. Wicks and H. Vold, "The $H_S$ Frequency Response Function Estimator," Proceedings of the 4th International Modal Analysis Conference, IMAC, pp. 897-899, 1986.

[11] J. Leuridan and D. De Vis, "A Comparison of Some Frequency Response Function Measurement Techniques," Proceedings of the 4th International Modal Analysis Conference, IMAC, pp. 908-918, 1986.

[12] R.J. Allemang and D.L. Brown, "Experimental Modal Analysis," Shock and Vibration Handbook, 4th Edition, C.M. Harris, McGraw Hill, 1996.

[13] P.R. White, M.H.Tan and J.K. Hammond, "Analysis of the Maximum Likelihood, Total Least Squares and Principal Component Approaches for Frequency Response Function Estimation," Journal of Sound and Vibration, Southampton-United Kingdom, Accepted in September 2004.

[14] H.L. Van Trees, "Detection, Estimation, and Modulation Theory: Part 1," John Wiley and Sons, New York, 1968.

[15] S.M. Kay, "Modern Spectral Estimation: Theory and Applications," Prentice-Hall, 1988.

[16] G. H. Golub and C. F. Van Loan, "An Analysis of the Total Least Squares Problem," SIAM Journal on Numerical Analysis, Vol. 17, No. 6, pp. 883-893, 1980.

[17] D. Brillinger and M. Rossenblatt, "Asymptotic Theory of $k^{th}$ Order Spectra, " Spectral Analysis of Time Series, B. Harris, John Wiley, New York:, pp. 153-188, 1967.

[18] D. Fotheringhame and R. Baddeley, "Non-Linear Principal Component Analysis of Neuronal Spike Train Data," Biological Cybernetics, Vol. 77, pp. 283-288, 1997.

[19] R.O. Schmidt, "A Signal Subspace Approach to Multiple Emitter Location and Spectral Estimation," Ph.D. Thesis, Stanford University, 1992.

[20] S. Haykin, "Adaptive Filter Theory," 3rd Edition, Prentice-Hall, New Jersey, 1996.

[21] P.R. White and W.B. Collis, "Analysis of the TLS Frequency Response Function Estimator," Proceedings of the 9th IEEE Workshop on Statistical Signal and Array Processing, IEEE, Portland-Oregon, 1998.

[22] B. Rost and J. Leuridan, "A Comparison of Least Squares and Total Least Squares for Multiple Input Estimation of Frequency Response Functions," ASME Design Engineering Division Conference and Exhibit on Mechanical Vibration and Noise, ASME, 85-DET-105, Cincinnati-Ohio, 1985.

[23] D. Otte, K. Fyfe and P. Sas, "Use of Principal Component Analysis for Dominant Noise Source Identification," IMechE Proceedings, 1988.

[24] M.H. Tan and J.K. Hammond, "Applications of Principal Component Analysis for the Detection and Interpretation of Non-Linearities in Measurement Systems," Proceedings of the 4th International Conference on Acoustical and Vibratory Surveillance Methods and Diagnostic Techniques, IMechE-IMEKO-SFM, Compiégne-France, 2001.

[25] M.H. Tan and J.K. Hammond, "Principal Component Analysis for Non-Linearity Detection and Linear Equivalent Transfer Function Estimation", Proceedings of ICASSP 2002 International Conference on Acoustics, Speech and Signal Processing, IEEE, Orlando-Florida, 2002.

[26] G. Efthymiatos, "Principal Component Analysis for Frequency Response Function Estimation," MSc. Thesis, Institute of Sound and Vibration Research, University of Southampton, Southampton-United Kingdom, 1999.

[27] S.V. Vaseghi, "Advanced Signal Processing and Digital Noise Reduction," John Wiley & Sons, Chicester-United Kingdom, 1996.

[28] G.H. Golub and C.F. Van Loan, "Matrix Computations," North Oxford Academic, Oxford-United Kingdom, 1983.

[29] J.K. Hammond, "Chapter 6 in Fundamentals of Noise and Vibration," F. Fahy and J. Walker, E&FN Spoon, London-United Kingdom, 1998.

[30] S. Daultrey, "Principal Component Analysis Series: Concepts and Techniques in Modern Geography," Geo Abstracts, Norwich-United Kingdom, 1976.

[31] J.K. Hammond and P.R. White, " The Analysis of Non-Stationary Signals Using Time-Frequency Methods," Journal of Sound and Vibration, Vol. 190(3), pp. 419-447, Academic Press Limited, 1996.

[32] S. Van Huffel and H. Zha, "The Total Least Squares Problem," Handbook of Statistics, Vol. 9, pp. 377-408, C.R. Rao, Elsevier Science Publishers, 1993.

[33] P.R. White, W.B. Collis, T.G. Leighton and J.K. Hammond, "Detection of Bubbles via Higher Order Statistics," Natural Physical Processes Associated with Sea Surface Sound, T.G. Leighton, Institute of Sound and Vibration Research, University of Southampton, United Kingdom, 1995.

[34] R. Dunia and S.J. Qin, "Joint Diagnosis of Process and Sensor Faults using Principal Component Analysis," Control Engineering Practice, Vol. 6, pp. 457-469, Pergamon, 1997.

[35] S. Edwards, A.W. Lees and M.I. Friswell, "Fault Diagnosis of Rotating Machinery," Shock and Vibration Digest, Vol. 30, No. 1, pp. 4-13, 1998.

[36] W. Li, F. Gu, A.D. Ball, A.Y.T. Leung and C.E. Phipps, "A Study of the Noise from Diesel Engines using the Independent Component Analysis," Mechanical Systems and Signal Processing, Vol. 15(6), pp. 1165-1184, Academic Press, 2001.

[37] K. Weltner, W.J. Webber, J. Grosjean and P. Schuster, "Mathematics for Engineers and Scientists," Nelson Thornes, 1995.

[38] R. Dunia, S.J Qin, T.F. Edgar and T.J. McAvoy, "Sensor Fault Identification and Reconstruction using Principal Component Analysis," Proceeding of the 13th Triennial World Congress, IFAC, San Francisco- USA, 1996.

[39] S.J. Qin and R. Dunia, "Determining the Number of Principal Components for Best Reconstruction," Priceedings of the 5th IFAC Symposium on Dynamcis and Control of Process Systems, IFAC, 1998.

# List of Publications

1. M.H. Tan and J.K. Hammond, "Applications of Principal Component Analysis for the Detection and Interpretation of Non-Linearities in Measurement Systems," Proceedings of the 4th International Conference on Acoustical and Vibratory Surveillance Methods and Diagnostic Techniques, IMechE-IMEKO-SFM, Compiégne-France, 2001.

2. M.H. Tan and J.K. Hammond, "Principal Component Analysis for Non-Linearity Detection and Linear Equivalent Transfer Function Estimation", Proceedings of ICASSP 2002 International Conference on Acoustics, Speech and Signal Processing, Student Forum, IEEE, Orlando-Florida, 2002.

3. P.R. White, M.H. Tan and J.K. Hammond, "Analysis of the Maximum Likelihood, Total Least Squares and Principal Component Approaches for Frequency Response Function Estimation," Journal of Sound and Vibration, Southampton-United Kingdom, Accepted in September 2004.